TRANSLATION

COSMIC RESEARCH

Volume 2 - Number 3 - 1964

FOREIGN TECHNOLOGY DIVISION

AIR FORCE SYSTEMS COMMAND

WRIGHT-PATTERSON AIR FORCE BASE

OHIO

FTD-TT- 64-770/1+2

UNEDITED ROUGH DRAFT TRANSLATION

COSMIC RESEARCH

English Pages: 239

THIS TRANSLATION IS A RENDITION OF THE ORIGINAL FOREIGN TEXT WITHOUT ANY ANALYTICAL OR EDITORIAL COMMENT. STATEMENTS OR THEORIES ADVOCATED OR IMPLIED ARE THOSE OF THE SOURCE AND DO NOT NECESSARILY REFLECT THE POSITION OR OPINION OF THE FOREIGN TECHNOLOGY DIVISION.	PREPARED BY: TRANSLATION DIVISION FOREIGN TECHNOLOGY DIVISION WP-AFB, OHIO.

Akademiya Nauk SSSR

KOSMICHESKIYE ISSLEDOVANIYA

Tom II

Vypusk 3

Izdatel'stvo Nauka

Moskva 1964

pages 355 - 504

TABLE OF CONTENTS

BLANK PAGE

COSMIC RESEARCH

Vol. II 1964 No. 3

THE "ELEKTRON" SPACE SYSTEM

A space system consisting of the two scientific stations "Elektron-1" and "Elektron-2 " was successfully launched in the Soviet Union on 30 January 1964, the two stations being ejected into substantially different orbits by a single powerful rocket vehicle. The creation of such a system opens new possibilities for study of circumterrestrial cosmic space and is of fundamental importance for the development of cosmic physics. A broad complex of measurements necessary for more profound understanding of the physical processes unfolding in various regions of circumterrestrial cosmic space is being accomplished with the aid of the scientific stations "Elektron-1" and "Elektron-2."

One of the basic assignments of the satellites "Elektron-1" and "Elektron-2" is to study the internal and external radiation belts of Earth. The streams of charged particles present in the radiation belts are highly intense, and the energy of many particles in the radiation belts is sufficient to allow them to penetrate inside space ships.

The "Elektron" satellites are also investigating the ultraviolet radiation of the Sun, cosmic rays, the magnetic field, and so forth. Below we present a full list of the scientific apparatus mounted on the "Elektron" satellites.

SCIENTIFIC APPARATUS ABOARD THE SATELLITE "ELEKTRON-1"

1. A package of instruments for study of the Earth's radiation belts, consisting of scintillation, gas-discharge and semiconductor radiation detectors. The instruments register electrons with energies

ranging from 40 kev to 10 Mev and protons with energies from 2 to 200 Mev.

2. Apparatus for study of the soft corpuscular radiation, consisting of scintillation counters with an auxiliary electron accelerator on one of the indicators and a magnet cutting off low-energy electrons on the other indicator. The apparatus registers electrons from 5 kev and protons from 150 kev.

3. A "Mayak" ["Beacon"] system, designed for study of the electromagnetic properties of the ionosphere and the interplanetary medium by means of coherent radio waves at the frequencies 20.005, 30.0075 and 90.0225 Mc.

4. Ballistic piezoelectric micrometeorite detectors having a sensitive surface area of 0.03 m^2. The minimum particle mass that can be registered is 10^{-8} g.

5. A mass spectrometer for study of the ionic composition of the atmosphere at high altitudes. This instrumentation is capable of registering mass numbers from 1 to 34 atomic mass units.

6. Solar energy cells, for study of the performance of solar batteries under the conditions of cosmic space.

SCIENTIFIC APPARATUS ABOARD THE SATELLITE "ELEKTRON-2"

1. Instrument package for studying the radiation belts of the Earth, consisting of the same instruments as aboard the satellite "Elektron-1."

2. An electrostatic spherical analyzer, which registers electrons and protons with energies E_0 of 100 ev, 200 ev, 400 ev, 1 kev, 2 kev, 4 kev and 10 kev in the band within $\pm 30\%$ of E_0.

3. Two ferromagnetic-probe magnetometers, which measure three mutually perpendicular components of the magnetic field in the ranges from 2-3 to 1200γ.

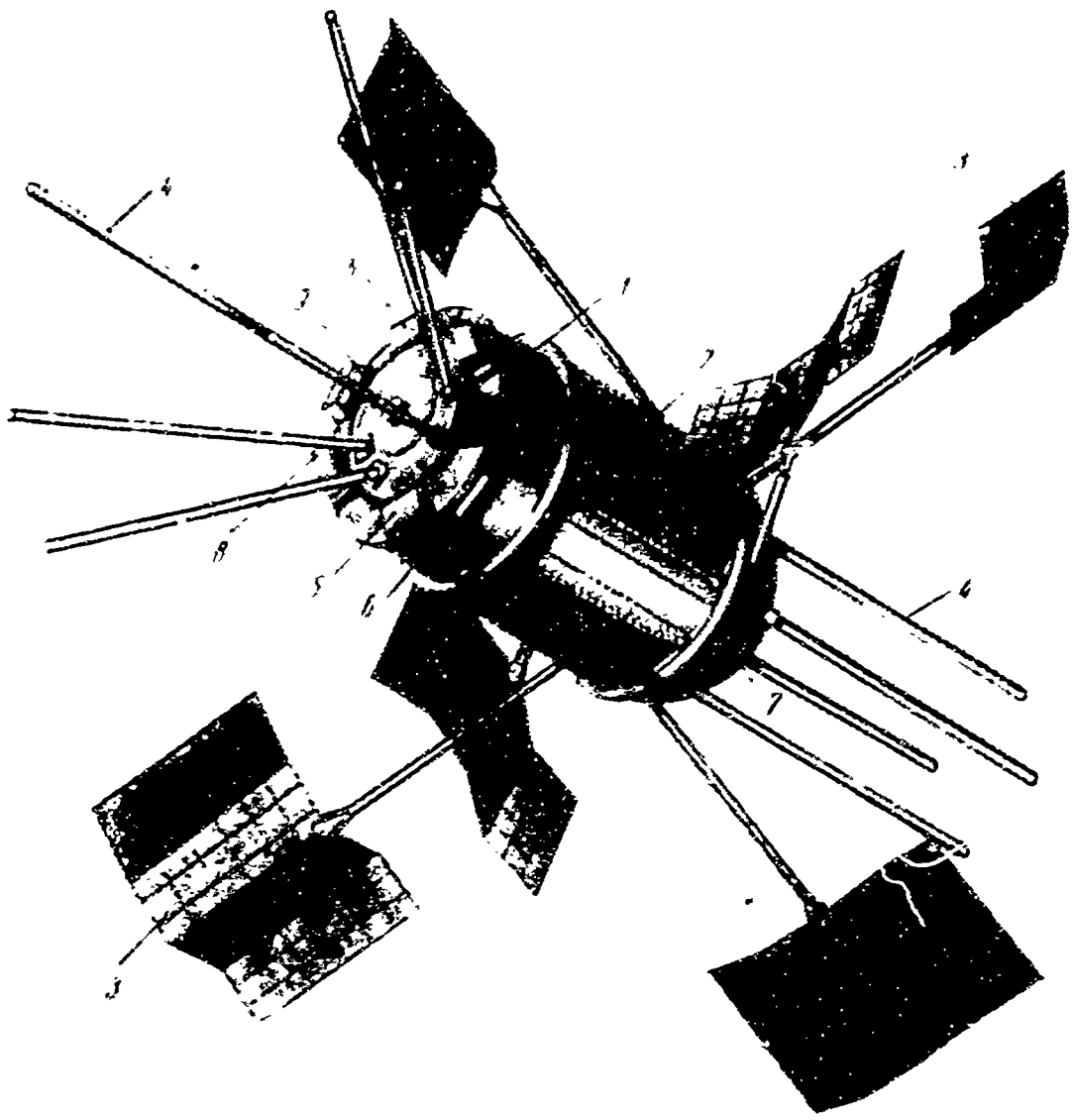

Fig. 1. The cosmic station "Elektron-1." 1) Sealed housing of station; 2) shutters of heat-regulation system; 3) solar batteries; 4) antennas; 5) micrometeor detector; 6) instrument for registering corpuscular radiation; 7) mass spectrometer; 8) proton detector; 9) device for studying the energy spectrum of radiation-belt electrons.

4. X-ray counters, which register the solar x-radiation in the ranges from 2 to 8 A and from 8 to 18 angstroms. The counters are mounted on a platform that automatically orients itself toward the Sun and "look" at the Sun almost continuously.

5. Apparatus for studying the composition of cosmic rays and the time variations of the fluxes of various nuclear groups. The instruments incorporate Cerenkov and scintillation counters, which register nuclei with charges $Z \geq 2$, $Z \geq 5$ and $Z \geq 15$ and heavier ones with energies exceeding 600 Mev/nucleon.

6. Apparatus for registering cosmic radio emission at the frequencies 725 kc and 1525 kc.

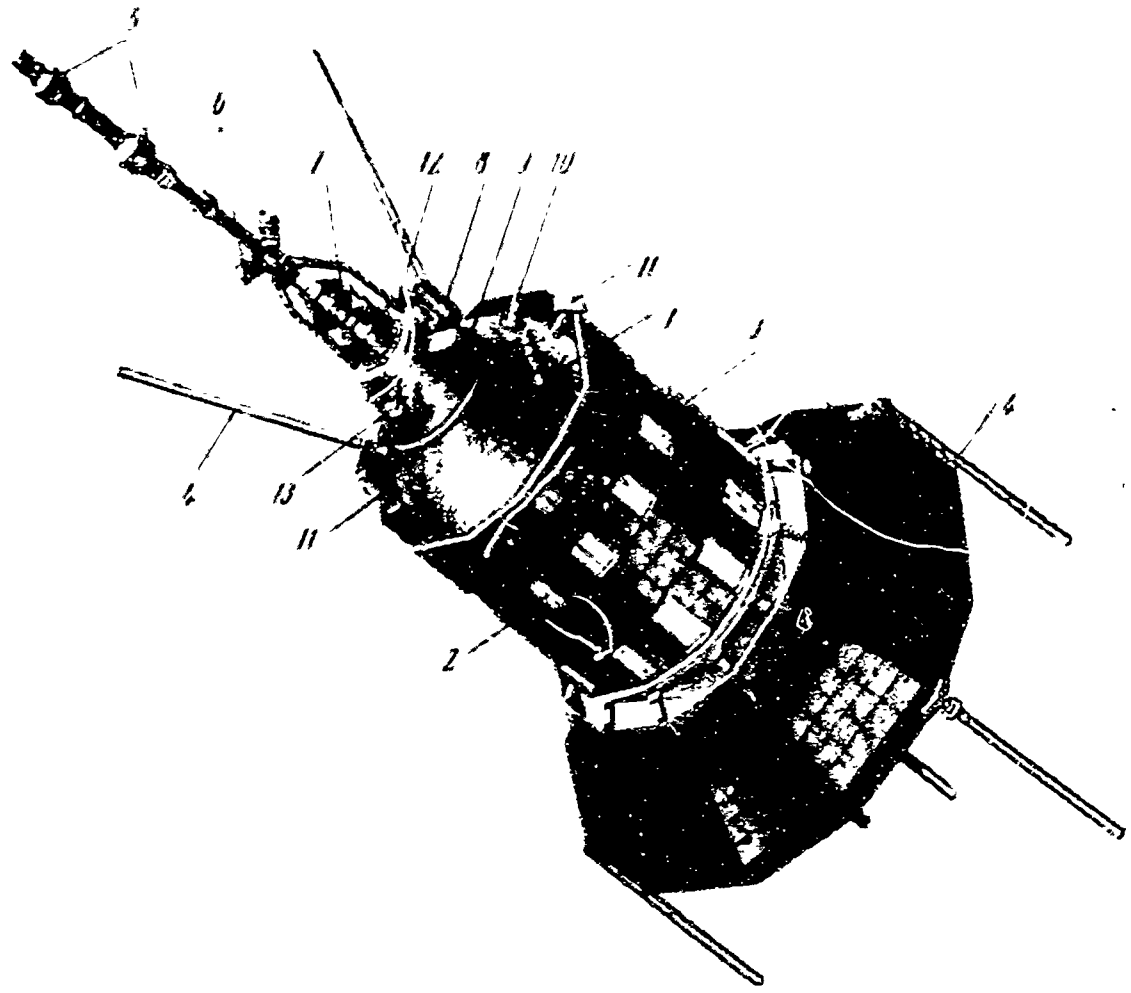

Fig. 2. The cosmic station "Elektron-2." 1) Sealed housing of station; 2) shutters of temperature-control system; 3) solar batteries; 4) antennas; 5) magnetometer; 6) solar orientation sensors; 7) spherical analyzer for studying the energy spectrum of low-energy particles; 8) instrument for studying the chemical composition of cosmic rays; 9) instrument for studying the energy spectrum of radiation-belt electrons; 10) mass spectrometer; 11) instrument for studying the solar x-radiation; 12) low-energy proton detector; 13) charged-particle traps.

7. A charged-particle trap similar to those used on all cosmic rockets. The trap registers positive masses in the plasma layer around the Earth and protons in the solar corpuscular streams. Electrons with energies > 100 ev are also registered by the trap, but they give rise to collector currents of the opposite sign.

8. A mass spectrometer for studying the ionic composition of the atmosphere at high altitudes. The instrument has the same parameters as the one aboard the satellite "Elektron-1."

9. Solar energy cells, for study of their performance under the conditions of cosmic space.

Two elliptical orbits with large eccentricities were selected for the "Elektron" cosmic system in order to provide for scientific inves-

tigations over the entire range of altitudes of interest to us – from the upper layers of the atmosphere to cosmic space beyond the limits of the radiation belts. The first orbit lies in the most interesting regions of the internal radiation belt, crosses parts of the external belt and covers the region of space with nonregular magnetic field and the unstable particle fluxes that produce the aurora. The second orbit crosses parts of the internal belt and the most interesting regions of the external radiation belt, and intersects a region with nonsteady fluxes of low-energy electrons situated outside the external radiation belt – the region that has come to be known in the literature as the outermost belt of charged particles. The apogee height of the satellite "Elektron-1" is 7000 km, which corresponds approximately to the upper boundary of the internal radiation belt, while the apogee of "Elektron-2" is 68,000 km. The perigee altitude lies in the range from 400 to 460 km for both orbits. The inclination is about 61°. The perigees are situated in the Northern Hemisphere, which guarantees optimum conditions for conducting radio communications sessions between the cosmic stations and ground monitoring points. Together with this, when the stations are situated in the perigee region of the orbits, the telemetry traffic is at its heaviest, since it is in this region that the measurements related to study of the upper atmosphere are made in addition to the radiation-belt studies.

Ejecting two satellites into substantially different orbits by means of a single booster presents significant technical difficulty. To eject the cosmic stations "Elektron-1" and "Elektron-2" into the specified orbits, the former was separated on the powered flight segment of the booster's last stage while its engine was still running. The "Elektron-1" station was separated by means of a special propulsion system that accomplished separation of the "Elektron-1" station from the last

tage of the booster rocket at a rigorously defined speed and with ractically no disturbing effects on the subsequent motion of the last tage. The "Elektron-1" station was designed in such a way that it ould be most compact at the time of separation and would not have arge projecting parts.

"Elektron-1" and "Elektron-2" are automatic stations - satellites eveloped for complex study of circumterrestrial cosmic space.

Figures 1 and 2 show the external appearance of the satellite stations "Elektron-1" and "Elektron-2."

On the outside of each station are the solar batteries, the antena systems, some of the instruments for scientific research and the solar-orientation sensors. The cylindrical part of the housing accommodates the rotating shutters of the temperature-control system. The 'Elektron-1" station is distinguished by its folding antennas and solar-battery panels, which open after separation of the station from the coster rocket on command from a programmed timer. This was necessary n connection with separation of this station on the powered part of he trajectory. The solar-battery panels are rigidly mounted on the 'Elektron-2" station. The scientific instrumentation installed on the 'Elektron" satellites takes measurements at all points of the orbits. he results of the measurements are read into storage devices carried n board. Scientific information and data on the performance of the on-oard systems are accumulated in the storage unit over one or several rbits (depending on the operating mode selected for the memory units).

During communications sessions, transmission of the stored information is accompanied by direct telemetric transmission of a large number of parameters registered by the scientific instruments, and data re transmitted on the performance of all systems aboard the station. peration of the on-board apparatus can be controlled by either of two

methods – autonomously or by commands transmitted to the stations from ground points on special command radio links. The power-supply systems include solar batteries and buffer storage batteries charged from the solar batteries.

The angular attitude of the "Elektron" stations in space is determined by the solar-orientation sensors, whose indications are registered in the storage units simultaneously with the measurement results from the scientific instrumentation.

A complex of control and monitoring points on the ground has the responsibility for controlling the flight of the "Elektron" cosmic system, measuring the parameters of the satellite-station orbits, receiving and recording the telemetry and scientific data, and issuing commands to switch on and off the apparatus carried by the devices.

The locations of the control and measuring stations in this complex permit communication with the "Elektron-1" and "Elektron-2" satellites on all orbits that pass over the territory of the USSR.

INTERPLANETARY FLIGHTS WITH CONSTANT OUTPUT ENGINES

V.V. Beletskiy and V.A. Yegorov

The problem of interplanetary flight of a jet-propelled vehicle with an ionic or plasma engine is investigated on the assumption that the jet-reaction power output is constant. The study is made basically by the "transporting-trajectory method" – a method of linearizing the equations with respect to a certain suitably selected reference trajectory. The method is convenient for the rapidity of its calculations and has high accuracy for a broad class of practically interesting trajectories. Flights with optimum control of the jet acceleration are studied, as well as flights with a constant jet-acceleration vector that changes direction once.

* * *

The present paper investigates the problem of cosmic flight of a jet-propelled apparatus with an ionic or plasma engine on the assumption that the power expenditure on jet reaction is constant. The maximum accelerations that these engines can impart to the rocket amount to only a few mm/sec^2. Due to the small magnitude of the reaction accelerations obtained as compared with the acceleration of gravity, the trajectory of the space flight consists of segments of two different types: segments of spiral motion in the vicinity of the planets and segments of flight between the planets' spheres of influence.

It is convenient to separate these segments by points at which the planetocentric velocity of the rocket is the same as the local parabolic velocity [1]. Here we may disregard the influence of the Sun in approximate calculations, at least until the parabolic velocity is

reached, and we may disregard the influence of the planet after this speed has been reached, taking the initial heliocentric velocity of the rocket as equal to the heliocentric velocity of the planet.

The present paper is concerned with flights between spheres of influence of planets. A method is proposed for calculating the trajectories and power characteristics of cosmic flight on the basis of the transporting trajectories and transporting coordinate system that are introduced. The basic inspiration for the method is due to T.M. Eneyev. This procedure is based on the assumption that the flight trajectory with small reaction acceleration does not differ greatly from a certain suitably selected known trajectory. Such a trajectory will be referred to as a transporting trajectory, and a system of coordinates that moves translationally along the transporting trajectory will be referred to as the transporting coordinate system.

In first approximation, we may, in this system of coordinates, disregard all forces other than the engine-thrust reaction force, since the basic part of the solar attraction is taken into account by the very introduction of the transporting trajectory. To take the gravitational attraction of the Sun into account with greater accuracy, it is expedient to linearize the equations of motion in the transporting coordinate system; this also takes into account the linear part of the perturbations of the rocket in the Sun's gravitational field, perturbations due to deviation of the rocket from the origin of the transporting-coordinate system.

It is shown in the present paper that a treatment of this type is sufficiently accurate for a broad class of trajectories. Moreover, this method first makes it possible in a number of cases to avoid numerical integration of the equations of motion, since the linearized equations are integrated in quadratures; secondly, it makes it possible to solve

the boundary-value problem without iterations, since the problem becomes linear. We shall apply the transporting-trajectory method to an arbitrary reaction-acceleration control law.

The paper submitted here contains seven sections.

Section 1 considers model problems and sets forth the transporting trajectory method for solution of the interplanetary-flight problem. Section 2 considers the variational problem for a rocket with a constant-power engine moving in an arbitrary force field; the method of transporting trajectories is used for solution of this problem in Section 3. The solution of the optimum problem in first approximation is studied in Section 4. In Section 5, we consider (in first approximation) the problem of flight with reaction acceleration constant in magnitude and changing direction once. In Section 6, the equations of optimum motion are integrated in the second approximation; Section 7 presents the results of calculations for certain flights to Mars, Venus, and Jupiter and analyzes the accuracy of the method used. The results of a series calculation of interplanetary-flight characteristics are set forth in another paper written by the authors in collaboration with V.G. Yershov.

The authors express their heartfelt gratitude to D.Ye. Okhotsimskiy and T.M. Eneyev for their invaluable assistance in the work, and to N.B. Myshetskiy, N.A. Malinina and Ye.A. Sidorova for running the calculations.

1. INITIAL CONSIDERATIONS. MODEL PROBLEMS. THE TRANSPORTING COORDINATE SYSTEM

Let N be that part of the power of the on-board powerplant that is converted into the kinetic energy of the reaction jet, V_r be the velocity of particle motion in the jet, $\underline{f}$ be the reaction acceleration and m(t) be the variable mass of the rocket. Then we have, by definition of reaction force and power,

$$f = -\frac{V_r}{m}\frac{dm}{dt}, \qquad (1.1)$$

$$N = -\frac{dm}{dt}\frac{V_r^2}{2}. \qquad (1.2)$$

We shall regard N as constant during the entire operating time of the engine. Excluding V_r with the aid of (1.1), we obtain $-\frac{1}{m^2}\frac{dm}{dt} = -\frac{f^2}{2N}$. Integrating, we find [2, 3]

$$\frac{m_0}{m} - 1 = \frac{m_0}{2N} J, \qquad (1.3)$$

$$J = \int_0^T f^2 dt. \qquad (1.4)$$

We note that by excluding dm/dt from (1.1) and (1.2), we obtain the formula

$$f = 2N/V_r m, \qquad (1.5)$$

from which it follows that at any fixed time during operation of the engine, the reaction acceleration will be the larger the lower the exhaust velocity at this moment.

It follows from Formula (1.3) that for any rocket with an engine producing a constant-power jet, the optimum operating mode will be that in which the integral J(1.4) reaches a minimum during the time of flight, with the expenditure of fuel from a small relative weight of fuel approximately proportional to J.

This permits making trajectory studies and calculating the reaction acceleration without using parameters for specific rockets, and the terminal relative weight and required fuel expenditures can then be calculated from the values of the integral J as soon as the parameters of the powerplant become known.

Problems of determining flight modes corresponding to the minimum of Functional (1.4) differ considerably from problems on the minimum of the functional $\int_0^T |f| dt$, which are normally solved for chemical-fuel

rockets. It is natural to begin a study of low-thrust motion from elementary model problems.

1) Let us consider rectilinear motion with a small constant reaction acceleration f over a given path 2s for a specified time 2T in the absence of external forces and under the condition that the initial and terminal velocities on the path are zero. We shall assume that the velocity rises uniformly on the first half of the path and diminishes uniformly on the second half.

We have

$$f = 2s/T^2 = 2V_0/T. \qquad (1.6)$$

During this process, the velocity $V_1 = 2s/T = 2V_0$ is gained and then lost, i.e., a velocity impulse $4V_0$ is expended. Here $V_0 = s/T$. We see that on the basis of the over-all velocity impulse, the expenditure for motion with small thrust is exactly twice the expenditure for impulse acceleration and deceleration of the rocket.

We have for the entire path

$$J_1 = 2f^2T = 8V_0^2/T. \qquad (1.7)$$

2) Let us now assume that a small constant acceleration acts not all of the time, but only at the beginning and the end of the assigned path, and that it is necessary to shut off the engine for this time in order to obtain the minimum of J in the assigned total flight time.

By virtue of the symmetry of the motion, it is sufficient to treat it, like Problem 1), only over half s of the entire path during a time T equal to half of the total flight time. Let τ be the time at which the engine is shut off. Then we obtain J and the assigned path:

$$J_2 = 2f^2\tau; \qquad (1.8)$$

$$2s = f\tau^2 + 2f\tau\,(T - \tau). \qquad (1.9)$$

Solving the problem for the minimum (1.8) with Condition (1.9), we get

$$\tau = \frac{2}{3}T,\ f = \frac{8}{4}\frac{V}{T},\ J_2 = \frac{27}{4}\frac{V_0^2}{T}. \qquad (1.10)$$

We see that $J_2 < J_1$ by $5/4 \cdot V_0^2/T$, i.e., by approximately 15.5%.

3) Let us now assume that the acceleration plot has two steps of height f_1 and f_2 and duration τ and $T - \tau$, and that it is necessary to select the parameters τ, f_1 and f_2 from the minimum condition (1.4) for the assigned path $\underline{s}$.

In this problem, we have instead of (1.8) and (1.9)

$$J_3 = 2\left[f_1^2\tau + f_2^2(T-\tau)\right], \quad 2s = f_1\tau^2 + 2f_1\tau(T-\tau) + f_2(T-\tau)^2,$$

which leads us, like the foregoing, to the formulas

$$\tau = \frac{1}{2}T,\ f_1 = \frac{12}{5}\frac{V}{T},\ f_2 = \frac{4}{5}\frac{V}{T};\ J_3 = \frac{32}{5}\frac{V^2}{T}. \qquad (1.11)$$

We see that $J_3 < J_2$, with the gain $J_3 - J_1$ already equal to 20% of J_1.

4) The maximum advantage can be obtained if we solve the variational isoperimetric problem for the minimum of Functional (1.4) for the assigned path

$$s = 2\int_0^T (T-t)f(t)\,dt. \qquad (1.12)$$

From the condition that the variation $\delta H = \int_0^T [2f + \lambda(T-t)]\,\delta f\,dt$ vanish (where λ is the constant Lagrange multiplier) and Condition (1.12), we find

$$f = 2\frac{V}{T}\left[\frac{3}{2}\left(1 - \frac{t}{T}\right)\right],\ s(t) = \frac{3}{2}VT\left(\frac{t}{T}\right)^2\left[1 - \frac{1}{3}\left(\frac{t}{T}\right)\right],\ J = 6\frac{V^2}{T}. \qquad (1.13)$$

We see that the reaction acceleration diminishes linearly to zero at t = T from an initial magnitude one-and-one half times larger than the constant acceleration of Problem 1), and the advantage in the value of J as compared with Problem 1) is 25%.

5) The variational problem can also be solved in a similar fashion with boundary velocities differing from zero. The solution is again a

linear law of variation of the reaction acceleration, and the advantage as compared with the case of constant reaction acceleration will be of the same order.

The elementary model problems that we have considered enable us to discern an essential peculiarity of the motion, namely that the introduction of a discontinuity into the engine's operation and a stepwise change in the magnitude of the reaction acceleration permits reducing the value of Integral (1.4) and, consequently, cutting fuel consumption. The maximum reduction of fuel consumption is attained by introducing continuous control of the acceleration $\underline{f}$ by an optimum law, which has been found to be linear in time in the case under consideration.

The problems set forth above represent something of an analogue of the problems of flight between planetary spheres of influence with assigned times t_1 of beginning and t_2 of completion of the flight, since these times fix the initial and terminal points of the path, the heliocentric velocities at these points, and the time of flight.

For approximate calculations of motion in specified spans of time between planetary spheres of influence, taking the attraction of the Sun into account, it is found more convenient to consider the motion not in a fixed, but in a translationally moving coordinate system. Suppose that the origin of this system is moving along a heliocentric conic section (according to Kepler's laws) during the same time t_1, t_2 between the same boundary points. In this system, the rocket will be acted upon not by the solar attraction itself, but only by the "perturbation" due to the Sun, i.e., the difference between the attractive forces exerted by the Sun on the rocket and on the coordinate origin or, more precisely, the difference between the force of solar gravitation and the inertial force due to the noninertial character of the reckoning system. We shall refer to the coordinate system introduced as the

transporting system and the trajectory of the coordinate origin as the transporting trajectory. The rocket's trajectory in this system will begin and end at the coordinate origin. Since the initial heliocentric velocity of the rocket is the same as the Earth's velocity for flight beginning at the Earth, the initial velocity of the rocket in the transporting system will be opposite in direction and equal in magnitude to the heliocentric initial velocity of the coordinate origin of the transporting system. Similarly, the terminal velocity of the rocket in the transporting system will be equal in magnitude and opposite in direction to the terminal planetocentric velocity of the transporting system coordinate origin.

When the trajectory in the transporting system deviates slightly from the coordinate origin, the perturbations may be disregarded as small by comparison with the reaction force, and we obtain motion in space without forces, so that the model problems examined above acquire even greater significance. Here and in everything that follows, we shall use the term "perturbations" to imply the above solar perturbations in the transporting coordinate system. It should be noted that in a specific calculation of interplanetary-flight trajectories, it is usually found advantageous to select a somewhat different transporting trajectory, namely, one located in the plane of the Ecliptic.

2. FORMULATION OF GENERAL VARIATIONAL PROBLEM

It was shown above that for engines with a reaction jet of constant power, the current relative mass m/m_0 and the reaction acceleration $\underline{f}$ are related by the integral relationship (1.3).

The problems that can be set up for rockets with low-thrust engines come in a wide variety. They include: acceleration of a rocket from the orbit of an Artificial Earth Satellite or planet to escape velocity and, conversely, return to such an orbit from cosmic space;

flight between planets, probing circumsolar space, and so forth. In all of these problems, it is reasonable to require that the rocket carry the largest payload consistent with execution of the given assignment.

As we see from (1.3), the problem of minimum mass expenditure in this flight reduces to minimization of Integral (1.4). As was shown in [2, 3], the problem of the minimum fuel and powerplant masses reduces to minimization of this same integral.

The problem can be formulated mathematically as follows. Let a force field with potential $\bar{U}$ and a reaction acceleration act on a rocket with mass $\underline{m}$. Let $U = \bar{U}/m$. Then the rocket's equation of motion will take the form

$$\dot{\mathbf{V}} - \operatorname{grad} U = \mathbf{f};\ \dot{\mathbf{r}} = \mathbf{V},\ \text{where } \mathbf{r} = (x, y, z);\ \mathbf{V} = (u, v, w);\ \mathbf{f} = (f_x, f_y, f_z). \quad (2.1)$$

It is necessary to determine the law of variation of the vector $\vec{f}$ such that the functional J (1.4) has an extreme at a given T with Relationships (2.1) prevailing. Let us introduce the Lagrange multipliers λ_x, λ_y, λ_z, λ_u, λ_v, λ_w, and write the auxiliary functional

$$J = \int_0^T \{f_x^2 + f_y^2 + f_z^2 + \lambda_x(\dot{u} - U_x - f_x) + \lambda_u(\dot{x} - u) + \lambda_y(\dot{v} - U_y - f_y) + \\ + \lambda_v(\dot{y} - v) + \lambda_z(\dot{w} - U_z - f_z) + \lambda_w(\dot{z} - w)\}\, dt.$$

The variation $\delta J = \delta_1 J + \delta_2 J$ where the term $\delta_1 J$ arises when the terminals are varied (with fixed terminals, $\delta_1 J \equiv 0$), and

$$\delta_2 J = \int_0^T \{-(\lambda_u + \dot{\lambda}_x)\,\delta u - (\lambda_v + \dot{\lambda}_y)\,\delta v - (\lambda_w + \dot{\lambda}_z)\,\delta w - \\ - (\lambda_x U_{xx} + \lambda_y U_{xy} + \lambda_z U_{xz} + \dot{\lambda}_u)\,\delta x - (\lambda_x U_{yx} + \lambda_y U_{yy} + \lambda_z U_{yz} + \dot{\lambda}_v)\,\delta y - \\ - (\lambda_x U_{xz} + \lambda_y U_{yz} + \lambda_z U_{zz} + \dot{\lambda}_w)\,\delta z + (2f_x - \lambda_x)\,\delta f_x + \\ + (2f_y - \lambda_y)\,\delta f_y + (2f_z - \lambda_z)\,\delta f_z\}\, dt.$$

Equating $\delta_2 J$ to zero, we obtain the Euler equations by virtue of the independence of the variations that appear:

$$2f_x - \lambda_x = 0, \quad 2f_y - \lambda_y = 0, \quad 2f_z - \lambda_z = 0,$$
$$\lambda_u + \dot{\lambda}_x = 0, \quad \lambda_v + \dot{\lambda}_y = 0, \quad \lambda_w + \dot{\lambda}_z = 0,$$
$$\lambda_x U_{xx} + \lambda_y U_{xy} + \lambda_z U_{xz} + \dot{\lambda}_u = 0,$$
$$\lambda_x U_{yx} + \lambda_y U_{yy} + \lambda_z U_{yz} + \dot{\lambda}_v = 0,$$
$$\lambda_x U_{zx} + \lambda_y U_{yz} + \lambda_z U_{zz} + \dot{\lambda}_w = 0.$$

Excluding the Lagrange multipliers from the above, we obtain for f_x, f_y and f_z the equations

$$\ddot{\mathbf{f}} - A\mathbf{f} = 0, \quad A = \begin{Vmatrix} U_{xx} & U_{xy} & U_{xz} \\ U_{yx} & U_{yy} & U_{yz} \\ U_{zx} & U_{zy} & U_{zz} \end{Vmatrix}. \qquad (2.2)$$

Simultaneous solution of Eqs. (2.1) and (2.2) gives the optimum trajectory $\vec{r}(t)$ and the optimum program $\vec{f}(t)$. In the general case, the solution of System (2.1)-(2.2) will depend on 12 arbitrary constants, with which, when we have them, we can satisfy various initial and final conditions.

Let us note one property of the equations of the variational problem. We introduce the function

$$H = up + vq + wn - U_x f_x - U_y f_y - U_z f_z - \frac{1}{2} f_x^2 - \frac{1}{2} f_y^2 - \frac{1}{2} f_z^2, \qquad (2.3)$$

where

$$p = f_x, \; q = f_y, \; n = f_z.$$

Then Eqs. (2.1)-(2.2) will be written in the following canonical form:

$$\begin{gathered} \dot{x} = H_p, \quad \dot{y} = H_q, \quad \dot{z} = H_n, \quad \dot{f}_x = H_u, \quad \dot{f}_y = H_v, \quad \dot{f}_z = H_w, \\ \dot{p} = -H_x, \quad \dot{q} = -H_y, \quad \dot{n} = -H_z, \quad \dot{u} = -H_{f_x}, \quad \dot{v} = -H_{f_y}, \quad \dot{w} = -H_{f_z}. \end{gathered} \qquad (2.4)$$

where the H with subscripts denote partial derivatives of H with respect to the argument indicated by the subscript. The first integral $H = H_0$ of the variational problem follows at once from this.

Let the potential U possess the properties:

$$\begin{gathered} U_{xz} - xU_{yz} \equiv 0, \quad zU_{xy} - xU_{xy} \equiv 0, \quad yU_{xz} - zU_{xy} \equiv 0, \\ U_x + yU_{xy} - xU_{yy} \equiv 0, \; U_x + zU_{xz} - xU_{zz} \equiv 0, \; U_y + zU_{zy} - yU_{zz} \equiv 0, \\ U_y + xU_{xy} - yU_{xx} \equiv 0, \quad U_z + xU_{xz} - zU_{xx} \equiv 0, \quad U_z + yU_{zy} - zU_{yy} \equiv 0. \end{gathered} \qquad (2.5)$$

These identities prevail, for example, for any central force field, including the Newtonian. Then Eqs. (2.1)-(2.2) or, what is the same thing, Eqs. (2.4) have another integral

$$\mathbf{r} \times \dot{\mathbf{f}} - \dot{\mathbf{r}} \times \mathbf{f} = \mathbf{k}. \qquad (2.6)$$

Thus we conclude that there are four integrals of the equations of

motion in the three-dimensional case and two integrals in the two-dimensional case. These integrals enable us to lower the order of the system: instead of Eqs. (2.2), we obtain, for example, in the two-dimensional case for the components f_x, f_y, the system

$$\begin{aligned}(x\dot{x}+y\dot{y})\,\dot{f}_x-f_x(xU_x+\dot{y}^2)+f_y(\dot{x}\dot{y}-xU_y)-\frac{1}{2}f^2x&=H_0x+k_1\dot{y},\\(x\dot{x}+y\dot{y})\,\dot{f}_y-f_x(\dot{x}\dot{y}-yU_x)-f_y(\dot{x}^2+yU_y)-\frac{1}{2}f^2y&=H_0y-k_1\dot{x}.\end{aligned}\tag{2.7}$$

Here $f^2 = f_x^2 + f_y^2$. Equations similar to (2.7) prevail in the three-dimensional case as well.

3. METHOD OF APPROXIMATE SOLUTION OF OPTIMUM-MOTION EQUATIONS

The Eqs. (2.1)-(2.2) of optimum motion in an arbitrary conservative force field with potential $U = U(x, y, z)$ may be written in the following vectorial form:

$$\ddot{\mathbf{r}}-\operatorname{grad}U=\mathbf{f},\tag{3.1}$$

$$\dot{\mathbf{f}}-A\mathbf{f}=0.\tag{3.2}$$

Here $\vec{r}$ is the radius vector of the trajectory and the matrix A is determined by Formula (2.2).

In the case of a Newtonian force field $U = \mu/r$ and the elements of the matrix in (2.2) take the form indicated in Section 6 (Formulas (6.4), the right members of which need only be multiplied by μ).

The twelve integration constants of System (3.1) should be defined in such a way that the 12 boundary conditions

$$\begin{aligned}\mathbf{r}=\mathbf{r}_0,\ \dot{\mathbf{r}}=\dot{\mathbf{r}}_0 \quad &\text{at} \quad t=t_1,\\ \mathbf{r}=\mathbf{r}_k,\ \dot{\mathbf{r}}=\dot{\mathbf{r}}_k \quad &\text{at} \quad t=t_2.\end{aligned}\tag{3.3}$$

are satisfied.

In the problem of flight between planetary spheres of influence, it is possible, as was shown in Section 1, to disregard the attraction of the planets and to take the coordinates and velocity components of the takeoff planet and the destination planet as the boundary condi-

tions.

Although System (3.1) has the first integrals indicated in Section 2, full integration of System (3.1) evidently cannot be accomplished by analytical methods. Numerical solution of the boundary-value problem (3.1)-(3.3) encounters the usual difficulties: the necessity for a large number of iterations requires a large amount of computer time and makes it hard to obtain series results. For this reason, it appears expedient to use an approximate technique for the calculation, one that possesses adequate accuracy and does not require iterations, namely: the method of linearizing Eqs. (3.1) about a suitably selected transporting trajectory. Let us assume that the trajectory of the motion is

$$r = r_0 + \rho, \tag{3.4}$$

where $\vec{r}_0$ defines a certain trajectory and the quantity $|\vec{\rho}|$ is small as compared with $|\vec{r}_0|$. The transporting trajectory $\vec{r}_0(t)$ satisfies the equation

$$\ddot{r}_0 - \operatorname{grad} U_0 = 0. \tag{3.5}$$

Substituting (3.5) into (3.1) and disregarding second-order infinitesimals (we include terms of the form $\vec{f}\vec{\rho}$ in this designation), we obtain the system of linear equations

$$\ddot{\rho} - A_0\rho = f, \tag{3.6}$$

$$\ddot{f} - A_0 f = 0. \tag{3.7}$$

Here U_0 and A_0 are the values of the function U and the matrix A along the transporting trajectory $\vec{r}_0(t)$. In first approximation, we may set $A_0 = 0$, and then we obtain for $\vec{\rho}$ and $\vec{f}$ formulas by means of which the calculations can be carried out in a particularly simple fashion (see Section 4). For more exact determination of $\vec{\rho}$ and $\vec{f}$, the linear system (3.6)-(3.7) should be integrated. This system contains periodic coefficients, but it must nevertheless be integrated at least in quadratures if Eq. (3.5) of the transporting trajectory is integrated in

quadratures. This will be the case, for example, for the Newtonian central force field $U = \mu/r$.

Henceforth we shall be considering precisely this value of U. The integrability of System (3.6)-(3.7) is evident from the following considerations. Equation (3.7) for the determination of $\vec{f}$ takes the same form as the homogeneous part of Eq. (3.6). But this homogeneous part has as a solution the variation of the Keplerian motion and, consequently, may be reduced to quadratures. Solution of the equation for $\vec{f}$ will be a linear combination of particular solutions of the homogeneous equation for $\vec{\rho}$; knowing $\vec{f}$, we may determine the particular solution of the nonhomogeneous equation (3.6) for $\vec{\rho}$, if only by the method of varying the constants. Thus, solution of the problem reduces to quadratures.

Among other things, it follows from these considerations (and from considerations of dimensionality) that in the approximation under consideration, the optimum control of the reaction-acceleration factor is given by the formula

$$f = \frac{g}{R}(r_* - r_0), \qquad (3.8)$$

where $\vec{r}_0$ is the transporting Keplerian ellipse, $\vec{r}_*$ is the Keplerian ellipse whose parameters are determined by the boundary conditions of the problem and g is the acceleration of Newtonian gravitation at a distance R from the center of attraction.

The integration process that has been described here and the solution of the boundary-value problem may be written in the following form. Let us now denote by $\vec{\rho}$ a six-dimensional vector incorporating both the coordinates and the velocity components. We have

$$\rho = \rho_0 + \rho_{ch}, \qquad (3.9)$$

where $\vec{\rho}_0$ is the solution of the homogeneous system (3.6), and $\vec{\rho}_{ch}$ is a particular solution of the nonhomogeneous system (3.6). We shall have

$$\rho_0 = \sum_{i=1}^{6} c_i \rho_i, \tag{3.10}$$

where $\vec{\rho}_i$ are particular solutions of the homogeneous system (3.6) and c_i are the integration constants. Then, according to what we said above,

$$f = \sum_{i=1}^{6} a_i \rho_i, \tag{3.11}$$

i.e., the six-dimensional vector $\vec{f}$ (which incorporates the components of the acceleration and its derivative) is a linear combination of the same particular solutions $\vec{\rho}_i$ that give the vector $\vec{\rho}_0$ in the other linear combination (3.10). The constants of integration a_i, together with c_i, enable us to satisfy the 12 boundary conditions.

Now, substituting (3.11) into (3.6), we find the particular solution $\vec{\rho}_{ch}$ by varying the constants:

$$\rho_* = \sum_{i=1}^{6} a_i \varphi_i, \tag{3.12}$$

selecting $\vec{\rho}_{ch}$ in such a way that $\vec{\rho}_{ch}(t_0) = 0$, i.e.,

$$\varphi_i(t_0) = 0. \tag{3.13}$$

We obtain

$$\rho = \sum_{i=1}^{6} c_i \rho_i + \sum_{i=1}^{6} a_i \varphi_i. \tag{3.14}$$

The actual integration of the system will be carried out in Section 6. We note at this juncture only that by virtue of (3.13), the constants c_i are defined only by the initial data, with finite formulas given for c_i; all functions $\vec{\rho}_i$ are given in finite form; the [Translator's note: letter symbol missing] $_i$ are determined by quadratures, which may be taken in finite form or obtained numerically. The constants a_i are subject to determination by the final data (at the time $t = t_k$) from the system of algebraic equations

$$\rho_k - \sum_{i=1}^{6} c_i \rho_i^k = \sum_{i=1}^{6} a_i \varphi_i^k. \tag{3.15}$$

Here the index $\underline{k}$ signifies that the quantities are taken for time $t = t_k$.

The algorithm written out above fully solves the boundary-value problem for the system of equations (3.6)-(3.7).

The approximate method proposed makes it possible first to avoid numerical integration in many cases, and, secondly, to solve the boundary-value problem without iterations. All of this significantly simplifies and shortens the calculation. Moreover, the proposed method possesses, as will be shown below, sufficiently high accuracy for a broad class of trajectories.

4. SOLUTION OF THE GENERAL VARIATIONAL PROBLEM WITHOUT TAKING PERTURBATIONS INTO ACCOUNT

For small deviations of the motion from the transporting motion, we may, in approximation, disregard in System (3.6)-(3.7) perturbations due to the basic (with reference to the thrust) force field, the more so because the principal portion of the effect of the basic potential is taken into account by the very introduction of the transporting system of coordinates. Then $A_0 \equiv 0$ and the equations of motion in the $\underline{x}$, $\underline{y}$ coordinate system, which moves translationally according to the laws of undisturbed motion along the transporting trajectory, will be written most simply:

$$\ddot{x} = f_x, \quad \ddot{y} = f_y, \quad \ddot{z} = f_z, \quad \dot{f}_x = 0, \quad \dot{f}_y = 0, \quad \dot{f}_z = 0. \qquad (4.1)$$

This means that in this approximation, the optimum thrust control law is linear in time:

$$\mathbf{f} = \mathbf{A}t + \mathbf{B}, \qquad (4.2)$$

while the trajectory $\vec{r}(t)$ in the coordinate system under consideration will be written in the form

$$\rho(t) = \mathbf{C}_0 + \mathbf{C}_1 t + \mathbf{B}t^2/2 + \mathbf{A}t^3/6. \qquad (4.3)$$

If it is required to provide for escape from the Earth's sphere of influence with zero relative velocity and arrive in the sphere of influence of another planet with zero relative velocity, then the boun-

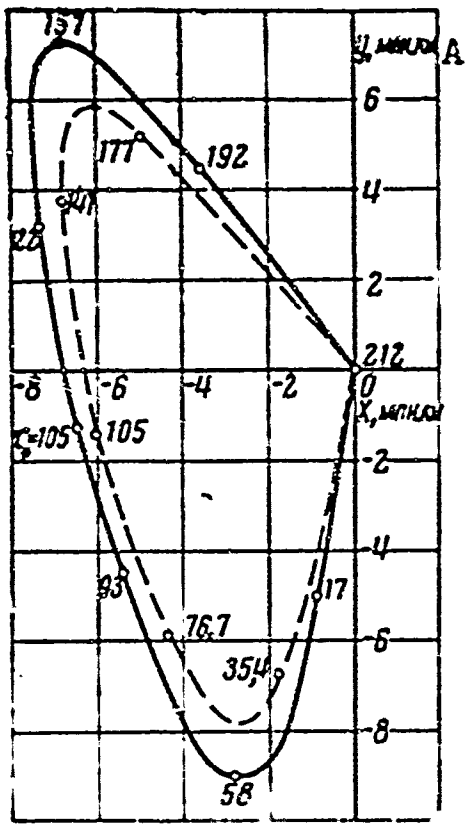

Fig. 1. Example of flight trajectory to Mars in transporting coordinate system with reaction acceleration constant in magnitude and changing direction once. The flight times and thrust-reversal time τ are marked on the trajectories in days. The dashed curve is the trajectory with the same boundary conditions, but with optimum thrust control (all curves without account of perturbations). A) Millions of kilometers.

dary conditions of the problem will be

$$\rho(0)=\rho_0,\quad \dot\rho(0)=-V_0=\dot\rho_0,$$
$$\rho(T)=\rho_k,\quad \dot\rho(T)=-V_k=\dot\rho_k, \qquad (4.4)$$

where T is the assigned flight time and $\vec V_0$ and $\vec V_k$ are the initial and final velocities on the transporting trajectory with respect to the Earth (planet of origin) and the destination planet, respectively. Then the constants of the problem are determined as follows through the boundary conditions:

$$C_0=\rho_0,\quad C_1=\dot\rho_0,$$
$$A=\frac{6}{T^2}(\dot\rho_0+\dot\rho_k)-\frac{12}{T^3}(\rho_k-\rho_0),$$
$$B=-\frac{2}{T}(2\rho_0+\dot\rho_k)+\frac{6}{T^2}(\rho_k-\rho_0). \qquad (4.5)$$

The value of the integral $J=\int f^2\,dt$ is given by the formula $J=|A|^2\frac{T^3}{3}+(A\cdot B)T^2+|B|^2T$.

Let us consider as an example calculation of a flight to Mars. Figures 1-2 show the trajectory $\vec\rho(t)$ and control law $\vec f(t)$ for the case in which Mars is moving in the plane of the ecliptic, departure occurs on 27 September 1960 and the flight time T is 212 days. Written in dimensionless form, the boundary conditions in this case will be

$$\dot x_0=-0{,}0145,\quad \dot y_0=-0{,}12826,$$
$$\dot x_k=-0{,}076884,\quad \dot y_k=-0{,}109856, \qquad (4.6)$$
$$x_0=y_0=x_k=y_k=0.$$

To obtain dimensional velocity values, it is necessary to multiply the values of (4.6) by the velocity of the Earth at the time of launching. The value of Integral (1.4), which determines the mass flow rate, is J = 0.0520 or, in dimensional form, 9.26 m^2/sec^3.

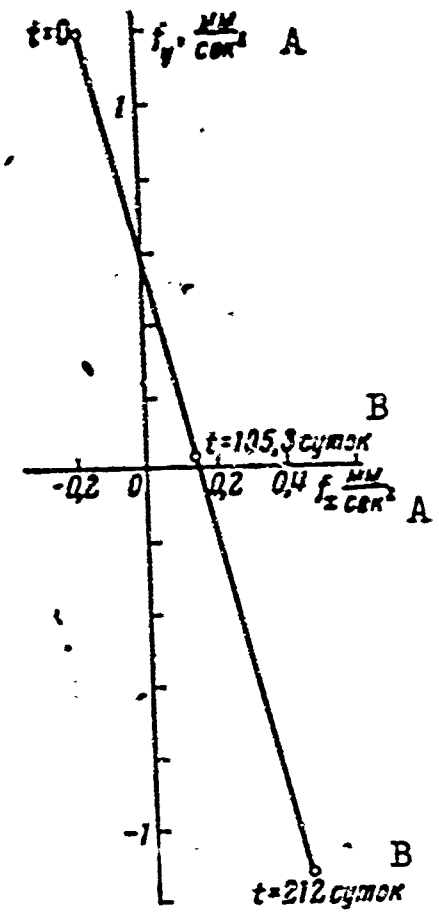

Fig. 2. Example of flight to Mars. Hodograph of small-thrust acceleration vector for optimum control without taking perturbations into account. A) mm/sec^2; B) days.

As will be seen from Fig. 2, the straight-line hodograph of the acceleration under consideration passes close by the coordinate origin. At the middle of the trajectory, therefore, the thrust changes quickly to almost exactly the opposite direction, and the absolute magnitude of the thrust acceleration changes substantially: from $f_0 = 1.20$ mm/sec^2, it diminishes (on the 105th day of flight) to a value near zero ($f_{min} = 0.15$ mm/sec^2) and then rises to $f_k = 1.22$ mm/sec^2.

Remarks.

1. Also of interest is the case in which the optimum (in the absence of perturbations) is flight with a constant acceleration vector. This case obtains, for example, when the coordinates of the end point are not assigned, but must be determined from the condition of minimum functional J(1.4).

With the flight time T, the initial data $\vec{\rho}_0$, $\dot{\vec{\rho}}_0$ and the terminal velocity $\dot{\vec{\rho}}_k$ given, vanishing of the term $\delta_1 J$ in the variation δJ, a term depending on the variation of the end coordinates, results in the condition A = 0, and we obtain

$$f = B = \frac{\dot{\rho}_k - \dot{\rho}_0}{T} = \text{const}, \quad \rho(t) = \rho_0 + \dot{\rho}_0 t + B\frac{t^2}{2},$$

i.e., the coordinates are quadratic and not cubic polynomials in t, as in the general case.

2. We can formulate and solve the problem of optimizing the direction of a reactive acceleration of constant absolute magnitude. If we do not take perturbations into account here, it is found that the ra-

tios of the reaction-acceleration vector components are piecewise-linear functions of time:

$$\frac{f_y}{f_x} = \frac{A_y t + B_y}{A_x t + B_x}, \quad \frac{f_z}{f_x} = \frac{A_z t + B_z}{A_x t + B_x},$$

where the coefficients are constant. Here the absolute magnitude of the reaction acceleration $\underline{f}$ is determined by the quadrature

$$f = \int_0^T \sqrt{a\tau^2 + b\tau + \gamma}\, d\tau, \text{ where } \tau = t/T,$$

$$a = (A_x^2 + A_y^2 + A_z^2) T^2/4, \qquad b = (A_x B_x + A_y B_y + A_z B_z)\, T/2,$$

$$\gamma = 1/4 (B_x^2 + B_y^2 + B_z^2).$$

The quadrature is taken in inverse hyperbolic functions. The constant coefficients are determined by the boundary conditions from a system of transcendental equations whose solution may be found numerically.

5. INTERPLANETARY FLIGHT WITH REACTIVE ACCELERATION CONSTANT IN MAGNITUDE AND CHANGING DIRECTION ONCE

Up to this point, we have been considering the problem of optimum flight between planets. However, the transporting-trajectory method is, of course, applicable to calculation of flights with arbitrary control of the reaction acceleration. The simplest form of control is obviously control in which the reaction acceleration is constant in magnitude and changes direction in space abruptly once. In the present section, we shall be considering flights with such control.

The problem of flight of a reaction-thrust vehicle under the influence of the Newtonian force field and a constant reaction-acceleration vector can be solved rigorously in Jacobian elliptical functions [4]. Due to the complexity of this solution, however, it will be expedient to resort to approximate investigation.

Let us consider motion in the transporting coordinate system. Just as in the case of optimum control (Section 4), we may disregard the so-

lar perturbations in first approximation for this motion. Then the equations of motion will assume the simplest form. Among other things, this will enable us to compute trajectories on a mass scale by varying the transporting-system parameters systematically.

To make it possible to satisfy six initial and six final conditions (the three velocity components and the three point coordinates), the motion must contain, in addition to six integration constants, six more absolute parameters. In the problem under consideration, the six absolute parameters are the following quantities: $\underline{f}$, the magnitude of the thrust acceleration, α_0 and i_0, two angles determining the position of the thrust vector before the change in direction, α_k and i_k, the same angles after the thrust vector has rotated and τ, the time of this rotation.

These six parameters must be selected in such a way as to satisfy the assigned boundary conditions. Here, α is the angle between the x-axis and the projection of the vector $\vec{f}$ onto the ecliptic plane xy, and $\underline{i}$ is the angle between the vector $\vec{f}$ and the z-axis. Without taking perturbations into account, the equations of motion in the transporting system take the form:

$$\ddot{x}_s = f_s^0,\ t<\tau,\ \ddot{x}_s = f_s^k,\ t>\tau;\ s=1,2,3. \qquad (5.1)$$

(Here we have adopted the designation $x = x_1$, $y = x_2$, $z = x_3$). The components f_s^0 and f_s^k are determined by the formulas

$$f_1^0 = f\cos\alpha_0\sin i_0,\ f_2^0 = f\sin\alpha_0\sin i_0,\ f_3^0 = f\cos i_0,$$
$$f_1^k = f\cos\alpha_k\sin i_k,\ f_2^k = f\sin\alpha_k\sin i_k,\ f_3^k = f\cos i_k.$$

Integrating Eqs. (5.1) and requiring that $x_s = x_s^0$ and $\dot{x}_s = \dot{x}_s^0$ at $t = 0$, and $x_s = x_s^k$ and $\dot{x}_s = \dot{x}_s^k$ at $t = T$, we obtain a system of algebraic equations for determining the parameters α_0, i_0, α_k, i_k, $\underline{f}$ and τ.

The solution to this system may be written as follows. Let us de-

note

$$\Delta V_{x_s} = \dot{x}_s^k - \dot{x}_s^0, \quad \Delta x_s = x_s^k - x_s^0 - \dot{x}_s^0 T, \quad v^2 = \sum_{s=1}^{3} (\Delta V_{x_s})^2,$$

$$\rho^2 = \sum_{s=1}^{3} (\Delta x_s)^2, \quad u = \frac{\rho}{T}, \quad \cos\theta = \frac{\sum_{s=1}^{3} (\Delta V_{x_s})(\Delta x_s)}{\rho V}.$$

Then the solution to the above system of algebraic equations will depend on three parameters: v, ρ, and cos θ and will be presented in the form

$$\frac{\tau}{T} = \frac{2(v^2 + 2u^2 - 3uv\cos\theta) \pm \sqrt{2(v^2 + 2u^2 - 3uv\cos\theta)^2 + 2(2u^2 - uv\cos\theta)^2}}{2(v^2 - 2uv\cos\theta)}$$

(the sign before the radical is selected from the condition $0 \leqslant \tau/T \leqslant 1$)

$$f = \frac{1}{T} \frac{\sqrt{v^2\left(1 - \frac{\tau}{T}\right)^2 + 4u^2 - 4uv\cos\theta\left(1 - \frac{\tau}{T}\right)}}{\left(\frac{\tau}{T}\right)}, \qquad (5.2)$$

$$\cos i_0 = \frac{-\Delta V_{x_3}(T-\tau) + 2\Delta x_3}{f\tau T}, \quad 0 \leqslant i_0 \leqslant 180°,$$

$$\sin\alpha_0 = \frac{-\Delta V_{x_3}(T-\tau) + 2\Delta x_2}{f\tau T \sin i_0}, \quad \cos\alpha_0 = \frac{-\Delta V_{x_1}(T-\tau) + 2\Delta x_1}{f\tau T \sin i_0},$$

$$\cos i_k = \frac{\Delta V_{x_3}(2T-\tau) - 2\Delta x_3}{fT(T-\tau)}, \quad 0 \leqslant i_k \leqslant 180°,$$

$$\sin\alpha_k = \frac{\Delta V_{x_3}(2T-\tau) - 2\Delta x_2}{fT(T-\tau)\sin i_k}, \quad \cos\alpha_k = \frac{\Delta V_{x_1}(2T-\tau) - 2\Delta x_1}{fT(T-\tau)\sin i_k}.$$

It is these formulas that determine the magnitude of the reaction acceleration, its direction before and after reversal and the reversal time from given boundary conditions and the total flight time T. These formulas include coordinates x_s and components $\dot{x}_s$ of the velocities in the transporting (moving) coordinate system.

In investigating a flight from the Earth to Mars, the transporting ellipse was selected in such a way as to pass through the Earth at time t = 0 and through the projection of Mars on the plane of the ecliptic at the time t_k. Let $V_x^\gamma, V_y^\gamma, V_z^\gamma = 0$ be the velocity components rela-

tive to the Earth at time t = 0, and let V_x^α, V_y^α, V_z^α be the velocity relative to Mars at $t = t_k$ in the transporting motion. Further, let the distance of Mars from the plane of the ecliptic be z_α at time $t = t_k$. Then $x_1^0 = x_2^0 = x_3^0 = 0$, $x_1^k = x_2^k = 0$, $x_3^k = z_\alpha$, $\dot{x}_1^0 = -V_x^\gamma$, $\dot{x}_2^0 = -V_y^\gamma$, $\dot{x}_3^0 = 0$, $\dot{x}_1^k = -V_x^\alpha$, $\dot{x}_2^k = -V_y^\alpha$, $\dot{x}_3^k = V_z^\alpha$.

This selection of the boundary conditions provides for departure from the Earth at zero velocity relative to the Earth and arrival at Mars with zero velocity with respect to Mars. (The Earth and Mars are regarded as nonattractive points.) For flight from Mars to Earth with the same conditions, the boundary data take the form

$$x_1^0 = x_2^0 = 0, \quad x_3^0 = z_\alpha, \quad x_1^k = x_2^k = x_3^k = 0,$$
$$\dot{x}_1^0 = -V_x^\alpha, \quad \dot{x}_2^0 = -V_y^\alpha, \quad \dot{x}_3^0 = V_z^\alpha, \quad \dot{x}_1^k = -V_x^\gamma, \quad \dot{x}_2^k = -V_y^\gamma,$$
$$\dot{x}_3^k = 0.$$

Let us dwell briefly on the general nature of the parameters f (magnitude of thrust acceleration) and τ (reversal time) as functions of the boundary conditions.

For this purpose, we shall consider the problem with zero initial and final values of the coordinates ($x_s^0 = x_s^k = 0$, $s = 1, 2, 3$). Let V_0 be the initial velocity, V_k the final velocity, and θ_0 the angle between $\vec{V}_0$ and $\vec{V}_k$; we shall denote $k = V_0 / V_к$, $k_0 = V_к / V_0 = 1/k$.

Then

$$\frac{\tau}{T} = \frac{2(1 + k\cos\theta_0) - \sqrt{(1 + k^2 + 2k\cos\theta_0)^2 + (1 - k^2)^2}}{2(1 - k^2)} \quad (5.3)$$

or

$$\frac{\tau}{T} = \frac{2(k_0^2 + k_0\cos\theta_0) - \sqrt{(k_0^2 + 1 + 2k_0\cos\theta_0)^2 + (k_0^2 - 1)^2}}{2(k_0^2 - 1)} . \quad (5.3a)$$

Whether it is more convenient to use the first or second of these formulas depends on the sign of the inequality $V_0 \lessgtr V_k$, namely on which of them has a velocity ratio smaller than unity. The reversal time τ depends on two parameters: k and θ_0. This relationship is represented

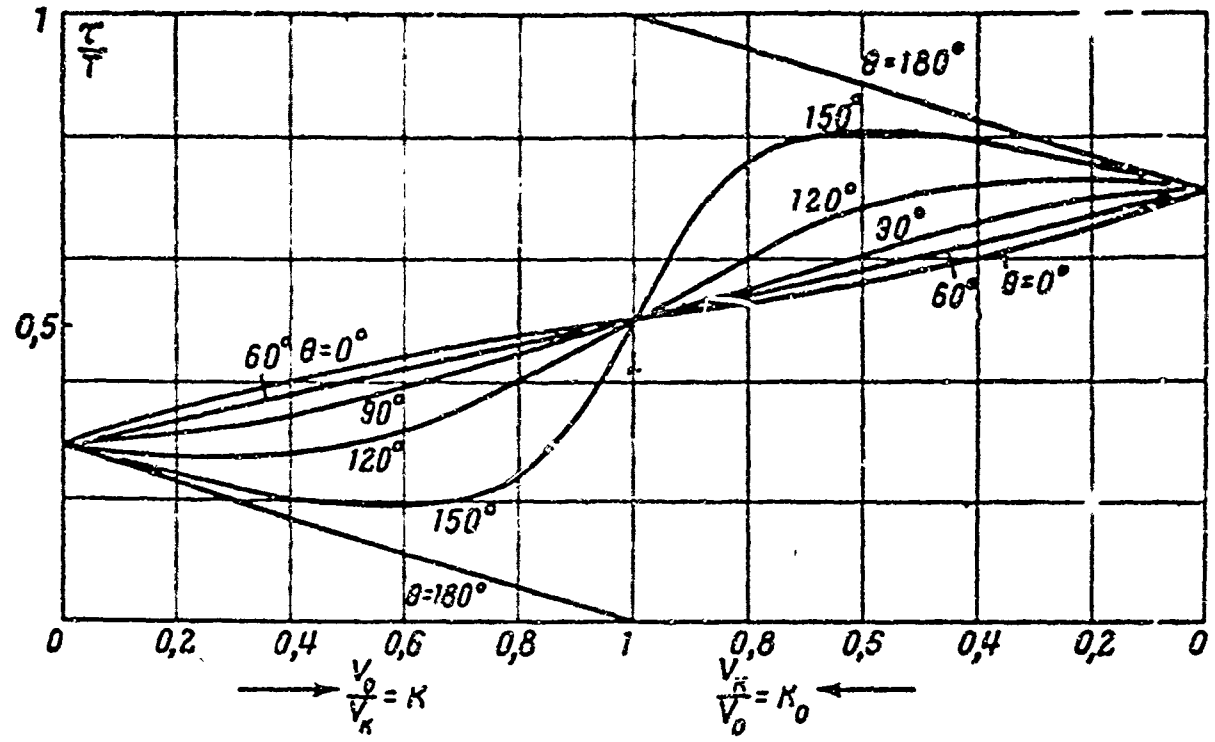

Fig. 3. Thrust vector reversal time T as a function of the ratio of the initial velocity V_0 to the final velocity V_k in the transporting system of coordinates and as a function of the angle θ between the vectors of these velocities.

in Fig. 3. We see that for a given ratio of the initial and final velocities, the reversal time is closer to the origin ($V_0 < V_k$) or to the terminal ($V_0 > V_k$) of the flight the larger the angle θ_0 between $\vec{V}_0$ and $\vec{V}_k$. For a fixed θ_0, the reversal time varies as a function of the ratio V_0/V_k.

Similarly, we have the following formula for the thrust acceleration f:

$$f = \frac{V_к}{T} \frac{\sqrt{\left(1 - \frac{\tau}{T}\right)^2 + k^2\left(1 + \frac{\tau}{T}\right)^2 + 2k\cos\theta_0\left(1 - \frac{\tau^2}{T^2}\right)}}{\left(\frac{\tau}{T}\right)} \quad (5.4)$$

or

$$f = \frac{V_0}{T} \frac{\sqrt{k_0^2\left(1 - \frac{\tau}{T}\right)^2 + \left(1 + \frac{\tau}{T}\right)^2 + 2k_0\cos\theta_0\left(1 - \frac{\tau^2}{T^2}\right)}}{\left(\frac{\tau}{T}\right)_0}. \quad (5.4a)$$

From Fig. 4, which shows a plot of Tf/V_k as a function of k and θ_0 and Tf/V_0 as a function of k_0 and θ_0, we see that

$$f = \alpha \frac{\max(V_0, V_к)}{T}, \quad 2 \leqslant \alpha \leqslant 4, \quad (5.5)$$

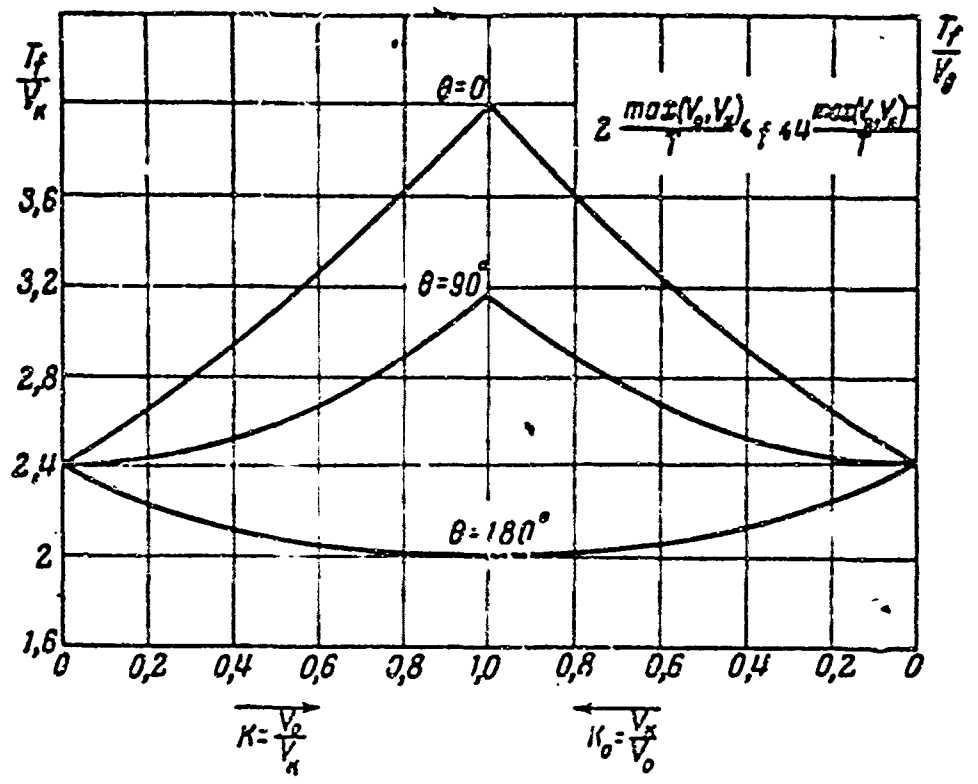

Fig. 4. Magnitude f of reaction acceleration as a function of ratio of initial V_0 and final V_k velocities, the angle θ between the vectors of these velocities, the largest of the velocities and the flight time T.

where α depends on the ratio V_0/V_k and the angle θ_0, but is bounded by the quantity($2 \leq \alpha \leq 4$).

Formula (5.5) permits immediate estimation of the value of f needed for the specified flight (T and V_0, V_k are given).

We note that V_0, V_k, θ_0 and, in the general case, z_a as well, are functions only of the takeoff time t_1 and the arrival time t_2 for specified orbits of the start and finish planets.

In concluding this section, let us consider an example of trajectory computation in the transporting coordinate system. The calculation is made for the same case of flight to Mars (with launching on 27 September 1960) for which we calculated the two-dimensional problem with optimum (perturbations disregarded) control (Section 4). The trajectory in the transporting system is represented in Fig. 1. For comparison, Fig. 1 showed the trajectory of the same flight but calculated for the optimum case, i.e., for linear components of the reactive acceleration. It was found that the necessary constant reactive acceleration f = 0.83 mm/sec^2, that the thrust-vector reversal takes place on the 105th day

of flight (with a total flight time of 212 days); the maximum deviation of the trajectory from the transporting ellipse was ~ 10 million kilometers. The dimensionless quantity $J = f^2T$ (where f and T are dimensionless) is 0.0695; comparing with the figure $J = 0.0520$ calculated (without taking perturbations into account) for the same example with optimum control, we see that optimum control gives an advantage of ~ 25%.

The question as to the accuracy of the approximate optimum-flight characteristics obtained is investigated further on, in Section 7. In the examples being considered, exact dimensionless values of J (obtained for the true gravitational field) are 0.092* and 0.065, respectively. Thus, both of the approximate values obtained above for the integral J differ from the exact ones by 23-24% in the same direction. The accuracy with which the gain due to optimization of control is determined is approximately the same. Such accuracy is obviously adequate for rough calculations. A second approximation (taking the linear part of the solar perturbations into account) gives a much more accurate result, as will be shown in Section 7.

6. INTEGRATION OF LINEARIZED SYSTEM OF EQUATIONS OF OPTIMUM MOTION

Let us now turn to the problem of optimum control of the reactive acceleration and consider its solution in second approximation, i.e., let us solve System (3.6)-(3.7).

We shall consider the dimensionless variables $\underline{r}$, $\underline{v}$, and $\underline{t}$, which are connected to the dimensional variables R, V, and T by the relationships

$$R = \tilde{r} \cdot r, \quad T = \sqrt{\frac{\tilde{r}}{g}}\, t, \quad V = \sqrt{\tilde{r} g}\, v, \quad g = \frac{\mu}{\tilde{r}^2}. \qquad (6.1)$$

Here $\tilde{r}$ is the initial distance from the center of attraction and $\underline{g}$ is the acceleration of gravity at this distance. The linearized equa-

tions (3.6) and (3.7) are written in full as follows:

$$\begin{aligned} \ddot{x} - U^0_{xx}x - U^0_{xy}y - U^0_{xz}z &= f_x, \\ \ddot{y} - U^0_{yx}x - U^0_{yy}y - U^0_{yz}z &= f_y, \\ \ddot{z} - U^0_{zx}x - U^0_{zy}y - U^0_{zz}z &= f_z, \end{aligned} \tag{6.2}$$

$$\begin{aligned} \dot{f}_x - U^0_{xx}f_x - U^0_{xy}f_y - U^0_{xz}f_z &= 0, \\ \dot{f}_y - U^0_{yx}f_x - U^0_{yy}f_y - U^0_{yz}f_z &= 0, \\ \dot{f}_z - U^0_{zx}f_x - U_{zy}f_y - U^0_{zz}f_z &= 0. \end{aligned} \tag{6.3}$$

The xyz coordinate system will move translationally along a Keplerian transporting trajectory. The superior number 0 signifies that the coefficients have been taken along the transporting trajectory.

We note the following. Solution of the homogeneous equations corresponding to System (6.2) yields simply the variation of the Keplerian motion. Knowledge of this variation is helpful in solving many problems of celestial ballistics. Hence the solution to the homogeneous part of Eqs. (6.2) is of independent interest. Solution of the nonhomogeneous equations in (6.2) is possible with any law of variation of f_x, f_y, f_z and, of course, is likewise of independent interest. Among other things, we might consider optimum control of the reaction-acceleration vector $\vec{f}$ (f_x, f_y, f_z) by Formulas (6.3).

The coefficients of Eqs. (6.2) and (6.3) are calculated by the formulas

$$\begin{gathered} U_x = -\frac{x}{r^3}, \quad U_y = \frac{-y}{r^3}, \quad U_z = \frac{z}{r^3}, \\ U_{xx} = -\frac{1}{r^3} + \frac{3x^2}{r^5}, \quad U_{yy} = -\frac{1}{r^3} + \frac{3y^2}{r^5}, \quad U_{zz} = -\frac{1}{r^3} + \frac{3z^2}{r^5}, \\ U_{xy} = \frac{3xy}{r^5}, \quad U_{xz} = \frac{3xz}{r^5}, \quad U_{yz} = \frac{3zy}{r^5}. \end{gathered} \tag{6.4}$$

Let us now select an absolute coordinate system XYZ with origin at the center of attraction such that the plane of the transporting trajectory will coincide with the XY plane, while the X-axis is directed toward the perihelion of the transporting trajectory (Fig. 5).

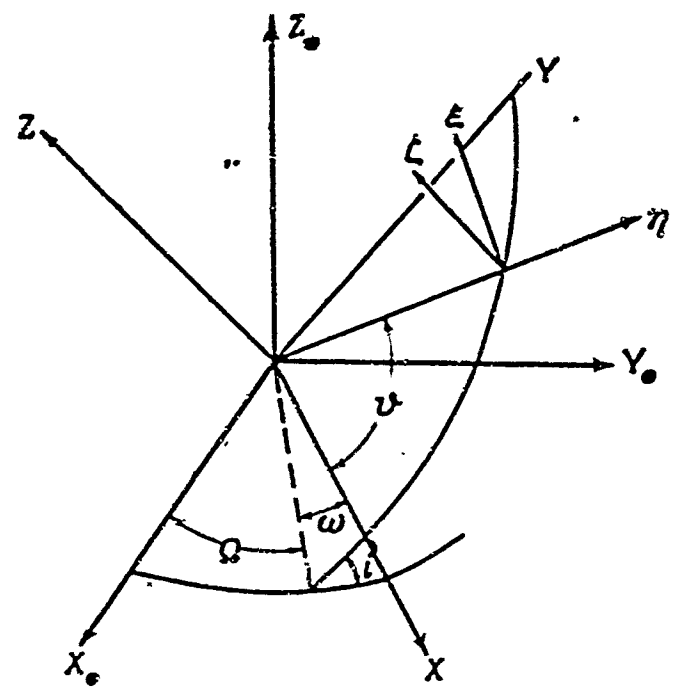

Fig. 5. Coordinate systems.

With a coordinate system selected in this way, we shall have along the transporting trajectory

$$U^0_{xx} = -\frac{1}{r_0^3} + \frac{3x_0^2}{r_0^5}, \quad U^0_{yy} = -\frac{1}{r_0^3} + \frac{3y^2}{r_0^5}, \quad U^0_{zz} = -\frac{1}{r_0^3},$$

$$U^0_{xy} = \frac{3x_0y_0}{r^5_0}, \quad U^0_{xz} = 0, \quad U^0_{yz} = 0,$$

since $z_0 \equiv 0$; remembering that $x_0 = r_0 \cos \vartheta$, $y_0 = r_0 \sin \vartheta$, where ϑ is the true anomaly, we get

$$U^0_{xx} = \frac{1}{r_0^3}(3\cos^2\vartheta - 1), \quad U^0_{yy} = \frac{1}{r_0^3}(3\sin^2\vartheta - 1), \quad U^0_{zz} = -\frac{1}{r_0^3},$$

$$U^0_{xy} = \frac{3\cos\vartheta\sin\vartheta}{r_0^3}, \quad U^0_{xz} = U^0_{yz} = 0. \qquad (6.5)$$

Thus, the coefficients in Eqs. (6.2)-(6.3) have the values (6.5).

To integrate the equation system (6.2), it is convenient to go over to a rotating system of coordinates whose origin coincides with that of the xyz system (i.e., with a point of the transporting trajectory), while its ζ-axis coincides with the z-axis, its η-axis is directed along the radius vector of the transporting trajectory, and its ξ-axis is directed along the transversal of the transporting trajectory in the direction of motion. We have

$$x = \eta\cos\vartheta - \xi\sin\vartheta, \; y = \eta\sin\vartheta + \xi\cos\vartheta, \; z = \zeta. \qquad (6.6)$$

Substituting (6.6) in Eq. (6.2), we obtain the equation of motion in the following form after certain manipulations:

$$\ddot{\eta} - 2\dot{\xi}\omega - \omega^2\eta - \dot{\omega}\xi - \frac{2}{r_0^3}\eta = f_\eta,$$

$$\ddot{\xi} + 2\dot{\eta}\omega - \omega^2\xi + \dot{\omega}\eta + \frac{1}{r_0^3}\xi = f_\xi, \qquad (6.7)$$

$$\ddot{\zeta} + \frac{1}{r_0^3}\zeta = f_\zeta.$$

Here ω is the angular velocity of the motion along the transporting trajectory and f_η, f_ξ and f_ζ are the projections of the reaction-acceleration vector on the η, ξ, and ζ-axes. Equations (6.7) could have been written at once, since the terms written in the left-hand members of the first two equations are the projections of the Coriolis and centrifugal accelerations onto the corresponding axes, the terms governed by the presence of the angular acceleration $\dot{\omega}$ and gravitational terms.

If $\vec{T}$ is determined by Eqs. (6.3), then the fundamental system of solutions to Eqs. (6.7) with zero right-hand members will give the fundamental system of solutions for (6.3) as well; thus, f_η, f_ξ and f_ζ will have been determined; then the motion will be found by integrating the nonhomogeneous linear system (6.7) with known right members.

Let us now concern ourselves with integration of System (6.7). For this purpose, we pass to the variable ϑ (the true anomaly). Let P be the dimensionless focal parameter of the orbit, and

$$\rho = (1 + e\cos\vartheta)^{-1}, \quad r = P\rho. \qquad (6.8)$$

Using the formulas for Keplerian motion $r^2 d\vartheta / dt = \sqrt{P}$, $\omega = d\vartheta / dt$, we reduce System (6.7) to the system

$$\eta'' - 2\frac{\rho'}{\rho}\eta' - 2\xi' - (1 + 2\rho)\eta + \frac{2\rho'}{\rho}\xi = P^3\rho^4 f_\eta,$$

$$\xi'' - 2\frac{\rho'}{\rho}\xi' + 2\eta' - (1 - \rho)\xi - \frac{2\rho'}{\rho}\eta = P^3\rho^4 f_\xi, \qquad (6.9)$$

$$\zeta'' - 2\frac{\rho'}{\rho}\zeta' + \rho\zeta = P^3\rho^4 f_\zeta.$$

Here the primes denote derivatives with respect to ϑ. Let us inte-

grate the third equation of (6.9). The substitution $\xi = \rho\nu$ results in an equation $\nu'' + \nu[\rho - 2(\rho'/\rho)^2 + \rho''/\rho) = P^3\rho^3 f_\zeta$. But it is not difficult to factor out $\rho - 2(\rho'/\rho)^2 + \rho''/\rho = 1$, from (6.8), and the equation assumes the form

$$\nu'' + \nu = P^3\rho^3 f_\zeta. \tag{6.10}$$

Writing the general solution to this equation and remembering that $\zeta = \rho\nu$, we obtain

$$\zeta = c_5\rho\sin\vartheta + c_6\rho\cos\vartheta + P^3\{\rho\sin\vartheta\int f_\zeta\rho^3\cos\vartheta\,d\vartheta - \\ - \rho\cos\vartheta\int f_\zeta\rho^3\sin\vartheta\,d\vartheta\}, \tag{6.11}$$

$$\zeta' = c_5\rho^2(e+\cos\vartheta) - c_6\rho^2\sin\vartheta + P^3\{\rho^2(e+\cos\vartheta)\int f_\zeta\rho^3\cos\vartheta\,d\vartheta + \\ + \rho^2\sin\vartheta\int f_\zeta\rho^3\sin\vartheta\,d\vartheta\}. \tag{6.12}$$

Henceforth we shall also use the notation

$$\zeta_5 = \rho\sin\vartheta,\quad \zeta_6 = \rho\cos\vartheta,\quad z_5 = P^3\int f_\zeta\rho^3\cos\vartheta\,d\vartheta, \\ z_6 = -P^3\int f_\zeta\rho^3\sin\vartheta\,d\vartheta. \tag{6.13}$$

We define the values of the integration constants c_5 and c_6 in terms of the initial data. For $\vartheta = \vartheta_0$ we have $\zeta = \zeta_0$, $\zeta' = \zeta_0'$, and the integrals in the curly brackets in (6.11) and (6.12) are zero. This gives

$$c_5 = \zeta_0\sin\vartheta_0 + \frac{\zeta_0'}{\rho_0}\cos\vartheta_0,\quad c_6 = \zeta_0(e+\cos\vartheta_0) - \frac{\zeta_0'}{\rho_0}\sin\vartheta_0.$$

Let us now turn to the first two equations of (6.9). The substitution

$$\xi = \rho\alpha,\quad \eta = \rho\beta \tag{6.14}$$

reduces these equations to the form

$$\beta'' - 3\rho\beta - 2\alpha' = P^3\rho^3 f_\eta,\quad \alpha'' + 2\beta' = P^3\rho^3 f_\xi \tag{6.15), (6.16}$$

We integrate Eq. (6.16) once. We obtain

$$\alpha' = c_1 - 2\beta + J_\xi. \tag{6.17}$$

which uses the notation

$$J_\xi = P^3\int\rho^3 f_\xi\,d\vartheta,\quad J_\xi(\vartheta_0) = 0. \tag{6.18}$$

Substituting (6.17) in (6.15), we get

$$\beta'' + (4 - 3\rho)\,\beta = 2c_1 + 2J_\xi + P^3\rho^3 f_\eta. \tag{6.19}$$

We make the inverse substitution to (6.14): $\beta = (1 + e\cos\vartheta)\,\eta$. Then (6.19) will be written as follows:

$$\eta'' - 2e\frac{\sin\vartheta}{1 + e\cos\vartheta}\eta' + \frac{1 + 3e\cos\vartheta}{1 + e\cos\vartheta}\eta = \frac{\Phi}{(1 + e\cos\vartheta)}. \tag{6.20}$$

Here

$$\Phi = 2c_1 + 2J_\xi + P^3\rho^3 f_\eta. \tag{6.21}$$

It can be verified easily that without a right member, Eq. (6.20) has the particular solution

$$\eta_2 = \sin\vartheta. \tag{6.22}$$

A second particular solution of Eq. (6.20) with zero right member is found from the familiar formula $\eta_3 = \eta_2\int\frac{e^{-\int P_1 d\vartheta}}{\eta_2^2}d\vartheta$,

$$P_1 = -2e\frac{\sin\vartheta}{(1 + e\cos\vartheta)}.$$

We obtain

$$\eta_3 = \sin\vartheta J^*,\quad J^* = \int\frac{\rho^2}{\sin^2\vartheta}d\vartheta. \tag{6.23}$$

Calculation of the quadratures J* gives:

$$J^* = -\rho^2\operatorname{ctg}\vartheta + \frac{1}{(1 - e^2)^2}\rho^2\sin\vartheta\,[e^3 + 2e + e^2(1 + e^2)\cos\vartheta] - 3\frac{e^2}{(1 - e^2)^2}\tilde{E}, \tag{6.24}$$

where $\tilde{E} = E/\sqrt{1 - e^2}$.

Here E is the eccentric anomaly:

$$\sin E = \sqrt{1 - e^2}\rho\sin\vartheta,\qquad \cos E = \rho(e + \cos\vartheta). \tag{6.25}$$

Now the solution of the nonhomogeneous equation (6.20) can be found by varying the constants.

It is then found that

$$\eta = c_1\eta_1 + c_2\eta_2 + c_3\eta_3 + \eta_2 F_2 + \eta_3 F_3, \tag{6.26}$$

where c_1, c_2, and c_3 are constants of integration, η_2 and η_3 are given by Formulas (6.22) and (6.23), and

$$\eta_1 = 2\left[f\sin\vartheta\int\frac{\sin\vartheta}{\rho}d\vartheta - \sin\vartheta\int\frac{f\sin\vartheta}{\rho}d\vartheta\right] = \frac{1}{e}\left\{f\sin\vartheta + \cos\vartheta\right\}, \quad (6.27)$$

$$F_2 = -p^2\int\frac{\eta_3}{\rho}\left(\frac{2J_\xi}{p^3} + \rho^3 f_n\right)d\vartheta, \quad F_3 = p^3\int\frac{\sin\vartheta}{\rho}\left(\frac{2J_\xi}{p^3} + \rho^3 f_n\right)d\vartheta. \quad (6.28)$$

From this we can also calculate $d\eta/d\vartheta = \eta'$:

$$\eta' = c_1\eta_1' + c_2\eta_2' + c_3\eta_3' + \eta_2' F_2 + \eta_3' F_3, \quad (6.29)$$

where η_1', η_2', and η_3' like η_1, η_2, η_3, will be written out in final form below, in the summary of formulas.

It remains to complete integration of the system of equations and determine $\xi(\vartheta)$. Let us turn to Eq. (6.17). Integrating it, we get $\alpha = c_1\vartheta - 2\int\frac{\eta}{\rho}\,d\vartheta + \int J_\xi d\vartheta + c_4$, $(\alpha = \xi/\rho)$. Substituting η from (6.26), we can then perform simple operations to take quadratures in the homogeneous part of the solution. As a result we obtain

$$\xi = c_1\xi_1 + c_2\xi_2 + c_3\xi_3 + c_4\xi_4 + \rho\Psi, \quad (6.30)$$

where c_1, c_2 and c_3 are the constants of integration and ξ_1, ξ_2, ξ_3, ξ_4, Ψ are calculated in final form below in the formulary.

We note that it follows from $\xi = \alpha\rho$ that $\xi' = \frac{\rho'}{\rho}\xi + \rho\alpha'$. Then by virtue of (6.17)

$$\xi' = \rho\,(e\sin\vartheta\xi + c_1 - 2\eta/\rho + J_\xi). \quad (6.31)$$

Now that we know general expressions for η, η', ξ, ξ', it is easy to determine the constants c_1, c_2, c_3, and c_4 in terms of the initial data η_0, η_0', ξ_0, ξ_0'. The values of these constants will be expanded below in the list of final formulas.

The solution derived in this paragraph describes the relative motion of a point under the action of an arbitrary reaction force. The motion is considered in a system of coordinates whose origin moves along a Keplerian trajectory. The problem was then linearized on the assumption that the deviations of the point from the origin are small (as compared with the distance from the coordinate origin to the center

of gravitational attraction). Since the solution obtained can be applied to a number of different types of problems (some of these will be indicated below), it will be helpful to give a summary of the formulas describing this motion.

Let us consider a motion in the neighborhood of a Keplerian trajectory with a focal parameter P (dimensionless), an eccentricity $\underline{e}$ and a true anomaly ϑ.

We shall consider the motion in the rotating system of coordinates η, ξ, ζ, whose origin moves along the indicated Keplerian trajectory, with the η-axis directed along the radius vector, the ξ-axis along the transversal and the ζ-axis along the normal to the plane of the Keplerian trajectory.

Now suppose that in addition to the gravitational forces, a reactive acceleration with the components f_η, f_ξ and f_ζ acts at a point. Further, let us use the prime to denote derivative with respect to ϑ: for example, $d\eta/d\vartheta = \eta'$. Conversion to the derivative with respect to (dimensionless) time is accomplished with the formulas $d\vartheta/dt = \sqrt{P}/r^2$, $r = P\rho$, $\rho = 1/(1 + e\cos\vartheta)$. As follows from the results of this section, the motion under consideration will be determined by the following summary of formulas:

$$\eta = c_1\eta_1 + c_2\eta_2 + c_3\eta_3 + \eta_2 F_2 + \eta_3 F_3, \quad \eta' = c_1\eta_1' + c_2\eta_2' + c_3\eta_3' + \eta_2' F_2 + \eta_3' F_3,$$

$$\eta_1 = \frac{1}{e}[\eta_3 + \cos\vartheta], \quad \eta_2 = \sin\vartheta,$$

$$\eta_3 = -\rho^2\cos\vartheta + \rho^2\frac{e}{1-e^2}\sin^2\vartheta + \sin\vartheta\frac{e}{(1-e^2)^2}\{(1+2e^2)\rho\sin\vartheta - 3e\tilde{E}\},$$

$$\eta_1' = \frac{1}{e}[\eta_3' - \sin\vartheta], \quad \eta_2' = \cos\vartheta,$$

$$\eta_3' = \rho^2\sin\vartheta\left[1 + \frac{e\cos\vartheta}{1-e^2}\right] + \frac{e\cos\vartheta}{(1-e^2)^2}\{(1+2e^2)\rho\sin\vartheta - 3e\tilde{E}\},$$

$$F_2 = -P^3\int\frac{\eta_3}{\rho}\left(\frac{2J_\xi}{P^3} + \rho^3 f_\eta\right)d\vartheta, \quad J_\xi = P^3\int\rho^3 f_\xi\, d\vartheta,$$

$$F_3 = P^3\int\frac{\sin\vartheta}{\rho}\left(\frac{2J_\xi}{P^3} + \rho^3 f_\eta\right)d\vartheta, \quad J_\xi(\vartheta_0) = 0,$$

$$\xi = c_1\xi_1 + c_2\xi_2 + c_3\xi_3 + c_4\xi_4 + \rho\psi, \quad \xi' = \rho\left(e\sin\vartheta\xi + c_1 - 2\frac{\eta}{\rho} + J_\xi\right), \qquad (6.32)$$

$$\xi_1 = \frac{e}{(1-e^2)^2}\rho \sin\vartheta\,(5 - 2e^2 + (4e - e^2)\cos\vartheta) - \frac{3\widetilde{E}}{(1-e^2)^2\rho},$$

$$\xi_2 = -\frac{\rho}{e}[1 - (1 + e\cos\vartheta)^2],$$

$$\xi_3 = \frac{\rho\sin\vartheta}{(1-e^2)^2}[2 + e^2 + e(1 + 2e^2)\cos\vartheta] - \frac{3e}{(1-e^2)^2}\frac{1}{\rho}\widetilde{E}, \quad \xi_4 = \rho,$$

$$\psi = \int\left\{J_\xi - \frac{2}{\rho}(\eta_2 F_2 + \eta_3 F_3)\right\}d\vartheta, \quad \widetilde{E} = \frac{E}{\sqrt{1-e^2}},$$

$$\cos E = \rho(e + \cos\vartheta), \quad \sin E = \sqrt{1-e^2}\,\rho\sin\vartheta,$$

$$\zeta = c_5\zeta_5 + c_6\zeta_6 + \zeta_5 z_5 + \zeta_6 z_6, \quad \zeta' = c_5\zeta_5' + c_6\zeta_6' + \zeta_5' z_5 + \zeta_6' z_6,$$

$$\zeta_5 = \rho\sin\vartheta, \quad \zeta_5' = \rho^2(e + \cos\vartheta), \quad \zeta_6 = \rho\cos\vartheta, \quad \zeta_6' = -\rho^2\sin\vartheta,$$

$$z_5 = P^3\int f_\zeta\cos\vartheta\rho^3\,d\vartheta, \quad z_6 = -P^3\int f_\zeta\rho^2\sin\vartheta\,d\vartheta,$$

$$c_1 = 2\frac{\eta_0}{\rho_0} + \frac{1}{\rho_0}(\xi_0' - \rho_0 e\sin\vartheta_0\xi_0), \quad c_2 = \frac{1}{\rho_0^2}(k_0\eta_3'^0 - k_0'\eta_3^0),$$

$$c_3 = -\frac{1}{\rho_0^2}(k_0\eta_2'^0 - k_0'\eta_2^0)$$

$$k_0 = \eta_0 - c_1\eta_1^0, \quad k_0' = \eta_0' - c_1\eta_1'^0,$$

$$c_4 = \frac{\xi_0}{\rho_0} - \xi_1^0\frac{c_1}{\rho_0} - \xi_2^0\frac{c_2}{\rho_0} - \xi_3^0\frac{c_3}{\rho_0},$$

$$c_5 = \zeta_0\sin\vartheta_0 + \frac{\zeta_0'}{\rho_0}\cos\vartheta_0,$$

$$c_6 = \zeta_0(e + \cos\vartheta) - \frac{\zeta_0'}{\rho_0}\sin\vartheta_0.$$

In the present paper, these formulas are used to compute cosmic flights with reaction acceleration between planetary spheres of influence. However, it is possible to indicate a number of other problems where the formulas given will be found useful. Some of these follow below:

1. Variation of Keplerian motion and isochrone derivatives. Setting $|\vec{f}| \equiv 0$ in the formulas, we obtain the variation of the Keplerian motion. Collecting terms for the initial coordinates and velocities (η_0, η_0', and so forth), we obtain expressions for the isochrone derivatives.

2. Problem of motion of a body in the vicinity of a satellite. For example, we might consider the motion of an astronaut in the neighborhood of a satellite station, both for the case in which he is provided with a "back-pack" jet-propulsion device ($f \neq 0$) and for the case in

which he does not wear such a device ($f \approx 0$). We can ascertain the "dangerous" regimes (or initial positions relative to the satellite), in which there is a danger of the astronaut's losing the satellite.

3. Problem of approach of two objects in space. Assuming that one cosmic object has already been ejected into the neighborhood of another during a preceding stage, we can consider the concluding stage – control of the reaction acceleration $\underline{f}$ in such a way that the objects will rendezvous with minimum relative velocity (docking of a rocket at a satellite station, assembly of a satellite station, and so forth), or with any other desired velocity. In this last problem, we may leave out the reactive acceleration ($f \equiv 0$) and seek the impulse (i.e., the initial values of the velocity components) that will provide for the rendezvous.

4. Motion of a cloud of particles ejected from a satellite relative to the satellite.

5. Securing a specified orbit by means of a correcting impulse or reactive acceleration, i.e., the problem of introducing a small change into the original orbit of a cosmic body.

6. Short-term effect of perturbing factors on the orbit, etc.

We note that for "satellite" problems, the formulas can be simplified considerably, since in this case the eccentricity $\underline{e}$ is frequently very small and we may set $\underline{e} = 0$ for preliminary investigation; this results in fundamental simplification of the formulas. For small $\underline{e}$, we can take account only of terms of the first order in $\underline{e}$. This simplifies calculation of quadratures significantly in the presence of a reactive acceleration $f \neq 0$.

The summarizing formulas (6.32) were written for arbitrary control of the reactive-acceleration vector $\vec{f}$.

Now let $\vec{f}$ satisfy the equations of optimum control. Then, as fol-

lows from Section 2, the components of the vector $\underline{f}$ along the ξ, η, and ζ-axes will be given by the formulas

$$f_\xi = \sum_{i=1}^{4} a_i \xi_i, \quad f_\eta = \sum_{i=1}^{3} a_i \eta_i, \quad f_\zeta = \sum_{j=5}^{6} a_j \zeta_j. \tag{6.33}$$

Here a_i and a_j are constants subject to determination in terms of the boundary conditions. Substituting (6.33) into Formula (6.32), we obtain, for example,

$$J_\xi = \sum_{i=1}^{4} a_i J_{\xi i}, \quad J_{\xi i} = P^3 \int \rho^3 \xi_i \, d\vartheta,$$

$$F_2 = \sum_{i=1}^{4} a_i F_{2i}, \quad F_{2i} = -P^3 \int \frac{J \sin\vartheta}{\rho} \left(\frac{2 J_{\xi i}}{P^3} + \rho^3 \eta_i \right) d\vartheta, \tag{6.34}$$

$$F_3 = \sum_{i=1}^{4} a_i F_{3i}, \quad F_{3i} = P^3 \int \frac{\sin\vartheta}{\rho} \left(\frac{2 J_{\xi i}}{P^3} + \rho^3 \eta_i \right) d\vartheta,$$

where

$$\eta_4 \equiv 0;$$

$$\psi = \sum_{i=1}^{4} a_i \psi_i, \quad \psi_i = \int \left\{ J_{\xi i} - \frac{2}{\rho} (\eta_2 F_{2i} + \eta_3 F_{3i}) \right\} d\vartheta,$$

$$z_5 = \sum_{j=5}^{6} a_j z_{5j}, \quad z_{5j} = P^3 \int \zeta_j \rho^3 \cos\vartheta \, d\vartheta,$$

$$z_6 = \sum_{j=5}^{6} a_j z_{6j}, \quad z_{6j} = -P^3 \int \zeta_j \rho^3 \sin\vartheta \, d\vartheta. \tag{6.35}$$

Now the a_i and a_j are determined from the system of algebraic equations

$$\eta^k - \sum_{i=1}^{3} c_i \eta_i{}^k = \sum_{i=1}^{4} a_i (\eta_2{}^k F_{2i}{}^k + \eta_3{}^k F_{3i}{}^k),$$

$$\eta'^k - \sum_{i=1}^{3} c_i \eta_i{}'^k = \sum_{i=1}^{4} a_i (\eta_2{}'^k F_{2i}{}^k + \eta_3{}'^k F_{3i}{}^k),$$

$$\xi^k - \sum_{i=1}^{4} c_i \xi_i{}^k = \rho_k \sum_{i=1}^{4} a_i \psi_i{}^k,$$

$$\xi'^k - \rho_k \left(c_1 + e \sin\vartheta_k \xi_k - 2 \frac{\eta_k}{\rho_k} \right) = \rho_k \sum_{i=1}^{4} a_i J_{\xi i}{}^k, \tag{6.36}$$

$$\zeta^k - \sum_{j=5}^{6} c_j \zeta_j{}^k = \sum_{j=5}^{6} a_j (\zeta_5{}^k z_{5j}{}^k + \zeta_6{}^k z_{6j}{}^k),$$

$$\zeta'^k - \sum_{j=5}^{6} c_j \zeta_j{}'^k = \sum_{j=5}^{6} a_j (\zeta_5{}'^k z_{5j}{}^k + \zeta_6{}'^k z_{6j}{}^k).$$

Here the index $\underline{k}$ denotes the final values of the variables.

Formulas (6.32)-(6.36) fully solve the linearized problem of opti-

mum rocket motion. The quadratures appearing in these formulas can be taken at least partially. The expressions for the quadratures in explicit form are extremely cumbersome. In practice, these quadratures have been computed numerically in series calculations for problems.

To the above formulas, we should add a formula for calculating the integral $J_P = \int f_P^2 dt$. Here f_P is the dimensional absolute value of the reactive acceleration, $\underline{t}$ is dimensional time and J_P is expressed in terms of the dimensionless value of J by the formula

$$J_P = \frac{1}{\bar{r}}\left(\frac{\mu}{\bar{r}}\right)^{3/2} J, \quad J = P^{3/2}\int f^2 \rho^2 d\vartheta. \tag{6.37}$$

It is also more convenient to find this quadrature numerically.

Let us write out the actual sequence used in computing trajectories. Let $X_0Y_0Z_0$ be the absolute system of coordinates, with the Z_0-axis perpendicular to the plane of the ecliptic and the X_0-axis directed toward the Vernal Equinox. The position of the η, ξ, ζ system introduced earlier relative to the $X_0Y_0Z_0$ system is given by the angles Ω, ω, $\underline{i}$ and ϑ (Fig. 5), which give, respectively, the position of the orbit's ascending node, the position of the orbit's pericenter, its inclination to the plane of the ecliptic and the true anomaly. Let the system xyz have axes parallel to the axes $X_0Y_0Z_0$, while its coordinate origin coincides with that of the ξ, η, ζ system.

The transition matrix between these systems and its derivatives are

$$A = \begin{pmatrix} a_{11} & a_{12} & a_{13} \\ a_{21} & a_{22} & a_{23} \\ a_{31} & a_{32} & a_{33} \end{pmatrix}, \qquad A' = \begin{pmatrix} -a_{21} & -a_{22} & -a_{23} \\ a_{11} & a_{12} & a_{13} \\ 0 & 0 & 0 \end{pmatrix}.$$

The matrix of the inverse transition and its derivative are

$$A^{-1} = \begin{pmatrix} a_{11} & a_{21} & a_{31} \\ a_{12} & a_{22} & a_{32} \\ a_{13} & a_{23} & a_{33} \end{pmatrix}, \qquad (A^{-1})' = \begin{pmatrix} -a_{21} & a_{11} & 0 \\ -a_{22} & a_{12} & 0 \\ -a_{23} & a_{13} & 0 \end{pmatrix}.$$

where

$$a_{11}=-\sin u\cos\Omega-\cos u\sin\Omega\cos i,\quad a_{12}=-\sin u\sin\Omega+\cos u\cos\Omega\cos i,$$
$$a_{21}=\cos u\cos\Omega-\sin u\sin\Omega\cos i,\quad a_{22}=\cos u\sin\Omega+\sin u\cos\Omega\cos i,$$
$$a_{31}=\sin i\sin\Omega.\qquad a_{32}=-\sin i\cos\Omega.$$
$$a_{13}=\cos u\sin i,\quad a_{23}=\sin u\sin i,\quad a_{33}=\cos i.$$
$$(u=\omega+\vartheta).$$

Thus,

$$\begin{pmatrix}\xi\\ \eta\\ \zeta\end{pmatrix}=(A)\begin{pmatrix}x\\ y\\ z\end{pmatrix},\quad \begin{pmatrix}\xi'\\ \eta'\\ \zeta'\end{pmatrix}=\begin{pmatrix}x'\\ y'\\ z'\end{pmatrix}A+\begin{pmatrix}x\\ y\\ z\end{pmatrix}A' \tag{6.38}$$

and, conversely,

$$\begin{pmatrix}x\\ y\\ z\end{pmatrix}=(A^{-1})\begin{pmatrix}\xi\\ \eta\\ \zeta\end{pmatrix},\quad \begin{pmatrix}x'\\ y'\\ z'\end{pmatrix}=(A^{-1})\begin{pmatrix}\xi'\\ \eta'\\ \zeta'\end{pmatrix}+(A^{-1})'\begin{pmatrix}\xi\\ \eta\\ \zeta\end{pmatrix}. \tag{6.39}$$

Here the prime denotes the derivative with respect to the true anomaly ϑ.

The calculation of the dynamic and energy characteristics of the trajectories takes the following sequence:

1. From the given launching time t_1 and arrival time t_2, we compute the transporting trajectory, which lies in the plane of the ecliptic and has at times t_1 and t_2 coordinates that coincide with those of the projections of the planets onto the plane of the ecliptic. The transporting trajectories are computed by the formulas of Keplerian motion.

2. The boundary conditions (x_0, y_0, z_0; $\dot{x}_0$, $\dot{y}_0$, $\dot{z}_0$; x_k, y_k, z_k; $\dot{x}_k$, $\dot{y}_k$, $\dot{z}_k$) are calculated in the relative system of coordinates and converted to the (ξ, η, ζ) coordinate system by Formulas (6.38).

3. Formulas (6.32)-(6.36) are used to solve the boundary-value problem and the characteristics of the trajectory are calculated in the rotating transporting coordinate system.

4. Formulas (6.39) may be used to convert the trajectory parame-

ters to a translationally moving transporting system.

If desired, the trajectories can also be calculated in the absolute coordinate system.

7. EXAMPLES OF CALCULATION FOR CERTAIN TRAJECTORIES. COMPARISON WITH EXACT SOLUTION

The trajectory characteristics obtained from the foregoing formulas can be used as a first approximation in handling the exact boundary value problem (3.1)-(3.3) by the conventional iteration method. It is interesting to compare the exact and approximate solutions and establish the region of applicability of the approximate solution and its exactness.

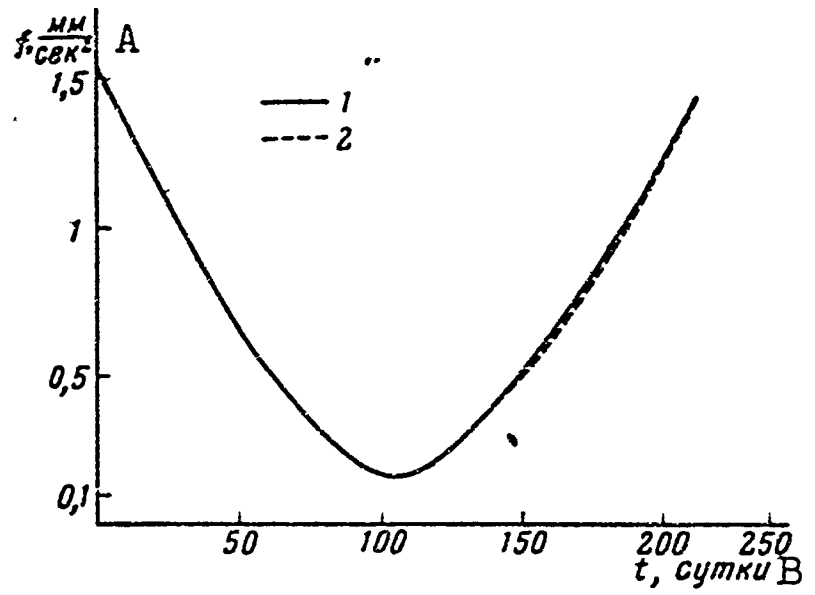

Fig. 6. Variation of magnitude of reactive acceleration over time. 1) Exact calculation; 2) approximate calculation. A) mm/sec^2; B) t, days.

Examples illustrating calculation of certain flight trajectories to Mars, Venus and Jupiter will be given in the present section. The exact and approximate calculations will be compared.

Figures 6-9 present certain characteristics of a flight to Mars. Figures 6-7 show the results of exact and approximate calculations of the reaction-acceleration modulus and its direction for a flight leaving on 28 September 1960 and ending on 28 April 1961. The excellent agreement between the approximate and exact calculations is evident.

(A more detailed analysis of the errors will be given below.) Figure 8 shows the trajectory characteristics of the same flight: the exact trajectory, the transporting ellipse, the trajectory calculated from the linear equations of the preceding section; Figure 9 shows the trajectory calculated from the linear equations and represented in the transporting system of coordinates. We see that the deviations from the coordinate origin, i.e., the deviations of the approximate trajectory from the transporting ellipse, are small (less than 7 million kilometers). Even smaller (by an order) are the deviations of the exact trajectory from the approximate one.

It is interesting to note that, as we pointed out in Section 4, the time dependence of the components f_x, f_y, and f_z is linear if we do not take perturbations into account. As it develops, accounting for the perturbations gives more accurate results the higher the maximum absolute value of the reactive acceleration. And the absolute acceleration figure is large if the flight time is short. For long flight times, the reactive acceleration is small, and, as shown by the exact and approximate calculations taking the perturbations into account, the acceleration hodograph differs greatly from the linear. Certain examples of hodographs f_y/f_x are shown in Figs. 7, 10 and 11. Figure 10 shows an f_y/f_x hodograph (exact calculation) for a flight to Mars lasting 420 days. (Departure 17 August 1964, arrival 11 October 1965.) We see that the hodograph is distinctly nonlinear. Figure 11 presents the relationship f_y/f_x for a flight to Mars lasting 130 days. (Departure 14 January 1965, arrival 24 May 1965.) In this case, the relationship f_y/f_x is close to linear. The importance of the component f_z is always minor. For comparison, Fig. 12 represents exact relationships $f_x(t)$, $f_y(t)$, $f_z(t)$ for a flight departing 15 November 1964 and arriving on 11 October 1965.

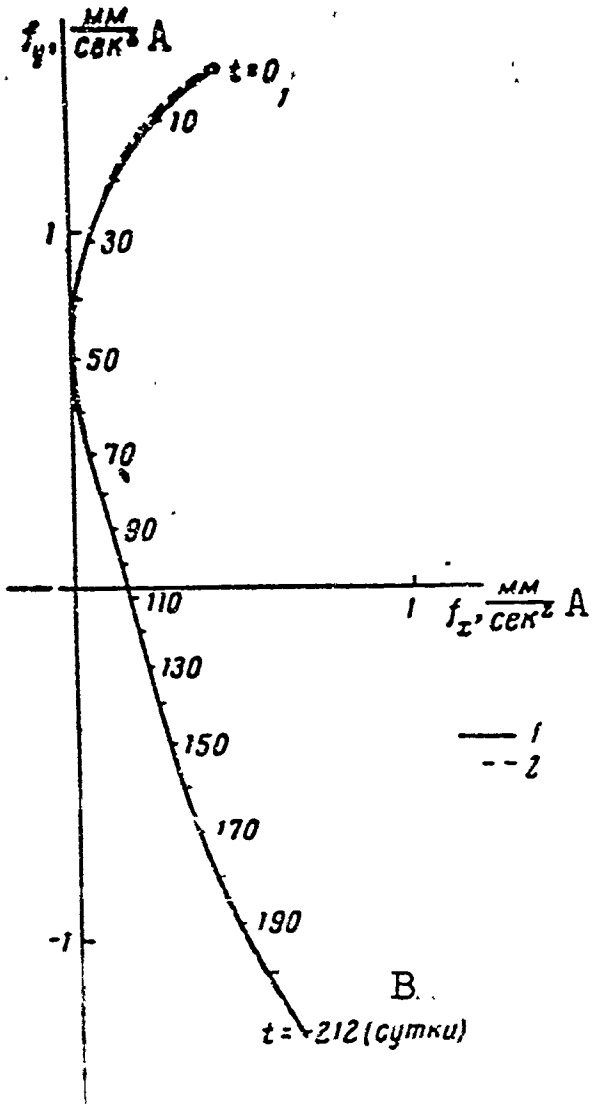

Fig. 7. Variation of magnitude and direction of reactive acceleration. 1) Exact calculation; 2) approximate calculation. A) mm/sec^2; B) days.

We note further that the true optimum trajectories in flights over long angular ranges require smaller fuel consumptions the longer the angular range and the flight time. Analytically, this means that the dependence of the integral (1.4) on the total flight time T is monotonic and that the integral J diminishes with increasing T. The approximate method, whether the perturbations are taken into account (Section 6) or even more so when they are not taken into account (Section 4), cannot yield adequate accuracy for flight over long angular distances. Consequently, the dependence of J on T as obtained by means of the approximate method will be close to the true dependence not everywhere, but only in a region corresponding to not very long flight angular ranges. Figure 13 shows the relationship $J(t_1)$, where t_1 is the departure time (the arrival time t_2 is fixed). This figure presents the results of exact and approximate calculations (with and without account of the solar perturbations in the transporting coordinate system); the flights under consideration go to Venus, with arrival on 18 July 1964. The region in which the approximate calculation gives excellent agreement with the ex one is readily recognized from this diagram.

More detailed information on the accuracy of the approximate calculations can be found in Tables 1 and 2. Table 1 presents the results of characteristic calculations for flights to Mars from the Earth, and (in the last column) from Mars to the Earth. Table 2 contains analogous

characteristics for flights from the Earth to Venus. The first column of the table indicates the departure and arrival dates. The columns that follow contain the following quantities: $J = \int f^2 dt$ in m^2/sec^3; T, the total flight time in days; Φ, the angular range of the flight; f_k, the terminal absolute value of the reaction acceleration in mm/sec^2; f_0, the initial absolute value of the reaction acceleration in mm/sec^2.

The boxes of the tables containing J, f_0 and f_k, show three values each for these quantities. The first figure was obtained by the method described in Section 4, i.e., without taking the solar perturbations into account in the transporting coordinate system. In other words, the first figure is a characteristic of the flight in first approximation. The second figure was derived by the method described in Section 6 and gives the second-approximation characteristic. Finally, the third figure was obtained by the conventional iterative treatment of the boundary-value problem (3.3) for the exact equations (3.1)-(3.2).

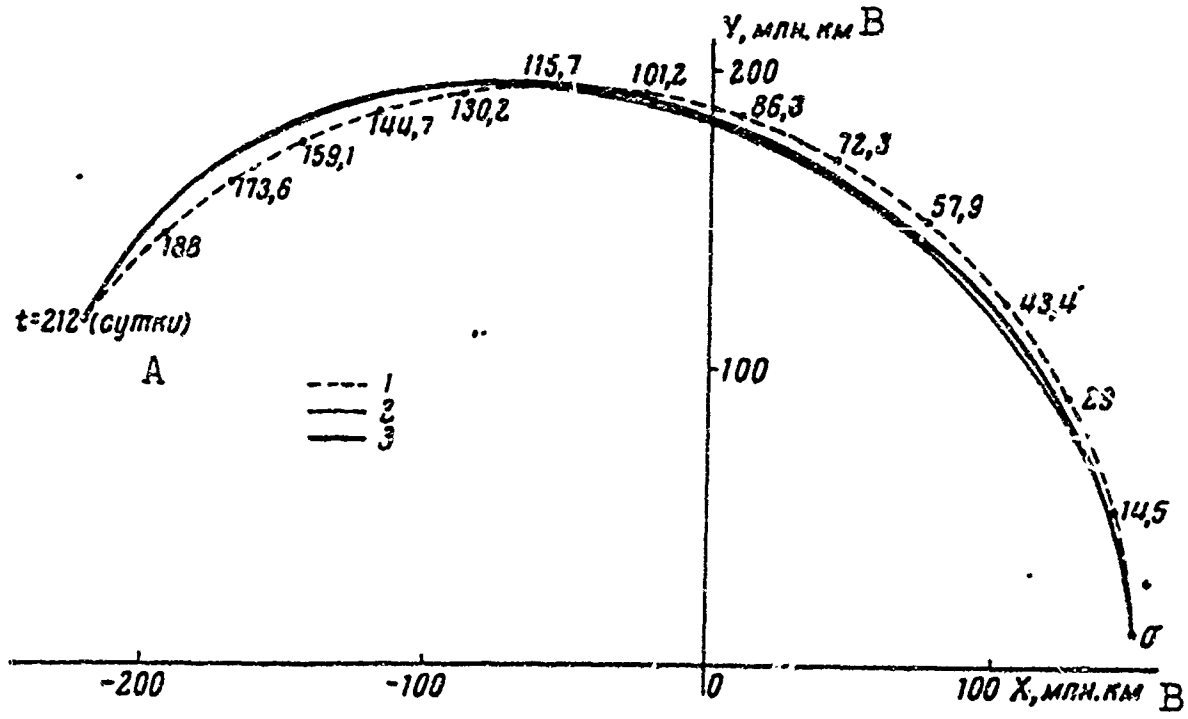

Fig. 8. Trajectory of a flight to Mars. 1) Transporting ellipse; 2) approximate trajectory; 3) exact trajectory. A) Days; B) millions of kilometers.

The seventh column of the table indicates the difference between the value of J in the second approximation (J_1) and the exact value J_t in percent of J_t.

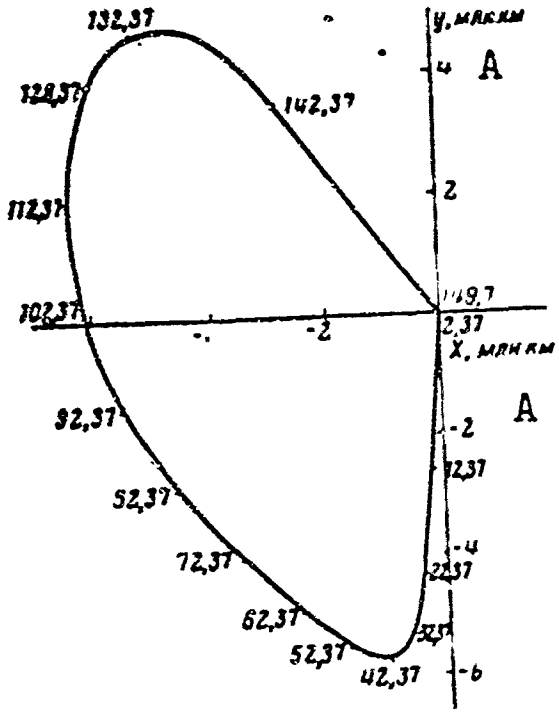

Fig. 9. Trajectory in transporting system of coordinates. Values of the true anomaly on the transporting ellipse are indicated along the trajectory. A) Millions of kilometers.

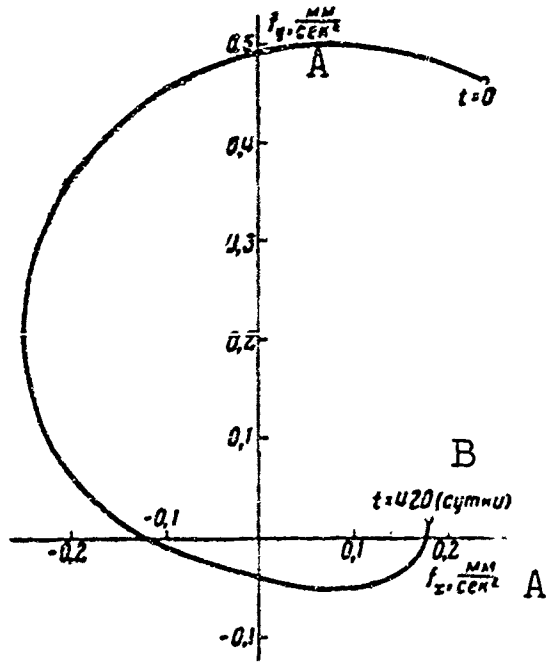

Fig. 10. Variation of magnitude and direction of reaction acceleration. A) mm/sec^2; B) days.

The first table also gives f_s and J_s for comparison; these are first approximations of the characteristics of nonoptimum flights, specifically flights with the reaction acceleration constant in magnitude and changing once. Here we have adopted the notation: f_s is the reaction in mm/sec^2 and J_s is the value of $\int f^2 dt = f_s{}^2 T$ in m^2/sec^3.

These characteristics were calculated without taking solar perturbations into account in the transporting coordinate system, using the method set forth in Section 5, and can be compared only with the first approximation of the optimum characteristics. However, when we remember that the influence of the solar perturbations is apparently almost identical percentagewise for flights made with different control laws (with identical departure and arrival dates), we may use the figures presented in Table 1 to estimate the correction for the influence of solar perturbations even for the present case of nonoptimum flight.

Analysis of Tables 1 and 2 indicates that the proposed calculation method possesses an accuracy adequately high for the cases of greatest interest, in which the total flight time is not very long. We might note a certain relationship between the accuracy of the method and the angular distance of flight. We see that in flights through an angular distance

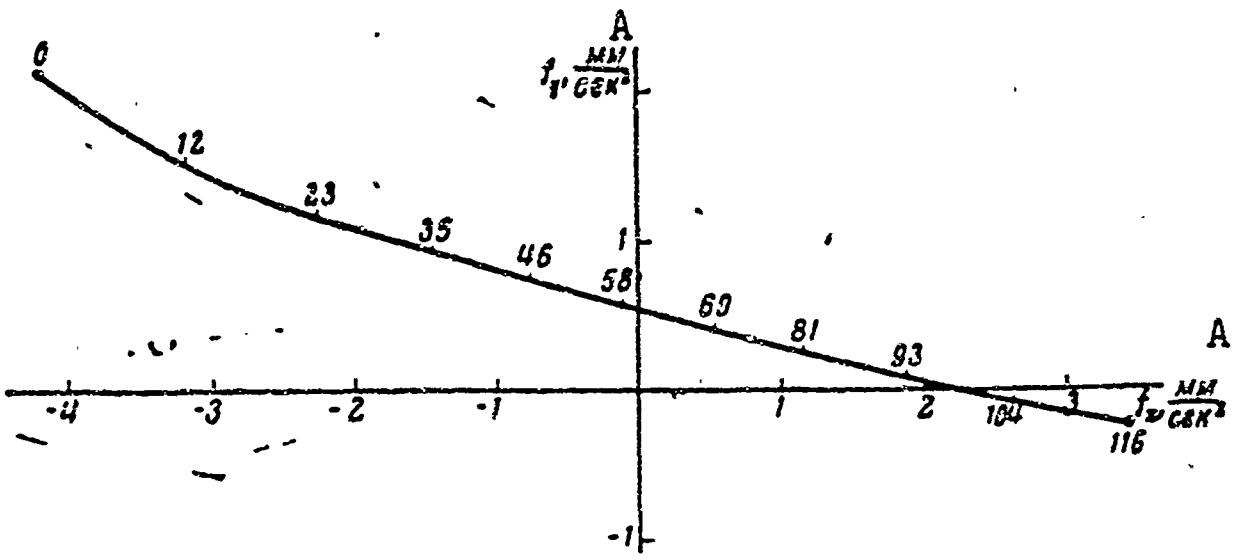

Fig. 11. Variation in magnitude and direction of reactive acceleration. Time of flight is indicated along the hodograph in days. A) mm/sec^2.

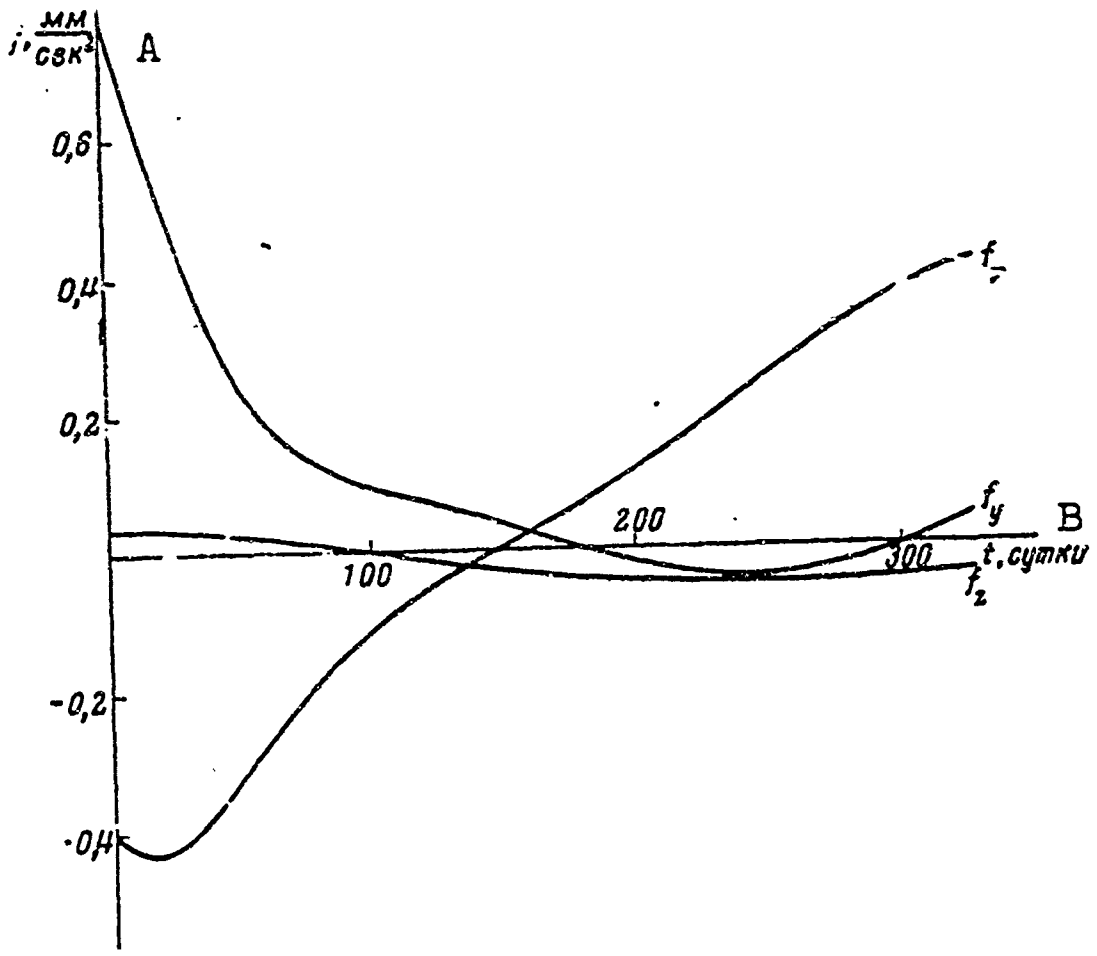

Fig. 12. Components of reactive acceleration. A) mm/sec^2; B) days.

of 225-235°, the calculation delivers an accuracy of 1-5% in the determination of J (and f as well). With increasing angular distance, the error of the calculation rises rapidly and, conversely, for angular distances shorter than 225-235°, the method is highly accurate and in some cases (with $\Phi < 180^\circ$), the calculated characteristics differ from the exact ones by tenths and hundredths of a percent. Figure 14 shows

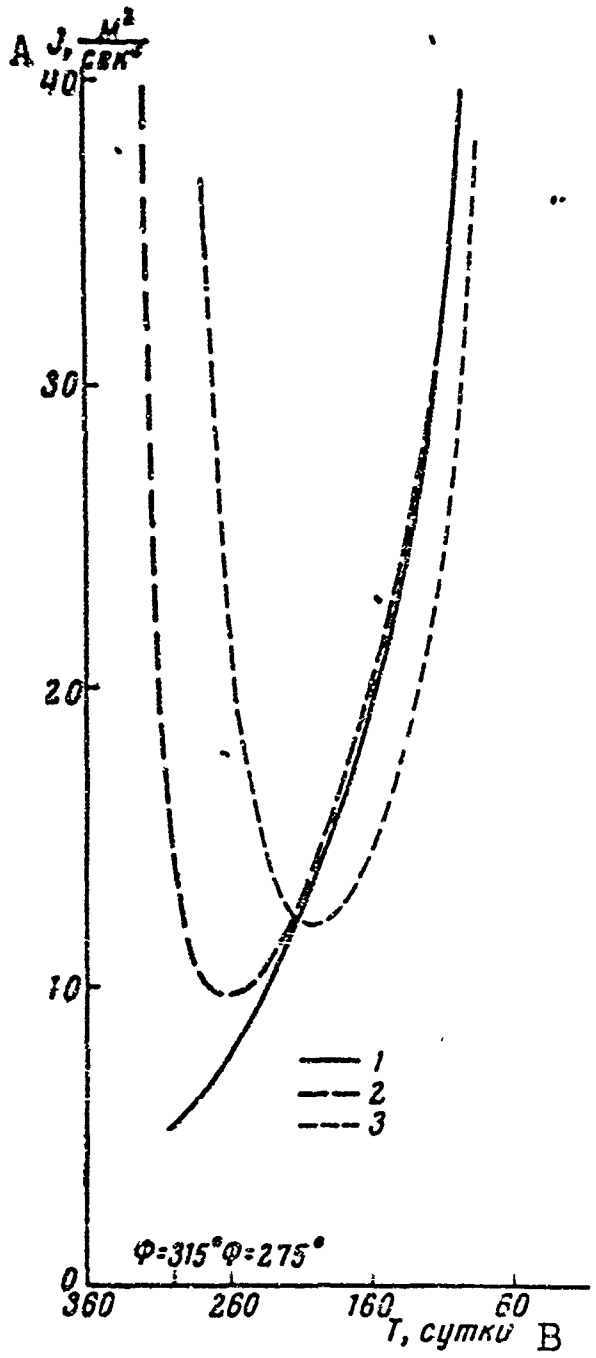

Fig. 13. J as a function of flight time T. The angular ranges Φ of the flight are also marked along the T-axis. 1) Exact calculation; 2) calculation in first approximation; 3) calculation in second approximation. A) J, m^2/sec^3; B) T, days.

the dependence of the quantity $\left|\frac{(J_1 - J_t)}{J_t}\right| \cdot 100\%$ on the angular distance Φ. Tis diagram is characteristic of the accuracy of the method.

We note that calculation by the proposed method requires approximately 1/10 times as much machine time as the conventional iterative calculation of the boundary-value problem for the exact equations.

Calculation of flights to Jupiter by the proposed method produces an error smaller than that of calculation for flights to Mars and Venus (with comparable flight angular distances). With a flight time of 549 days and an angular distance of 200°, the difference between the approximate and exact values of J amounts to about 12% (on the high side), i.e., the accuracy is an order poorer than for calculations of Mars and Venus flights. With shorter angular distances (150-170°), the error will be of the order of 1-5%, i.e., quite acceptable.

For flights to Jupiter, the deviations of the approximate trajectory from the transporting ellipse reach 50-60 million kilometers, which is larger not only absolutely, but also relatively (relative to the distance traversed) larger than for flights to Mars and Venus (by approximately an order). Hence the accuracy of calculation for flights to Jupiter is also found to be lower.

To provide some notion of the characteristics of flight to Jupiter,

TABLE 1

Characteristics of Flights to Mars

Даты старта и финиша 1	J, км²/сек² 2	T, сутки 3	Φ, градусы 4	$f_к$, мм/сек² 5	f_0, мм/сек² 6	$\frac{J_п - J_т}{J_т} \cdot 100\%$ 7	$f_с$, мм/сек² 8	$J_с$, км²/сек² 9
10 14.I 1965	60,88			4,08	3,80		2,67	80,13
	71,29	130	89,06	4,54	4,64	0,13		
11 24.V 1965	71,20			4,485	4,71			
28.IX 1960	9,33			1,22	1,21		0,82	12,30
	11,53	212	147,38	1,44	1,51	0,09		
23.IV 1961	11,54			1,43	1,52			
15.XI 1964	3,60			0,62	0,61		0,41	4,80
	3,23	330	222,65	0,405	0,29	0,94		
11.X 1965	3,20			0,42	0,88			
8.VII 1964*	3,67			0,61	0,58		0,40	4,90
	3,32	360	227,33	0,935	0,31	1,84		
3.VII 1965	3,36			0,925	0,315			

* Flight from Mars to the Earth.

1) Dates of departure and arrival; 2) J, m^2/sec^3; 3) T, days; 4) Φ, degrees; 5) f_k, mm/sec^2; 6) f_0, mm/sec^2; 7) $(J_1 - J_t)/J_t \cdot 100\%$; 8) f_s, mm/sec^2; 9) J_s, m^2/sec^3; 10) 14 January 1965; 11) 24 May 1965.

TABLE 2

Characteristics of flights to Venus

Даты старта и финиша 1	J, км²/сек² 2	T, сутки 3	Φ, градусы 4	$f_к$, мм/сек² 5	f_0, мм/сек² 6	$\frac{J_п - J_т}{J_т} \cdot 100\%$ 7
8 22.III 1964	19,03			2,51	2,09	
	26,44	121	136,35	4,02	1,85	0,04
21.VII 1964	26,43			4,08	1,845	
11.XII 1963	12,65			1,29	1,50	
	11,975	220	234,79	2,25	1,26	5,18
18.VII 1964	11,385			2,24	1,15	
21.XI 1963	15,45			1,37	1,58	
	10,39	240	255,05	2,01	1,19	11,48
18.VII 1964	9,32			1,95	1,04	
1.XI 1963	22,11			1,62	1,77	
	9,65	260	275,16	1,85	1,17	25,81
18.VII 1964	7,67			1,70	0,93	

1) Dates of departure and arrival; 2) J, m^2/sec^3; 3) T, days; 4) Φ, degrees; 5) f_k, mm/sec^2; 6) f_0, mm/sec^2; 7) $(J_1 - J_t)/J_t \cdot 100\%$; 8) 22 March 1964.

we have assembled certain calculated results in Table 3, where the symbols used are the same as those in Tables 1 and 2, except that f_0 and f_k have been replaced by f_{max}, the larger of the two values f_0 and f_k; the only calculated results presented are the second-approximation fig-

TABLE 3

Characteristics of Flights to Jupiter

Даты старта и финиша 1	J, м²/сек³ 2	T, сутки 3	4 Φ, градусы	5 f_{max}, мм/сек²
6 1.VII 1965 1.I 1967	36,71	549	198	1,60
31.VII 1965 1.I 1967	39,80	519	170	1,92
30.VIII 1965 1.I 1967	49,01	489	144	2,60

1) Dates of departure and arrival; 2) J, m^2/sec^3; 3) T, days; 4) Φ, degrees; 5) f_{max}, mm/sec^2; 6) 1 July 1965.

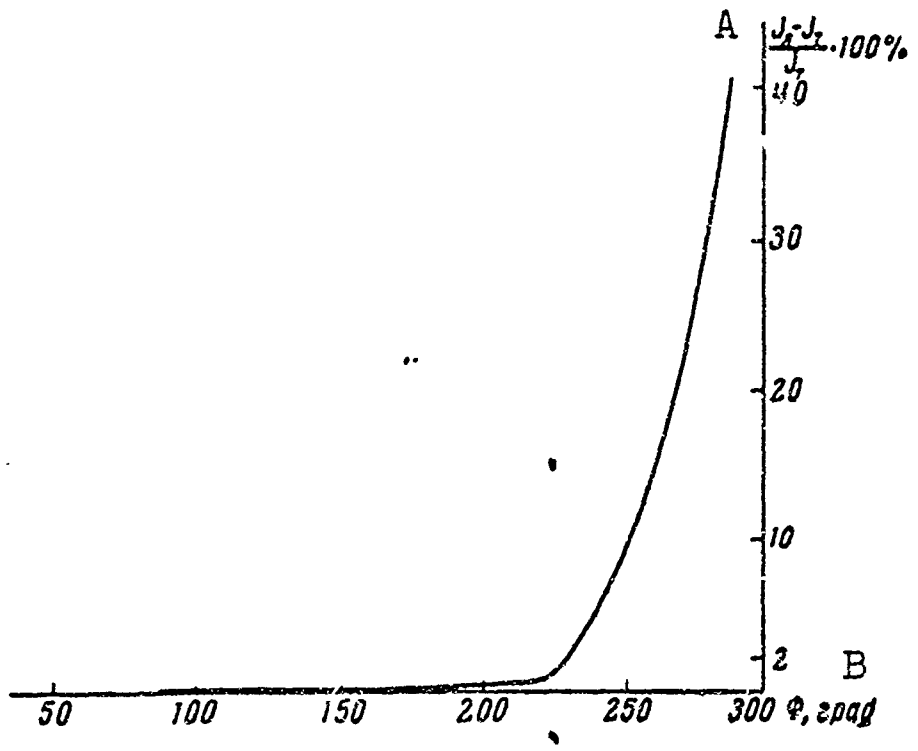

Fig. 14. Error of approximate calculation of the quantity J as a function of the flight angular distance Φ (for flights to Mars and Venus). A) $(J_1 - J_t)/J_t \cdot 100\%$; B) Φ, degrees.

ures obtained by the approximate method (Section 6).

CONCLUSIONS

1. In flights by jet-propelled vehicles with constant power output into jet reaction, the trajectories that are optimal in the sense of minimum fuel consumption are those for which the integral J of the squared reaction acceleration over the time of motion reaches a minimum.

2. Equations of motion that have been linearized with respect to a transporting trajectory can be used to solve a number of problems in the dynamics of cosmic flight (interplanetary flight with reaction acceler-

BLANK PAGE

ation, motion of a body in the neighborhood of a cosmic object, rendezvous of two cosmic objects, calculation of isochrone derivatives, and so forth).

3. The transporting-trajectory method enables us to calculate, quickly and rather accurately, the characteristics of cosmic flights made with a reactive acceleration operating. The error in determining the basic flight characteristics amounts to 1-2% for flights to Mars and Venus with angular distances of the order of 200-220°. When the angular distances are reduced, the accuracy increases, and it drops sharply when they are increased. Accuracy also diminishes with increasing distance to the orbit of the destination planet, and for this reason flights to Jupiter are calculated less accurately than flights to Mars and Venus (for comparable angular distances).

4. Given optimum control of the reactive acceleration, flights with reactive accelerations, fuel reserves, and values of the integral J all as small as we please become possible. However, such a flight would require a very long total flight time, and this would become longer the smaller the value of the integral J.

5. With optimum control of the reactive acceleration for flights to Mars and Venus with return to the Earth within a span of approximately a year and a half, maximum reactive accelerations of 1.5-3 mm/sec^2 and an integral consumption of several tens of m^2/sec^3 are required.

For round-trip flights to Jupiter lasting approximately three years, the value of J required with a maximum reactive acceleration of 2-3 mm/sec^2 is of the order of 100 m^2/sec^3.

6. For flights of the same duration between planetary spheres of influence with a constant reactive-acceleration vector that changes direction once, the energy outlay required is 20-25% larger (according to

the value of the integral J) than for optimum thrust control.

7. The results presented in the last section show, among other things, that optimum control of the reactive acceleration is complex in nature, both as regards the variation of its absolute magnitude and as regards its change in direction. In absolute magnitude, the reactive acceleration changes greatly, for example, from values of 1.5-2 mm/sec^2 at the beginning and end of the flight to a value of 0.1 mm/sec^2 in the middle of the flight. It is possible that difficulties will be encountered in realizing such control. This gives rise to the question of replacing optimum control by a control law that has very similar energetics but is simpler. We might propose the following "stepwise" scheme: on the first segment, the reactive-acceleration vector is constant; on the second segment, there is no reactive acceleration; on the third segment, the reactive-acceleration vector is again constant but, generally speaking, different from the acceleration vector in the first segment. By specifying the acceleration-vector values for the first and third segments, together with the times of stopping and starting the engine on the second segment, we can provide for satisfaction of the boundary conditions and minimize the integral (1.4).

As we see from the results given here, the error of the calculation increases with increasing angular distance. But the transporting-trajectory method can also be extended to the case of flights over long angular distances. For this purpose, we might, for example, employ transporting trajectories consisting of several segments of various elliptical trajectories, segments that do not necessarily have to meet. Two circular trajectories with different radii situated between the orbits of the Earth and Mars might also serve as transporting trajectories for calculating a flight from the Earth to Mars with long angular distance. Investigations in this direction would appear to be appro-

priate.

Received 20 February 1964

REFERENCES

1. V.V. Beletskiy, V.A. Yegorov. Kosmich. issled. [Cosmic Research]. This issue, page 392.

2. I.H. Irving, E.K. Blum. Vistas in Astronautics, II. Second Annual Astronautics Symposium, 1959.

3. G.L. Grozdovskiy, Yu.N. Ivanov, V.V. Tokarev, Dokl. AN SSSR [Proceedings of the Academy of Sciences of the USSR], 137, No. 5, 1082, 1961.

4. V.V. Beletskiy. Kosmich. issled., this issue, page 408.

Manuscript Page No.

[Footnote]

31 This example was calculated by V.V. Golubkov.

Manuscript Page No.

[Transliterated Symbols]

20 ч = ch = chastnyy = particular

28 к = k = konechnyy = final

47 л = l [not identified]

47 т = t = tochnyy = exact

48 с = s [= sravneniya = comparison]

THE ACCELERATION OF A SPACECRAFT WITHIN THE RANGE OF PLANETARY INFLUENCE

V.V. Beletskiy, V.A. Yegorov

An investigation is presented of the space acceleration trajectories within the range of planetary influence in the case of low reaction-thrust acceleration. An approximate solution is presented for the problem pertaining to the optimum control of reaction-thrust acceleration. Formulas are presented for the computation of trajectory parameters at the end of the acceleration phase. Calculation results for a number of trajectories are presented.

* * *

Reference [1] considers the problem of flight between planetary spheres of influence through use of constant-power engines. The present work considers the acceleration trajectories of a spacecraft within such a planetary sphere of influence.

The variation problem of determining the optimum acceleration trajectories prior to the attainment of the parabolic velocity is presented in Section 1; approximate solutions for this problem are also presented. Section 2 presents an analysis of a number of acceleration trajectories, particular attention being devoted to trajectories close to the optimum. Section 3 presents results obtained in calculating the acceleration trajectories prior to attainment of parabolic velocity, with constant tangential reaction-thrust acceleration.

The authors wish to express their gratitude to O.S. Ryzhina for the programming and execution of the numerical computations on the EVM [computer].

1. THE OPTIMUM ACCELERATION PROBLEM

It has been demonstrated [1] that the optimum trajectory $\vec{\rho}$ (in the sense of the minimum of the integral $J = \int_0^\tau f dt)'$ and the optimum control of the reaction-thrust acceleration $\vec{f}$ in an arbitrary force field having the force function $U(\underline{x}, \underline{y}, \underline{z})$ are described by the [following] equations

$$\ddot{\rho} - \operatorname{grad} U = \mathfrak{f};\ \mathfrak{f} - Af = 0,\quad A = \left\| \begin{matrix} U_{xx} U_{xy} U_{xz} \\ U_{yx} U_{yy} U_{yz} \\ U_{zx} U_{zy} U_{zz} \end{matrix} \right\|. \qquad (1.1)$$

We will hold Eqs. (1.1) to have been written for nondimensional quantities. The nondimensional distances ρ, velocity V, time $\underline{t}$, and acceleration $\underline{f}$ are related to the corresponding dimensional quantities r_r, V_r, t_r, and f_r by the following relationships

$$r_p = r_0 \rho,\quad V_p = \sqrt{g r_0}\, V,\quad t_p = \sqrt{\frac{r_0}{g}}\, t,\quad f_p = fg, \qquad (1.2)$$

where $\underline{g}$ is the acceleration of the force of gravity at a distance r_0 from the center of attraction.

If the field of force is Newtonian, $U = 1/r$ and the trajectory of optimum acceleration will thus be flat. In this case eight integration constants for Eqs. (1.1) will be defined by the four initial conditions and the conditions at the instant $t = T$ at which acceleration ceases (T is given):

$$V^2/2 - U = h_k,\ +v_x f_y - v_y f_x = 0,\ -v_x f_z + f_z U_x = 0,$$
$$-v_x f_y + f_z U_y = 0. \qquad (1.3)$$

The first of the conditions in (1.3) is the condition that the given energy h_K be attained (for example, $h_K = 0$), the remaining three conditions being comprised of the conditions of transversality which provide for zero variation of the functional in the case of unattached ends.

The first of the conditions of transversality indicates that at the end of the powered phase of the flight the thrust vector must coin-

cide with the velocity vector in terms of direction: $f = kV|_{t=T}$. As a result, the two remaining transversality conditions lead to the requirement

$$\frac{d}{dt}\left(\frac{v_x}{f_x}\right)\Big|_{t=T} = \frac{d}{dt}\left(\frac{v_y}{f_y}\right)\Big|_{t=T} = \left[\frac{d}{dt}\left(\frac{V}{f}\right)\right]_{t=T} = 1,$$

i.e., the derivative with respect to $\underline{t}$ of the ratio between the modulus of velocity and the modulus of thrust acceleration must be equal to unity. Analogous conditions prevail in the three-dimensional case for an arbitrary U.

Through simple substitution it is possible to prove that Eqs. (1.1) for a three-dimensional trajectory in the arbitrary field U satisfy the following law of change in the vector $\underline{\vec{f}}$ for reaction-thrust acceleration:

$$f = \frac{\beta}{1+\frac{\beta}{2}t}V, \qquad (1.4)$$

where β is an arbitrary constant.

In view of (1.4), the total energy $\underline{h}$ has the derivative

$$\frac{dh}{dt} = \frac{\beta}{1+\frac{\beta}{2}t}V^2.$$

When $\beta > 0$, $dh/dt > 0$ and with Eq. (1.4) it is possible to derive the acceleration. In this case, the initial value of the reaction-thrust acceleration f_0 is governed by the given value of h_k for the final energy, the latter having been determined from the following equation:

$$h_k - h_0 = \beta\int_0^T \frac{V^2(\beta, t)}{1+\frac{\beta}{2}t}dt, \quad \beta = \frac{f_0}{V_0}.$$

However, on the basis of (1.4) we obtain

$$\left[\frac{d}{dt}\left(\frac{V}{f}\right)\right]_{t=T} = \frac{1}{2},$$

i.e., the conditions of tranversality will not be satisfied. This means that Eq. (1.4) yields the best acceleration from the arbitrary point $(\vec{\rho}_0, \vec{V}_0)$ to the point $(\vec{\rho}_k^*, \vec{V}_k^*)$, the latter point having been determined by integration of the first system of equations in (1.1) under the condition given by (1.4); the acceleration is best in comparison with all other accelerations from the point $(\vec{\rho}_0, \vec{V}_0)$ to the same fixed point $(\vec{\rho}_k^*, \vec{V}_k^*)$. However, acceleration based on the control law (1.4) is not the best in comparison with other accelerations from the same point $(\vec{\rho}_0, \vec{V}_0)$ to some other terminal point $(\vec{\rho}_k, \vec{V}_k)$ selected from the condition of the minimum for the functional J. However, it can be demonstrated that in case of low accelerations $\underline{f}$ the control law (1.4) is close to the best even in the indicated sense; it develops that the value of the integral J is close to the minimum with motion according to Law (1.4) at low reaction-thrust accelerations, since the ratio $\Delta J/J \approx f$. Here ΔJ represents the difference between the values of the integral J on attainment of the exact optimum acceleration and the acceleration derived from Law (1.4). Correspondingly, the difference in fuel flow rates, referred to the minimum flow rate, is also a magnitude of the order of $\underline{f}$.

Let us now attempt to derive a more exact solution of the variation problem, presenting a more specific statement of the problem. Let us consider acceleration from a circular orbit in a Newtonian field of forces to energy values of $h|_{t=T} = h_k < 0$, but not too close to zero, in the conventional polar coordinates ρ and φ to which we will convert Eq. (1.1):

$$\ddot{\rho} - f_\rho = \rho\dot{\varphi}^2 - \frac{1}{\rho^2}, \quad \frac{1}{\rho}\frac{d}{dt}(\rho^2\dot{\varphi}) = f_\tau. \qquad (1.5)$$

The radius of the initial circular orbit is here taken as the unit of length. The last term in the first equation represents the Newtonian, f_ρ and f_τ representing the radial and transversal components of reac-

tion-thrust acceleration.

Assuming ρ and f_ρ to be free functions, the functional of the problem can be presented in the following form:

$$J = \int_0^T F(\rho, \dot\rho, \ddot\rho, \dddot\rho, f_\rho, \dot f_\rho)\, dt, \quad F = f_\rho^2 + \frac{1}{\rho^3}\left[\frac{d}{dt}\sqrt{\rho^3(\ddot\rho - f_\rho) + \rho}\right]^2. \quad (1.6)$$

If the variation of the functional were to be written out and equated to zero, holding the ends for f_{ρ_0}, ρ_k, $\dot\rho_k$ and $\ddot\rho_k$ to be moveable, the flight time T being given, we would obtain two Euler equations (of second and sixth orders) and four transversality conditions at the ends. The transversality conditions together with the condition $h(T) = h_k$ and the three initial conditions define eight integration constants for the Euler equations. The indicated initial conditions are:

$$\rho_0 = 1, \quad \dot\rho_0 = 0, \quad \ddot\rho_0 = f_{\rho 0}.$$

Let us now take note of the fact that in the case of low maximum reaction-thrust accelerations f_m the given times T of acceleration from the initial energy $h = -1/2$ to the given h_k must be large, i.e., of the order of $1/f_m$, since it follows from the equation $dh/dt = fV\cos(f, V)$ that $\int_0^t fV dt$ is of the order of unity and with the mean-value theorem we obtain $T \geqslant \frac{1}{f_m}\frac{h_k - h_0}{V_{cp}}$, where the velocity V_{sr} is a magnitude of the order of unity. It is therefore natural to assume that with low thrust the quantities $\dot\rho$ and f_ρ are small in comparison with ρ, that they change slowly with time, i.e., that $\ddot\rho$ and $\dot f_\rho$ are second-order infinitesimals, and that each differentiation raises the order of smallness by unity. This hypothesis indicates that acceleration is accomplished along a spiral whose turns are nearly circular.

Neglecting the third-order infinitesimals, we bring the second of the Euler equations to the following form:

$$f_\rho = \frac{5\dot\rho^2 - 2\rho\ddot\rho}{8\rho}. \quad (1.7)$$

Thus we see that f_ρ should not be regarded as a first-order infin-

itesimal, but rather as one of the second order.

Further, holding $f_\rho \approx \dot{\rho}^2$, we can use the Euler equations to verify the fact that (1.7) is valid with consideration of the third-order infinitesimals which we earlier neglected. Consequently, (1.7) is accurate to infinitesimals of the fourth order.

The second Euler equation, the fourth-order infinitesimals being neglected, is brought to the form $\ddot{\rho}/\dot{\rho} = 3\dot{\rho}/2\rho$, from which, considering that $\rho(0) = 1$, we obtain

$$\rho = 1/(1-ct)^2. \qquad (1.8)$$

Then from (1.7) for the radial component f_ρ of reactive acceleration we obtain the expression:

$$f_\rho = c^2/(1-ct)^4. \qquad (1.9)$$

To determine the constant $\underline{c}$, using the condition $h|_{t=T} = h_к$, we obtain the equation

$$-x^2 + (3c/x^3)^2 = 2h_к,$$

where $x = 1 - cT$.

Because T is of the order of $1/f_m$ this equation has a small root $\underline{c}$ defined by the formula $c = (1-x)/T$ where at values of h_k not close to zero in first approximation $x = (-2h_k)^{1/2}$, and in second approximation

$$x = \sqrt{-2h_к}\left[1 + \frac{1}{2}\left(\frac{3c_0}{4h_к^2}\right)^2\right],$$

$$c_0 = \frac{1-\sqrt{-2h_к}}{T} \text{ etc.}$$

Now let us find the quantity f_τ from the equations of motion. With an accuracy to c^5

$$f_\tau = c\left[1 + \frac{45}{2}\frac{c^2}{(1-ct)^8}\right].$$

Moreover, we have $f = f_\tau$ accurate to c^3. Accurate to c^2

$$f(t) = f_\tau(t) = \text{const}, \quad f_\rho(t) = 0.$$

Having compared the ratios of angular coefficients $k_f = f_\rho/f_\tau$ and $k_v = \dot{\rho}/\rho\dot{\Phi}$, we see that $k_v = 2k_f$ is accurate to c^3. Hence it follows that the direction of thrust bisects the angle formed by the tangent and the transversal.

Let us now take note of the fact that the derived approximate solution to the Euler equations also only satisfies the conditions at the ends in approximate terms. We have reference here to the fact that instead of $\dot{\rho}_0 = 0$ and $\ddot{\rho}_0 = f_{\rho 0}$ in (1.6), according to (1.8) and (1.9) we have

$$\dot{\rho}_0 = 2c \neq 0, \quad \ddot{\rho}_0 - f_{\rho 0} = 5c^2 \neq 0.$$

Having compared the derived approximate solution with the true solution of the variation problem, we can maintain that

$$\Delta\dot{\rho}_0 = 2c, \quad \Delta(\ddot{\rho}_0 - f_{\rho 0}) = 5c^2. \tag{1.10}$$

The approximate solution (1.8)-(1.9) and the incremental values (1.10) make it possible to evaluate the increment ΔJ of the functional J with transition from the true solution to the derived solution. It turns out that $\Delta J \approx c^3$.

Since the quantity $J \approx c^2 T \approx c$, $\Delta J/J \approx c^2$, i.e., we have a higher order of smallness than for the particular solution (1.4).

Let us note that the derived result cannot simply be extended to the value of $h_k = 0$. Actually, in this case the quantity $1 - cT$ is of order 1/4 with respect to $\underline{c}$ rather than of zeroth order, and the evaluations carried out in the equations and the boundary conditions are no longer valid.

Thus the investigation shows that in the problem pertaining to the accumulation of the given energy $h_k < 0$ the optimum control of the magnitude and direction of thrust is very close to the control in which the acceleration of the force of thrust is constant along the modulus and bisects the angle between the tangent and the transversal. This re-

sult was obtained only for energy values that were not close to zero; this result is valid so long as the spiral along which the acceleration is proceeding is close to being circular; the direction of thrust is close to the tangent along such a spiral. On the other hand, as follows from the exact consideration of the boundary conditions in the acceleration problems considered above, with optimum control the thrust acceleration at the end of the acceleration phase must be directed exactly along the tangent to the trajectory. Because of continuity the direction of acceleration must be close to the tangent even in the vicinity of the end of the acceleration pnase. Having compared this fact with the result of the approximate solution, we can draw the conclusion that the optimum direction of thrust acceleration over virtually the entire acceleration phase is close to the tangent, and the magnitude of acceleration is close to constant.

In conclusion let us note that the basic results of this section are applicable to the problem of probing the space around the sun. Indeed, with such probing it would be expedient, from the standpoint of deriving information, to direct the rocket toward the sun along a trajectory between, let us say, the orbits of the earth and Mercury. Since in this case only a certain finite nonzero value of h_k is obtained, the assumptions made at this point prove justified and the derived approximate solution of the variation problem will be close to the exact solution over the entire probe trajectory.

When probing the space within the earth's orbit, it should be assumed in Formulas (1.8) and in the following that $c < 0$; the motion follows a spiral tightening toward the sun; the direction of thrust bisects the angle between the directional lines opposite to those of the direction of velocity and the transversal.

2. ANALYSIS OF CERTAIN ACCELERATION TRAJECTORIES

It is interesting to examine other acceleration trajectories prior to the attainment of parabolic velocity and to compare these with the optimum. Let us undertake an analysis of these trajectories, devoting particular attention to trajectories with constant tangential acceleration, since these trajectories, as demonstrated in the previous section, are close to the optimum.

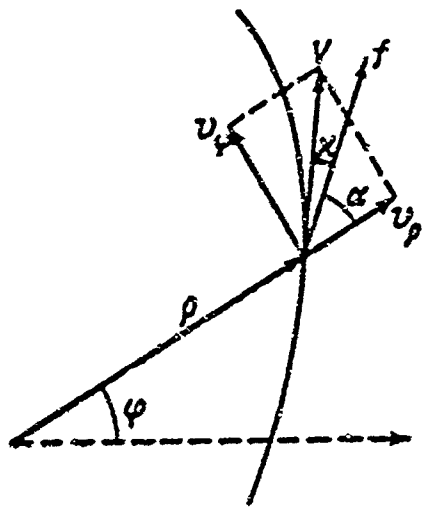

Fig. 1. Coordinate system and mutual position of velocity and thrust-acceleration vectors.

Let α and $\varkappa$ be the angles between the direction of the reactive acceleration and, respectively, the radius vector and the velocity vector (Fig. 1). Let $\sigma = \rho^2\dot{\varphi}$ be the sectorial velocity.

We have

$$\frac{dh}{dt} = fV\cos\varkappa, \quad \frac{d\sigma}{dt} = f\rho\sin\alpha. \quad (2.1)$$

If the thrust is directed along the normal to the trajectory ($\varkappa = 90^\circ$), it [the thrust] will perform no work; in this case h = const; regardless of the magnitude of the thrust, it is impossible to develop any acceleration. If the thrust is directed along the radius vector of the orbit we have $\alpha = 0$ and σ = const, and with f = const the equations of motion, as first demonstrated by Tsien [2], are integrated in quadratures. It turns out that with $f < 1/8$ it is impossible to achieve acceleration, i.e., the orbit remains limited and the work of thrust is used exclusively for the rotation of the line of apsides of an osculating orbit about the center of attraction. Acceleration achieved with the aid of the constant radial acceleration f is possible only if the values of f are sufficiently high, i.e., $f \geq 1/8$.

Given thrust tangential to the trajectory we have $\varkappa = 0$ and $dh/dt = fV > 0$, i.e., h increases monotonically, and it can be demonstra-

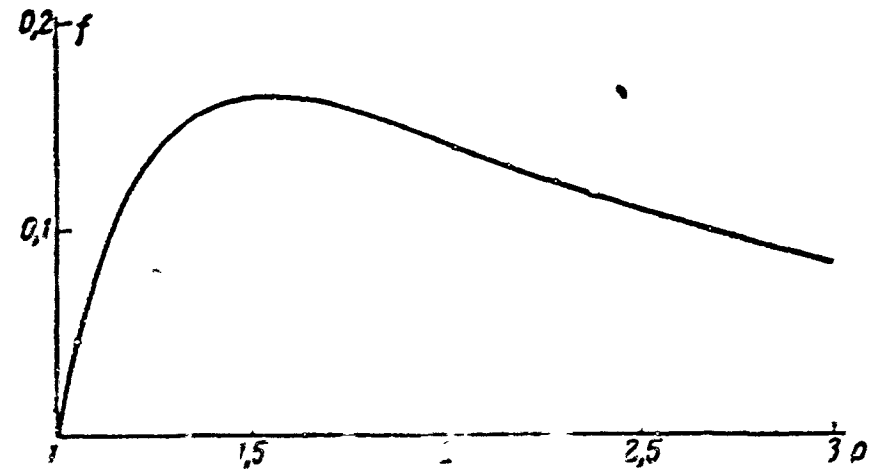

Fig. 2. Change in reactive acceleration for acceleration with constant velocity.

ted that $h \to \infty$ when $t \to \infty$.

In this case it is convenient to use the following closed system of equations for purposes of the analysis:

$$\frac{dV}{dt} = f - \frac{1}{\rho^2}\cos\alpha, \quad \frac{d\rho}{dt} = V\cos\alpha,$$
$$\frac{d}{dt}\cos\alpha = \frac{\sin^2\alpha}{V}\frac{1}{\rho}\left(\frac{V^2}{2} + h\right), \qquad (2.2)$$
$$h = \frac{V^2}{2} - \frac{1}{\rho}.$$

This system in particular makes it possible easily to construct examples of certain simple trajectories (given appropriate selection of control laws for tangential acceleration).

Example 1. Logarithmic spiral [3]. Here $\alpha = \text{const}$, $f = f_0/\rho^2$, $f_0 = \cos\alpha/2$, and $V^2 = 1/\rho$. Parabolic velocity at a finite distance is not attained.

Example 2. Acceleration with constant velocity. Here $V = V_0$

$$f = \frac{1}{\rho^2}\sqrt{1 - \frac{\rho_0^2\sin^2\alpha_0}{\rho^2}\exp\frac{2}{V_0^2}\left(\frac{1}{\rho_0} - \frac{1}{\rho}\right)} \equiv \frac{1}{\rho^2}\cos\alpha.$$

With a start from a nearly circular orbit $\alpha_0 \approx \pi/2$, $V_0 \approx 1$, and $\rho_0 \approx 1$ (Fig. 2). Parabolic velocity is attained at $\rho = 2/V_0^2$.

Let us now consider the basic properties of acceleration from a circular orbit to parabolic velocity with constant tangential reactive

acceleration.

Because of the monotonic increase in h (and consequently, in the orbit's semimajor axis a) and the focal parameter p (satisfying the equation $dp/dt = 2fp/V > 0$), an osculating orbit continually enlarges its linear dimensions, the motion proceeding along an expanding spiral. Because of the increasing orbital dimensions the osculating period of revolution will increase, the mean velocity of motion diminishing with each revolution.

As demonstrated by an analysis of Formulas (2.2) and calculations, eccentricities of the order of f and deviations in velocity B from the mean value of V_{sr} of the same order result because of the effect of low accelerations, i.e., $f \approx 0.001\text{-}0.0001$; $\Delta V/V_{sr} \approx f$. In the case of acceleration from a circular orbit it may be maintained that the average velocity of motion diminishes monotonically so long as $h < 0$. When $h > 0$, as can be shown with Eqs. (2.2), $\cos\alpha$ and ρ will increase monotonically, with $\cos\alpha \to 1$, and $\rho \to \infty$ for $t \to \infty$. Consequently, the term $\cos\alpha/\rho^2$ in the first of the equations (2.2) will become as small as desired and with $t \to \infty$ we will have $dV/dt \approx f > 0$.

Thus the mean velocity V_{sr} diminishes monotonically when $h < 0$ and increases monotonically with $h > 0$. This means that in the vicinity of $h \approx 0$, the velocity V exhibits an absolute minimum and $dV/dt = 0$. Let us assume that this occurs exactly when $h = 0$. In this case it is not difficult to determine the parameters of the trajectory at the end of the acceleration phase (i.e., when $h = 0$). These values of the parameters will be marked with an asterisk. The first of the equations (2.2) and the condition $h = 0$ itself yield

$$\rho^* = \sqrt{\frac{\cos\alpha^*}{f}}, \qquad V^* = \sqrt[3]{\frac{4f}{\cos\alpha^*}}. \tag{2.3}$$

Further, we have

$$h^* = h_0 - f\int_0^{t^*} V\,dt = h_0 + f\bar{V}T, \quad T = t^*,$$

where $\bar{V}$ is the mean value of V over the interval (0, T), with T the time of acceleration. For the case of a circular initial orbit we can assume

$$\bar{V} = \frac{V_0 + V^*}{2} = \frac{1 + \sqrt[4]{4\frac{f}{\cos\alpha^*}}}{2}.$$

Also bearing in mind that $h^* = 0$, and that for a circular initial orbit $h_0 = -1/2$, we finally obtain

$$T = \frac{1}{f\left(1 + \sqrt[4]{\frac{4f}{\cos\alpha^*}}\right)}. \qquad (2.4)$$

Since as $t \to \infty$ we have asymptotically $\cos\alpha = 1$, in first approximation Formulas (2.3)-(2.4) take the form

$$r_* = \sqrt{\frac{1}{f}}, \quad V_* = \sqrt[4]{4f},$$

$$T = \frac{1}{f(1 + \sqrt[4]{4f})}, \qquad \bar{V} = \frac{1 + \sqrt[4]{4f}}{2}. \qquad (2.5)$$

As demonstrated by a comparison with numerical integration, the approximate formulas yield an accuracy of 5-10% which is completely adequate for estimation purposes. However, computation on the basis of these formulas can be even further refined by deriving an approximate formula for α^*. This can be done by using the second of the equations in (2.1), this equation being presented in the form $d\sigma/dt = f\sigma/V$ and $\sigma = \rho V \sin\alpha$, having approximately

$$V = 1 - \frac{1 - V^*}{T}t.$$

Having completed the integration, after modification we obtain

$$\sin\alpha^* = \frac{1}{2}\left(\sqrt[4]{4f}\right)^{\frac{2\sqrt{T}}{2\sqrt{T}-1}}. \qquad (2.6)$$

Having determined α^* from (2.6) and having carried out the substi-

tution into (2.3)-(2.4), we obtain the second approximation of the parametric values of the end of the acceleration phase.

As shown by calculations, these formulas yield velocity values at the end of the acceleration phase with an accuracy of up to 3% and distance values with an accuracy to 5%. However, the acceleration time in second approximation is less precisely determined than in the first, since with more exact determination of the terminal velocity the error resulting from the assumption of a linear change in velocity becomes more pronounced. For approximate determination of acceleration time it is best to use the first-approximation formula from (2.5), the inaccuracy of the hypothesis pertaining to the linearity of the change in velocity and the inaccuracy in the determination of the terminal velocity partially offsetting one another in this formula. The formula for T from (2.5) yields an accuracy of 5-6% for the acceleration of thrust $f = 10^{-5}$-10^{-4} and 7-8% for $f = 10^{-3}$-10^{-2}.

Let us also note that there is an exact relationship $s = (h - h_0)/f$ in which $\underline{s}$ is the nondimensional path traveled by the rocket over the trajectory. For example, if the initial orbit is circular ($h_0 = -1/2$) and $f = 10^{-4}$, the dimensional magnitude of the path s_r covered prior to attainment of the parabolic velocity ($h = 0$) is determined from the relationship $s = s_r/r_0 = 0.5 \cdot 10^4$, where r_0 is the radius of the initial circular orbit. When r_0 is equal to 7000 km, $s_r = 35$ million km.

Remarks. 1. Let us compare the acceleration of a rocket under conditions of low thrust with impulsive acceleration from the standpoint of the momentum expended. In the case of impulsive acceleration it can be assumed that there is an instantaneous increase in the velocity from the circular (V_0) to the parabolic $V_p = V_0 \cdot (2)^{1/2}$ over the same distance from the earth, i.e., the increment in velocity $\Delta_1 V = V_p - V_0 =$

$[(2)^{1/2} - 1]\ V_0 = 0.41\ V_0$ expended on acceleration. In the case of low-thrust acceleration, according to (2.5) for the velocity increment we obtain

$$\frac{\Delta_2 V}{V_0} = \int_0^T f dt = \frac{1}{1 + \sqrt[4]{4f}} \approx 1 - \sqrt[4]{4f},$$

whence

$$\delta = \left| \frac{\Delta_2 V}{\Delta_1 V} \right| \approx 2{,}41\ (1 - \sqrt{2}\sqrt[4]{f}).$$

In the case of very small f($f \approx 0$) low-thrust acceleration requires a momentum greater by a factor of approximately 2.4 than is required in the case of impulsive acceleration. With $f = 10^{-4}$ (i.e., of the order of 1 mm/sec^2 in the case of acceleration from an orbital altitude of ~ 300 km) we will have $\delta = 2.1$; with $f = 5 \cdot 10^{-4}$, $\delta = 1.9$, i.e., the momentum expended on low-thrust acceleration is greater by a factor of approximately two than the momentum required for impulsive acceleration.

2. The segment of spiral motion closer to the planet is separated from the phase of flight between the spheres of planetary influence by the point at which the planetocentric velocity attains the local parabolic velocity. In this case, the initial heliocentric velocity in the segment of motion between the spheres of influence is held to coincide with the heliocentric velocity of the planet, i.e., the planetocentric velocity is held to be equal to zero. This contention is valid on the basis of the following. In the case of planetocentric motion with tangential constant reactive acceleration f the energy integralstake the following form:

1) in the absence of an initial velocity and gravitational pull

$$V_1^2 / 2 = f\ (s - s_*),$$

2) with an initial (parabolic) velocity $V_*^2 = \sqrt{2\mu / \rho_*}$ and gravity

$$V_2^2 / 2 = f\ (s - s_*) + \mu / \rho.$$

Here s is the covered path, μ is the product of planetary mass by the gravitational constant. These integrals in cases 1) and 2) yield ever closer magnitudes for velocities V_1 and V_2 as the distance ρ increases.

However, in terms of the characteristic velocity the expenditures over an identical period of flight time $t \geq \tau_*$ in the second case will be lower than in the first, as is evident if the equations of motion are integrated once with respect to time, holding the motion to be radial for the sake of simplicity:

$$1)\ V_1 = jt, \quad 2)\ V_2 = V_* - \int_0^t \frac{\mu}{\rho^2} dt + jt.$$

We have $V_* - \int_0^t \frac{\mu}{\rho^2} dt > 0$, since $\rho(t)$ increases more rapidly under the action of thrust and in the case in which there is no thrust.

Let us calculate $V^- \equiv \int_0^\infty \frac{\mu}{\rho^2} dt$, assuming ρ_* as the distance unit and V_* as the velocity unit. In this case $\mu = 1$, and considering that $f = 1/\rho_*^2$ from the energy integral we will have $V = \sqrt{\frac{1}{\rho} + \rho - 1}$, whence $dt = [(1/\rho) + \rho - 1]^{-1/2}\, d\rho$ and

$$V_1^- = + \frac{V_*}{2} \int_1^\infty \frac{d\rho}{\rho^2 \sqrt{\frac{1}{\rho} + \rho - 1}} = \frac{V_*}{2} \int_0^1 \frac{d\lambda}{\sqrt{\frac{1}{\lambda} + \lambda - 1}}.$$

The last integral is approximately equal to $\pi/4$. Consequently, the expenditures of characteristic velocity in case 2) are lower than in case 1), by the quantity $V_* - V^- \cong 0{,}6V_*$.

3. Departing from purely radial motion and taking into consideration that with reactive accelerations that are not too low acceleration upon attainment of the parabolic velocity V_* proceeds for a rather long period of time inside the sphere of planetary influence in which solar perturbations are small, we can derive an approximate method for the planetocentric calculation of acceleration at constant tangential ac-

celeration $f = 1/\rho_*^2$. In this case it is convenient to take advantage of the fact that the covered path s(t) increases approximately as the distance $\rho(t)$ in purely radial motion.

The expression dt presented in Remark 2 for purely radial motion in the case of high ρ is easily integrated, whereas in the case of low ρ, e.g., $1 \leq \rho \leq 7$, the quadratic approximation $dt/d\rho = \rho^2/60 - 0.2324\rho + 1.216$ can be integrated to obtain $t = -1.1056 + 1.216\rho - 0.1162\rho^2 + + 0.00555\rho^3$, so that for $\rho > 7$ we have $t = t_1 + 2[(\rho - 1)^{1/2} - (\rho_1 - - 1)^{1/2}]$, where $t_1 = 3.62$ corresponds to the value of $\rho_1 = 7$. In order to calculate the angle α between the velocity and the radius vector the equation of motion can be integrated in projection onto the normal to the trajectory with respect to the variable s:

$$\frac{d\alpha}{ds} = -\frac{\sin\alpha}{\rho}\left(1 - \frac{1}{2\rho V^2}\right),$$

assuming in the integrand that $s = \rho$, in which case we will obtain

$$\operatorname{tg}\frac{\alpha}{2} = \frac{\operatorname{tg}\frac{\alpha_0}{2}}{\rho}\exp\left(\operatorname{arctg}\frac{2\rho - 1}{\sqrt{3}} - \alpha_0\right)/\sqrt{3}.$$

The difference $\Delta = s - \rho : \Delta' = 1 - \cos\alpha$ is associated with the angle α. Using the formula for tan $\alpha/2$, it is possible to evaluate $\Delta' < \frac{2\operatorname{tg}\alpha_0/2}{\sigma^2}$ $\exp 2/\sqrt{3}$, , from which $\Delta_\infty < 2$ is obtained for sufficiently high ρ. It turns out that the relative quantity Δ/ρ initially increases and then diminishes, after attaining the maximum (of less than 10%) at $\rho \approx 2$.

4. Let us undertake a comparison with the previous motion involving a low constant transversal component f_τ of reactive acceleration where the centrifugal term in the nondimensional equations is exactly equal to the gravitational term. This is possible only when the radial-component of reactive acceleration $f_\rho \equiv \ddot{\rho}$ [4]. In this case the equation in projection to the transversal is easily integrated, and with $\rho_0 = 1$ we obtain

$$\rho = \frac{1}{(1 - f_\tau t)^2}, \quad \dot{\rho} = \frac{2f_\tau}{(1 - f_\tau t)^3}, \quad f_\rho = \ddot{\rho} = \frac{6f_\tau^2}{(1 - f_\tau t)^4}.$$

With $t = 0$ we obtain $\dot{\rho} = 2f_\tau$, i.e., this motion is not possible for any initial data.

The considered motion involving the component $f_\tau = \text{const}$ is the optimum of all of the motions with $f_\rho = \ddot{\rho}$ in the sense of the minimum of $J_1 = \int_0^T f_\tau^2 dt$, as acceleration is continued to a value of h_k not close to zero [4].

Let us show that this motion in the case of sufficiently low f_τ and $h_k \neq 0$ is close to the optimum as well in the sense of the complete integral $J = \int_0^T (f_\rho^2 + f_\tau^2)\, d\tau$. Indeed, through simple calculation we find

$$J = J_1 + \frac{36}{7} f_\tau \left(\sqrt[4]{\frac{f_\tau}{2^7}} - f_\tau^2 \right), \quad J_1 \approx f_\tau,$$

i.e., $(J_1 - J)/J$ is an infinitesimal quantity of the order of $\sqrt[4]{f_\tau}$.

For the motion under consideration we have the following values of the terminal parameters:

$$\rho_* = \frac{1}{\sqrt{2f_\tau}}, \quad \dot{\rho}_* = (2f_\tau)^{1/4}, \quad f_\rho^* = 3f_\tau, \quad f_* = f_\tau \sqrt{10}, \quad V_* = \sqrt[4]{8f_\tau},$$

$$\lg(\widehat{\rho f}) = \frac{1}{3}, \quad \angle(\rho, f) \approx 18°25': \quad \angle(V, \rho) = 45°, \quad T = \frac{1 - \sqrt[4]{2f_\tau}}{f_\tau},$$

where $f^2 = f_\rho^2 + f_\tau^2$, and V_* is the terminal velocity.

Comparing the case of acceleration at $\ddot{\rho} = f_\rho$ with the case of constant reactive acceleration, we see that the orders of the terminal quantities with respect to f_τ coincide. However, because of the more rapid increase in acceleration when $\ddot{\rho} = f_\rho$, the parabolic velocity is attained at distances smaller by a factor of $(2)^{1/2}$ from the center of attraction and the velocity itself correspondingly is of greater magnitude. The acceleration time in the case of constant tangential acceleration f_τ will be smaller. Correspondingly, in the case of tangential acceleration the expenditures of energy will be lower (i.e., the magnitude of the integral $J = \int_0^T f^2 dt$). . A comparison of the energy expendi-

tures should be carried out for identical periods of acceleration time T. In this case, in approximate terms, we will have the following for the tangential acceleration (see Section 2), accurate to the infinitesimals of higher order:

$$J_1 = \int_0^T f^2 dt \approx \frac{1}{T}\left(1 - \sqrt[4]{\frac{4}{T}}\right),$$

while for the acceleration considered in Section 1, with $\rho = f_\rho$

$$J_2 = \int_0^T f_\tau^2 dt \approx \frac{1}{T}\left(1 - \sqrt{\frac{2}{T}}\right).$$

It is obvious that $J_1 < J_2$, i.e., the tangential acceleration with constant acceleration is more advantageous from the standpoint of energy expenditure than acceleration with constant transversal acceleration and the centrifugal acceleration compensated by gravity. However, as can be seen from the formulas for J_1 and J_2, the gain is not great. Thus for T = 10,000, which corresponds, for example, to acceleration about the earth from an altitude of ~ 300 km over a period of approximately 100 days, the gain in J_1 relative to J_2 amounts to ~ 2%.

3. RESULTS OF ACCELERATION-TRAJECTORY CALCULATIONS IN THE CASE OF TANGENTIAL CONSTANT ACCELERATION

Certain results obtained through calculation of the acceleration trajectories in the case of constant tangential acceleration are presented in the following tables and in Figs. 3-6.

Tables 1-4 show the calculations of acceleration from an initially circular orbit on the basis of Formulas (2.3), (2.4), (2.5), and (2.6); in addition, these tables show the results of the numerical integration of the differential equations of motion. The results of the numerical integration are shown in graphs.

In addition to the dimensionless values of the parameters in Tables 1-4, their dimensional values for acceleration around the earth

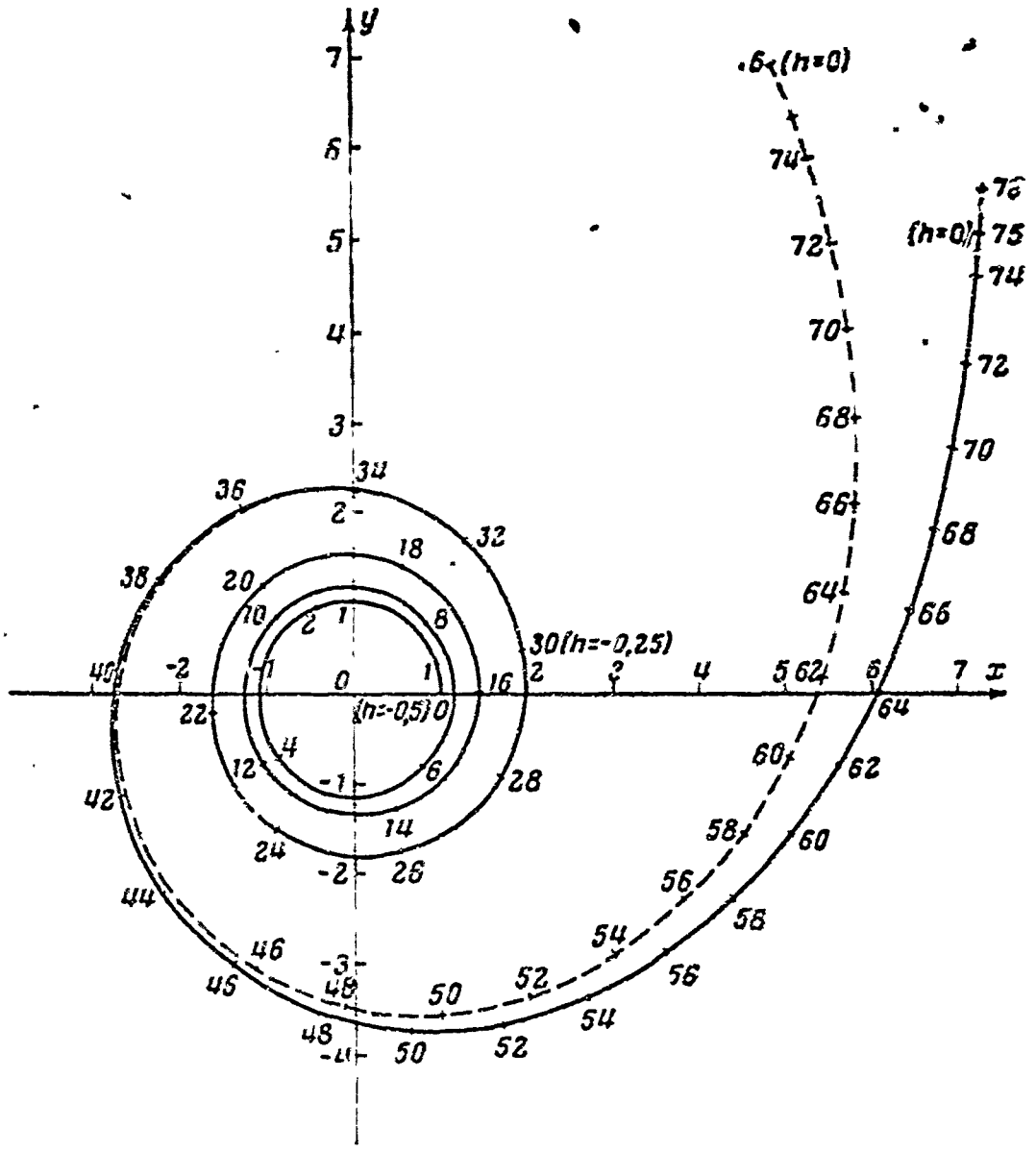

Fig. 3. Example of acceleration trajectory with departure from initial circular orbit (in dimensionless variables). Solid line - trajectory in the case of constant tangential acceleration f = 0.01. Dashed line - trajectory in the case of transversal acceleration of identical magnitude. Dimensionless flight time indicated along trajectory. Dimensionless values of total energy indicated in parentheses.

and Mars are also presented, these having been calculated on the assumption that the altitude of the initial circular orbit is equal to 300 and 6000 km for the earth and 300 km for Mars.

Calculations for greater initial altitudes of the initial orbit (6000 km in Table 3) are of some advantage because these orbits lie beyond the first radiation belt. The energy expenditures required for the insertion of the vehicle at this altitude may be offset by a reduction in the weight of the antiradiation shielding. The denotations in the table coincide with the previous, subscripts 1 and 2 denoting the parameters calculated in first and second approximations on the basis of

TABLE 1

Acceleration from Circular Orbit

f	T_1	T_2	T	δ_T	ρ_1	ρ_2	ρ	δ_ρ
10^{-1}	5,3	5,3	—	—	3,16	2,50	—	—
10^{-2}	69,1	67,8	75	—0,078	10,00	8,89	8,939	0,005
$5\cdot10^{-3}$	145	143	157	—0,074	14,14	12,72	12,438	0,023
10^{-3}	703	702	856	—0,066	31,62	28,01	27,846	0,038
$5\cdot10^{-4}$	1651	1638	1738	—0,061	44,72	41,06	39,506	0,039
10^{-4}	8761	8717	9192	—0,047	100,00	92,10	87,715	0,053
$5\cdot10^{-5}$	17874	17800	—	—	141,4	130,91	—	—

TABLE 1 (Cont'd)

f	V_1	V_2	V	δ_{r_2}	φ, градусы [1]	α, градусы [1]	n
10^{-1}	0,795	0,878	—	—	—	48	1 *
10^{-2}	0,447	0,471	0,473	+0,002	35	37,5	4
$5\cdot10^{-3}$	0,375	0,396	0,401	—0,011	20	36	8
10^{-3}	0,251	0,263	0,268	—0,019	325	33	39
$5\cdot10^{-4}$	0,213	0,221	0,225	—0,019	240	32,5	79
10^{-4}	0,141	0,147	0,151	—0,026	2	31,5	398
$5\cdot10^{-5}$	0,119	0,124	—	—	—	31,0	800 *

* According to Formula (3.1).

1) Degrees.

TABLE 2

Acceleration Around the earth, $h_0 = 300$ km

f	f_r, мм/сек² [1]	T_r, сутки [2]	r, км	V, км/сек
10^{-1}	895	0,054	17 280	6,79 *
10^{-2}	89,5	0,75	50 630	3,65
$5\cdot10^{-3}$	44,7	1,5	82 970	3,10
10^{-3}	8,95	8,5	185 760	2,07
$5\cdot10^{-4}$	4,5	17,5	263 545	1,74
10^{-4}	0,9	92	585 150	1,17
$5\cdot10^{-5}$	0,45	178	873 310	0,955 *

*According to approximate formulas.

1) f_r, in mm/sec^2; 2) T_r, per day.

Formulas (2.3)-(2.6), with the parameters without subscripts derived through numerical integration. The angle between the radius vectors at the beginning and conclusion of acceleration is denoted by φ; $\underline{n}$ represents the number of turns in the acceleration-trajectory spiral; δ_ρ, δ_V, and δ_T are the relative errors in calculation with the approximate formulas (second approximation for V and ρ and first [approximation] for T)

TABLE 3

Acceleration Around the earth, $h_0 = 6000$ km

f	f_r, мм/сек² 1	T_r, сутки 2	r, км	V_r, км/сек
10^{-1}	260	0,13	32 040	4,18
10^{-2}	26	2	110 580	2,68
$5\cdot10^{-3}$	13	4	153 870	2,275
10^{-3}	2,6	21,5	344 483	1,52
$5\cdot10^{-4}$	1,3	44	488 730	1,28
10^{-4}	0,26	232	1085 120	0,86
$5\cdot10^{-5}$	0,13	449	1619 500	0,70

1) f_r, in mm/sec^2; 2) T_r, per day.

TABLE 4

Acceleration Around Mars, $h_0 = 300$ km

f	f_r, мм/сек² 1	T_r, сутки 2	r, км	V_r, км/сек
10^{-1}	316	0,07	9 562	3,00
10^{-2}	31,6	0,93	43 000	1,61
$5\cdot10^{-3}$	15,8	2	65 920	1,37
10^{-3}	3,16	11	102 810	0,91
$5\cdot10^{-4}$	1,6	22	145 800	0,77
10^{-4}	0,3	115	323 840	0,51
$5\cdot10^{-5}$	0,16	223	483 323	0,42

1) f_r, in mm/sec^2; 2) T_r, per day.

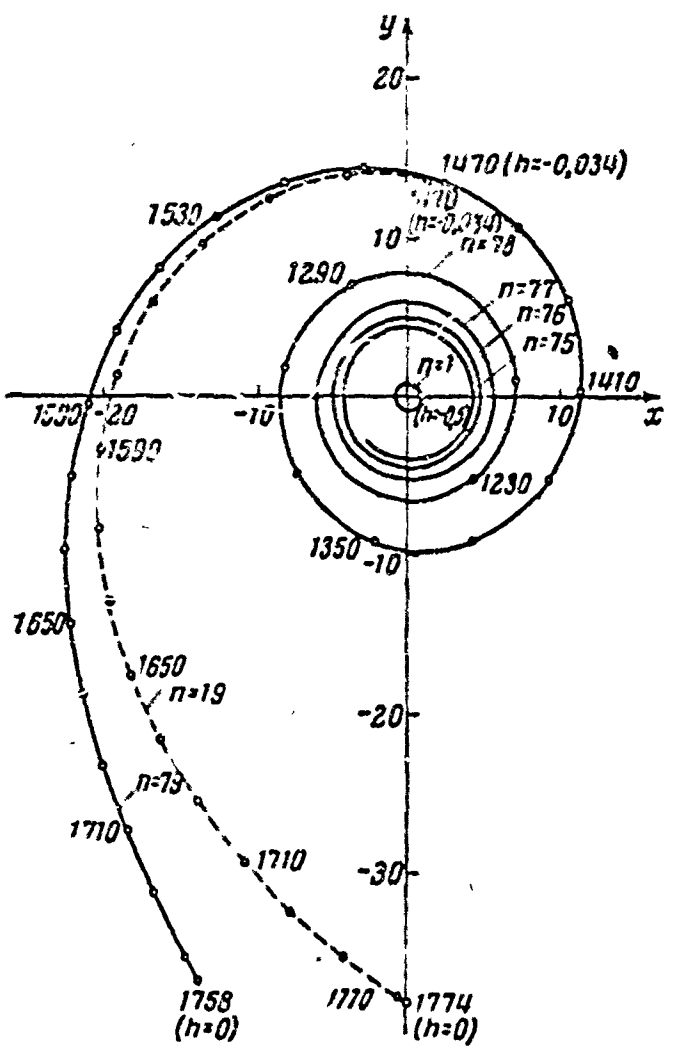

Fig. 4. Example of acceleration trajectory departing from an initially circular orbit (in dimensionless variables). Solid line – trajectory at constant tangential acceleration f = 0.0005. Dashed line – trajectory

for transversal acceleration of same magnitude. Dimensionless flight times and number n of turns indicated along trajectory. Turns 2-74 not shown. Dimensionless values of total energy shown in parentheses.

in comparison with numerical integration. All parameters have been taken at the end of the acceleration phase, i.e., at the instant that the parabolic velocity is attained.

As can be seen from Table 1, the number of turns as a function of the dimensionless f is clearly shown by the formula

$$n = 4/100f. \qquad (3.1)$$

From Tables 2-4 we can draw the conclusion that the acceleration time in the case of acceleration of the order of 1 mm/sec from a circular orbit at an altitude of 300 km above the surface of the planet amounts to approximately 100 days in the case of motion around the earth and 30 days in the case of acceleration about Mars. The same times are required for deceleration with the same gravity forces from the parabolic velocity to the circular [velocity], with entry into a circular orbit 300 km high. For acceleration with the same gravity forces from an orbit around the earth at an altitude of 6000 km above the surface of the earth, approximately 40 days will be required. With a reduction in the magnitude of f of reactive acceleration, the acceleration time increases approximately as 1/f.

Table 5 compares the parameters for the end of the acceleration phase from circular and elliptical orbits, the coordinates and direction of the velocity vector at the initial instant of time coinciding; the initial point is the perigee of the elliptical orbit. For purposes of comparing acceleration from circular and elliptical orbits it is convenient to select the elliptical orbit with comparatively great eccentricity in order to make the differences between the two cases more pronounced.

We can see that the acceleration time (given the indicated eccen-

TABLE 5

Acceleration from Circular and Elliptical Orbits

e = 0					e = 0,442			
f	V	ρ	T	n	V	ρ	T	n
0,01	0,457	8,9[illegible]	7[illegible]	4	0,457	9,6	48	1
0,001	0,251	27,846	856	39	0,285	21,65	617	13

tricity of the initial orbit) diminishes by 30-40%, while the number of turns in the acceleration spiral diminishes by a factor of 3-4. However, economies in acceleration time from an elliptical orbit and the corresponding savings in consumption can hardly offset the energy expenditures required for the insertion of an object from the earth into an extended elliptical orbit (instead of insertion into a circular orbit). The problem of orbital energy gains in the case of orbits exhibiting various eccentricities requires further investigation.

TABLE 6

f = 0,01		T	ρ	V	n
Касательная	1	75	8,9	0,473	4
Трансверсаль	2	76,15	8,5	0,485	4

1) Tangential; 2) transversal.

Tables 6 and 7 compare accelerations involving identical initial data with the same constant acceleration, but directed in one case along the tangent to the trajectory and directed along the transversal in the other case (in Table 6 it is assumed that f = 0.01, while the assumption in Table 7 is that f = 0.0005).

TABLE 7

f = 0,0005		T	ρ	V	n
Касательная	1	1758	39,3	0,225	79
Трансверсаль	2	1774	38,2	0,229	79

1) Tangential; 2) transversal.

We can see that the dimensionless parameters of the end of the acceleration phase are virtually identical in both cases. The acceleration time and, consequently, the values of the integral J in the case of transversal acceleration are somewhat greater than in the case of tangential [acceleration] (by ~ 1.5% in Table 6 and by less than 1% in Table 7); the parabolic velocity is attained somewhat closer to the earth. Both corresponding trajectories are presented in Figs. 3 and 4. We can see that so long as the "unwinding" is taking place in the vicinity of the earth, the trajectories are virtually coincident, the difference between the trajectories visible only in the last turn. For $f = 0.01$ starting approximately after half the total acceleration time has elapsed, and with 4/5 T for $f = 0.0005$, i.e., with the last turn, the trajectories turn into branches that do not envelop the earth; prior to this point the trajectories retain their quasicircular character. In this case the eccentricity increases rapidly and both trajectories deviate significantly from the "quasicircular" spiral. The trajectory branch with transversal thrust exhibits a somewhat greater curvature than the trajectory branch with tangential thrust. The parabolic velocity is attained somewhat closer to the earth along the "transversal" trajectory than in the case of the "tangential" [trajectory]. Thus we can draw the conclusion that the difference between accelerations in the case of transversal and tangential acceleration is found primarily in the last turn of the trajectory.

Figure 5 provides some idea as to the nature of the change in parameters, this figure showing the dimensionless acceleration parameters for $\underline{f} = 0.01$ as a function of time. The time is carried to values at which $\underline{h}$ is considerably greater than zero. We can see that the modulus of velocity actually changes as was indicated in Section 2, attaining its minimum values close to $h \approx 0$. At other values of $\underline{f}$ the nature of

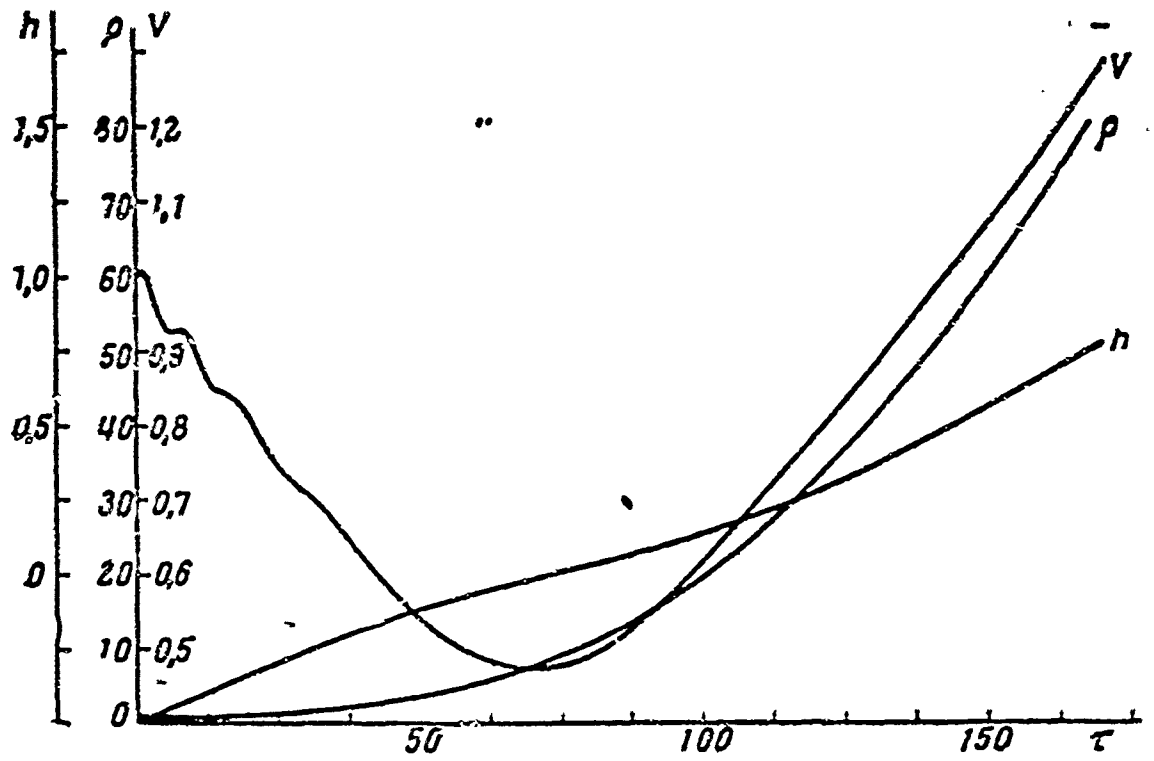

Fig. 5. Trajectory parameters for acceleration from circular orbit as function of time (dimensionless variables); f = 0.01.

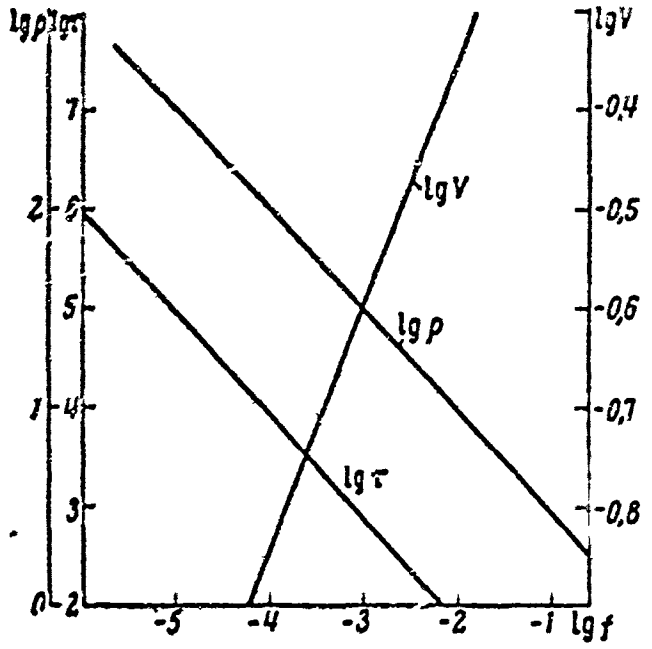

Fig. 6. Logarithmic dimensionless trajectory parameters for acceleration from an initially circular orbit.

the changes in the parameters is retained.

The calculation of the acceleration parameters is most conveniently carried out with curves showing the the logarithms of dimensionless parameters as functions of the logarithm of dimensionless thrust acceleration. These curves are universal and simple. They are shown in Fig. 6.

CONCLUSIONS

The analysis carried out here makes it possible to draw the following basic conclusions.

In the case of acceleration to the local parabolic velocity, the (approximately) constant-magnitude reactive acceleration directed along the bisectrix of the angle between the tangential and transversal tra-

jectories will be the optimum in the sense of the minimum of the integral $J=\int_0^T f^2 dt$. The acceleration [gain in velocity] with tangential constant reactive acceleration is close to the optimum.

Reactive acceleration in the range from 0.5 to 5 mm/sec^2 ensures vehicle acceleration about the earth to the parabolic velocity (or deceleration from the parabolic velocity to circular velocity) in 7 months to 2 weeks, respectively; the corresponding values of J lie within the range from 4.5 to 45 m^2/sec^3. The same values of reactive acceleration provide for deceleration (or acceleration) around Mars in 2 months to one week, respectively, with the values of J ranging from 1.5 to 15 m^2/sec^3.

Received 20 February 1964

REFERENCE

1. V.V. Beletskiy, V.A. Yegorov. Kosmich. issled., nast. nomer, [Cosmic Research, present Issue], page 360.

2. H.S. Tsien, J. Amer. Roc. Soc., 23, 233, 1953.

3. H.S. London, J. Amer. Roc. Soc., 30, 198, 1960.

4. G.L. Grozdovskiy, Yu.N. Ivanov, V.V. Tokarev, Dokl. AN SSSR, [Proc. Acad. Sci. USSR], 137, No. 5, 1082, 1961.

Manuscript Page No. [Transliterated Symbols]

57 p = r = razmernyy = dimensional

58 к = k = konechnaya = terminal

61 м = m = maksimal'noye = maximum

61 ср = sr = sredniy = average

ON SPACE-FLIGHT TRAJECTORIES WITH A CONSTANT-REACTION ACCELERATION VECTOR

V.V. Beletskiy

The equations of motion of a space vehicle in a Newtonian force field are investigated for a constant reaction-acceleration vector. Two dimensional trajectories are classified.

* * *

Plans for space flights using ionic, plasma and other types of engines [1] that generate reaction thrust over a very long span of time have recently been discussed in the literature.

In the present note, we consider the possible trajectories of a space vehicle in one of the simple cases, namely that in which it moves in a Newtonian field with one attracting center in the presence of a constant reactive-acceleration vector. We integrate the equations of motion and classify the two-dimensional trajectories.

We introduce the dimensionless variables

$$\{r\} = \frac{\{r_R\}}{r_0}, \quad \{v\} = \frac{\{V_R\}}{\sqrt{r_0 g}}, \quad t = \frac{t}{\sqrt{\frac{r_0}{g}}}, \quad \{f\} = \frac{\{f_R\}}{g};$$

where

$$g = \frac{\mu}{r_0^2}.$$

Here $\{r\}$, $\{v\}$, $\{f\}$, t are the dimensionless coordinates, the velocity components, the reactive-acceleration components and the time, respectively, $\{r_R\}$, $\{V_R\}$, $\{f_R\}$, t_R are the analogous dimensional quantities, r_0 is a fixed (for example, the initial) distance from the center of attraction, g is the acceleration of gravity at the distance r_0 from the at-

tracting center and $\mu = fM$ is the product of the mass by the gravitation constant.

Let us direct the x-axis of a fixed coordinate system xyz along the constant vector $\vec{f}$ of the reactive acceleration. Then the equations of motion assume the form

$$\ddot{x} = -\frac{x}{r^3} + f, \quad \ddot{y} = -\frac{y}{r^3}, \quad \ddot{z} = -\frac{z}{r^3}, \quad r = \sqrt{x^2 + y^2 + z^2} \tag{1}$$

and have the following first integrals:

the energy integral

$$\frac{1}{2}(\dot{x}^2 + \dot{y}^2 + \dot{z}^2) - \frac{1}{r} - fx = h, \tag{2}$$

the area integral

$$z\dot{y} - y\dot{z} = -k_0 \tag{3}$$

and the third integral

$$x\dot{r} - \frac{x}{r} - \frac{3}{2}fx^2 - \frac{1}{2}fr^2 - 2hx = c. \tag{4}$$

The presence of the three first integrals (2)-(4) makes it possible to reduce the problem to quadratures. We introduce the new variables

$$u = r - x, \quad v = r + x, \tag{5}$$

so that

$$r = (u + v)/2, \quad x = (u - v)/2, \tag{6}$$

and define the third variable φ by the relationships

$$\cos\varphi = \frac{y}{r_1}, \quad \sin\varphi = \frac{z}{r_1}, \quad r_1 = \sqrt{y^2 + z^2}. \tag{7}$$

The coordinate surfaces u = const and v = const are paraboloids of rotation.

To replace the time T, we introduce the parameter τ, which increases monotonically with time, by the relationship

$$d\tau = dt/r. \tag{8}$$

Then

$$\int \frac{dv}{\sqrt{V(v)}} = \tau + c_1, \int \frac{du}{\sqrt{U(u)}} = \tau + c_2, \tag{9}$$

where

$$V(v) = fv^3 + 2hv^2 + 2(1+c)v - k^2,$$
$$U(u) = -fu^3 + 2hu^2 + 2(1-c)u - k^2. \qquad (10)$$

Inversion of the elliptical integrals (10) gives the parametric equations of the trajectory in the rotating plane containing the radius vector $\vec{r}$ and the x-axis, i.e., the vector $\vec{f}$. The rotation angle φ of this plane about the axis is determined, according to (3) and (7), by the formula

$$\varphi - \varphi_0 = k_0 \int_0^\tau \frac{r d\tau}{r^2 - x^2}, \qquad (11)$$

where, of course, $\underline{r}$ and $\underline{x}$ are regarded as already known functions of τ [by virtue of (6) and the inverse integrals (9)]. We see that φ_0 varies monotonically over τ. From (8) we obtain

$$t - t_0 = \int_0^\tau r d\tau. \qquad (12)$$

The problem is reduced completely to quadratures.

Let us consider the motion in the x, y-plane. Then $k_0 = 0$ and $\varphi = \varphi_0$. The polynomials (10) can be presented in the form

$$V = fv(v - v_2)(v - v_3), \quad U = -fu(u - u_2)(u - u_3), \quad (13)$$

where the roots of Polynomial (13) have the values

$$v_1 = 0, \; v_2 = \frac{-h + \sqrt{h^2 - 2f(1+c)}}{f}, \quad v_3 = \frac{-h - \sqrt{h^2 - 2f(1+c)}}{f},$$
$$u_1 = 0, \; u_2 = \frac{h + \sqrt{h^2 + 2f(1-c)}}{f}, \quad u_3 = \frac{h - \sqrt{h^2 - 2f(1-c)}}{f}. \quad (14)$$

The roots v_i and u_i have different signs and complexities depending on the values of $\underline{h}$ and $\underline{c}$. Hence classification of the motions is conveniently carried out in the $\underline{h}$, c-plane for a fixed value of $f \neq 0$. A breakdown of the (h, c) plane into regions with trajectories of uniform type is shown in Fig. 1.

For each of the regions represented, inversion of Integrals (9) gives a particular form to the parametric trajectory equations. For a

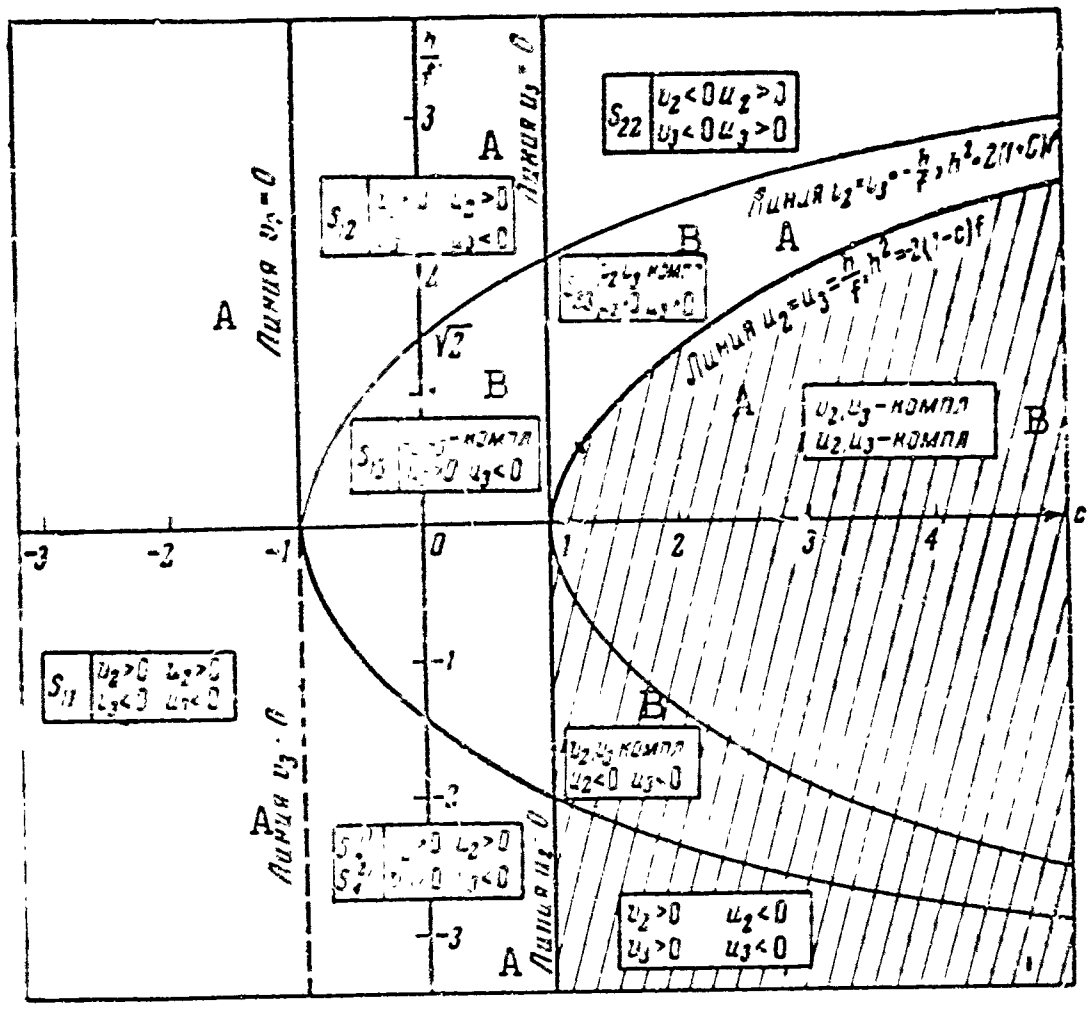

Fig. 1. A) Line; B) complex.

real motion $V \geq 0$, $U \geq 0$ (since the parameter τ is a real quantity). In all cases, $U(0) = 0$, $V(0) = 0$, $U \to \pm \infty$ as $u \to \pm \infty$; $V \to \pm \infty$ as $\to \pm \infty$; moreover, we have $u \geq 0$; $v \geq 0$ according to the sense of the variables u and v. The trajectory classes will be denoted by S_{ij}, where the subscript i corresponds to the type of the polynomial U (i.e., to the nature of the roots of this polynomial) and the subscript j corresponds to the type of polynomial V. As is shown by analysis, two types of polynomial U and four types of polynomial V may be encountered in a real motion; we write out the relationships $u(\tau)$ and $v(\tau)$ for each of these types. We shall denote by T_u and T_v the periods of the functions $u(\tau)$ and $v(\tau)$; by K(k) the complete elliptic integral of the first kind; by F the incomplete elliptic integral of the first kind and by k its modulus. In all cases, $u = u_0$ and $v = v_0$ at $\tau = 0$.

1. FORMULAS FOR $u(\tau)$

Type 1. $u_3 < 0 \leqslant u \leqslant u_2$

$$u = u_2 \operatorname{cn}^2 \varphi, \quad \varphi = \frac{\sqrt{u_1 - u_3}}{2}(\tau - \tau_0^u), \quad k^2 = \frac{u_2}{u_1 - u_3},$$

$$T_u = \frac{4}{\sqrt{u_1 - u_3}} K(k), \quad \tau_0^u = \frac{2}{\sqrt{u_1 - u_3}} F\left(\arcsin \sqrt{\frac{u_1 - u_0}{u_2}}, \ k\right),$$

Type 2. $0 < u_3 \leqslant u \leqslant u_2$

$$u = u_2 \operatorname{cn}^2 \varphi + u_3 \operatorname{sn}^2 \varphi, \ \varphi = \frac{\sqrt{u_1}}{2}(\tau - \tau_0^u),$$

$$\tau_0^u = \frac{2}{\sqrt{u_1}} F\left(\arcsin \sqrt{\frac{u_1 - u_0}{u_2 - u_3}}, \ k\right), \quad k^2 = \frac{u_2 - u_3}{u_2}, \ T_u = \frac{4}{\sqrt{u_1}} K(k).$$

2. FORMULAS FOR $v(\tau)$

Type 1. $v_3 < 0 < v_2 \leqslant v$

$$v = \frac{v_1}{\operatorname{cn}^2 \Psi}, \ \Psi = \frac{\sqrt{v_1 - v_3}}{2}(\tau + \tau_0^v), \ \tau_0^v = \frac{2}{\sqrt{v_1 - v_3}} \times$$

$$\times F\left(\arcsin \sqrt{\frac{v_0 - v_1}{v_0}}, \ k\right),$$

$$k^2 = -\frac{v_3}{v_1 - v_3}, \quad T_v = \frac{4}{\sqrt{v_1 - v_3}} K(k).$$

Type 2. $v_3 < v_2 < 0 \leqslant v$

$$v = -v_2 \frac{\operatorname{sn}^2 \Psi}{\operatorname{cn}^2 \Psi}, \quad \Psi = \frac{\sqrt{-v_3}}{2}(\tau + \tau_0^v),$$

$$\tau_0^v = F\left(\arcsin \sqrt{\frac{v_0}{v_0 - v_2}}, \ k\right), \ k^2 = -\frac{v_1 - v_2}{v_3}, \quad T_v = \frac{4}{\sqrt{-v_3}} K(k).$$

Type 3. v_2 and v_3 are complex and $v \geq 0$

$$v = p \frac{\operatorname{sn}^2 \Psi}{(1 + \operatorname{cn}^2 \Psi)^2}, \quad \Psi = \sqrt{p}(\tau + \tau_0^v), \ \tau_0^v = \frac{1}{\sqrt{p}} \times$$

$$\times F\left(2 \operatorname{arc\,tg} \sqrt{\frac{v_0}{p}}, \ \sqrt{\frac{p + m}{2m}}\right),$$

$$k^2 = \frac{p + m}{2p}, \quad T_v = \frac{2K(k)}{\sqrt{p}}, \quad p = \sqrt{2(1 + c)}, \quad m = -h.$$

Type 4. $0 < v_3 < v_2 \leqslant v$

$$v = \frac{v_1 - v_3 \operatorname{sn}^2 \Psi}{\operatorname{cn}^2 \Psi}, \quad \Psi = \frac{\sqrt{v_1}}{2}(\tau + \tau_0^v),$$

$$\tau_0^v = \frac{2}{\sqrt{v_1}} F\left(\arcsin \sqrt{\frac{v_0 - v_1}{v_0 - v_3}}, \ k\right), \ k^2 = \frac{v_3}{v_1}, \quad T_v = \frac{4}{\sqrt{v_1}} K(k).$$

Type 4^2. $0 \leqslant v \leqslant v_3 < v_2$

$$v = v_3 \operatorname{sn}^2 \Psi, \quad \Psi = \frac{\sqrt{v_2}}{2}(\tau - \tau_0^v), \quad \tau_0^v = \frac{2}{\sqrt{v_2}} F\left(\arcsin \sqrt{\frac{v_3}{v_2}}, k\right),$$

$$k^2 = \frac{v_3}{v_2}, \quad T_v = \frac{4}{\sqrt{v_2}} K(k).$$

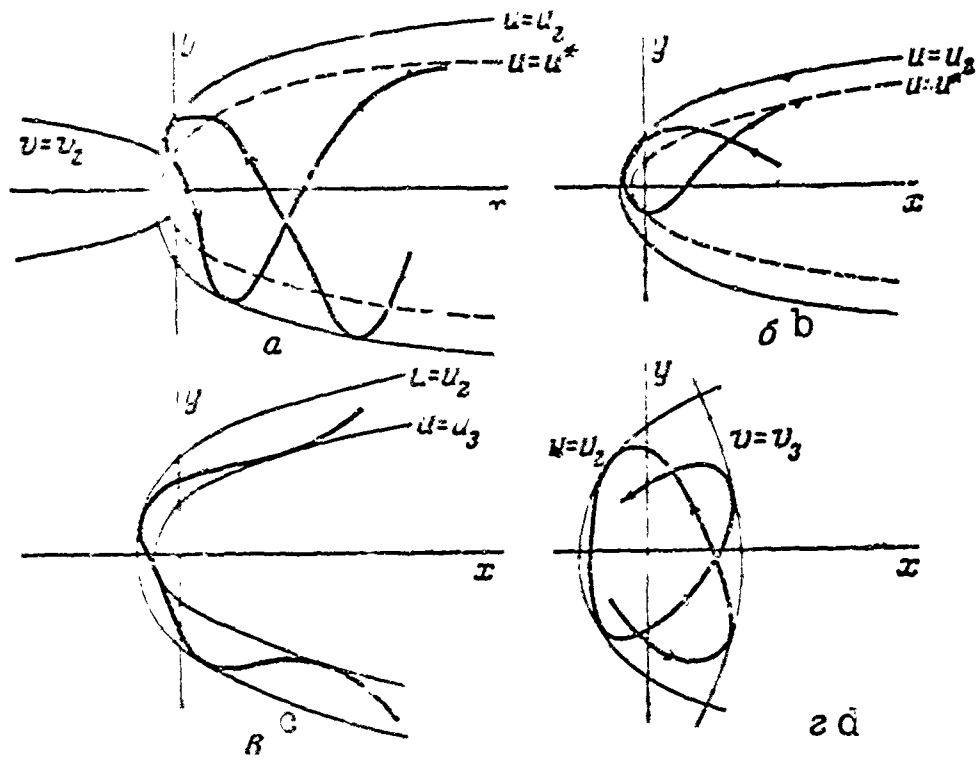

Fig. 2.

For Type 4, the motion may take either of two forms depending on the initial value of v_0 ($v_0 \geq v_2$ in the first case and $0 \leq v_0 \leq v_3$ in the second case). We shall mark trajectory classes in these cases by an additional superior number ($S_{14}^{(1)}$, $S_{14}^{(2)}$). Figure 1 shows the regions corresponding to the trajectory classes S_{ij}, and indicates the nature of the polynomials U and V in these cases. Further, the heavy lines delineate those groups of regions in which the trajectories are qualitatively of the same nature. The region of values of the parameters h, c that does not correspond to real motions is shaded.

In regions S_{11} and S_{14}, the motions will be qualitatively different in the case $S_{14}^{(2)}$ and qualitatively similar in the case of $S_{14}^{(1)}$; for this reason, these regions are separated by a heavy dashed line. Let us pass to a description of the trajectories.

Class S_{11}. In this case, the motion is unbounded: $v \to \infty$ as $\tau \to \tau^*$ (recession to ∞ in a finite τ and in an infinite $\underline{t}$, since $dt = rd\tau$, $r \to \infty$). Here, $u \to u(\tau^*) \equiv u_*$, i.e., the motion tends to some parabola u_*. This is the first characteristic peculiarity of all unbounded motions (and not only those of class S_{11}). In the present case $u^* \leq u_2$. Since it may be the case that $T_u \ll T_v$, then before receding to infinity , the rocket may execute a finite number of oscillations in the region $0 \leq u \leq u_2$. The resultant motion is of the undulating type; this represents the second characteristic peculiarity of all the unbounded motions. Since $v > v_2$, the trajectories of class S_{11} do not embrace the attracting center. This is a characteristic peculiarity of the present class of motions – S_{11}. A trajectory of the S_{11} type is shown in Fig. 2a.

Class S_{12}. The departure from the preceding class consists only in that $\underline{v}$ may reach zero, i.e., the trajectory may envelop the center of attraction (Fig. 2b).

Generally speaking, trajectories of classes S_{11} and S_{12} intersect themselves.

Class S_{13}. The trajectories are qualitatively the same as those in S_{12}.

Class S_{22}. The trajectories lie within the region bounded by the parabolas $u = u_2$ and $u = u_3$; they envelop the center of attraction (since $\underline{v}$ reaches zero) and cannot intersect themselves (Fig. 2c).

Class S_{23}. The trajectories are qualitatively the same as in class S_{22}.

Class $S_{14}^{(1)}$. Contains trajectories qualitatively similar to the trajectories of class S_{11}, but here the trajectories may be somewhat less "smooth," since extremes of $\underline{v}$ may be reached not only at the points $\Psi = 0, 4K, 8K, \ldots$, but also at certain intermediate points.

Class $S_{14}^{(2)}$, gives bounded trajectories, since here $0 \leq u \leq u_2$, $0 \leq v \leq v_3$ (Fig. 2d). In terms of the Keplerian osculating elements, these trajectories are clearly described as osculating ellipses exhibiting secular motion of the line of apsides and long-period oscillations of the semimajor axis and eccentricity.

Thus, the two-dimensional trajectories can be broken down into four basic qualitative forms.

Form I. Unbounded self-intersecting trajectories that do not envelop the center of attraction.

Form II. Unbounded self-intersecting trajectories that envelop the center of attraction.

Form III. Unbounded non-self-intersecting trajectories.

Form IV. Bounded trajectories.

The three dimensional trajectories are classified into the same basic forms, at least for small values of the area constant k_0 in the plane $(\vec{r}, \vec{f})$ rotating about $\vec{f}$.

Suppose that the space vehicle starts from a circular orbit of radius r = 1 and let the initial radius vector and the velocity vector form angles α and up to $90^\circ - \alpha$, respectively, with the reactive acceleration vector $\vec{f}$. Then if the conditions

$$f < \frac{1}{2}, \quad f^2 - f[2 - \cos\alpha] + \frac{1}{4} > 0,$$

are simultaneously satisfied, the motion is bounded. With f > 1/2, the motion is unbounded for any α. For $\alpha = 0$, the motion is bounded if $0 < f < 1/2$; at $\alpha = 180^\circ$, the motion is bounded if $0 < f < 3/2 - \sqrt{2} = 0.086$. The maximum value of f that still permits bounded motion increases monotonically from $f_1 = 3/2 - \sqrt{2}$ to $f_2 = 1/2$ as α diminishes from 180° to 0. At $\alpha = 180^\circ$ and $f = 3/2 - \sqrt{2} = 0.086$, the largest attainable $r \approx 3.4$. With $\alpha = 0$ and f = 0.5, the largest attainable $r \approx 1.4$. Thus it is easier (the f-values are smaller) to cover long distances and

easier to obtain unbounded trajectories when α is large.

Received 14 February 1964

REFERENCES

1. U. Korliss. Raketnyye dvigateli dlya kosmicheskikh poletov [Rocket Engines for Cosmic Flights]. IL [Foreign Literature Press]. Moscow, 1962.

OPTIMUM TRAJECTORIES AND OPTIMUM PARAMETERS FOR SPACE VEHICLES WITH ENGINES OF LIMITED OUTPUT

Yu.N. Ivanov, V.V. Tokarev and Yu.V. Shalayev

The subject of discussion is the two-dimensional problem of flight of a space vehicle from the earth's sphere of influence to the sphere of influence of another planet and back. The trajectories of motion and vehicle parameters corresponding to maximum payload at the end of the flight are derived for space vehicles with engines of limited power.

* * *

The present paper investigates the problem of optimizing the parameters of an engine of limited output and the trajectories of interplanetary flights; it represents a continuation of [1].

A special point in the control of limited-output engines consists in maximum utilization of the power available from the source. In the absence of other limitations on control, the determining functional of the problem takes the form [1, 2]

$$J = \int_0^T a^2 dt,$$

where a(t) is the acceleration due to the thrust and T is the time of motion.

Here, the optimum weight components of the apparatus are expressed as follows [1, 2]:

$$G_n / G_0 = \sqrt{(\alpha / 2g) J} - (\alpha / 2g) J, \quad G_m / G_0 = \sqrt{(\alpha / 2g) J},$$
$$G_a / G_0 = (1 - \sqrt{(\alpha / 2g) J})^2, \qquad (2)$$

where G_n is the weight of the power source, G_m is the weight of working fluid, G_n is the weight of the payload, G_0 is the initial weight of the

vehicle and α is the specific weight of the power source.

The variational problem of achieving maximum payload consists in determining the optimum trajectories and optimum control laws for the thrust-acceleration vector so as to minimize the functional (1), followed by selection of the optimum weight components by Formulas (2).

The trajectory part of the problem is described by a system of differential equations and boundary conditions:

$$\ddot{\mathbf{r}} = \mathbf{a} + \mathbf{R}(\mathbf{r}, t), \quad \mathbf{r}(0) = \mathbf{r}_0, \quad \dot{\mathbf{r}}(0) = \dot{\mathbf{r}}_0, \quad \mathbf{r}(T) = \mathbf{r}_1, \quad \dot{\mathbf{r}}(T) = \dot{\mathbf{r}}_1. \quad (3)$$

Here $\vec{r}$ is the radius vector of the point and $\vec{R}(\vec{r}, t)$ is the acceleration vector due to gravity.

In the first part, we consider the problem of interplanetary flight from the earth to the planet and back. The trajectory of such a flight has two qualitatively different segments: a segment of motion in a region where the influence of the planets predominates, with a perturbing influence from the sun, and a segment of motion in a region where the influence of the sun predominates with the planets exerting the perturbing influence. The boundary between these characteristic segments of the trajectory is determined from examination of the Jacobi's integral for the bounded three-body problem [3].

The natural approximation for the problem of flight in the region where the sun's influence predominates is that of disregarding the influence of the planets, i.e., motion in the central field of the sun. The corrections required by the gravitational fields of the planets are found to be nonessential in the integral characteristics. To a certain degree, this makes it possible to consider the two motion segments independently of one another.

In the second part of the paper, we publish the results of numerical trajectory calculations for interplanetary flight.

For simplicity of analysis, it is assumed that the orbits of the

planets are circular and coplanar.

Symbols.

a_x, a_y Projections of the reaction-thrust acceleration on the axes of a rectangular coordinate system

a_r, a_φ Radial and transversal components of the acceleration in the polar coordinate system

$k = \gamma_r M$, γ_r Gravitational constant

M Mass of the central body

T_σ Residence time in planetary spheres of influence

T + T' Time of flight from orbit "0" to orbit "1" and back:

$$T_n = T - T' + T_\sigma$$

E Total energy in the gravitational field

ω Average angular velocity of planet's revolution around the sun

r_0 Radius of planet's orbit

τ_0 Period of revolution of the planet

r Current distance of point from center

$\varphi = \psi + \omega t$ Angle in polar coordinate system

v Absolute magnitude of velocity

θ Angle between velocity vector and tangent to circle at the given point

γ Angle between velocity vector and thrust vector.

Subscripts: 1 – planetary system; 2 – heliocentric system; Z – earth; P – planet; 0 – initial index; 1 – final index; orb – orbital.

ANALYSIS OF THE EQUATIONS OF THE VARIATIONAL PROBLEM

1. Formulation of the Optimum-Trajectory Problem for Interplanetary Flights

Let us consider the problem of flight of a space vehicle from the sphere of influence of the earth to the sphere of influence of a planet

and back. The trajectory of such a flight consists of the following characteristic parts:

a) acceleration in the earth's sphere of influence from a certain satellite orbit around the earth;

b) flight in the region in which the sun's influence predominates;

c) deceleration in the region of the destination planet's influence with injection into a certain orbit;

d) subsequent acceleration from this orbit;

e) the return flight;

f) deceleration in the neighborhood of the earth to a certain orbit about the earth.

We shall study two-dimensional motion in the gravitational field of the sun and nearest planets, disregarding the influence of other celestial bodies. Here, the influence of the nearest planet is taken into

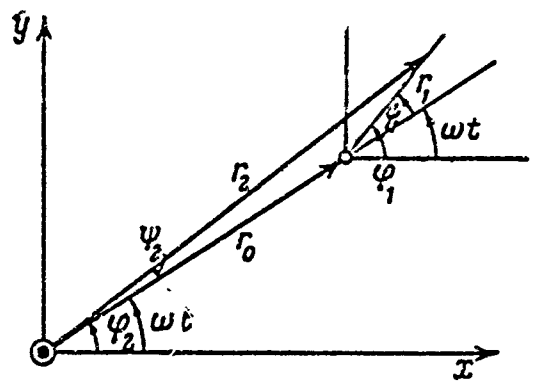

Fig. 1

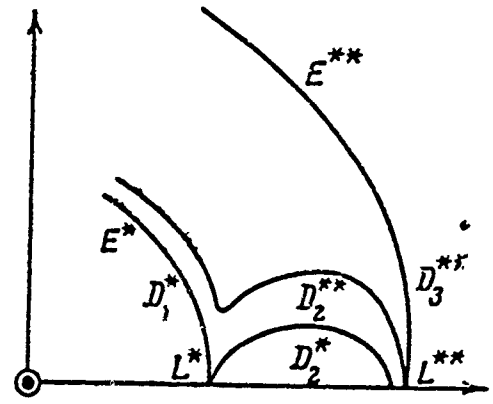

Fig. 2

account in the vicinity of this planet for the flight segment in the sphere of the sun's dominating influence. In this formulation, we can indicate a criterion for distinguishing between fields of influence.

The law of energy variation for a unit mass in a system of coordinates revolving together with the planet at a constant angular velocity ω takes the following form (Fig. 1):

$$v_1^2/2 - k_1/r_1 - k_2/r_2 - r_2^2\omega^2/2 = E_0 + \int_0^T (a_1, v_1)\,dt. \qquad (1.1)$$

Let us first investigate the behavior of a material point in the

neighborhood of a planet without the influence of a reaction force ($a_1 = 0$). Suppose that the velocity v_{10} is known at point (r_{10}, r_{20}) at the initial point in time; it is required to find the region D of possible displacements of the material point for a known total energy

$$E_0 = r_{10}^2/2 - k_1/r_{10} - k_2/r_{20} - r_{20}^2\omega^2/2.$$

Let us examine (1.1) for $a_1 = 0$. Since $v_1^2 \geq 0$, region D is bounded by $v_1 = 0$:

$$k_1/r_1 + k_2/r_2 + r_2^2\omega^2/2 + E_0 = 0. \qquad (1.2)$$

This determines the boundary of region D for the given E_0. For large negative E_0, region D consists of three subregions [3]: D_1 about the sun, D_2 about the planet and D_3, which encompasses both bodies. As E_0 increases, the boundaries of the regions come closer together until, at a certain point L* (libration point) the regions D_2 and D_1 come into contact; then $E_0 = E_0^*$; with $E_0 = E_0^{**}$ ($E^{**} > E^*$), regions D_2 and D_3 touch at point L**. Below we give numerical values of r_2^*, r_1^*, E_0^* and r_2^{**}, r_1^{**} and E_0^{**} for the earth (the distances are referred to the radius of the corresponding planetary orbit and the velocities to the corresponding planetary orbital velocities):

$$E_0^* = -1{,}5004511, \quad r_1^* = 0{,}0099665, \quad r_2^* = 0{,}9900335$$
$$E_0^{**} = -1{,}5004490, \quad r_1^{**} = 0{,}0100333, \quad r_2^{**} = 1{,}0100333.$$

We note that the points of libration L*, L** lie on a ray connecting the sun and the planet ($r_2^* = r_0 - r_1^*$, $r_2^{**} = r_0 + r_1^{**}$) and that the function $E_0(r_1)$ has a maximum at these points. As E_0 increases further, necks connecting regions D_1, D_2, and D_3 make their appearance near the libration points and, finally, at a certain $E_0 = E_0^{***}$, the region of possible movements occupies the entire plane. From the known values of E** and E*, we can determine the $D_2^{**} - D_3^{**}$ and $D_2^* - D_1^*$ boundaries. Figure 2 shows the qualitative appearance of these regions. It will be seen that the boundary of region D_2^* encircles only the pla-

net, unlike the boundary of region D_2**, which encompasses both the planet and the sun.

Thus, suppose that at the initial time t = 0, a material point with the coordinates r_{10}, r_{20} from D_2* possesses a velocity v_{10}. If

$$E_0 = v_{10}^2/2 - k_1/r_{10} - k_2/r_{20} - r_{20}^2\omega^2/2 < E_0^*, \qquad (1.3)$$

then the material point will not escape region D_2*.

If within the region D_2*, the quantity $a_1 \neq 0$, then the conclusion remains valid for

$$\int_0^t (a_1, v_1)\, dt \leqslant 0 \qquad (1.4)$$

(here the energy will diminish and the point will "fall" to the center $r_1 = 0$).

On completing the investigation, we can clearly define the boundaries of the flight segment from the earth's orbit to the orbit of the other planet: this is the trajectory from the pcint $N_Z^*(r_{1z}, \psi_{1Z})$ in D_{2Z}*, where $E_{0Z} = E_{0Z}^*$ with respect to the earth, to point N_P^* (r_{2P}, ψ_{2P}) within D_2*, where $E_{0P} = E^*_{0P}$ with respect to the planet.

For the segment of the trajectory in the region of the sun's influence, extending from point N^*_{Z0} (the origin of the flight near the earth) to point N^*_{Z1} (the end point of the return flight near the earth), the essential parameter is the time T_n: the time T of flight from N^*_{Z0} to N^*_{P0} plus the time T_σ of residence in the region D^*_2 near the planet plus the time T' for the return flight from N^*_{P1} to N^*_{Z1}.

The formula obtained for T_n from comparison of the angular displacements of the material point and the points N* of the beginning and end of the flight near the earth is as follows:

$$T_n = [1/(\omega_1 - \omega_2)][\varphi + \varphi' - \omega_2(T + T') - \delta\psi_3 + \delta\psi_\pi \pm 2k\pi], \quad (1.5)$$

where

$$T_\sigma = [(1/\omega_1 - \omega_2)][\varphi + \varphi' - \omega_1(T - T') - \delta\psi_3 + \delta\psi_\pi \pm 2k\pi]. \quad (1.6)$$

Here φ and φ' are the angular displacements of the point during the flight (earth to planet when unprimed and planet to earth when primed); T and T' are the corresponding times; ω_1 and ω_2 are the angular velocities of revolution of the earth and planet about the sun (the orbits are assumed circular); $\delta\psi_Z$ and $\delta\psi_P$ are the angular distances between the points N* for the earth and for the planet; k = 0, 1, 2,... In (1.5) and (1.6), the plus sign is read for $\omega_1 > \omega_2$ and the minus sign for $\omega_1 < \omega_2$.

Most interesting from the standpoint of minimum waiting time is the case with k = 0:

$$[1/(T+T')](\varphi+\varphi'-\delta\psi_3-\delta\psi_\pi) < \omega_1 \text{ for } \omega_1 < \omega_2. \qquad (1.7)$$
$$[1/(T+T')](\varphi+\varphi'-\delta\psi_3+\delta\psi_\pi) > \omega_1 \text{ for } \omega_1 > \omega_2.$$

For accelerations a_2 that are small as compared with the characteristic accelerations from the sun, the trajectories of these flights leave the region between the orbits.

Let us formulate the variational problem. From among the set of trajectories $\vec{r}(t)$ passing successively through the points $N^*_{Z)}$, N^*_{PO}, N^*_{P1}, and N^*_{Z1}, it is required to select a class of trajectories that minimize the functional J and satisfy the following conditions:

a) the time of transit T_n between points N^*_{ZO} and N^*_{Z1} is assigned;

b) the time of residence T_σ in the region D_{2P} near the planet is assigned.

Further assignment of the coordinates of the four points N* and the directions of the velocity vector θ_1 at these points with respect to the corresponding planets* determines the boundary-value problem formulated if the quantities φ, φ', T, and T' are known separately (the sums $\varphi + \varphi'$ and T + T' are determined by Expressions (1.5) and (1.6) for assigned T_n and T_e).

The trajectory obtained as a result of solving this boundary-value problem can be extended continuously or discontinuously in the sense of the projections of the acceleration and their derivatives in the regions D_{2Z} and D_{2P} from the points N*. (Cauchy problem). In the continuous extension of the trajectory, there correspond to each set of three quantities r_1, Ψ_1, and θ_1 for a specified motion time T_R from N* within D^*_2 until a certain orbit is reached three elements that define an osculating ellipse (for example, the orientation of the ellipse and the minimum and maximum distances from the center).

2. EQUATION OF THE VARIATIONAL PROBLEM

Two-dimensional motion in the gravitational field of two gravitating bodies – the sun and the planet – was analyzed in [1] (we disregard the influence of the second planet in the neighborhood of the first).

Suppose that the planet revolves about the sun with an angular velocity ω_0 in a circular orbit of radius r_0. In the region where the influence of one of the bodies predominates, the equations of motion may be written in the following form in the system of coordinates attached to this body (Fig. 1):

$$\ddot{r}_i - r_i(\dot{\psi}_i + \omega)^2 = a_{r_i} - k_i / r_i^2 + R_i,\quad r_i\ddot{\psi}_i + 2\dot{r}_i(\dot{\psi}_i + \omega) = a_{\psi_i} + \Psi_i \qquad (i = 1, 2), \tag{2.1}$$

where

$$R_1 = (k_2 / r^2_0)\cos\psi_1 - (k_2 / r^2_2)\cos(\psi_1 - \psi_2),$$
$$R_2 = (k_1 / r^2_1)\cos(\psi_1 - \psi_2)$$
$$\Psi_1 = (k_2 / r^2_0)\sin\psi_1 + (k_2 / r^2_2)\sin(\psi_1 - \psi_2),$$
$$\Psi_2 = (k_1 / r^2_1)\sin(\psi_1 - \psi_2).$$

The angles Ψ_1 and distances r_1 are presented in Fig. 1.

Integral (1) is expressed in terms of the kinematic acceleration projections as follows:

$$J_i = \int_0^T \left\{ [\ddot{r}_i - r_i(\dot{\psi}_i + \omega)^2 + k_i / r_i^2 - R_i]^2 + [r_i\ddot{\psi}_i + 2\dot{r}_i(\dot{\psi}_i + \omega) - \Psi_i]^2 \right\} dt =$$

$$= \int_0^T \Phi_i(r_i, \dot{r}_i, \ddot{r}_i; \psi_i, \dot{\psi}_i, \ddot{\psi}_i)\, dt. \qquad (2.2)$$

The first variation of the functional is

$$\delta J_i = \frac{\partial \Phi_i}{\partial \ddot{r}_i}\delta\dot{r}_i - \left(\frac{d}{dt}\frac{\partial \Phi_i}{\partial \ddot{r}_i} - \frac{\partial \Phi_i}{\partial \dot{r}_i}\right)\delta r_i + \frac{\partial \Phi_i}{\partial \ddot{\psi}_i}\delta\dot{\psi}_i - \left(\frac{d}{dt}\frac{\partial \Phi_i}{\partial \ddot{\psi}_i} - \frac{\partial \Phi_i}{\partial \dot{\psi}_i}\right)\delta\psi_i +$$

$$+ \left[2\Phi_i - \frac{\partial \Phi_i}{\partial \ddot{r}_i}\ddot{r}_i + \left(\frac{d}{dt}\frac{\partial \Phi_i}{\partial \ddot{r}_i} - \frac{\partial \Phi_i}{\partial \dot{r}_i}\right)\dot{r}_i - \frac{\partial \Phi_i}{\partial \ddot{\psi}_i}\ddot{\psi}_i + \right.$$

$$\left. + \left(\frac{d}{dt}\frac{\partial \Phi_i}{\partial \ddot{\psi}_i} - \frac{\partial \Phi_i}{\partial \dot{\psi}_i}\right)\dot{\psi}_i\right]\delta t\Big|_0^T + \int_0^T \left[\left(\frac{d^2}{dt^2}\frac{\partial \Phi_i}{\partial \ddot{r}_i} - \frac{d}{dt}\frac{\partial \Phi_i}{\partial \dot{r}_i} + \frac{\partial \Phi_i}{\partial r_i}\right)\delta r_i + \right.$$

$$\left. + \left(\frac{d^2}{dt^2}\frac{\partial \Phi_i}{\partial \ddot{\psi}_i} - \frac{d}{dt}\frac{\partial \Phi_i}{\partial \dot{\psi}_i} + \frac{\partial \Phi_i}{\partial \psi_i}\right)\delta\psi_i\right] dt. \qquad (2.3)$$

When the initial and final points are assigned, the variations of the boundary conditions in (2.3) drop out; equating to zero the expressions standing before the variations δr_i and $\delta\psi_i$ in the integrand, we obtain the Euler equations of this variational problem. On introduction of two new functions $\nu_i(t)$ and $\lambda_i(t)$, the system acquires the form

$$\dot{a}_{r_i} = (1/v_{r_i})\left[\frac{a_{r_i}^2 + a_{\varphi_i}^2}{2} + a_{r_i}\left(\frac{v_{\varphi_i}^2}{r_i} - \frac{k_i}{r_i^2}\right) - \lambda_i - \nu_i\frac{v_{\varphi_i}}{r_i}\right],$$

$$\dot{a}_{\varphi_i} = (1/r_i)(a_{\varphi_i}v_{r_i} - 2a_{r_i}v_{\varphi_i} + \nu), \quad \dot{\nu}_i = a_{\varphi_i}\Psi'_{i\psi_i} + a_{r_i}R'_{i\psi_i},$$

$$\dot{\lambda}_i = -v_{r_i}\left(a_{\varphi_i}\Psi'_{ir_i} + a_{r_i}R'_{ir_i} + \frac{\Psi_i}{r_i}a_{\varphi_i}\right) - \nu_i\frac{\Psi_i}{r_i} - R_i\dot{a}_{r_i} - \qquad (2.4)$$

$$- \frac{v_{\varphi_i}}{r_i}(\nu_i - 2a_{r_i}\Psi_i) \qquad (\dot{r}_i = v_{r_i},\ r_i(\dot{\psi}_i + \omega) = v_{\varphi_i}).$$

3. VARIATIONAL PROBLEM FOR FLIGHTS BETWEEN ORBITS IN A CENTRAL FIELD

Let us examine the problem of optimum flight in the sense of Integral (1) in a central field from a plane circular orbit 0:

$$r = r_0, \quad v_{r_0} = 0, \quad v_{\varphi_0} = v_{\text{орб}3} = \sqrt{k/r_0} \qquad (3.1)$$

to a plane circular orbit 1

$$r = r_1, \ v_{r_1} = 0, \ v_{\varphi_1} = v_{\text{орб.1}} = \sqrt{k/r_1} \qquad (3.2)$$

followed by return to orbit 0. Suppose that the total flight time $T_\Sigma = T + T'$ and the total angular displacement $\varphi_\Sigma = \varphi + \varphi'$ are given for this case.

The solution of the problem formulated may serve as a first approximation for the flight trajectory, taking the influence of the planets into account. The assigned values of the total flight time T + T' and the total angle φ + φ' determine T_n and T_σ by Formulas (1.5), (1.6), where $\delta\Psi_P = \delta\varphi_Z = 0$. 110

The optimum programming law for the thrust vector, given constant power, is determined by the extremals of Functional (1).

$$\dot{r} = v_r, \quad r\dot{\varphi} = v_\varphi, \quad \dot{v}_r = a_r + v_\varphi^2/r - k/r^2, \quad \dot{v}_\varphi = a_\varphi - v_r v_\varphi/r$$
$$\dot{a}_r = (1/v_r)\left[\frac{a_r^2 + a_\varphi^2}{2} + a_r\left(\frac{v_\varphi^2}{r} - \frac{k}{r^2}\right) - \lambda - \nu\frac{v_\varphi}{r}\right] \qquad (3.3)$$
$$\dot{a}_\varphi = (1/v_r)(a_\varphi v_r - 2a_r v_\varphi + \nu).$$

The optimum boundary conditions for the boundary-value problem are found from the vanishing condition for the terms outside the integral sign in the first variation of the functional. The variation of the functional's boundary values is written in the form (see (2.3)):

for the 0-1 flight:

$$\delta J = -2\nu\delta\varphi - 2\lambda\delta T, \qquad (3.4)$$

for the return flight 1-0:

$$\delta J' = -2\nu'\delta\varphi' - 2\lambda'\delta T'. \qquad (3.5)$$

At the initial and final points, $\underline{r}$, v_r and v_φ are assigned, so that the variations of these quantities have dropped out of (3.4) and (3.5). The minimum of the functional

$$\int_0^{T_\Sigma} a^2 dt = \int_0^{T} a^2 dt + \int_T^{T+T'} a^2 dt$$

with respect to the boundary values corresponds to vanishing of the sum of the boundary-value variations:

$$\delta J + \delta J' = -2(\nu\delta\varphi + \nu'\delta\varphi' + \lambda\delta T + \lambda'\delta T') =$$
$$= -2[\nu\delta(\varphi + \varphi') - \nu\delta\varphi' + \nu'\delta\varphi + \lambda\delta(T + T') - \lambda\delta T' + \lambda'\delta T']. \qquad (3.6)$$

Since T + T' = T_Σ and φ + φ' = φ_Σ are assigned, then δ(T + T') = = δ(φ + φ') = 0 and the vanishing condition for Expression (3.5) is

satisfied if

$$\nu = \nu', \quad \lambda = \lambda'. \tag{3.7}$$

Substitution of variables as follows in the equation system (3.3) for the central field –

$$t \to -t, \quad \varphi \to -\varphi, \quad v_r \to -v_r, \quad a_\varphi \to a_\varphi \tag{3.8}$$

does not affect the form of the equations, i.e., for each outgoing trajectory from 0 to 1 we can construct a return trajectory from 1 to 0 symmetrical to it according to the law (3.8). This property makes it possible to limit ourselves to calculation of trajectories from orbit 0 to orbit 1; the family of return trajectories is obtained by conversion using Formulas (3.8). The integral characteristics of the outgoing trajectory and the return trajectory symmetrical to it are the same:

$$T = T', \ \varphi = \varphi', \int_0^T a^2 dt = \int_0^{T'} (a')^2 dt, \ \nu = \nu', \ \lambda = \lambda'. \tag{3.9}$$

It should be noted that the necessary condition (3.7) for the optimum combination of the outgoing and return voyages is satisfied when a flight (3.9) symmetrical to the outgoing flight is used as the return flight.

It follows from the above that the initial and final points of the trajectory (3.1), (3.2) are singular points, i.e., the relationship

$$^1/_2 a_0^2 - \lambda - \nu v_{\varphi_0}/r_0 = 0, \ ^1/_2 a_1^2 - \lambda - \nu v_{\varphi_1}/r_1 = 0.$$

is satisfied at these points (see [1]).

Let us express $\frac{1}{2} a_1^2$ in terms of $\frac{1}{2} a_0^2$ and ν:

$$^1/_2 a_1^2 = {}^1/_2 a_0^2 - \nu (v_{\varphi_0}/r_0 - v_{\varphi_1}/r_1).$$

If $r_1 > r_0$ then it follows from the condition $a_1^2 \geq 0$ that

$$\nu \leqslant \frac{a_0^2}{2(v_{\varphi_0}/r_0 - v_{\varphi_1}/r_1)}, \tag{3.10}$$

i.e., for an assigned value of a_0, the possible values of the parameter ν have an upper bound.

Let us write the system of equations (3.3) in dimensionless form; for this purpose, we refer $\underline{r}$ to r_0, $\underline{t}$ to $t_0 = 1/\omega_0$ and all derivative quantities (v_r, v_φ, a_r, a_φ, ν, λ) to the corresponding combinations of r_0 and ω_0. If $r_0^3\omega_0^2 = k$, then the coefficient $\underline{k}$ vanishes in the equations. In the new system of equations, we vary the scale of the radial distance $r^* = r\underline{l}$. If simultaneously we set

$$t^* = l^{3/2}t, \quad v_r^* = l^{-1/2}v_r, \quad v_\varphi^* = l^{-1/2}v_\varphi, \quad a_r^* = a_r l^{-2}, \quad a_\varphi^* = a_\varphi l^{-2}, \quad (3.11)$$
$$\lambda^* = \lambda l^{-4}, \quad \nu^* = \nu l^{-3/2},$$

then the form of the equations will not be affected. This means that flight in a central field from orbit r_0 to orbit r_1 may be converted by Formulas (3.11) to flight from orbit $r_0\underline{l}$ to orbit $r_1\underline{l}$.

Flights whose trajectories do not enter the planet's sphere of influence but pass close to it (flybys) are of interest. The average angular-displacement velocity of flights of this type must be exactly equal to the angular velocity of the earth's revolution about the sun:

$$\Delta\varphi = \omega_1 T. \quad (3.12)$$

The boundary conditions at the beginning of the trajectory remain the same (3.1), while at the end the condition $v_{\varphi_1} = v_{\varphi_{orb.}}$ is replaced by the condition of continuous conjugation of the outgoing and return trajectories (3.8):

$$a_\varphi(T) = 0. \quad (3.13)$$

It is this condition that is optimal in the sense of minimizing the functional of J with respect to the boundary values. Actually,

$$\delta J = 2a_\varphi \, \delta v_\varphi|_{t=T}, \quad (3.14)$$

from which (3.13) follows.

4. FLIGHTS IN THE REGION WHERE THE SUN'S INFLUENCE PREDOMINATES, TAKING THE PLANETARY GRAVITATIONAL FORCES INTO ACCOUNT

As was indicated earlier, the boundary-value problem of flight in the sphere of predominant influence of the sun is fully defined by as-

signing the coordinates of the points N* and the directions of the velocity θ_1 vector at these points, together with the angular displacement φ and the time T of this displacement between the points N*. Below, in Section 8, it is shown that taking the planetary forces into account has little effect on the integral characteristics $I, q, \int a dt$ of the flight, so that it is appropriate to employ the same values of a_0 and v as correspond to the assigned φ and T in the central field. Leaving aside selection of the coordinates for the N* points, let us consider what must be the optimum direction of the velocity θ_1 vector.

We write out the first variation of the functional boundary values, regarding all quantities except θ_1 as assigned at the N* points:

$$\delta J = 2a_1 r_1 \sin\gamma_1 \delta\theta_1 \Big|_0^T. \qquad (4.1)$$

We have the following relationships between the quantities in the heliocentric and planetary coordinate systems:

$$\theta_1 + \gamma_1 - \psi_1 = \theta_2 + \gamma_2 - \psi_2,$$
$$\sin(\theta_2 - \gamma_2) = (v_1 / v_{\infty}) \sin(\gamma_2 - \gamma_1), \qquad (4.2)$$

so that assigning γ_1 with ψ_1, ψ_2, v_1 and γ_2 known defines θ_1. The condition for vanishing of the variation at the terminals reduces to the condition

$$\sin\gamma_1 = 0, \text{ i.e., } \gamma = 0 \text{ or } \pi \qquad (4.3)$$

This means that the direction of the velocity θ_1 vector at the N* points must coincide with the direction of the thrust vector or be proportional to it.

Let us note certain limitations imposed on the coordinates of the N* points. For a given energy $E = E^*$ with respect to the planet corresponding to "capture" of the material point by the planet, and given coordinates of the point N* (r_1, ψ_1), the absolute magnitude of the velocity v_1 is uniquely determined. Here, the closer N* is to the boundary of region D_2*, the smaller will be the magnitude of v_1, which tends

to zero as a limit. Since the acceleration vector $\vec{a}$ due to the reaction thrust must be opposed to the velocity vector $\vec{v}_1$ at point N*, then for any value of $|\vec{a}|$ we find a point $N^*(r_1, \psi_1)$ with its own value of v_1 such that the absolute magnitude of v_1 will first diminish to zero under the influence of the acceleration $\vec{a}$ and will then increase; here, the direction of the vector $\vec{v}_1$ coincides with that of the acceleration vector $\vec{a}$ and the energy E with respect to the planet will increase monotonically according to (1.1). Here the "capture" condition (1.3) is violated. Consequently, for each value of the acceleration $\vec{a}$ there exists a certain limiting value, bounded from below, for the velocity modulus and, accordingly, a limiting position of the points $N^*(r_1, \psi_1)$.

The trajectories of optimum flights in a two-body field (field of the sun and the first planet up to the point where the gravitational forces from the two planets are equal, and from that point on that of the sun and the second planet) are described by the differential equation system (2.1), (2.4) (where i = 2) with the following boundary conditions, which are written in the heliocentric coordinate system:

for t = 0

$$r_2 = \sqrt{r_{03}^2 + r_{13}^2 + 2r_{03}r_{13}\cos\psi_{13}}, \quad \operatorname{tg}\psi_2 = r_{13}\sin\psi_{13}/(r_{03} + r_{13}\cos\psi_{13})$$
$$v_{r_2} = v_{13}\sin(\theta_{13} - \psi_{13} + \psi_{23}) + r_{03}\omega_3\cos\psi_{23}, \qquad (4.4)$$
$$v_{\varphi_2} = v_{13}\cos(\theta_{13} - \psi_{13} + \psi_{23}) + r_{03}\omega_3\sin\psi_{23}, \quad \varphi_2 = 0,$$

for t = T:

$$r_2 = \sqrt{r_{0\text{П}}^2 + r_{1\text{П}}^2 + 2r_{0\text{П}}r_{1\text{П}}\cos\psi_{1\text{П}}}, \quad \operatorname{tg}\psi_2 = r_{1\text{П}}\sin\psi_{1\text{П}}/(r_{0\text{П}} + r_{1\text{П}}\cos\psi_{1\text{П}})$$
$$v_{r_2} = v_{1\text{П}}\sin(\theta_{1\text{П}} - \psi_{1\text{П}} + \psi_{2\text{П}}) + r_{0\text{П}}\omega_{\text{П}}\cos\psi_{2\text{П}} \qquad (4.5)$$
$$v_{\varphi_2} = v_{1\text{П}}\cos(\theta_{1\text{П}} - \psi_{1\text{П}} + \psi_{2\text{П}}) + r_{0\text{П}}\omega_{\text{П}}\sin\psi_{2\text{П}}, \quad \varphi_2 = \Delta\varphi,$$

where θ_{1Z} and θ_{1P} are determined from Conditions (4.2)-(4.3).

In numerical integration of this system, as for the case of the central field, the boundary-value problem was reduced to the Cauchy problem, and the two parameters a_{r0} and γ_{20} at the beginning of the

trajectory were selected to make the velocity vector $\overline{V}_{1P}$ (v_{1P}, θ_{1P}) with respect to the planet fall on the projections specified for the end of the trajectory. The initial angle between the radius vectors of the two planets φ_P was specified in such a way that when the assigned $r_{2\,P}$ was reached, the angle $\psi_{2P} = \varphi - \omega_P T$ would be equal to the assigned angle.

5. Acceleration and Deceleration Trajectories in the Planetary Field of Influence

If the coordinates of the point N* satisfy the condition indicated above under heading 4, the flight trajectory can be extended into the region D_2*. As was indicated earlier, three elements defining an osculating ellipse for a specified time T_R correspond to each set of three quantities r_1, ψ_1 and θ_1, when the trajectory is extended continuously. We subject the angle θ to Condition (4.3).

The search for optimum trajectories in region D_2* is the Cauchy problem for Eqs. (2.1) and (2.4), where $(i = 1)$ we have from a point N* with the following initial conditions:

$$t = 0, \quad r_1 = r_{1N^*}, \quad \psi_1 = \psi_{1N^*}, \quad v_{r_1} = v_1 \sin\theta_1, \quad v_{\varphi_1} = v_1 \cos\theta_1,$$
$$a_{r_1} = a_1 \sin(\theta_1 + \gamma_1), \quad a_{\varphi_1} = a_1 \cos(\theta_1 + \gamma_1), \quad \dot{v}_1 = \dot{a}_{\varphi_1} r_1 - a_{\varphi_1} v_{r_1} + 2 a_{r_1} v_{\varphi_1}, \tag{5.1}$$
$$\dot{\lambda}_1 = -\dot{a}_{r_1} v_{r_1} + \tfrac{1}{2} a_1^2 + a_{r_1}(v_{\varphi_1}^2 / r_1 - 1/r_1^2) - v_1 v_{\varphi_1} / r_1,$$

where

$$\dot{a}_{r_1} = \dot{a}_{r_2} \cos(\psi_1 - \psi_2) - \dot{a}_{\varphi_2} \sin(\psi_1 - \psi_2) + a_{\varphi_1}(v_{\varphi_1}/r_1 - v_{\varphi_2}/r_2),$$
$$\dot{a}_{\varphi_1} = \dot{a}_{\varphi_2} \cos(\psi_1 - \psi_2) - \dot{a}_{r_2} \sin(\psi_1 - \psi_2) - a_{r_1}(v_{\varphi_1}/r_1 - v_{\varphi_2}/r_2).$$

Here the deceleration from point N* is characterized by $t > 0$ and $\gamma_1 = 0$, and the acceleration to point N* by $t < 0$ and $\gamma_1 = \pi$.

RESULTS OF OPTIMUM-TRAJECTORY CALCULATIONS

6. Optimum Flights Between Planetary Orbits

At the boundary of the planet's sphere of influence, the velocity of the apparatus in a system of coordinates connected to the planet is small by comparison with the orbital velocity of the planet, and the

dimensions of the planet's sphere of influence are small as compared with the radius of its orbit. In first approximation, therefore, the flight between orbits may be regarded as taking place in the central field of the sun's gravitational forces.

At the start of the earth-to-planet flight (t = 0), the rocket is on the earth's orbit, $r_0 = R_0$, and has a zero radial velocity component $v_r = 0$ and a tangential component equal to the orbital velocity of the earth $v_\varphi(0) = v_{orb.Z}$; at the end of the flight from the earth to the planet, t = T, $r(T) = R_1$, $v_r(T) = 0$ and $v_\varphi(T) = v_{orb.P}$ (R_1 is the radius of the planet's orbit and $v_{orb.P}$ is the planet's orbital velocity).

In analyzing interorbital round-trip flights, it has been assumed universally that the return trajectory is symmetrical to the outgoing trajectory ($T = T'$, $\varphi = \varphi'$).

The calculations employed dimensionless parameters as follows: the radius was referred to the orbit radius of the inner planet; time to the period of revolution of the inner planet about the sun, divided by 2π; velocity to the angular velocity on the orbit of the inner planet; acceleration to the acceleration due to the sun's attraction at this orbit; angular velocity to the angular velocity of the inner planet.

The distances from Venus, the earth, and Mars to the sun, the accelerations due to the sun on the orbits of these planets and the periods of their revolution about the sun are listed in Table 1.

The ratios of the radii of the planets' orbits were assumed equal to their mean values, as follows:

for earth-to-Mars-to-earth flights:

$$r_1 = 1{,}52, \tag{6.2}$$

here,

$$v_{\text{орб.З}} = 1, \quad v_{\text{орб.М}} = 0{,}811, \quad \omega_З = 1, \quad \omega_М = 0{,}5335;$$

For earth-to-Venus-to-earth flights

$$r_1 = 1{,}38, \tag{6.3}$$

here

$$r_{\text{орб. в}} = 1, \quad v_{\text{орб. з}} = 0{,}852; \quad \omega_в = 1; \quad \omega_з = 0{,}617.$$

TABLE 1

Показатели 1	2 Венера	3 Земля	4 Марс
5 R_0 [млн. км]	108+1	149,5+2,5	228+20
6 g_0 [м/сек²]	0,0114	0,00594	0,00255
7 τ_0 [земн. сутки]	225	365	685

1) Quantity; 2) Venus; 3) earth; 4) Mars; 5) R_0 [millions of kilometers]; 6) g_0 [m/sec^2]; 7) τ_0 [terrestrial days].

The problem with boundary conditions (1.2), (1.3) for the differential system (3.3) of the variational problem was reduced to the Cauchy problem, which was then solved on electronic digital computers using the method of selected initial values.

The results of integration are presented in Table 2 for the a_0, ν, $\dot{a}_{r0}$, γ_0, T, φ_1 values for each of the flight trajectories for which the calculation was carried through. The trajectories are classified by initial values of the acceleration absolute magnitude $|a_0|$ and values of the parameter ν, which, in the boundary-value problem, correspond to certain values of the polar angle $\Delta\varphi$ of the flight and the flight time T between the orbits (to one terminal). We also present for each trajectory the initial values of the angle γ_0 between the thrust vector and the velocity vector and the initial value of the radial acceleration component time derivative $\dot{a}_{r0}$ that give the assigned v_{r_1} and v_{φ_1} for $r = r_1$.

Examples of the calculated trajectories are given in Figs. 3-5, and the time variation of the absolute-value acceleration $\underline{a}$ in Figs. 6-8. Figures 9-11 present plots of $a_y = f(a_x)$. It is seen that for large values of a_0, this relationship approaches the linear, which cor-

responds to the case of motion in a force-free field [1].

The appearance of the constant ν in Eqs. (3.3) makes it possible to obtain, for each value of the initial acceleration a_0, a set of trajectories with different values of the average rate of angular displacement $\omega_{sr} = \varphi(T)/T$; here, ω_{sr} diminishes with increasing ν (Fig. 12).

The case $\nu = 0$ corresponds to the minimum of the functional J for the assigned flight time between orbits (one way). With increasing initial acceleration, the time of flight between orbits will naturally be shortened and the functional J will increase accordingly (Fig. 13), but the minimum time of residence T_σ near the planet will remain large (Fig. 14):

$$T_{\sigma_{min}} = [2T/(\omega_2 - \omega_{II})](\omega_{cp} - \omega_3 + \pi k_{min}/T), \qquad (6.4)$$

where k_{min} is an integer corresponding to the minimum positive value of $T_\sigma \to T_{\sigma_{min}}$.

With $\nu = 0$, therefore, an increase in the initial acceleration (and the functional J) will reduce insignificantly the round-trip flight time from the earth to the planet and back.

Let us consider the influence of the parameter ν on the total flight time from the orbit of the earth to the planet and back.

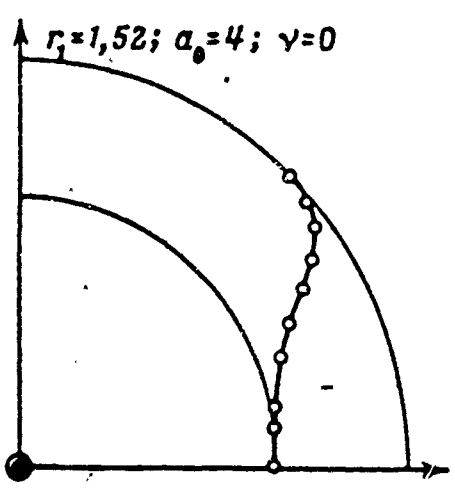

Fig. 3

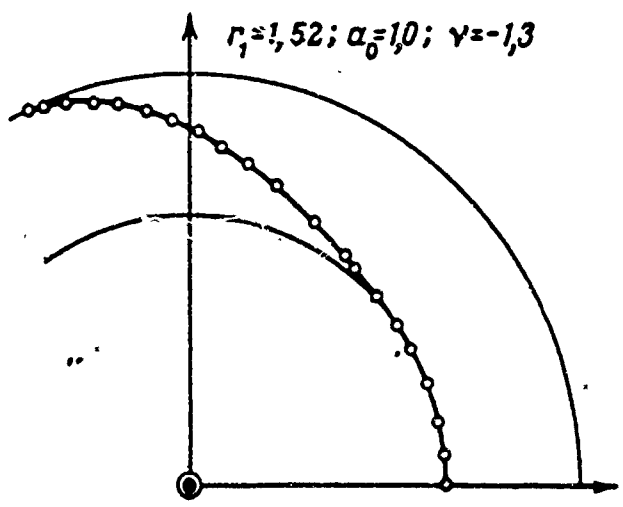

Fig. 4

Flight to an outer planet (Mars). In the case under consideration,

110

BLANK PAGE

TABLE 2

$r_1 = 1{,}52$

Значения 1	$a_0 = 0{,}02$	$a_0 = 0{,}2$			$a_0 = 0{,}5$				$a_0 = 1$				
v	0,000	—0,200	0,000	0,020	—0,500	0,000	0,100	0,200	—1,300	—1,240	—1,200	—1,100	—1,000
$\dot{a}_{r_0}$	0,001	0,020	0,015	—0,011	0,685	—0,125	—0,247	—0,324	1,326	1,273	0,830	0,835	0,089
γ_0	0,044	0,413	0,420	0,525	0,527	0,703	0,865	1,048	—0,604	—0,370	—0,176	—0,035	0,104
T	9,183	3,699	3,478	4,011	2,551	2,420	2,489	3,164	1,947	1,832	1,776	1,730	1,704
φ_1	6,987	2,730	2,636	2,880	2,361	1,812	1,845	2,051	1,973	1,776	1,6[illegible]	1,592	1,529
$\int_0^T a^2 dt$	0,004	0,042	0,037	0,032	0,403	0,178	0,138	0,126	1,053	0,972	0,933	0,871	0,826

	$a_0 = 1$						$a_0 = 2$	$a_0 = 3$	$a_0 = 4$			
v	—0,500	—0,400	—0,200	0,000	0,500	0,600	0,000	0,000	—7,000	—6,000	—1,000	0,000
$\dot{a}_{r_0}$	—0,100	—0,230	—0,461	—0,670	—1,095	—1,161	—2,170	—1,940	—0,100	—1,850	—7,300	—7,950
γ_0	0,556	0,626	0,764	0,898	1,251	1,337	1,065	1,150	0,350	0,520	1,100	1,205
T	1,673	1,681	1,700	1,741	1,966	2,085	1,239	0,935	0,920	0,901	0,874	0,880
φ_1	1,372	1,361	1,334	1,312	1,302	1,319	0,940	0,758	0,988	0,000	0,700	0,664
$\int_0^T a^2 dt$	0,652	0,632	0,586	0,538	0,447	0,444	1,578	2,769	5,920	5,625	4,696	4,561

1) Value of.

TABLE 2 (Cont'd)

$r_1 = 1{,}38$

Значения 1	$a_0 = 1$										$a_0 = 2{,}85$
ν	0,000	0,200	0,700	0,750	0,800	0,801	0,803	0,804	0,810	0,820	—4,200
$\dot{a}_{r_0}$	—0,908	—1,068	—1,372	—1,387	—1,389	—1,389	—1,388	—1,388	—1,386	—1,372	—1,380
$\dot{\gamma}_0$	0,980	1,103	1,441	1,488	1,546	1,548	1,551	1,853	1,562	1,588	0,525
T	1,492	1,516	1,786	1,864	1,974	2,003	2,009	2,000	2,069	2,140	0,908
φ_1	1,196	1,174	1,224	1,243	1,260	1,275	1,275	1,257	1,299	1,298	0,913
$\int_0^T a^2 dt$	0,465	0,420	0,399	0,406	0,415	0,424	0,425	0,420	0,440	0,446	2,930

	$a_0 = 3$			$a_0 = 3{,}5$					
ν	—4,500	—3,000	0,000	—5,440	—5,000	—4,400	—4,300	—3,500	0,000
$\dot{a}_{r_0}$	—1,600	—3,599	—6,070	—2,500	—3,250	—4,050	—4,150	—5,050	—7,788
$\dot{\gamma}_0$	0,535	0,950	1,207	0,570	0,649	0,730	0,700	0,843	1,232
T	0,888	0,864	0,864	0,824	0,818	0,810	0,810	0,800	0,801
φ_1	0,896	0,807	0,697	0,844	0,816	0,790	0,785	0,754	0,656
$\int_0^T a^2 dt$	3,160	2,884	2,502	3,927	3,835	3,730	3,719	3,601	3,173

1) Value of.

BLANK PAGE

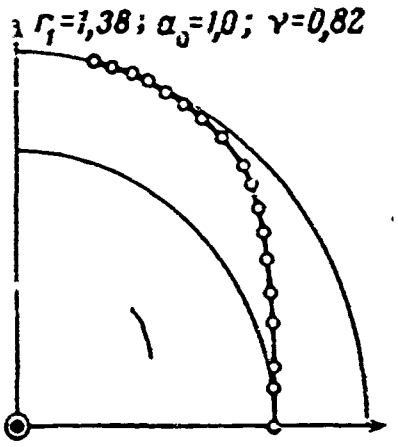

Fig. 5

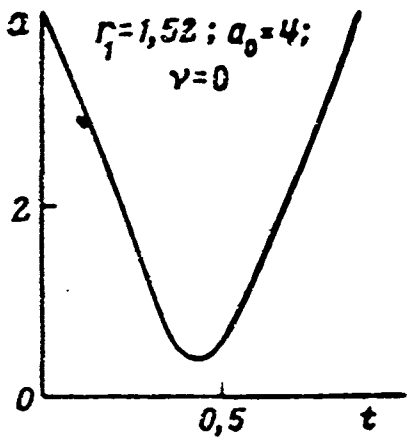

Fig. 6

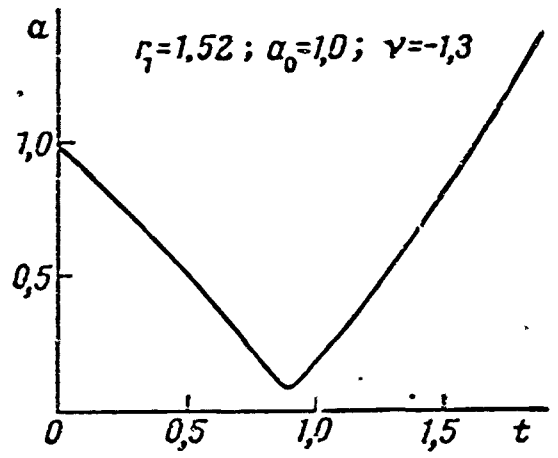

Fig. 7

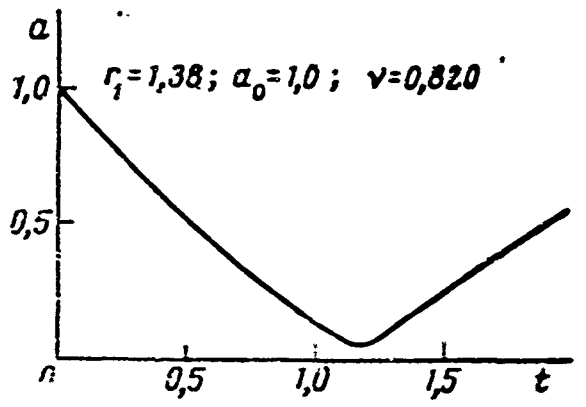

Fig. 8

$R_1 = 1.52$, $\omega_Z = 1$, $\omega_P = 0.5335$ and the total flight time will be given by the relationship

$$T_n = 2T + T_{c_{min}} = 2T + (2T/0{,}4665)\left(\omega_{cp} - 1 + \frac{\pi k_{min}}{T}\right). \quad (6.5)$$

With $\omega_{sr} < 1$, it follows from the condition $T_\sigma > 0$ that $k_{min} \geq 1$. Since an increase in ν reduces ω_{sr} (see Fig. 12), it is necessary to increase the value of ν in this region of ω_{sr} in order to shorten the round-trip flight time T_n. When ν is reduced, the values of ω_{sr} and T_n increase. But at $\omega_{sr} = 1$, the value of k_{min} changes abruptly from unity to zero. Accordingly, the total flight time also changes jumpwise to a value $T_n = 2T(T_\sigma = 0)$ for $\omega_{sr} = 1$ which corresponds to the "fast" flight to the planet and back. As ν is reduced further, the value $\omega_{sr} > 1$ and the residence time T_σ near the planet increases accordingly.

The analysis made is illustrated in Fig. 15 by the law of variation of the functional $J_n = 2\int_0^T a^2 dt$ (over two symmetrical flights: earth

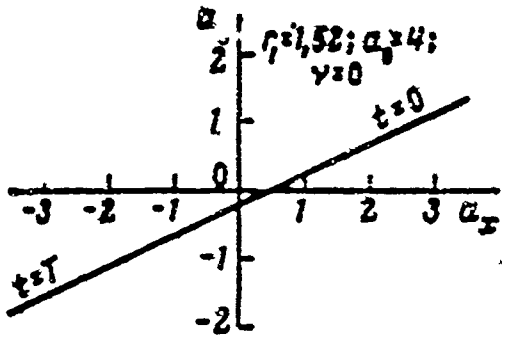

Fig. 9

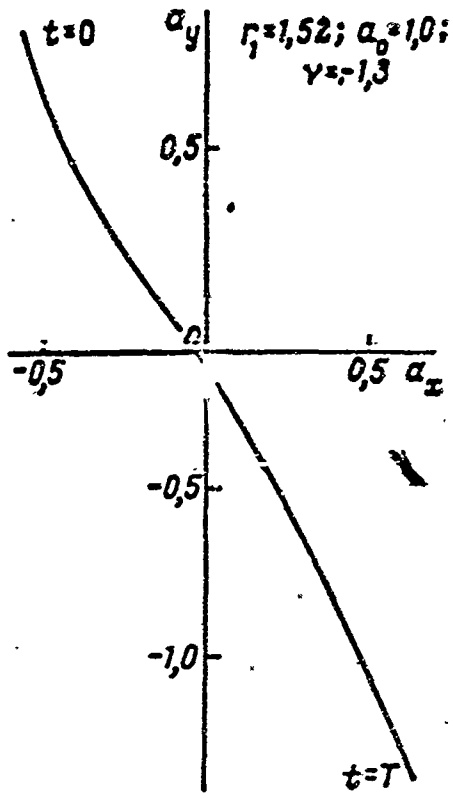

Fig. 10

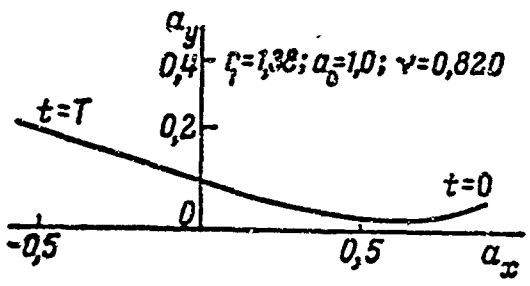

Fig. 11

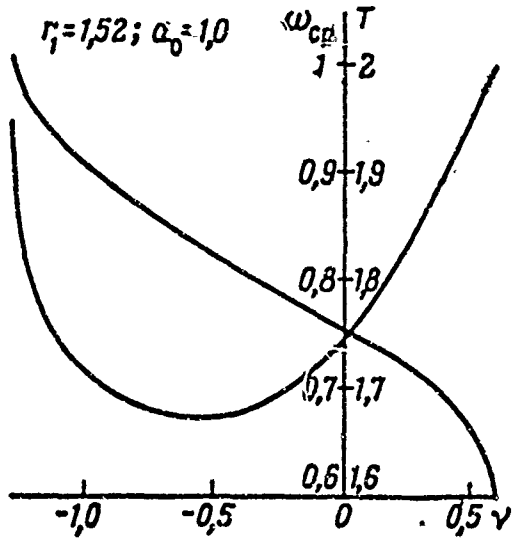

Fig. 12. ω_{sr}

to Mars and Mars to earth). The data of Fig. 15 permit indicating an optimum value of the parameter ν, one that provides for a minimum of J_n, i.e., maximum payload, for specified total flight time T_n and time of residence T_σ near the planet.

Similarly, nonsymmetrical flights (in which the trajectories of the flights to the planet and back to the earth do not coincide) can also be analyzed on the basis of the data in Table 2.

Flight to an inner planet (Venus). In this example, $R_1 = 1.38$; $\omega_Z = 1/R^{3/2} = 0.617$, $\omega_P = 1$. The minimum total flight time will be determined by the relationship

$$T_n = 2T + T_\sigma = 2T + (2T/0{,}383)(0{,}617 - \omega_{cp} - \pi k_{min}/T). \quad (6.6)$$

In consequence of the difference between Formulas (6.5) and (6.6), the effect will be the reverse of that examined above in the case of a flight to an outer planet.

For $\omega_{sr} > 0.617$ and $k_{min} = -1$, an increase in ν reduces ω_{sr} and T. With $\omega_{sr} = 0.617$, the value of k_{min} changes stepwise from -1 to zero; accordingly, the total flight time T_n also diminishes stepwise to a value $T_n = 2T$ ($T_\sigma = 0$).

As ν is further increased, we have $\omega_{sr} <$ < 0.617, and the time of residence near the

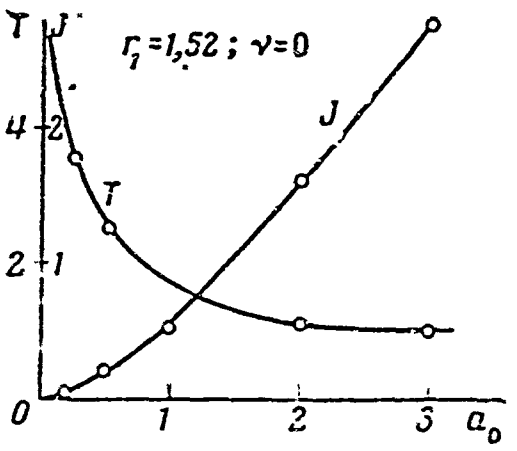

Fig. 13

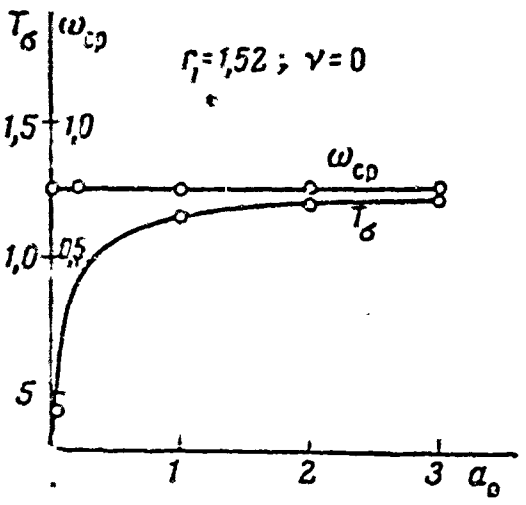

Fig. 14. ω_{sr}.

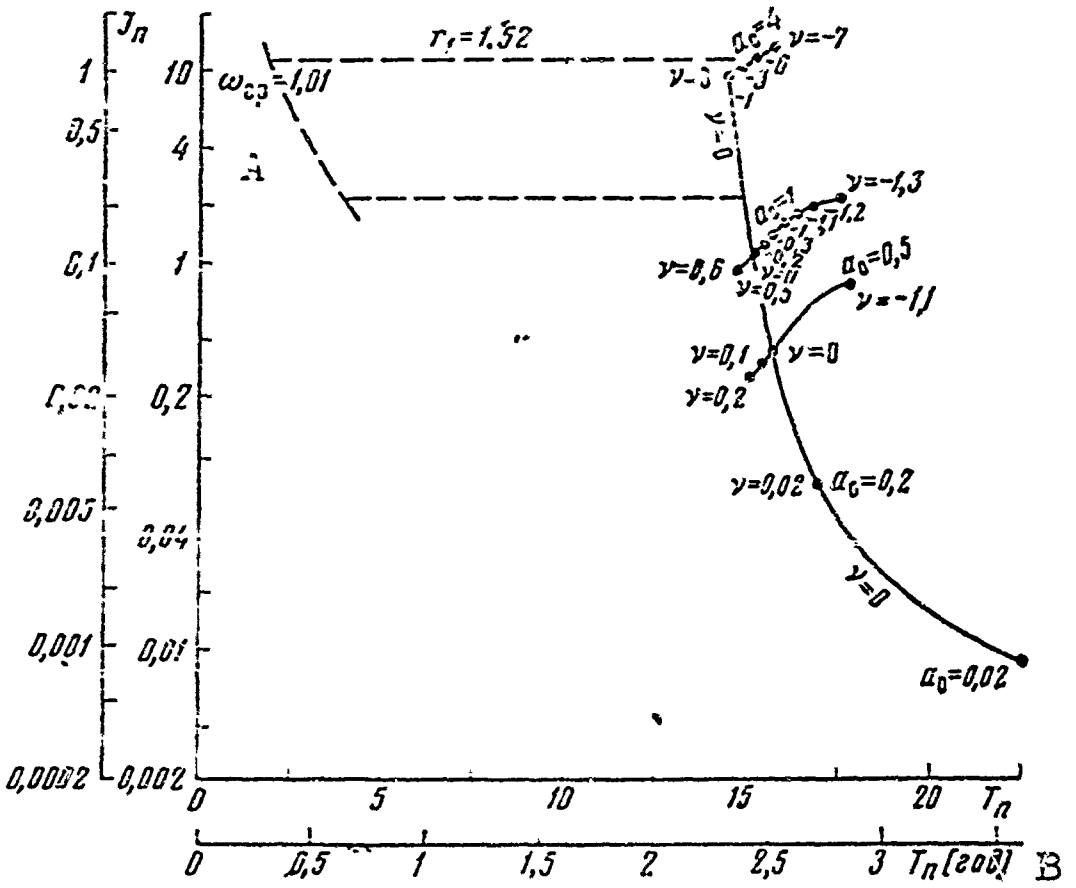

Fig. 15. A) ω_{sr}; B) [years].

TABLE 3

Значения 1	$a_0 = 1{,}45$		$a_0 = 1{,}5$	$a_0 = 2$
	$r_1 = 1{,}38$, $a_{0_1} = 0$			
ν	−1,940	−1,900	−2,000	−3,000
a_{r_0}	0,594	0,594	0,595	0,575
$\tilde{r}_0$	0,191	0,191	0,192	0,200
T	1,275	1,300	1,276	1,140
φ_1	1,279	1,297	1,284	1,216
$\int_0^T a^2 dt$	1,247	1,289	1,339	2,086

1) Value of.

planet increases accordingly.

Figure 16 presents an example of the variation of J_n as a function

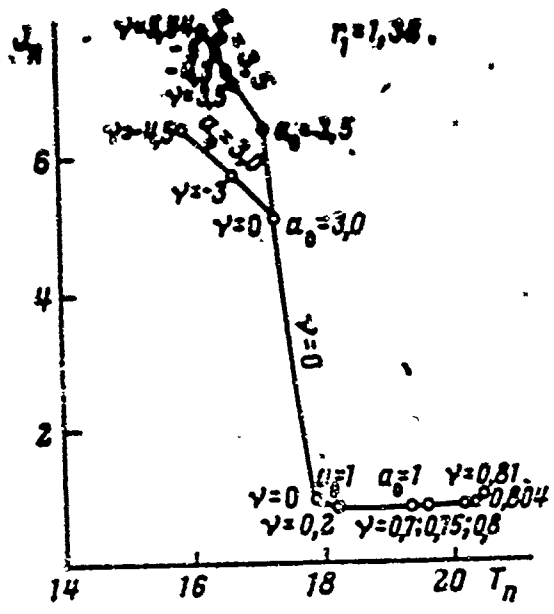

Fig. 16

of T_n for an earth-to-Venus-to-earth flight, in dimensionless quantities.

For flybys, the average velocity of angular displacement on flights of this type must be exactly equal to the angular velocity of the earth's revolution about the sun. As before, the flight "out" is regarded as symmetrical to the flight "back," and for this reason we compute only the first half of the voyage.

The boundary conditions at the origin of the trajectory remain the same (6.2), (6.3), and at the end the condition $v_\varphi(T) = v_{\varphi orb.P}$ is replaced by the optimum condition $a_\varphi(T) = 0$ (3.14), and the condition of equal angular displacements of the vehicle and the earth is written in the form (3.12).

Table 3 shows examples of this type of trajectory for $r_1 = 1.38$ and $\omega_{sr} = 1$, which corresponds to flight to an outer planet (for example, to Mars at a major opposition).

7. Optimum Segments for Acceleration and Deceleration Near Planets

For the accelerating and decelerating segments near the planet, the solution of the variational problem in its exact formulation (2.1), (2.4) and (5.1) was replaced by a calculation of the vehicle's motion from a certain initial circular orbit about the planet to a point E = = E** without "merging" of the resulting trajectory with the trajectory of the interorbital flight.

The radius of the initial circular orbit and the acceleration of the planet's gravity on this orbit were taken as characteristic quantities r_0 and g_0 (see (6.1)).

The calculations were made taking the influence of the sun into

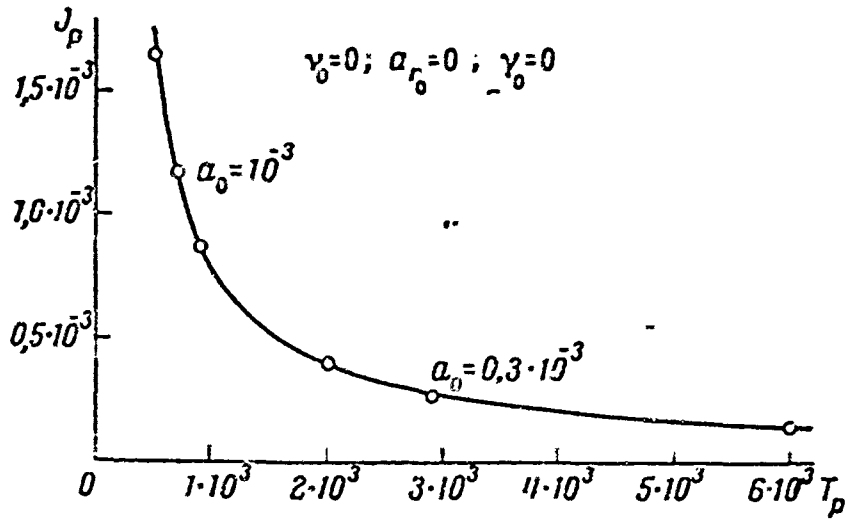

Fig. 17

account for a specific initial orbit about the earth, but the influence of the sun on the value of the functional J_p was found to be small, so that the gravitational field near the planet may be regarded as central within the framework of the approximation adopted, and we may use the results cited for computing acceleration trajectories at other planets, using other values of r_0 and g_0, in accordance with the similarity criteria for trajectories in a central field (3.11). Due to the "reversibility" property of trajectories in a central field (3.8), these results can also be used for the case of deceleration near planets.

In the case of optimum acceleration to the "breakaway" point in a specified time T_p, the initial value of the parameter ν is zero. The results of the calculation are shown in Fig. 17. The data obtained indicate that for optimum acceleration (deceleration) near the planet, the reaction-thrust acceleration $\vec{a}$ has practically the same direction as the velocity, varies only slightly along the trajectory, and increases somewhat toward the breakaway point (by 10-20%).

8. Influence of Planetary Gravitational Forces on Section of Flight Between Planet Orbits

Let us consider flights in the region where the sun's influence predominates, taking the gravitational forces from the planets into account with the object of studying the differences from the central

TABLE 4

r_{1M}	ψ_{1M}	T	$\int_0^T a^2 dt$	Δv
0,00700	3,1416	1,6905	0,5421	1,3060
0,00200	3,1416	1,6930	0,5414	1,3070
0,00200	3,0500	1,6940	0,5426	1,3080
0,00200	3,0000	1,6920	0,5404	1,3070
0,00200	2,9000	1,6925	0,5408	1,3070
0,00200	2,8500	1,6930	0,5410	1,3070
0,00050	3,1416	1,6870	0,5380	1,3040
0,00050	3,1300	1,6850	0,5359	1,3030
0,00050	3,1000	1,6850	0,5359	1,3030
0,00050	3,0500	1,6855	0,5361	1,3040
0,00050	2,9500	1,6860	0,5365	1,3040
0,00050	2,9000	1,6860	0,5368	1,3036
0,00050	2,8800	1,6860	0,5369	1,3037
0,00050	2,8500	1,6860	0,5372	1,3038
0,00025	3,1416	1,6860	0,5390	1,3030
A Центральное поле	—	1,7420	0,5390	1,3120

A) Central field.

TABLE 5

r_{13}	ψ_{13}	T	$\int_0^T a^2 dt$	Δv
0,0090	0	1,7487	0,4780	1,4528
0,0030	1,00	1,7551	0,4663	1,4815
0,0030	0,50	1,7506	0,4665	1,4736
0,0030	0,10	1,7466	0,4653	1,4682
0,0030	0,02	1,7449	0,4645	1,4665
0,0030	—0,50	1,7405	0,4617	1,4625
0,0010	0	1,7210	0,4491	1,4465
0,0005	0	1,7210	0,4485	1,4496
A Центральное поле	—	1,7400	0,4623	1,4574

A) Central field.

field; we shall limit ourselves to consideration of one-way flights. As our starting variant, we select a flight from the orbit of the earth to the orbit of Mars in a central field with $a_0 = 1$, $\nu = 0$ (see Table 2) and calculate a series of trajectories beginning near the libration point N^*_Z in the vicinity of the earth ($r_1 = 0.009$ and $\psi_1 = 0$) for various positions of N^*_M. The dependence of the integral characteristics $T, \varphi, \int_0^T a^2 dt$ on the positions of the point N^*_M is illustrated in Table 4. This table also gives the values of $T, \varphi, \int_0^T a^2 dt$ for the central field. Table 5 presents a list of the final parameter values for the return calculation from point $N^*_M(r_{1M} = 0.0005, \psi_{1M} = 3.14139)$ to various

BLANK PAGE

points N^*_Z corresponding in the central field to trajectories of flight with $a_0 = 0.786$, and $\nu = -0.554$.

As we see from Tables 4 and 5, taking the influence of planetary attraction into account for the flight segment between their orbits has little effect on the integral characteristics T, φ, and J. The results obtained testify to the possibility of evaluating the flight characteristics from the results of calculations in the central field.

Received 21 August 1963

REFERENCES

1. G.L. Grodzovskiy, Yu.N. Ivanov, V.V. Tokarev. Dokl. AN SSSR [Proc. Acad. Sci. USSR], 137, No. 5, 1081, 1961.
2. I.H. Irving, E.K. Blum. Vistas in Astronautics, 2, N.Y., 1959, page 191.
3. M.F. Subbotin. Kurs nebesnoy mekhaniki [Course in Celestial Mechanics], 2, ONTI [United Scientific and Technical Publishers], 1937.

Manuscript Page No.

[Footnotes]

97 The vector modulus of the velocity v_1 is determined from the coordinates $N^*(r_1, \psi_1)$:

$$v_1 = \sqrt{2E_{II}^* + 2k_1/r_1 + 2k_2/r_2 + r_2^2\omega^2}.$$

Manuscript Page No.

[Transliterated Symbols]

93 П = P = planeta = planet

93 З = Z = zemlya = earth

93 орб = orb = orbital'nyy = orbital

98 P = R [not identified]

Manu-
script
Page
No.

[Transliterated Symbols Cont'd]

106 M = M = Mars = Mars

107 B = V = Venera = Venus

108 cp = sr = sredniy = average

METHOD OF QUICKEST DESCENT AS APPLIED TO COMPUTATION OF INTERORBITAL TRAJECTORIES WITH ENGINES OF LIMITED POWER

Yu.N. Ivanov and Yu.V. Shalayev

In the variational problem of space-vehicle flights using an engine of limited power between coplanar circular orbits in a central gravitational field, two solution methods are considered: the Ritz method with the coefficients determined by the quickest-descent method and the method of functional quickest descent. The results of calculations are presented and the efficiencies of solving the problem by the two methods are compared.

* * *

Selection of optimum trajectories and optimum operating modes for the ideal limited-power engine reduces to finding the minimum extremals of the functional [1, 2]

$$J = \int_0^T a^2 dt,$$

where a is the reaction-thrust acceleration and T is the time of motion. For the two-dimensional flights between circular orbits in a central field, as considered in the present paper, the functional J and the boundary conditions are expressed in terms of Cartesian coordinates and their derivatives, as follows (Fig. 1):

$$J = \int_0^T \{[\ddot{x} - x/(x^2+y^2)^{3/2}]^2 + [\ddot{y} + y/(x^2+y^2)^{3/2}]^2\}\, dt, \qquad (1)$$

$$x(0) = 1, \quad y(0) = 0, \quad \dot{x}(0) = 0, \quad \dot{y}(0) = 1,$$

$$x(T) = r_1 \cos\varphi_1, \quad y(T) = r_1 \sin\varphi_1, \quad \dot{x}(T) = -\frac{1}{\sqrt{r_1}} \sin\varphi_1,$$

$$\dot{y}(T) = \frac{1}{\sqrt{r_1}} \cos\varphi_1.$$

Here φ_1 is the angle of the flight, r_1 is the radius of the final orbit, with the radius of the initial orbit taken as the unit of distance and the period of revolution on the initial orbit divided by 2π taken as the unit of time. All calculations are made for $r_1 = 1.52$, and the quantities φ_1 and T are parameters of the problem.

The problem of minimizing Functional (1) was solved by two methods: the Ritz method with the coefficients determined by quickest descent and the method of functional quickest descent.

1. THE RITZ METHOD WITH THE COEFFICIENTS DETERMINED BY QUICKEST DESCENT

The algorithm of the classical Ritz method as applied to find the minimum extremals of Integral (1) consists in the following [3]. A complete system of N linearly independent basis functions $\{\varphi_i(t)\}$ is selected such that

$$\varphi_i(0) = \dot{\varphi}_i(0) = \varphi_i(T) = \dot{\varphi}_i(T) = 0 \qquad (1.1)$$

together with functions $x^{(0)}(t)$, $y^{(0)}(t)$ that satisfy the boundary conditions (1). The solution is sought in the form of a linear combination

$$x_N(t) = x^0(t) + \sum_1^N a_i\varphi_i(t), \quad y_N(t) = y^{(0)}(t) + \sum_1^N b_i\varphi_i(t). \qquad (1.2)$$

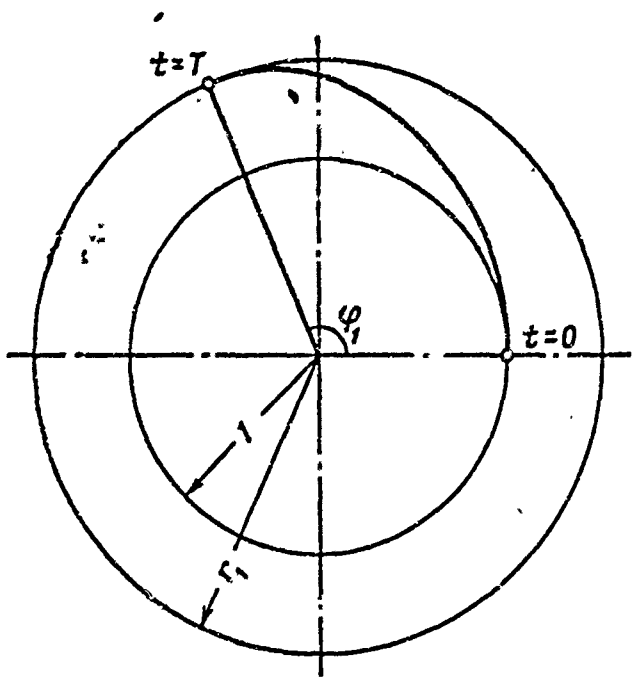

Fig. 1

After substituting $x_N(t)$, $y_N(t)$ in (1) in place of $\underline{x}$, $\underline{y}$, the latter is found to be a function of the coefficients a_i and b_i:

$$J = J(a_i, b_i). \qquad (1.3)$$

The problem of finding the minimum extremals of Functional (1) has thus been reduced to minimization of the function $J(a_i, b_i)$ with respect to a finite number of variables.

The function $J(a_i, b_i)$ can be minimized by the quickest-descent method, whose algorithm consists in the following [3].

Suppose that an initial approximation is known for the coefficients $a_i^{(0)}$, $b_i^{(0)}$; the next approximation is presented in the form

$$a_i^{(1)} = a_i^{(0)} - \lambda\,(\partial J/\partial a_i)^{(0)},\quad b_i^{(1)} = b_i^{(0)} - \lambda\,(\partial J/\partial b_i)^{(0)}$$
$$(\partial J/\partial a_i)^{(0)} = \frac{\partial J}{\partial a_i}(a_j^{(0)}, b_j^{(0)}),\quad (\partial J/\partial b_i)^{(0)} = \frac{\partial J}{\partial b_i}(a_j^{(0)}, b_j^{(0)}). \qquad (1.4)$$

The descent parameter λ is determined from the minimum condition for the function $J(\lambda) = J[a_i^{(0)} - \lambda(\partial J/\partial a_i)^{(0)}, b_i^{(0)} - \lambda(\partial J/\partial b_i)^{(0)}]$.

Thus, the minimization procedure proposed here consists of the following three iteration processes, which enclose one another sequentially:

1) the Ritz iteration process, which consists in increasing the number N of coefficients a_i, b_i from step to step in Expansion (1.2);

2) the iteration process of quickest descent, which consists in finding the minimum of Function (1.3) on each step of the Ritz iteration process;

3) the iterative process of finding the descent parameter λ on each step of the quickest-descent iteration process.

Basis functions $\varphi_i(t)$ of power-series form

$$\varphi_i(t) = (t/T)^{i+2}(i - t/T)^2 \quad (i = 0, 1, \ldots, N), \qquad (1.5)$$

were selected for the solution of Problem (1), while the zeroth-approximation functions selected were solutions of Problem (1) for a field of zero force [1]:

$$x^{(0)}(t) = 1 + \left[\frac{3(r_1\cos\varphi_1 - 1)}{T^2} + \frac{\sin\varphi_1}{\sqrt{r_1}T}\right]t^2 - \left[\frac{2(r_1\cos\varphi_1 - 1)}{T^3} + \frac{\sin\varphi_1}{\sqrt{r_1}T^2}\right]t^3$$
$$y^{(0)}(t) = t + \left(\frac{3r_1\sin\varphi_1 - 2T}{T^2} - \frac{\cos\varphi_1}{\sqrt{r_1}T}\right)t^2 + \left(-\frac{2r_1\sin\varphi_1 - T}{T^3} + \frac{\cos\varphi_1}{\sqrt{r_1}T^2}\right)t^3. \qquad (1.6)$$

The law of convergence of the functional J by iteration numbers K of the Ritz process ($T = 2$, $\varphi_1 = 2$) is presented in Fig. 2, where the

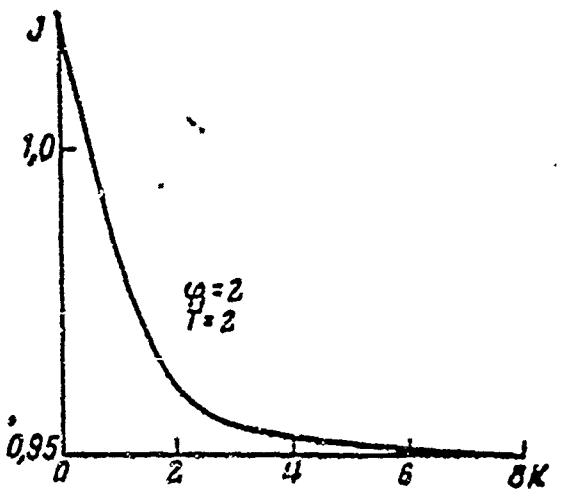

Fig. 2

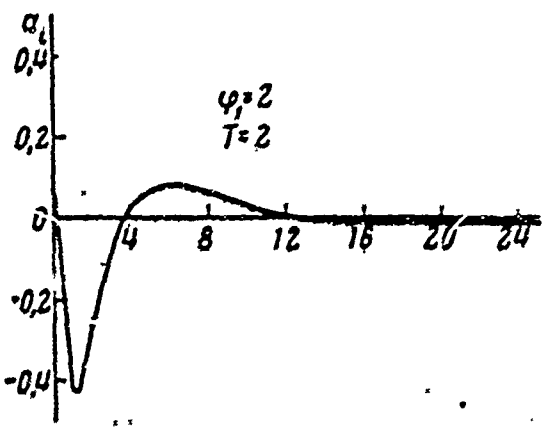

Fig. 3

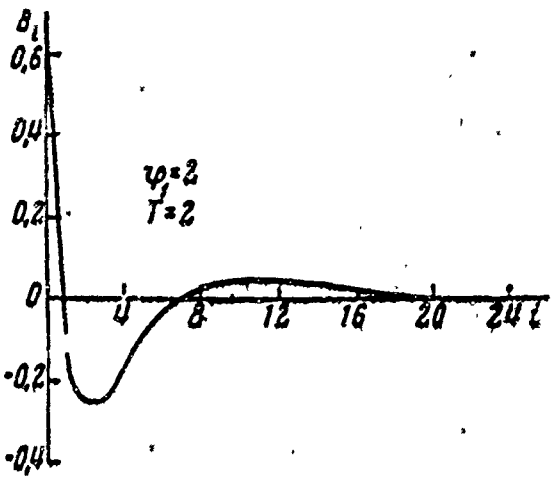

Fig. 4

solid line connects discrete points $J^{(0)}$, $J^{(1)}$, ..., $J^{(8)}$ (K = 0 corresponds to the zero-force field). Five coefficients a_i, b_i (N = 5) each are considered on the first iteration; on passage to each subsequent iteration, the number of coefficients is increased by 10 ($\Delta N = 5$), with the initial values of the ten new coefficients zero, while the initial values taken for the old coefficients are their values from the preceding iteration. The quantities a_i, b_i are indicated arbitrarily by the unbroken line in Figs. 3 and 4 as functions of the number i for K = 8.

2. METHOD OF FUNCTIONAL QUICKEST DESCENT

The iterative process of functional quickest descent as applied to Problem (1) consists in the following [4-7].

From the known zeroth approximation $x^{(0)}(t)$, $y^{(0)}(t)$, which satisfies the boundary conditions (1), we determine functions $\eta_x(t)$, $\eta_y(t)$, which vanish together with their first derivatives at the ends of the interval; for example, the expression for η_x takes the form

$$\eta_x = \int_0^t\int_0^t\int_0^t\int_0^t E_x^{(0)}dt^4 - \frac{t^3}{T^3}\left(T\int_0^T\int_0^t\int_0^t\int_0^t E_x^{(0)}dt^3 - 2\int_0^T\int_0^t\int_0^t\int_0^t\int_0^t E_x^{(0)}dt^4\right) - \frac{t^2}{T^2}\left(3\int_0^T\int_0^t\int_0^t\int_0^t\int_0^t E_x^{(0)}dt^4 - T\int_0^T\int_0^t\int_0^t\int_0^t E_x^{(0)}dt^3\right), \qquad (2.1)$$

where

$$E_x^{(0)} = \left(\frac{d^2}{dt^2}\frac{\partial}{\partial \ddot{x}} + \frac{\partial}{\partial x}\right) \Phi\left(x^{(0)}(t),\ y^{(0)}(t),\ \ddot{x}^{(0)}(t),\ \ddot{y}^{(0)}(t)\right),$$

$$\Phi = [\ddot{x} + x/(x^2+y^2)^{3/2}]^2 + [\ddot{y} + y/(x^2+y^2)^{3/2}]^2.$$

We may replace $\underline{x}$ with $\underline{y}$ to obtain the expression for η_y.

The sought function on the next step of the iteration process is presented in the form

$$x^{(1)}(t) = x^{(0)}(t) + \lambda_x \eta_x(t), \quad y^{(1)}(t) = y^{(0)}(t) + \lambda_y \eta_y(t). \qquad (2.2)$$

The descent parameters λ_x and λ_y are found from the minimum condition of the function $J(\lambda_x, \lambda_y)$ on the step in question:

$$\partial J / \partial \lambda_x = 0, \quad \partial J / \partial \lambda_y = 0. \qquad (2.3)$$

The approximation to the sought solution takes place together with a step-to-step diminution of the two quantities $(\partial J / \partial \lambda_x)_{\lambda_x=\lambda_y=0}$, $(\partial J / \partial \lambda_y)_{\lambda_x=\lambda_y=0}$ concerning which we know that they are nonpositive. The moment at which the sought minimum is reached can be determined with a specified accuracy from these two integral characteristics.

To avoid numerical differentiation in determining the functions η_x and η_y (2.1), let us present the double integral as follows:

$$\int_0^t\int_0^t E_x^{(0)} dt^2 = \frac{\partial \Phi^{(0)}}{\partial \ddot{x}}(t) - \frac{\partial \Phi^{(0)}}{\partial x}(0) + \int_0^t\int_0^t \frac{\partial \Phi}{\partial x} dt^2 - t\frac{d^2}{dt^2}\frac{\partial \Phi^{(0)}}{\partial \ddot{x}}(0)$$

and proceed analogously for the variable $\underline{y}$. This makes it possible to get by with values of the functions $x^{(0)}(t)$, $y^{(0)}(t)$ and their second derivatives $\ddot{x}^{(0)}(t)$, $\ddot{y}^{(0)}(t)$ in calculating the functions η_x and η_y without resorting to calculation of third and fourth derivatives. Consequently, it is necessary to "store" for the computation process only tables of the functions $x(t)$, $y(t)$ and the second derivatives $\ddot{x}(t)$, $\ddot{y}(t)$. Correspondingly, the second derivatives $\ddot{\eta}_x(t)$, $\ddot{\eta}_y(t)$ are stored together with the functions $\eta_x(t)$, $\eta_y(t)$. Taking this remark into account, we shall present the functions η_x, η_y and their second derivatives $\ddot{\eta}_x$, $\ddot{\eta}_y$ in the form

$$\eta_{1x} = t\int_0^t M_x dt - \int_0^t tM_x dt - {}^1/_6 c_{0x} t^3 - {}^1/_2 c_{1x} t^2, \qquad \ddot{\eta}_{1x} = M_x - c_{0x} t - c_{1x}, \quad (2.4)$$

where

$$M_x = t\int_0^t \frac{\partial \Phi}{\partial x} dt - \int_0^t t\frac{\partial \Phi}{\partial x} dt + \frac{\partial \Phi}{\partial \dot{x}},$$

$$c_{1x} = \frac{6}{T^2}\int_0^T ({}^2/_3 T - t) M_x dt, \qquad c_{0x} = \frac{6}{T^3}\int_0^T (2t - T) M_x dt.$$

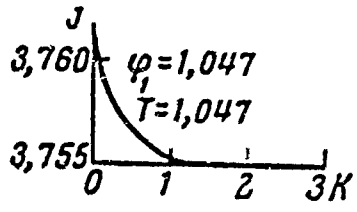

Fig. 5

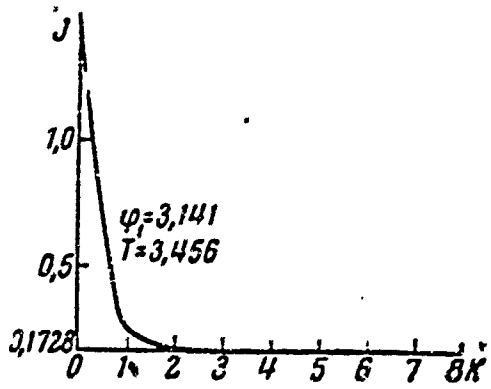

Fig. 6

Use of the method of functional quickest descent was found to be highly effective for Problem (1). While the computer time for one variant on an ETsVM [Electronic Digital Computer] using the Ritz method in combination with the quickest-descent method is approximately 100 minutes, this variant can be figured in 1-2 minutes by the method of functional quickest descent, and with the same accuracy (4-5 places).

The nature of the method's convergence is shown in Figs. 5 and 6, where the iteration numbers are laid off on the axis of abscissas and the corresponding values of the functional are plotted against the axis of ordinates; the discrete points are connected by a curve. For both examples, the initial approximation selected was an optimum trajectory satisfying the boundary conditions in a zero-force field. Comparison of the numbers of iterations in the two cases makes it possible to judge of the applicability of the zero-force-field optimum trajectory as the zeroth approximation: the shorter the trajectory and the shorter the time of motion along it, the better will the zero-force field approximate the central field.

A network of optimum flights was computed by the described method

for parameter values $0 \leqslant \varphi_1 \leqslant \varphi_1^* \sim \pi$, $0 \leqslant T \leqslant T^* \sim \pi$, $r_1 = 1{,}52$. An attempt to use the optimum trajectory in a zero-force field for angles $\varphi_1 > \varphi_1^*$ as the zeroth approximation came up against the following difficulty. It was found that for these flight angles, the functional being investigated does not possess a unique minimum and that use of the solution in the zero-force field as the zeroth element gives values of the minimum that exceed those expected. This signifies impossibility of using the zeroth element alone for the entire range of parameter variation.

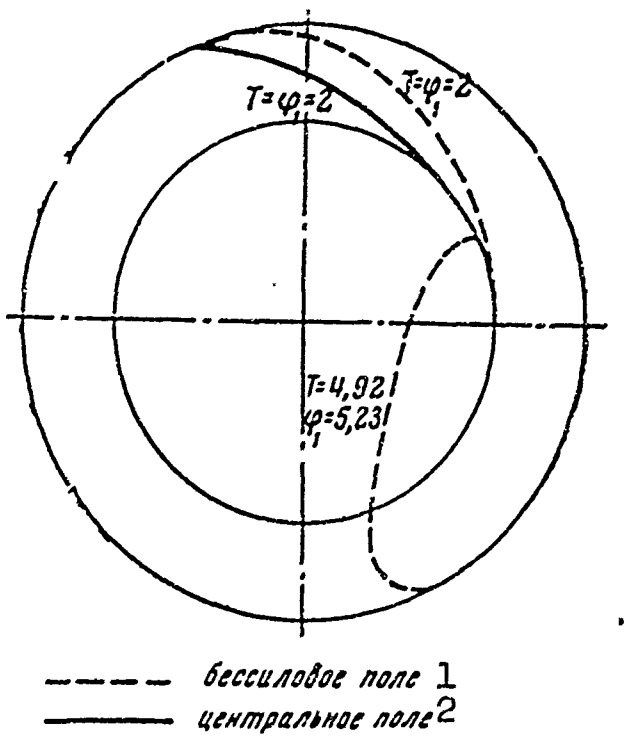

Fig. 7. 1) Zero-force field; 2) central field.

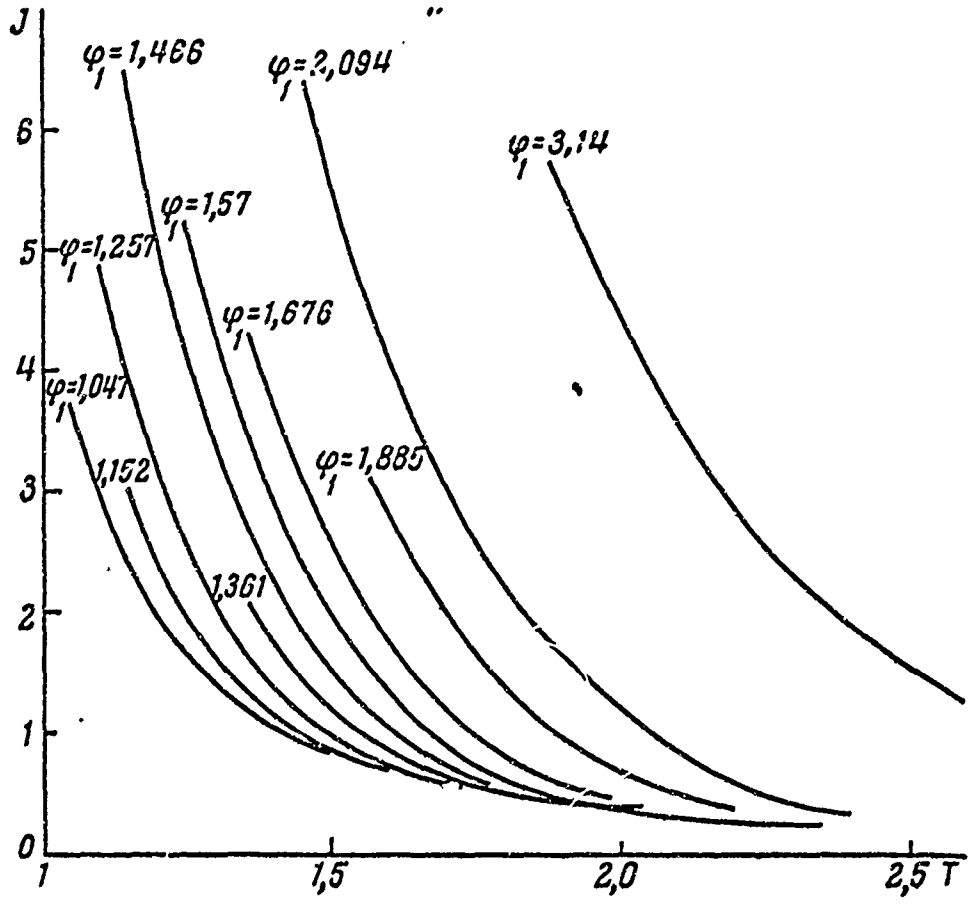

Fig. 8

The above is illustrated in Fig. 7, which gives optimum trajectories for the zero-force and central fields for $\varphi_1 = 2$, $T = 2$ and the optimum trajectory of the zero-force field for $\varphi_1 = 5.23$ and $T = 4.93$.

The latter does not envelop the gravitation center. This can apparently serve as a superficial criterion for the unsuitability of this trajectory as the zeroth element of the iterative process.

The following procedure can be recommend for finding the initial element in constructing a network with one or several parameters.

Let the optimum trajectory be known for certain values of the parameters and let it be required to construct a new optimum trajectory for parameter values close to the former; the boundary conditions imposed on the new trajectory differ from the old boundary conditions.

We transform the old trajectory, for example, by multiplying by a certain arbitrary function differing little from unity, a function that provides for satisfaction of the assigned boundary conditions on the new trajectory. The latter can be used as the zeroth element.

3. RESULTS OF CALCULATIONS

Figure 8 shows a plot of the functional J as a function of T for various φ_1.

An important problem related to that of one-way interorbital flight is the problem of finding optimum flights with return to the initial orbit. The problem of the optimum combination of outgoing and return trajectories in a central field is formulated as follows [8]: find the optimum angular displacements φ_1, φ_1' and times T, T' for the outgoing and return flights (the prime denotes that the quantity belongs to the return flight) that produce a minimum of the resultant functional $J_\Sigma = J + J'$ for the assigned $\varphi_{1\Sigma} = \varphi_1 + \varphi_1'$, $T_\Sigma = T + T'$.

It is shown in Reference [8] that any outgoing flight from r_0 to r_1 can be transformed into a return flight from r_1 to r_0 that is "symmetrical" to the outgoing flight. Thus, it is sufficient to have a network of one-way flights to construct round-trip flights between circular orbits.

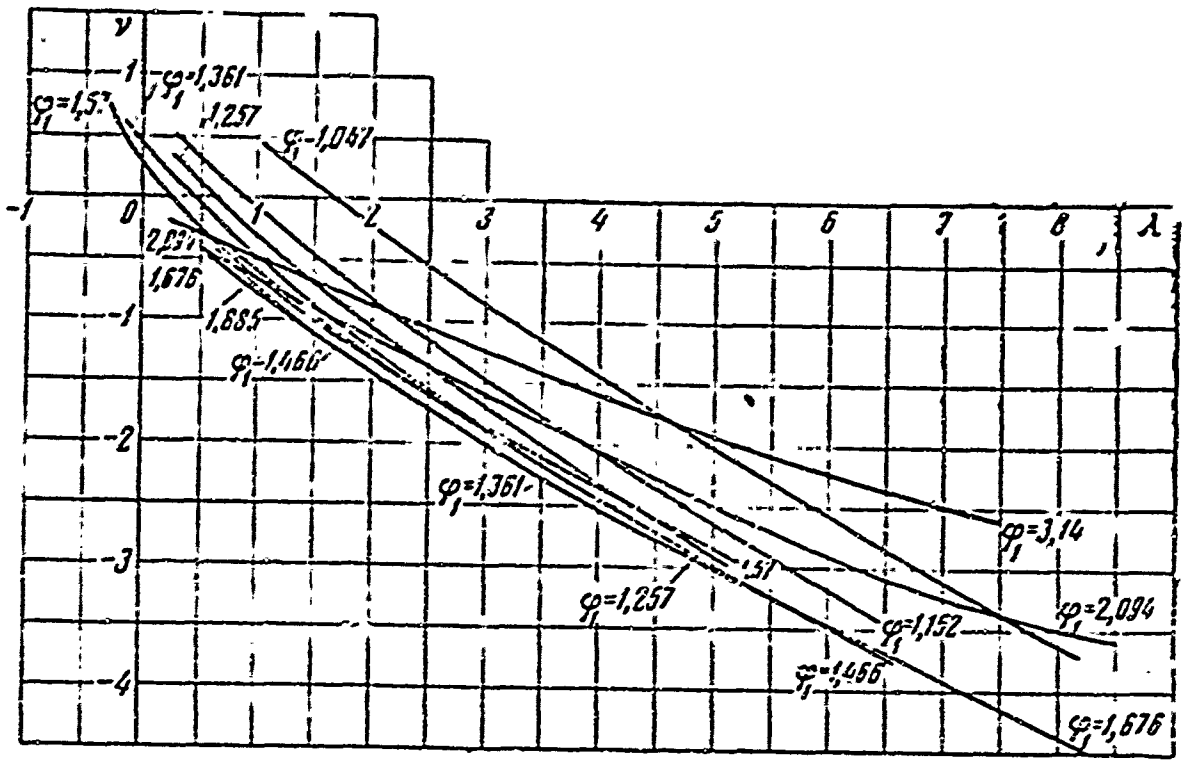

Fig. 9

The optimum condition for combining outgoing and return flights is equality of the two integrals introduced in Reference [1] for the outgoing and return motions:

$$\nu = \nu', \quad \lambda = \lambda'. \tag{3.1}$$

These integrals can be expressed with the aid of the initial and final parameters on the optimum trajectory [8]:

$$\nu = \frac{a_0^2 - a_1^2}{2(1 - v_1/r_1)}, \qquad \lambda = \frac{a_1^2 - a_0^2 v_1/r_1}{2(1 - v_1/r_1)}. \tag{3.2}$$

Here a_0 and a_1 are the absolute acceleration values for the beginning and end of the trajectory, v_1 and r_1 are the orbital velocity and radius of the terminal circular orbit (for $r_1 = 1.52$, $v_1 = 0.811$).

Condition (3.1) is definitely satisfied when a flight "symmetrical" to the outgoing flight is used as a return flight; then $\varphi_1 = \varphi_1'$, $T = T'$. This same condition can be satisfied on nonsymmetrical flights, a confirmation of which is provided in the fact that the curves intersect in Fig. 9, where the flight network is given in the coordinates ν, λ for various values of φ_1. As an example, we have found a "nonsymmetrical" flight that gives an advantage over the "symmetrical" flight amounting

to 16% in the functional J_Σ.

The parameters of the nonsymmetrical flight are: $T_\Sigma = 3{,}76$, $\varphi_{1\Sigma} = 4{,}29$, $T = 2{,}41$, $T' = 1{,}35$, $\varphi_1 = 3{,}14$, $\varphi_1' = 1{,}15$; $J^\Sigma = 3{,}20$.

The parameters of the corresponding symmetrical flight are: 10

$T_\Sigma = 3{,}76$, $\varphi_{1\Sigma} = 4{,}29$, $T = 1{,}88$, $T' = 1{,}88$, $\varphi_1 = 2{,}14$, $\varphi_1' = 2{,}14$, $J_\Sigma = 3{,}80$. Typical advantages gained by nonsymmetrical flight are given in [9-11].

Received 21 August 1963

REFERENCES

1. G.L. Grodzovskiy, Yu.N. Ivanov, V.V. Tokarev. Dokl. AN SSSR [Proceedings of the Academy of Sciences USSR], 137, No. 5, 1086, 1961.
2. J.H. Irving, E.K. Blum. Vistas in Astronaut., II, N.Y., 1959, page 191.
3. I.S. Berezin, N.P. Zhidkov. Metody vychisleniy [Calculation Methods] 2, Fizmatgiz [State Publishing House for Physicomathematical Literature], 1960.
4. L.V. Kantorovich. Dokl. AN SSSR, 56, No. 3, 233, 1947.
5. L.V. Kantorovich. Uspekhi matem. nauk [Advances in the Mathematical Sciences] 3, No. 6, 89, 1948.
6. M.L. Stein. J. Res. Nat. Bur. Standards, 50, No. 5, 277, 1953.
7. Sovremennaya matematika dlya inzhenerov [Contemporary Mathematics for Engineers], edited by E.F. Bekkenbakh, IL [Foreign Literature Press], 1959.
8. Yu.N. Ivanov, V.V. Tokarev, Yu.V. Shalayev. Kosmich. issledov. [Cosmic Research], this issue, 414.
9. V.K. Isayev, V.V. Sonin. Avtomatika i telemekhanika [Automation and Remote Control], 23, No. 9, 1117, 1962.
10. W.G. Melbourn, C.G. Sauer, D.E. Richardson. Proc. IAS Symp., N.Y.,

1961, page 138.

11. W.G. Melbourn, C.G. Sauer. Astronaut. Acta, 8, No. 4, 205, 1962.

Manu-
script
Page
No.

[Transliterated Symbols]

10

124 ЭЦВМ = ETsVM = elektronnaya tsifrovaya vychislitel'naya mashina = electronic digital computer.

RADIATIVE HEATING IN HYPERSONIC FLOW

L.M. Biberman, V.S. Vorob'yev, G.E. Norman, I.T. Yakubov

This article deals with the heating of a blunted body by the emission of a shock wave generated by that body in hypersonic flow. General expressions are presented for the calculation of the radiant flux. Particular attention is devoted to heating in the case of streamlining under conditions in which the gas behind the compression shock is virtually completely dissociated. An analysis has been carried out of the elementary radiation processes; the basic and decisive optical properties of the plasma formed behind the shock under these conditions are indicated. There is a discussion of the methods employed to calculate the contribution of individual radiation processes to the emissive power of hot air. Emission in the continuous spectrum and over the entire range of spectral lines is considered. Values have been calculated to cover a wide range of temperatures, pressures, and layer thicknesses for spectral and integral radiant fluxes, incident on the streamlined body. Regions of streamlining-parameter values have been found for which the radiation heat flow may exceed the convection heat flow and thus define the aerodynamic heating. The problems associated with the determination of the state of the gas behind the front of the shock wave are discussed. The analysis of the factors responsible for deviations from equilibrium made it possible to reveal relaxation and quasi steady nonequilibrium regions. The basic processes determining the structure of the nonequilibrium zone at great streamlining flow velocities are clarified. The decisive role of radiant processes is shown.

* * *

In the early works devoted to aerodynamic heating, only the immediate interaction between the streamlined surface and the boundary laye (convective heating) was considered.

L.M. Biberman indicated the existence of a second heating method,

i.e., the radiation of a shock wave generated by the gas flow in front of a streamlined surface (radiative heating), and in work performed in 1955-1957 he demonstrated that this mechanism offers a significant contribution to the aerodynamic heating.

A method has been worked out for the calculation of radiant flux as a function of free-stream parameters, the chemical composition of the gas, and the shape of the streamlined body. It is assumed that in the plasma formed behind the compression shock the distribution of particles by states, as well as the degree of dissociation and ionization correspond to a state of thermodynamic equilibrium. The basic elementary processes governing the optical properties of the plasma have been ascertained, and approximate methods of accounting for these processes have been proposed. In the case of air in a region of low temperatures corresponding to velocities below 8 km/sec the vibrational transitions of NO and the electron transitions in the molecules proved to be the most significant: the O_2 Schumann-Runge bands, the first and second positive N_2 systems, the β-, γ-, δ-, and the ε-systems of NO, and the first negative N_2^+ system. The photoionization of atoms was evaluated, as were the photoseparation of an electron from the O^- ion and the free transitions in the ion and neutral-particle field.

The calculations that were carried out showed that radiative heating may be comparable to convective heating.

Analogous calculations have subsequently been carried out in the USA [1-6]. Let us take note of the fact that the calculation method and the selection of elementary processes determining emissive power coincide. The results of these calculations also confirmed the significance of radiative heating.

The present work is devoted to radiative heating for flows moving at velocities in excess of 8 km/sec, i.e., and analysis has been car-

ried out and a theory of elementary radiation processes determining the optical properties of the plasma formed behind the wave front under these conditions has been evolved; the values of the spectral and integral radiant fluxes incident on the streamlined body have been calculated for a wide interval of parameters; the theoretical and experimental data available in the literature have been compared; a comparison of radiative and convective heat flows shows that there exist extensive regions of streamlining parameters at which radiative heating considerably exceeds convective [heating]; the trends in the further development of the theory of radiative heating are discussed, the primary problems are formulated, and ways are indicated for the solution of these problems.

GENERAL EXPRESSIONS FOR THE CALCULATION OF RADIANT FLUXES

The radiant-energy flow I incident on a unit area of the streamlined surface is equal to

$$I=\int_0^\infty d\nu \int_{(V)} dV \frac{\varepsilon_\nu(r')}{4\pi(r-r')^2}\exp\left[-\int_0^{|r-r'|} k_\nu'(r'')\,dr''\right]\cos[n,\widehat{(r-r')}], \quad (1)$$

where $\vec{r}$ and $\vec{n}$ characterize the position and orientation of the unit area; $\vec{r}'$ determines the position of the volume element dV of the radiating gas; $\varepsilon_\nu(\vec{r}')$ is the spectral emissive power at the point determined by $\vec{r}'$; $k_\nu'(\vec{r}'')$ is the coefficient of absorption calculated with consideration of induced emission, with the points given by $\vec{r}''$ taken on the straight line $(\vec{r}-\vec{r}')$; ν is the frequency.

Expression (1) is extremely general. This expression takes into consideration the nonuniformity of the radiating gas, the geometry of the streamlined body, and, what is extremely important, the absorption of radiation inside the radiating gas. The state of the radiating gas is close to the equilibrium state over a wide range of streamlining parameters. It is also significant that 1 - the magnitude of shock de-

tachment – is small in comparison with the characteristic dimension of the streamlined body. With consideration of these circumstances (1) is considerably simplified

$$I = \int_0^\infty B_\nu (1 - e^{-k'(\nu)l})\, d\nu + \int_0^\infty d\nu B_\nu k'(\nu)\, l \int_1^\infty e^{-k'(\nu)lu} \frac{du}{u^2}, \qquad (2)$$

$$k'(\nu) = (1 - e^{-h\nu/kT}) \sum_i k_i(\nu), \qquad (3)$$

where B_ν is the Planck function; $k_i(\nu)$ is the coefficient of absorption governed by the ith elementary process. The factor [1 – exp (– hν/ /kT)], as is usual, permits consideration of the forced emission.

Expression (2) defines the emissive power of the uniform gas layer bounded by two parallel planes separated from one another by a distance l. The first term (let us denote it by I_1) is the energy emitted by the hemispherical volume inscribed in the flat layer through the unit area in the center of the base of the hemisphere. The second term reflects the role of the remaining part of the flat layer. The actual geometry of the radiating layer behind the compression shock lies somewhere between a flat layer and a hemispheric volume. As a result of the relative smallness of the shock detachment, the configuration of the radiating volume is close to that of a flat layer. Further refinement of this problem seems premature to us, since it [the refinement] does not correspond to the level of accuracy at which the optical properties of the plasma are known. Let us take note of the fact that the quantity I may be greater than I_1 by a factor of no more than two (for an optically thin layer); the contributions of heavily reabsorbed spectral segments to I and I_1 prove to be identical. For lines exhibiting dispersion contours, reaching the "square root" section of the growth curves, the contribution to I amounts to 1.33 of the contribution to I_1.

In practical terms, it is convenient to introduce the emissivity of a flat layer and a hemispherical volume, these terms being defined by the expressions

$$\varepsilon = I / \sigma T^4, \qquad \varepsilon_1 = I_1 / \sigma T^4, \tag{4}$$

where σ is the Stefan-Boltzmann constant.

According to (2) and (3), the calculation of the radiant fluxes reduces to a consideration of the individual elementary processes and the summing of the found $k_i(\nu)$, with subsequent integration in accordance with Expression (2). Occasionally, the coefficient of absorption changes sharply with frequency (the atomic and ionic lines, the rotational-vibrational molecule bands). In this case, it is convenient to present $k(\nu)$ in the form of the sum $k(\nu) = k_1(\nu) + k_2(\nu)$, where $k_1(\nu)$ slowly changes with frequency (the continuous spectrum) and $k_2(\nu)$ changes rapidly with frequency (the spectral line). In this case, for example, for I_1 we obtain

$$I_1 = \int_0^\infty B_\nu (1 - e^{-k_1'(\nu) l})\, d\nu + \sum_i B_{\nu_i} e^{-k_1'(\nu_i) l} \int_0^\infty (1 - e^{-k_{2i}'(\nu) l})\, d\nu, \tag{5}$$

where ν_i is the frequency corresponding to the center of the ith spectral line. Thus it becomes possible to take into consideration the superposition of the lines on the reabsorbed sections of the background, while at the same time separating the calculations pertaining to the continuous spectrum and the spectral lines.

ELEMENTARY RADIATION PROCESSES

With increasing temperature the role of individual elementary processes changes. A preliminary analysis has shown that given sufficiently high temperatures, photoionization and absorption by electrons in ion fields become decisive. Moreover, in addition to the continuous spectrum, it became necessary also to take into consideration the spectral lines of atoms and ions. In connection with the virtually total

absence of literature data, we evolved theoretical methods of accounting for a number of elementary processes, and it seems to us that this is of some independent interest.

Below there follows a brief discussion of the methods employed to take into consideration the primary elementary processes. Particular attention is devoted to the air plasma.

1. The continuous absorption spectrum in the visible and near-ultraviolet region is defined by the photoionization of excited atoms. It is the general practice in the literature to determine the resulting coefficient of absorption on the basis of the Unsoeld formula [7, 8] based on the utilization of hydrogen characteristics for complex atoms. The Unsoeld formula has no theoretical or experimental foundation. This problem was again considered in References [9-11]. This [reconsideration] was based on the quantum-defect method [12, 13] rigorously validated in [14]. This method makes it possible to take into consideration the features of the internal structure of complex atoms. The comparison carried out in [9, 11] showed that the derived results proved to be in good agreement with existing experimental data for various elements. The measurements carried out subsequently for argon [15] and nitrogen [16] also confirmed our theoretical calculations. Let us take note that in the case of nitrogen and oxygen the Unsoeld formula yields values exaggerated by an order of magnitude.

2. In the infrared and visible regions, particularly in the case of high temperatures, the free-free transitions in ion fields play an important role. It has been the practice in the literature either to include these in the Unsoeld formula or to take them into consideration in purely Coulomb approximation. The reasoning presented in [11, 17] made it possible to take into consideration the structural features of complex ions. The resulting refinements were also quite significant

here.

3. The continuous spectrum in the ultraviolet region (~ 1000 A) is defined by the photoionization of atoms from the ground and lower excitation levels. It turned out that the energy emitted in these spectral segments is very substantial at high temperatures. The sections for the ground levels of O and N atoms were taken from [18]. The photoionization sections from the 2^2D^0 and 2^2P^0 levels of the nitrogen atom were calculated in [19].

4. At pressures of the order of atmospheric pressure and higher and in the case of noticeable ionization, the effects of interaction begin to make themselves felt. This leads to a shift in the photoionization threshold toward the long waves.* There is a lack of reliable methods of accounting for these phenomena in the literature. We assumed that the effect of the interaction on the spectra reduces only to the fact that the upper terms of the spectral series convert to a continuous spectrum in accordance with the unperturbed density of their oscillator forces, and thus the photoionization section is found to be extended toward the long waves.** The shifted photoionization threshold was determined on the basis of the last bound state achieveable in the plasma. Corresponding changes were introduced into both the individual sections and into the integral formulas.

5. In certain cases, when calculating the continuous spectrum, we should take into consideration the electron transitions in the molecules, the photoseparation of electrons from negative ions, and the free-free transitions in the neutral-systems field.

Molecular bands were taken into consideration by means of the method which we evolved earlier, according to which the absorption coefficient averaged with respect to the rotational structure is defined by the probability of electron transition and the Franck-Condon fac-

tors.* In [21] an approximate method is proposed for the calculation of the Franck-Condon factors, this method being suitable for large vibrational quantum numbers. The result obtained by means of this method for the Schumann-Runge bands [22] were subsequently confirmed by extremely cumbersome machine [computer] calculations [23].

The photoionization section of the NO molecule from the ground state was taken from [24], the O^- photoseparation section having been taken from [25]. We turned our attention to the role of photoseparation from the negative N^- nitrogen ion. The contribution of this process was calculated in accordance with evaluations carried out in [26]. The contribution of the free-free transitions in the neutral-systems field was calculated according to semiempirical formulas standardized on the basis of existing experimental data.

6. We devoted our attention to the role played by emission in the spectral lines. It turned out that this process makes a decisive contribution at low pressures and at intermediate and high temperatures. The number of emitted lines may be quite large. In this connection, an approximate method has been developed to make possible the calculation of the energy emitted by the plasma over the entire range of spectral lines [27, 28]. Some of the strongest lines of the basic series are considered individually, all of the remaining lines being separated into groups of adjacent lines; in order to compute their contribution, integral formulas have been derived. When taking reabsorption into consideration, the nature of the expansion of the various atomic and ionic lines was taken into consideration, as were multiplet splitting, the overlapping of equivalent line widths, etc.

The results of the calculations show that: a) there exists a sufficiently wide interval of temperatures, pressures, and radiating-layer thicknesses in which the lines provide the basic contribution to the

energy emitted by the plasma; b) the total energy of a large number of weak lines, considered integrally, may markedly exceed the contribution of the individually considered strong lines with increasing optical density; c) in addition to the visible lines, the lines situated in the ultraviolet and corresponding to the transitions to the ground configuration may play an important role. The oscillator forces of the O and N lines lacking in the literature were calculated by us [19].

Let us take note of the fact that in recent experiments [16] with a nitrogen plasma produced in shock tubes it was found that the emission in the lines plays a significant role. Thus direct experimentation has confirmed the validity of the problem posed by us with regard to the role of the lines in the emission of a low-temperature plasma.

THE COEFFICIENT OF ABSORPTION AND THE EMISSIVITY OF AIR

We calculated the absorption coefficients and emissivities of air for the interval of pressures p = 0.001-100 atm and for temperatures below 20,000° K. The data pertaining to the composition of the air were taken from [20].

Figure 1 shows some of the derived resulting continuous absorption spectra (T = 14,000° K). At frequencies below ~ 80,000 cm^{-1}, the photoionization of the upper excited states of nitrogen and oxygen atoms plays a basic role; at low frequencies, the free-free transitions in the ion field are significant. The combined contribution of these two processes was calculated on the basis of the formulas presented in [11], with a correction for the shift in the photoionization threshold. Because of the integral nature of these formulas, smooth jumps corresponding to the ionization threshold from individually excited states appear on the curves.

At higher pressures the free-free transitions in the atom field begin to play a certain role, as does photoseparation from negative

ions, and the NO δ- and ε-systems.

The threshold frequency of the photoeffect from the 2^2P^0 state of the nitrogen atom lies at about 88,000 cm^{-1}. At this frequency the absorption coefficient for air increases abruptly by a considerable magnitude. With a further increase in the frequency, the absorption coefficient again increases abruptly several times at frequency values equal to the threshold values for nitrogen and oxygen atoms. At greater pressures these jumps due to the interaction shift to the left. Let us note that in the absence of saturation, the energy emitted in the continuous spectrum is defined by the spectral segment $\nu > 80{,}000$ cm^{-1}.

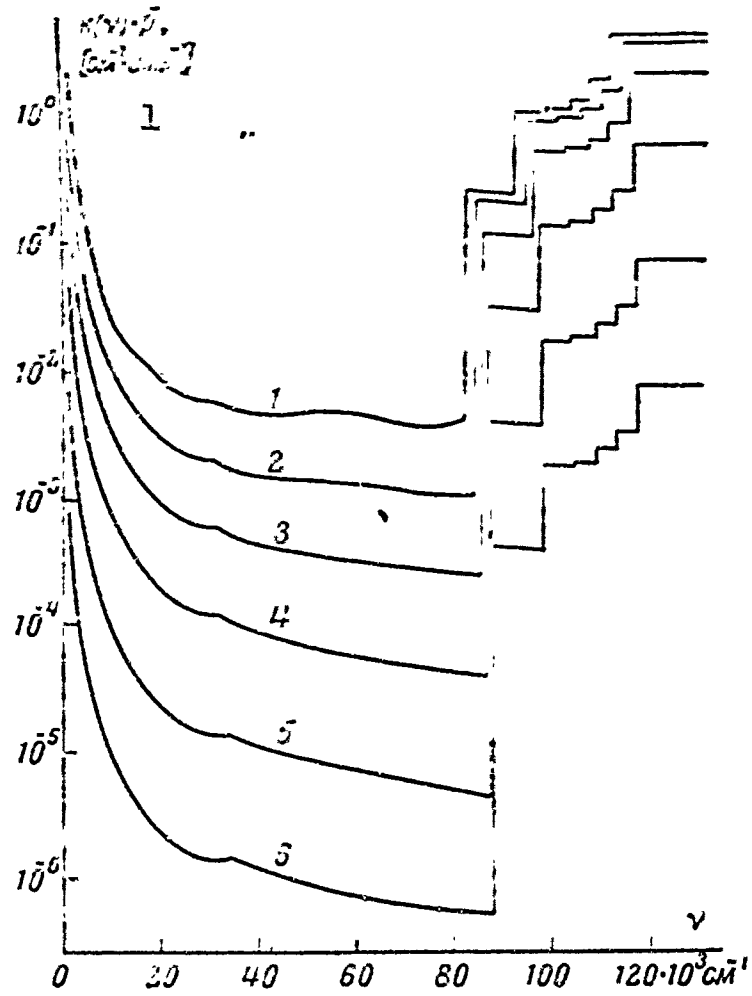

Fig. 1. Absorption coefficients $\underline{k}'(\nu)$ for air at a temperature T = = 14,000°K and for various pressures (p, in atm): 1) 100; 2) 10; 3) 1; 4) 0.1; 5) 0.01; 6) 0.001 atm. For the sake of keeping the figure compact, the graph has been plotted with the coefficients divided by pressure. Thus, for example, the absorption coefficient at a pressure of 100 atm is reduced by a factor of 100, while the absorption coefficient at a pressure of 0.001 atm is increased by a factor of 1000. 1) $k(\nu)\cdot p^{-1}$, $[cm^{-1}\cdot atm^{-1}]$.

If we know the absorption coefficients for air, we can use Formulas (2) and (4) to determine the emissivity governed by the continuous

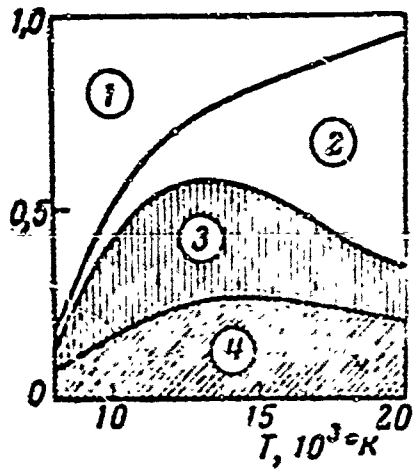

Fig. 2. Balance of energy emitted by air plasma, with p = 1 atm and l = 10 cm. The relative contribution of the continuous spectrum: 1) Regions of frequencies ν = 0-80,000 cm^{-1}; 2) regions of frequencies ν > > 80,000 cm^{-1}. Relative contribution of spectral lines: 3) Sets of weak lines considered integrally; 4) contribution of several strong lines considered individually.

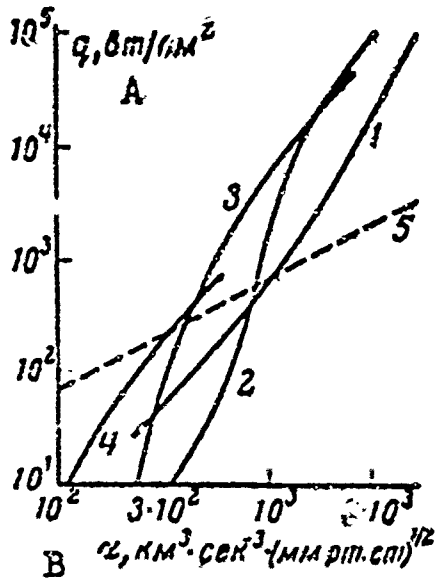

Fig. 3. Radiation and convection heat flows as functions of the parameter α for various pressures p_1 in front of the compression shock. Radiant flux: 1) 10; 2) 1; 3) 0.1; 4) 0.01 mm Hg; convective flow; 5) for all p_1; A) Q, w/cm^2; B) α, $km^3 \cdot sec^{-3} \cdot (mm\ Hg)^{1/2}$.

T, °K	l, см	p, atm [1]											
		0,001		0,01		0,1		1		10		100	
		A	r	A	r	A	r	A	r	A	r	A	r
6 000	1	1,2	7	5,9	7								
	10	3,6	7	3,0	6								
	100	1,4	6	2,5	5								
8 000	1	2,2	6	9,3	6	2,9	5						
	10	1,1	5	3,1	5	2,0	4						
	100	4,0	5	1,4	4	1,3	3						
10 000	1	8,7	6	6,5	5	3,9	4	2,9	3				
	10	3,5	5	2,4	4	1,5	3	1,6	2				
	100	1,2	4	1,0	3	8,5	3	[illegible]	2				
12 000	1	1,7	5	1,3	4	1,3	3	[illegible]	2	4,7	[illegible]		
	10	3,8	5	4,8	4	5,2	3	4,5	2	2,2	[illegible]		
	100	1,3	4	2,2	3	2,5	2	2,3	1	8,8	1		
14 000	1	3,7	5	1,6	4	1,7	3	[illegible]	2	9,3	2	6,5	1
	10	5,6	5	6,3	4	7,6	3	9,5	2	3,2	1	1,0	0
	100	1,3	4	2,5	3	3,3	2	3,4	1	9,4	1	1,0	0
17 000	1	1,1	4	2,7	4	1,1	3	[illegible]	2	1,9	1	6,0	1
	10	1,6	4	6,3	4	4,7	3	[illegible]	1	5,0	[illegible]	1,0	0
	100	2,3	4	1,8	3	2,2	2	3,5	1	1,0	0	1,0	0
20 000	1	2,1	4	4,1	4	9,8	4	1,5	2	2,8	1	7,5	1
	10	3,2	4	6,8	4	3,1	3	[illegible]	2	[illegible]	1	1,0	0
	100	4,8	4	1,1	3	1,4	2	2,5	1	1,0	0	1,0	0

1) p, in atm.

spectrum. The contribution of the spectral lines is determined separately, in accordance with the method evolved in [27, 28]. To illustrate the relative role of the individual processes, Fig. 2 shows the balance of energy emitted by the air plasma at p = 1 atm and $\underline{l}$ = 10 cm. Under these conditions all of the basic processes make a significant contribution. This problem is considered in greater detail in [27] for hydrogen plasma, and in [28] for nitrogen plasma. The basic qualitative results considered in [27, 28] prove to be valid for an air plasma as well.

The table shows air emissivity values for shock detachments $\underline{l}$ = = 1-100 cm ($\varepsilon = A \cdot 10^{-r}$). The range of temperatures and pressures has been chosen so as to encompass the entire region in which the atoms and ions dominate. Let us note that at low pressures the emissivity does not vary in proportion to $\underline{l}$, as is customarily held, but rather it varies more slowly, despite the fact that $\varepsilon \ll 1$. This is a result of the reabsorption of the lines which under these conditions represent the primary contribution to ε. In the case of comparatively large ε, when the basic contribution is provided by the continuous spectrum, the relationship between ε and $\underline{l}$ pertaining to the visible and near-ultraviolet region, exhibiting no pronounced fluctuations with respect to frequency, comes closer to being a linear function, subsequently attaining saturation. At the same time, it should be pointed out that it is impossible to compute the contribution of the continuous spectrum on the basis of formulas for an optically thin layer, since in the region of low and high frequencies the absorption coefficient of the continuous spectrum assumes greater values and reabsorption at this point begins to make itself felt even though the resulting ε is still considerably smaller than unity.

DISCUSSION OF RESULTS

There are absolutely no reliable measurements of the integral values of emissivity available at the present time. However, as was pointed out earlier, our theoretical data satisfactorily coincide with the experiments for all existing elementary processes as well as for individual and large spectral intervals. This indicates that the results of our calculations of the integral emissivity are reliable. On the whole, the emissivity values cited in the present report are apparently reliable and accurate to several tens of percent.

The derived results make it possible to compare radiative and convective heat flows. We have $q_{\text{конв}} \sim v^3\sqrt{p_1}$ [29], at the stagnation [critical] point for a convective heat flow in the case of a laminar boundary layer [29], where $\underline{v}$ is the velocity of the free [approaching] stream, and p_1 is the pressure in front of the compression shock. The radiative heat flow $q_{rad} \sim \varepsilon T^4$ is a considerably stronger function of $\underline{v}$ (an increase in velocity leads to a rise in temperature, and this directly affects the magnitude of q_{rad}; moreover, with increasing $\underline{v}$ the pressure behind the shock rises; a rise in temperature and pressure, in turn, leads to a pronounced increase in ε). It is natural to expect that if at low velocities the convection flow exceeds the radiation [flow], given sufficiently great velocities the situation will reverse (Fig. 3). Figure 3 shows both flows plotted as a function of the parameter $a = v^3\sqrt{p_1}$ (the radius of the streamlined [swept] body was assumed to be 1 meter, while the length of the shock detachment distance was taken as $\underline{l}$ = 10 cm). As we can see, there is an extensive region in which radiative heating considerably exceeds convective [heating].

Let us compare our values for emissivity with data available in the literature. References [30-32] summarize the results of investigations carried out independently in three laboratories in the USA. For

the conditions under which molecular bands prevail, these references are basically in agreement with our data both with respect to the method of calculation and in terms of the results.* From the standpoint of radiative heating, the most important are the regions of values for p and T at which the radiation of atoms and ions is basic. The values of the shock-wave parameters at which radiative heating exceeds convective heating correspond to precisely these conditions. For these conditions substantial errors have been tolerated in [30-32].

The basic processes considered by Kivel [30] are the photoionization of nitrogen atoms from the upper excited levels and the free-free transitions in the N^+ field. For these Kivel uses the Unsoeld formula, selecting the value of the effective charge $Z^{*2} = 3$, relying on the measurements of argon luminescence in a shock tube [33], although the structure and the properties of N and Ar atoms are completely different (see [11]). With respect to these processes Kivel assumed an exaggeration in excess of an order of magnitude, and this is apparently explained by the fact that Kivel made use not only of an excessively larger value of Z^{*2}, but of an exaggerated value for the boundary frequency ν_g (for the definition of ν_g see [11]). At the same time, Kivel failed to take into consideration the recombination that occurs with the formation of the O and N atoms in the ground and lower excited states. A particularly significant error on Kivel's part is the fact that he neglected the emission in the spectral lines.

At a pressure of ~1 atm we find accidental compensation of all errors permitted in Reference in [30], as a result of which the results of [30] coincide with ours. At lower pressures bright-line emission and recombination to lower levels predominate; therefore the data contained in [30] prove to be considerably on the low side. Let us also take note of the fact that in [30] the calculation is carried out for an optical-

ly thin layer. In this connection, for the actual values of shock detachment the emissivity curves presented in [30] attain values equal to unity considerably earlier than is the case in actual fact.

The authors of [31] also consider an optically thin layer and for recombination emission make use of formulas that are valid for hydrogen, exaggerating the role of this process thereby virtually by an order of magnitude. Unlike [30], the photoionization from each level is considered separately, thus markedly increasing the volume of computations without raising the level of computational accuracy in any manner whatever.

Reference [31] poses the problem of the necessity of considering bright-line emission. Having noted the difficulties involved in such a computation, the authors of [31] as their first step evaluated, for a number of specific conditions, the radiation energy of an optically thin layer of nitrogen plasma, for which purpose they examined individually more than 700 multiplets, supermultiplets, and individual transitions. For the spectral lines in the case of pressures of practical interest, reabsorption appears at thicknesses of the order of tenths of a millimeter. Therefore, the evaluation carried out in [31] is of no practical interest.

In Reference [32] air is considered at temperatures below 9000° K. The spectral lines and photoionization are not taken into consideration, although at low optical densities these processes become decisive, even at these comparatively low temperatures.

TRENDS IN THE FUTURE DEVELOPMENT OF THE THEORY OF RADIATIVE HEATING

The further evolution of the theory of radiative heating is, of course, associated with the refinement of the probability values and the sections of individual radiation transitions for atoms, molecules, and ions; in addition, it is associated with bremsstrahlung radiation

in the field of neutral systems, and with the consideration of the influence exerted by the interaction of particles in the plasma. The solution of this group of problems will make it possible considerably to reduce the error in the calculated radiant fluxes.

However, the basic trend in the evolution of the theory of radiative heating are associated with more thorough investigation of the state of the gas behind the wave front. The examination presented above is based on the assumption that equilibrium prevails for the distribution of particles with respect to the energy state as well as for the degrees of dissociation and ionization. In actuality there are two factors which may result in significant deviations from equilibrium.

Relaxation nonequilibrium. With the passage of the compression shock the state of the gas is subjected to pronounced change. The energy of the directed translational motion transforms into the energy of random translational motion, and this results in a sharp rise in the kinetic temperature. Then there follows the development of excitation processes in the rotational and vibrational states, dissociation, chemical reactions, the excitation of the electron states in atoms and molecules, and ionization. As a result of the finite rates of these processes, a region forms behind the compression shock in which the chemical composition of the gas, the distribution of molecules, atoms, and ions over the energy states, and the degrees of dissociation and ionization sharply differ from values corresponding to the local kinetic temperature. Then during the course of the process of gradual relaxation the gas approaches a state of equilibrium.

Quasisteady nonequilibrium. Strictly speaking, equilbrium can prevail only in closed systems. The gas behind the front of the wave is not in this state. The emission, as well as the diffusion of particles in the direction of the streamlined [swept] surface, lead to uncompen-

sated loss in excited and ionized particles. The emission is apparently the more significant factor, since it encompasses the entire luminescent volume, whereas diffusion acts primarily in the vicinity of the swept surface.

Relaxation nonequilibrium is a decisive factor which defines the state immediately behind the wave front where the kinetic temperature noticeably exceeds the equilibrium temperature and it is a strong function of the coordinates. Quasisteady nonequilibrium determines the state of the gas in the deeper regions behind the compression shock. In this region the kinetic temperature is a weak function of the coordinates. This provides a basis for the individual consideration of each of the factors responsible for nonequilibrium.

The result of a theoretical examination of relaxation nonequilibrium must be the determination of the concentrations of molecules, atoms and ions as functions of the coordinates, including the distribution of these systems over the energy state. This can be achieved by solving the corresponding systems of kinetic equations simultaneously with the gasdynamic equations of conservation. The kinetic equations must take into consideration not only the results of the various gas-particle collisions, but the transfer of these gas particles in the flow. These equations must also contain provision for consideration of the transfer of shock-wave radiation from one region of the streamlining gas to another.

The main difficulty encountered in studying relaxation nonequilibrium in air is the virtually total absence of reliable data as to the effectiveness of atomic and molecular collisions. Therefore the quantitative results of a number of works devoted to the study of weak shock waves in air (for example, [34, 35]) are of doubtful value.

Let us now consider the problem of relaxation in strong shock

waves, there being no consideration of this problem in the literature. We assume that this case exhibits extremely interesting features.

Having passed through the front of a strong shock wave, molecules rapidly dissociate as a result of direct collisions between one another and with atoms.* Our estimates have shown that only after this phenomenon do significant concentrations of electrons appear. For this reason it is possible to speak of a division of the zone of relaxation into an extremely short zone of dissociation relaxation and into a considerably more extended zone of ionization relaxation.

The proposed mechanism for the progress of nonequilibrium processes is considerably different from the nature of relaxation in weak shock waves. In the latter case the nitrogen molecules dissociate through the formation of NO molecules (the Zel'dovich mechanism), while the processes of dissociation and ionization proceed simultaneously.

The situation here is that at low temperatures the relationship between the rates of the various processes is determined primarily by the difference in the energies of their activation. With a rise in the streamlining velocity there is a pronounced increase in the kinetic temperature in the zone of relaxation nonequilibrium. Large temperature values significantly weaken the influence of the magnitude of the activation energy on the rate of the process. The relationship between the velocities of the various collisions is now determined primarily by the relationships of the effective sections. Thus, for example, it is extremely significant that the sections for dissociation are considerably larger than the ionization sections.

Thus, the investigation of the complex problem of relaxation nonequilibrium in the case of a streamlining molecular gas at great velocities of streamlining becomes very much simpler. In practical terms, the matter reduces to the study of relaxation in an atomic gas. In this

connection, we will consider relaxation nonequilibrium in atomic gases.

The study of relaxation in an atomic gas [36-38] has shown the need for taking into consideration the processes resulting in the formation of excited atoms. The rate of their appearance determines the rate at which the concentration of ions and electrons increases. In this case, it was significant that the excited atoms are formed not only as a result of collisions, but during the absorption of radiation as well.

The transfer of radiation energy exerts a certain effect on the entire nature of the relaxation. In [39, 40] it was shown that the radiation of a hot gas propagating before the front (advance radiation) is partially absorbed there. Noticeable concentrations of excited atoms and electrons are formed in a cold gas before the front. These are then carried to the compression shock and, consequently, determine the initial conditions for the relaxation processes behind the front. Their presence may accelerate the process of relaxation.

Moreover it was demonstrated in [37] that the radiation of the deep-lying regions of the shock wave, having been absorbed in the zone of relaxation, may lead to a reduction in the extent of this zone. In the case of a wave in argon, consideration of this phenomenon reduced the time of relaxation by an order of magnitude.

During the last stage of relaxation, excitation and ionization are achieved primarily through collisions with electrons [36]. It is significant that the magnitudes of the sections and potentials of excitation and ionization exert extremely limited effect on the efficiency of the electron impact. The rate of excitation and ionization through electrons is very rigidly limited by the rate of heating for the electron gas in elastic collisions with ions and atoms [37]. Inadequate attention is generally devoted to the need for knowledge of reliable

elastic-collision sections.

The most complete experimental data in the literature pertain to argon. The analysis discussed above made it possible to derive theoretical values for the times of relaxation, these values in sensible agreement with experiment.

Apparently the fundamental qualitative relationships derived in the analysis of relaxation in atomic gases retain their validity for air in the case of high velocities of streamlining. As a matter of fact, the examination may easily be extended to a wave in a mixture of atomic gases. In this case it should be borne in mind that the processes of generating excited atoms are determined by specific streamlining conditions. For example, in argon with an admixture of cesium vapor there are extremely collisions of argon and cesium atoms in the ground states, this leading to the excitation of the cesium [38].

The quasisteady nonequilibrium caused by the yield of radiation was examined in [41] on the basis of the earlier evolved theory of radiation transfer in spectral lines [42]. It was shown that the population of the excited state may be considerably below equilibrium if $\beta = j_{II}\tau_{eff} < 1$. In this criterion j_{II} is the probability of deactivation of the excited state through collisions; $\tau_{eff} = \tau/\theta$, where τ is the natural duration of the excited state and θ is the probability of a photon passing beyond the limits of the radiating volume without absorption [43]. In the literature (for example, [44]) frequent use is made of another criterion, i.e., $\beta = j_{II}\tau < 1$, which fails to take into consideration the reabsorption of radiation and is valid only for an optically thin layer. Under actual conditions such a simplified approach may lead to errors in terms of order of magnitude.

Note should be taken of the fact that in [41] it was assumed that there are two energy states that correspond to the atom (or molecule).

In actual atoms and molecules the population of any of the multiplicity of states is a significant function of the population in all of the remaining states. In particular, since the ionization occurs primarily in stepwise fashion [45], the concentration of electrons depends significantly on the concentration of excited atoms. In turn, the concentration of excited atoms in great measure is defined by the collisions with electrons. The corresponding system of nonlinear equations was derived and solved in approximate terms in [46] for a hydrogen plasma. It was shown that for conditions close to gasdynamic, the concentrations of electrons and excited atoms may be smaller than the equilibrium [concentrations] by an order of magnitude.

The low pressures and temperatures at which the processes of shock excitation and ionization fail to compensate the nonequilibrium of corresponding radiation processes promote the withdrawal from equilibrium. This result is valid for any gas. It should be noted that the yield of radiation may markedly reduce the concentration of excited atoms, even if the energy losses associated with this process are insignificant.

The derived numerical result for actual conditions of air streamlining are also complicated by the inadequacy of information regarding sections of inelastic processes.

It should be noted that both factors responsible for nonequilibrium differ in their effect on the radiant fluxes. The radiation appears as a result of transitions from higher energy states to lower [energy states]. In the relaxation region the kinetic temperature is considerably greater than the equilibrium [temperature]. There is therefore no basis for the contention that the concentrations of excited, dissociated, and ionized systems will approach the equilibrium values monotonically. Consequently, it is possible that the emissive power of a unit volume of the relaxation region will exceed the corresponding

magnitude calculated in the assumption that equilibrium had already been attained. This was found to be the case in the experiments described in [44]. On the other hand, in the region in which the quasisteady nonequilibrium was significant, the concentrations of excited and ionized states were lower than those calculated in the assumption of equilibrium. This leads to a reduction in the radiant fluxes.

Another phenomenon arises in the case of strong shock waves when the temperature, pressure, and the emissivity are great. Under these conditions the quasisteady nonequilibrium may be small. However, the radiation energy losses may become significant. As a result the temperature behind the relaxation region will be smaller than that calculated without consideration of radiation losses, gradually diminishing with increasing distance from the front of the wave.

Reference [47] is devoted to the radiation cooling of an atomic gas, and the relationship associating the temperature of the gas with the distance from the front was derived in this work. The utilization of this relationship requires knowledge of the radiation losses of energy per unit volume of gas. For the case of a wave in argon, the theoretical rate of cooling is in satisfactory agreement with the measurements carried out in [33]. The results of the examination may be extended to air which, at high temperatures, represents a mixture of two atomic gases. It turned out that radiation cooling, reducing the temperature of the gas, may noticeably reduce radiative heating. Note should be taken of the fact that even a comparatively small reduction in temperature is significant, since the radiant flux is proportional to εT^4, where ε also diminishes with temperature.

The shock wave will also be subjected to additional cooling, this being associated with the removal of heat to the swept surface.

It is possible that conditions may arise under which relaxation

and quasisteady nonequilibrium, as well as radiation cooling, will make themselves felt in concert.

In conclusion let us note that the further development of the theory of radiative heating is associated with consideration of the extremely complex process of the streamlining of a blunted body by a nonequilibrium flow of gas exhibiting a high kinetic temperature at which the radiation processes affect both the kinetics and the parameters of the shock wave. The shock-wave radiation may also alter the boundary-layer parameters, this naturally affecting convection heat transfer (Academician G.I. Petrov indicated this circumstance in 1957).

Thus the radiation processes play an extremely important role in hypersonic streamlining. In this connection, the processes of radiation transfer in many cases become decisive. It should be noted that even the continuous emission spectrum under actual conditions is extremely far removed from the grey. Moreover, the spectral lines of atoms and ions play an important role, and at lower temperatures the molecular bands play an important part. Radiation transfer in a discrete spectrum differs qualitatively from the transfer in the continuous spectrum [42]. Therefore the utilization of mean absorption coefficients independent of frequency, as is frequently encountered in works devoted to hypersonic streamlining, can produce no satisfactory results. Even under limiting conditions when the diffusion approximation is applicable to radiation transfer, the consideration of the lines may alter the Rosseland mean by an order of magnitude [48].

Received 3 January 1964

REFERENCES

1. R.E. Meyerott. Threshold of Space. Proc.Conf. Chem. Aeron, 1957, page 259.

2. J. Keck, B. Kivel, T. Wentink. Heat Transfer Fluid Mech. Inst., Preprint of Papers, Stanford University Press, 1957, page 279.

3. B. Kivel, H. Meyer, H. Bethe. Ann. Phys., 2, 57, 1957.

4. T. Wentink, W. Planet, P. Hammerling, B. Kivel. J. Appl. Phys., 29, 472, 1958.

5. R.E. Meyerott. Third AGARD Colloquium, 1958, page 431.

6. J. Keck, J. Camm, B. Kivel, T. Wentink. Ann. Phys. [Annals of Physics], 7, 1, 1959.

7. A. Unsöld. Ann. Phys., 33, 607, 1938.

8. W. Finkelnburg, T. Peters. Handbuch der Physik [Handbook of Physics], Vol. 28, Springer Verlag, Berlin, 1957, page 79.

9. L.M. Biberman, G.E. Norman. Optika i spektroskopiya [Optics and Spectroscopy] 8, 433, 1960.

10. L.M. Biberman, G.E. Norman. K.N. Ul'yanov. Astron. Zh. [Astronomy Journal] 3, 107, 1962.

11. L.M. Biberman, G.E. Norman. J. Quant. Spectrosc. Radiat. Transfer, 3, 221, 1963.

12. A. Burgess, M.J. Seaton. Monthly Notices Roy. Astron. Soc., 120, 121, 1960.

13. M.J. Seaton. Monthly Notices Roy. Astron. Soc., 118, 504, 1958.

14. G.E. Norman. Optika i spektroskopiya, 12, 333, 1962.

15. D. Schlüter. Z. Astrophys. [Journal of Astrophysics], 56, 43, 1962.

16. R.A. Allen, R.L. Taylor, J.C. Camm. VI^{eme} conference internationale sur les Phenomenes d'Ionisation dans les Gas. 8 au 13 Juillet 1963 a Paris. Resumes dans communications [6th International Conference on Ionization Phenomena in a Gas Held from 8 through 13 July 1963 in Paris. Abstracts of Articles] page 233.

17. G.E. Norman. Optika i spektroskopiya, 14, 521, 1963.

18. D.R. Bates, M.J. Seaton. Monthly Notices Roy. Astron. Soc., 109, 698, 1949.

19. G.E. Norman. Optika i spektroskopiya, 14, 593, 1963.

20. Tablitsy termodinamicheskikh funktsiy vozdukha dlya temperatur 6000-12,000-20,000° K (pod red. A.S. Predvoditeleva). Izd-vo AN SSSR [Tables of Thermodynamic Functions for Air at Temperatures of 6000-12,000-20,000° K (edited by A.S. Predvoditelev). Acad. Sci. USSR Press], 1957, 1959.

21. L.M. Biberman, I.T. Yakubov. Optika i spektroskopiya, 8, 294, 1960.

22. I.T. Yakubov. Optika i spektroskopiya,9, 409, 1960.

23. R. Nicholls. Canad. J. Phys., 38, 1705, 1960.

24. K. Watanabe. J. Chem. Phys., 22, 1564, 1954.

25. L.M. Branscomb. Optical spectrometric measurements of high temperatures (ed. P. Dickerman), Univ. Chicago Press, 1961, page 235.

26. G.E. Norman. Optika i spektroskopiya, 17, 176, 1964.

27. L.M. Biberman, V.S. Vorob'yev, G.E. Norman. Optika i spektroskopiya, 14, 3[illegible] 1963.

28. V.S. Vorob'yev, G.E. Norman. Optika i spektroskopiya, 17, 180, 1964.

29. N.H. Kemp, F.R. Riddel. Jet. Propuls., 27, 132, 1957. J. Fay, F. Riddel. J. Aeron. Sci., 25, 73, 1958.

30. B. Kivel. J. Aerospace Sci., 28, 96, 1961.

31. B. Armstrong, J. Sokoloff, R. Nicholls, D. Holland, R. Meyerott. J. Quant. Spectrosc. Radiat. Transfer, 1, 143, 1961.

32. R.G. Breene, Jr., M.C. Narsone. J. Quant. Spectrosc. Radiat. Transfer, 2, 272, 1962.

33. H.E. Petschek, P. Rose, H. Glick, A. Kane, A. Kantrowitz. J. Appl. Phys., 26, 83, 1955.

34. K.L. Wray. Hypersonic Flow Researches (ed. F.R. Riddel), Academic

OPTICAL PROPERTIES OF CLOUDS

Ye.M. Feygel'son

A brief survey of the present state of research in cloud optics is presented. Most attention is devoted to theoretical studies on radiation transfer in clouds and the qualitative laws governing reflection and transmission of radiation by clouds without taking the influence of the atmosphere outside the cloud into account.

* * *

One of the most important tasks of weather satellites is to collect data pertaining to cloud cover. These data get to the satellite only in the form of radiation sensed by instruments at various wavelengths. Processing of the signals in the instruments into information on the state of the cloud cover presupposes knowledge of the optical properties of clouds and the influence of the atmosphere above the cloud on the radiation that the clouds emanate upward.

The present paper represents a brief survey of studies made at the Institute of Atmospheric Physics of the Academy of Sciences USSR into the optics of the clouds themselves. The second aspect of the problem under consideration, i.e., the influence of the atmosphere above the clouds, is not treated here.

The peculiarities of radiant-energy propagation in clouds are determined by three factors:

a) the scattering on water droplets is great at all wavelengths in the range $0.3\ \mu \leq \lambda \leq 40\ \mu$,

b) the absorption at $\lambda \geq 1.5\ \mu$ is an order greater than the absorption by water vapor,

c) the drop-scattering indicatrix is distinguished by sharp forward distension.

For comparison of the optical properties of a cloud and the cloudless atmosphere, we note, for example, that the optical thickness of the cloud in the visible region of the spectrum is two orders greater than that of the cloudless atmosphere. The latter's scattering indicatrix may be presented as a ten-term expansion in Legendre polynomials [1]. To form a sufficiently accurate conception of the cloud indicatrix, it is necessary to take into account about one hundred terms of this series [2]. The severe distension of the scattering indicatrix and the high optical thickness render the problem of radiation transfer in clouds exceedingly difficult, and it requires the design of special solution methods. The development of such methods at the Institute has taken three trends.

L.M. Romanova [3-5] elaborated numerical methods for solving the exact transfer equations that are adapted to high-speed computers and deliver high accuracy in the results obtained.

Ye.M. Feygel'son [2], using Romanova's data and known exact solutions as controls, derived analytical expressions for an approximate solution to the exact transfer equations. The comparative simplicity of the formulas made it possible to give the study a geophysical tendency and to examine real cloud types.

G.V. Rozenberg [6, 7] derived an approximate solution to the transfer equation for arbitrary indicatrix shape, taking polarization effects into account in analytical form for cases in which absorption is large or small by comparison with scattering. These studies have a spectroscopic orientation. The formulas obtained make it possible to judge of the absorption properties of a substance from measurements of the brightness of radiation reflected from a layer of it. Since the

studies of G.V. Rozenberg are more or less in a group by themselves, we shall dwell on them first.

The fundamental relationships in the case of weak absorption take the form:

$$R_\infty(r, r_0) = \frac{\mu_0}{\pi} h(r, r_0) \exp[-s(r, r_0) y], \tag{1}$$

$$t(r, r_0) = \frac{\omega}{\pi} \mu_0 g(\mu_0) g(\mu) \frac{\operatorname{sh} y}{\operatorname{sh}(\varkappa + y)} + \begin{cases} \exp\left(-\frac{\tau_0}{\mu_0}\right) \delta_{r,r_0} & \text{for } \omega > \omega_0, \\ \frac{\omega}{\omega_0} \exp\left(-\frac{\tau_0}{\mu_0}\right) \delta_{r,r_0} & \text{for } \omega \leqslant \omega_0, \end{cases} \tag{2}$$

$$R(r, r_0) = \frac{\mu_0}{\pi} \left\{ h(r, r_0) \exp[-s(r, r_0) y] - g(\mu_0) g(\mu) \frac{e^{-x-y} \operatorname{sh} y}{\operatorname{sh}(x+y)} \right\}. \tag{3}$$

Here r_0 is the propagation direction of the light from the source, θ_0 is the polar angle of the ray r_0, $\mu_0 = \cos \theta_0$, $R_\infty(r, r_0)$ is the brightness coefficient of a semiinfinite layer, $t(r, r_0)$ is the transparency of a layer of finite optical thickness, $R(r, r_0)$ is the brightness coefficient of such a layer, $\underline{r}$ is the line-of-sight direction, $\mu = \cos \theta$, θ is the polar angle of the ray $\underline{r}$, r_0 is the direction of a parallel pencil of incident radiation, $\beta = \alpha/\sigma$, α and σ are the absorption and scattering coefficients of the medium being studied, δ_{r,r_0} is the Kronecker symbol, $y = \eta\sqrt{\beta}$, $x = 4\tau_0/\eta\sqrt{\beta}$, τ_0 is the optical thickness of the cloud, ω_0 is the angular divergence of the illuminating pencil and ω is the angular divergence of the receiver.

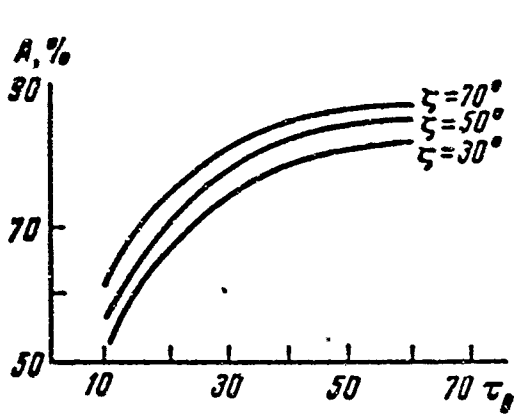

Fig. 1. Albedo of clouds in the visible region of the spectrum.

The functions $h(r, r_0)$, $s(r, r_0)$, $g(\mu)$ and the parameter η depend on the scattering function and are not determined from the theory of G. V. Rozenberg.

If they are determined from experiment or from some other theory,

then Formulas (1)-(3) enable us to calculate β, i.e., to determine the relationship between absorption and scattering in the medium.

It follows from this that effective utilization of the relationships derived by G.V. Rozenberg is possible only for sufficiently weak dependence of the quantities $h(r, r_0)$, $s(r, r_0)$, $g(\mu)$ and η on the optical properties of the medium. Attempts at experimental verification of these quantities have given encouraging results.

L.M. Romanova calculated the functions $h(r, r_0)$, $s(r, r_0)$ and $g(\mu)$ for the cases of spherical and severely distended scattering indicatrices. The calculations indicated that we may speak of general applicability for these quantities in the sense of their weak dependence on the shape of the indicatrix with $0 \leq \beta \leq 0.1$, i.e., over the entire interval of variation of the parameter β for which the theory is valid. We note that according to data presented in [2], the resultant water-vapor and water-droplet absorption spectrum in the near infrared region ($\lambda \leq 2\mu$) corresponds to values of $\beta \leq 0.1$ everywhere except in the central regions of the strongest Ψ and Ω absorption bands, and outside individual high-intensity lines.

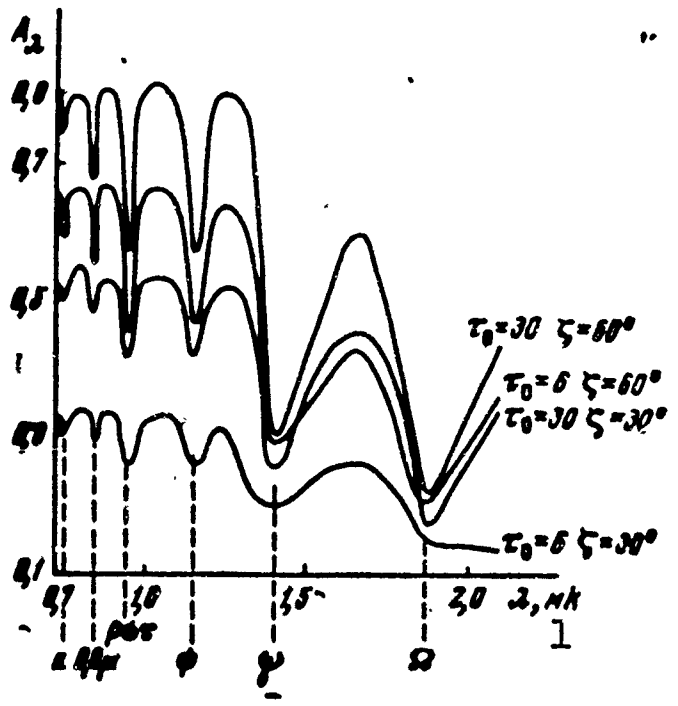

Fig. 2. Albedo of clouds in the near infrared region. 1) Microns.

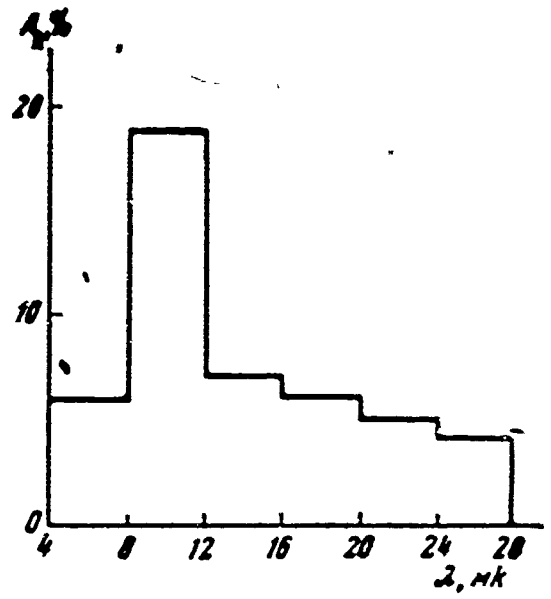

Fig. 3. Albedo of clouds in the long-wave region. ρ_v = = 0.2 g/m^3; t = 0°.

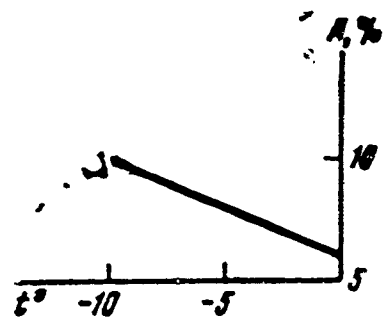

Fig. 4. Albedo in the interval (4, 8μ) as a function of cloud temperature.

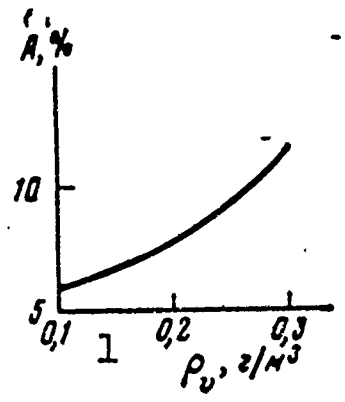

Fig. 5. Albedo in the interval (4, 8μ) as a function of cloud wetness. 1) ρ_v, g/m^3.

We now present a summary of the basic results that we obtained with L.M. Romanova. Let us note first of all that all calculations were carried out for an infinite, horizontally stratified cloud layer with flat boundaries. It was assumed that $k = \sigma/(\alpha + \sigma) = \text{const}$ and the scattering indicatrices used were those for an individual drop calculated without taking absorption into account. The calculations were made for $\rho = 10$, 20, and 30, where $\rho = 2\pi a/s$ and a is the drop radius.

The spectral albedo of the clouds was calculated as a function of the optical thickness τ_0 of the cloud and the zenith distance ζ of the sun.

Figure 1 shows the albedo in the visible part of the spectrum as a function of τ_0 for various values of ζ. The albedo is not a function of wavelength here because $\lambda \ll a$.

Figure 2 shows the spectral albedo in the region 0.7 micron $\leq \lambda \leq$ 2.5 microns for thin ($\tau_0 = 6$) and thick ($\tau_0 = 30$) clouds for high ($\zeta = 30°$) and low ($\zeta = 60°$) solar altitudes. The positions of the basic water-vapor absorption bands are indicated.

Figure 3 shows the spectral albedo in the long-wave region of the spectrum. The curve is stepped, since values of α_λ and σ_λ that had been averaged over 4-micron spectral intervals were used in calculating the

Вид облака 1	2 H, км	2 Z_2, км	3 a, мк	τ_0	A, % ζ°=30	50	70
Sb	0,5	1	5	14	59	63	69
Sc	0,5	1,5	5	20	68	72	76
Ns—As	2,5	3	5	65	88	88	90
4 Отдельные слои As	0,9	4,5	5	17	63	68	73

1) Type of cloud; 2) kilometers; 3) microns; 4) isolated As layers.

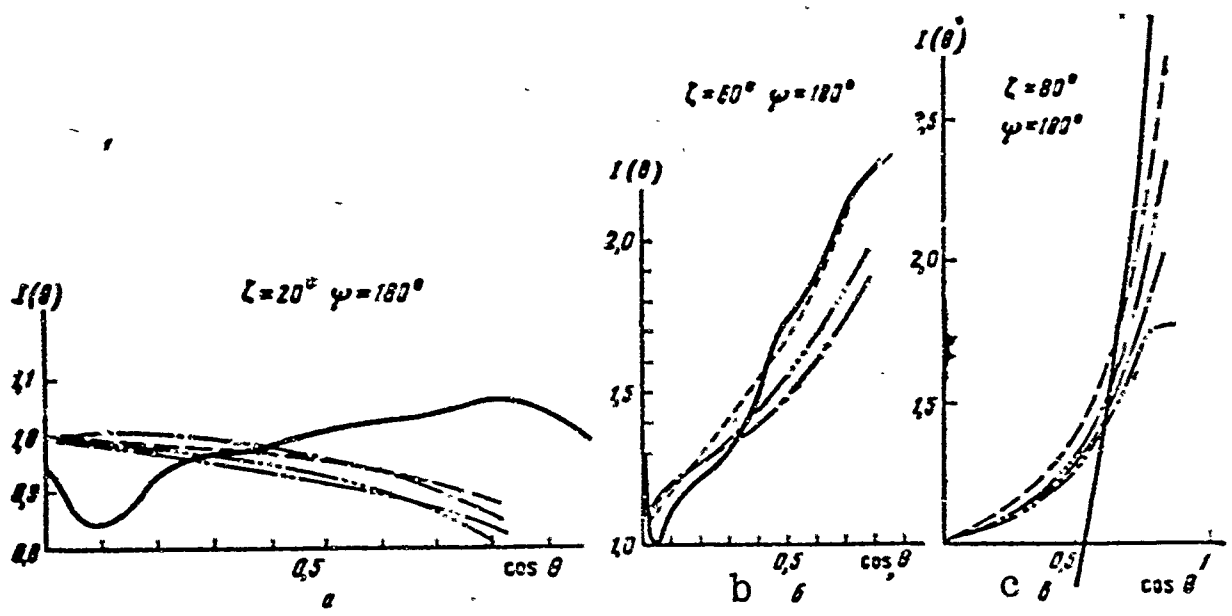

Fig. 6. Variation of brightness of light reflected from a cloud (solid curve) and from snow (dashed curves) as a function of the incidence direction of a parallel pencil of light: a) with $\zeta = 20^\circ$; b) with $\zeta = 60^\circ$; c) with $\zeta = 80^\circ$; $\psi = 180^\circ$.

A_λ. The albedo in this region of the spectrum depends the more heavily on the temperature t° and wetness ρ_v of the cloud the greater the absorption. Figures 4 and 5 present examples of this relationship in the interval 4 microns $\leq \lambda \leq$ 8 microns.

An attempt was made to determine average parameters for various types of stratified clouds on the basis of observational data: their thickness H, the altitude of the upper boundary Z_2, the average radius $\underline{a}$, and the optical thickness τ_0. Then these figures were used to determine average values for the cloud albedos in the visible region of the spectrum as a function of the sun's zenith distance. The results are presented in the table.

Intensity calculations for the light reflected from the cloud permitted establishing a number of interesting qualitative laws for the

optical situation in clouds observed from above. First of all, it was noted that the intensity of the reflected light is distributed quite uniformly among the directions, with the exception of the region of the antisolar vertical. Here, with the sun at low altitudes, we observe the so-called indicatrix effect (see [2]) – a rapid increase in brightness in the direction toward the horizon that becomes more rapid as the sun descends. This effect is represented in Fig. 6. Here θ is the polar angle of the sighting direction, ψ is the azimuth angle reckoned from the sun's vertical, and $\psi = 180^\circ$ corresponds to the antisolar vertical. The unbroken lines on the figures represent the brightness of the light reflected from the cloud; the dashed lines represent reflection from a snow mantle in various cases. The figures show a rotation of the brightness curves with increasing ζ, with the same qualitative effect taking place for snow.

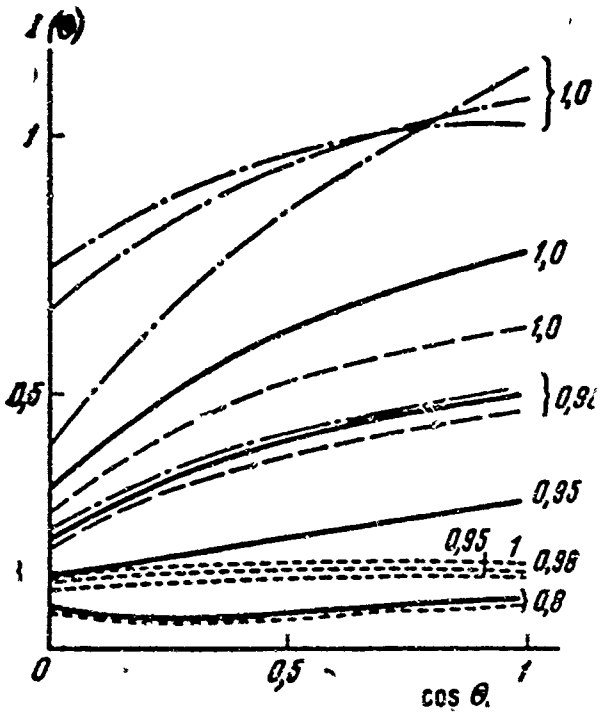

Fig. 7. Change in brightness of reflected light as a function of cloud-layer thickness, shape of scattering indicatrix, and absorption. $\zeta = 0$, $\rho = 20$; dot-dash line: $\tau_0 = \infty$ (upper curve for spherical indicatrix, middle curve for Rayleigh indicatrix, lower curve for $\rho = 20$; solid curve: $\tau_0 = 20$; dashed curve $\tau_0 = 12$; short dashes: $\tau = 2.5$.

Figure 7 shows the reflected radiation as a function of the cloud-layer thickness ($\tau_0 = \infty$; 20; 12; 2.5) and of the relationship between absorption and scattering ($k = 1$, 0.98, 0.95 and 0.8; the values of k are keyed on the curves). We see that the great difference between the brightness of clouds having different thickness in the absence of absorption ($k = 1$) are largely reconciled when absorption is introduced ($k = 0.98$). The role of absorption consists in reducing the free path of the radiation in the cloud; an effective reflecting layer with a

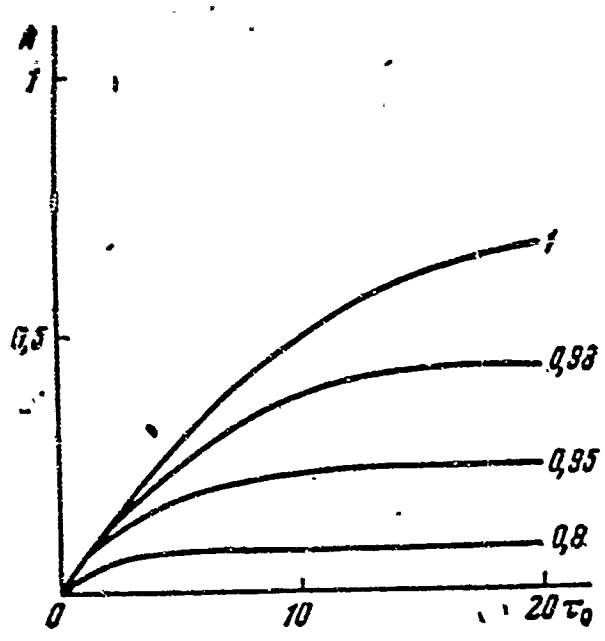

Fig. 8. Albedo as a function of optical thickness and the parameter $\underline{k}$. $\zeta = 0$, $\rho = 20$.

thickness that becomes smaller the greater the absorption forms in the vicinity of the upper boundary. It is seen from the figure that at $\underline{k} = 0.98$, the thickness of this layer is definitely greater than 2.5, since the curve ($\tau_0 = 2.5$, $k = 0.98$) is far removed from the group composed by the remaining curves corresponding to $\underline{k} = 0.98$. At $\underline{k} = 0.8$, the effective-layer thickness obviously does not exceed 2.5. The presence of the effective reflecting layer is clearly seen in Fig. 8 as well. Beginning at a certain value of τ_0, which is the smaller the larger $\underline{k}$, the albedo of the cloud ceases to change.

Returning to Fig. 7, we draw attention to an essential difference between the curves corresponding to different scattering indicatrices (the case $\tau_0' = \infty$, $k = 1$).

It should be noted, however, that the Rayleigh and isotropic scattering are by no means observed in clouds. If we remain within the limits of the scattering laws peculiar to clouds, the difference between brightness curves is found to be insignificant. Figure 9 compares the brightness of the reflected light for $\rho = 10$ and 20.

The relative influence of indicatrix shape becomes stronger with increasing absorption, since then the effective reflecting layer becomes thinner and the number of scatterings, which smooth the indicatrix effect, diminishes.

On the whole, the figures presented here indicate a decisive influence of absorption on the nature of light reflection from a cloud. Figure 10 enables us to establish further that the region of weak ab-

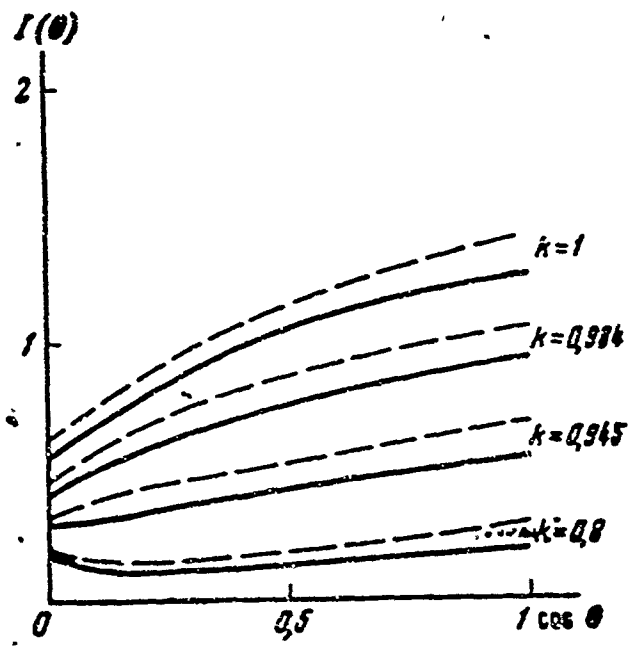

Fig. 9. Brightness of reflected light as a function of indicatrix shape. $\zeta = 0$, $\tau_0 = 12$; solid line $\rho = 20$; dashed line $\rho = 10$.

sorption, where a small change in the absorptivity results in a large change in the reflected radiation, is particularly critical.

The information obtained would appear useful for solving problems of cloud identification from satellite observations.

As we noted at the beginning of the paper, the transformation of radiation emanating from the clouds into the atmosphere above the clouds must be taken into account simultaneously.

The propagation of radiation in the atmosphere with cloud cover taken into account has not yet been studied thoroughly enough. We made a preliminary attempt to use the cloud-optics data enumerated above to ascertain the possibility of cloud differentiation. The distorting effect of the haze above the cloud was taken into account.

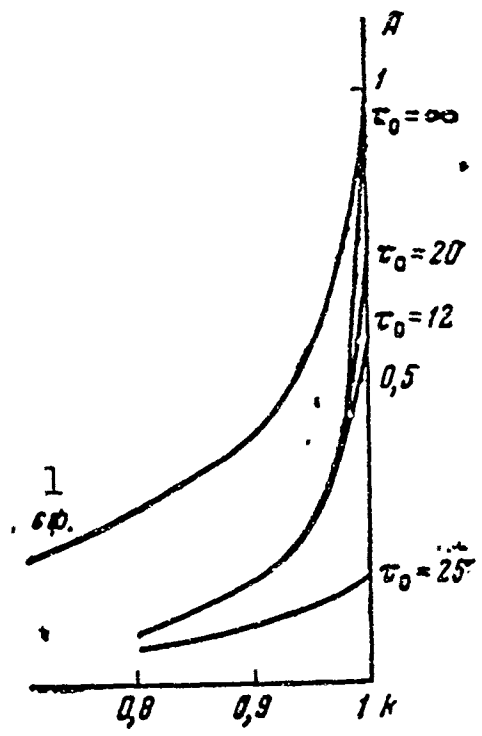

Fig. 10. Change in albedo with increasing absorptivity of the medium. $\zeta = 0$, $\rho = 20$; the curve marked sf corresponds to the case of the spherical indicatrix. 1) sf.

We arrived at the following conclusions, which are, unfortunately, of a negative nature. These conclusions do not by any means pretend to be definitive.

1. In the visible region of the spectrum, the scattered light of the haze significantly distorts the light arriving at the upper boundary of the atmosphere from the cloud.

2. The haze luminosity above clouds does

not depend on wavelength any more than it does on cloud albedo. Thus it is impossible to count on differentiation of clouds situated at different levels on the basis of their spectral brightness curves.

3. Low-lying clouds may be brighter than clouds at high altitude by virtue of the greater thickness and scattering ability of the former. Hence the possibility of distinguishing cloud levels on the basis of differences in their brightness would also seem rather doubtful.

4. The angular distribution of the light reflected from a cloud is relatively uniform, except for the regions of the azimuth angles $135^\circ \leq \leq \psi \leq 180^\circ$. Here, with the sun at low altitudes, we observe a rapid increase in brightness in the direction toward the horizon. It will hardly be possible to exploit this peculiarity of the angular distribution for interpretation purposes, since it is also a property of snow and atmospheric haze.

5. The difference between the albedos at the center ($\lambda = 0.76$ microns) and on the skirt of the oxygen absorption band may introduce an error of the order of 10-20% in the determination of the atmosphere's optical thickness above the cloud.

6. Clouds that are not transilluminated may be regarded as black bodies with an error of 5-10% in the spectral intervals (4 microns $\leq \leq \lambda \leq 7$ microns) and (12 microns $\leq \lambda \leq 40$ microns). In the atmospheric transparency window (8 microns $\leq \lambda \leq 12$ microns), this error amounts to 15-25%.

In conclusion, let us indicate a number of cloud-optics problems that are, from our standpoint, of the first importance.

It is necessary to expand experimental research in clouds - study of the micro- and macrooptical conditions in clouds with simultaneous following of their physical properties.

It is necessary to supplement the tables of absorption and scat-

tering coefficients of water droplets in the absorption region, calculate the scattering indicatrix with absorption and determine the optical properties of ice crystals.

An important task is the calculation of the optical characteristics of real clouds – a project that must be preceded by cloud classification and the elaboration of average representative parameters for the various groups: average droplet radius, wetness, altitude level, thickness, etc.

In the field of radiation transfer, we may regard as basically complete the work to determine the fluxes of radiation reflected and transmitted by a two-dimensional cloud layer and the qualitative laws governing its behavior as a function of wavelength, the sun's position and the optical thickness of the cloud.

The principal problems here are to correct for the irregular shapes of the cloud surface and determine the optical conditions set up by clouds of limited extent distributed statistically in space. The interaction of the luminous fields inside and outside the clouds must also be studied, i.e., we must trace the path of a sunbeam through the atmosphere and the cloud, its reflection from the earth's surface and its return to the upper boundary of the atmosphere.

Received 23 December 1963

REFERENCES

1. Ye.M. Feygel'son, M.S. Malkevich, S.Ya. Kogan et al., Tr. In-ta fiziki atmosfery AN SSSR [Transactions of the Institute of Atmospheric Physics of the Academy of Sciences USSR], No. 1, 1958.
2. Ye.M. Feygel'son. Radiatsionnyye protsessy v sloistoobraznykh oblakakh. [Radiation Processes in Stratified Clouds] Izd-vo AN SSSR [Publishing House of the Academy of Sciences USSR], 1964.

3. L.M. Romanova. Optika i spektroskopiya [Optics and Spectroscopy] 13, No. 3, 429, 1962.

4. L.M. Romanova. Optika i spektroskopiya, 13, No. 6, 819, 1962.

5. L.M. Romanova. Optika i spektroskopiya, 14 No. 2, 262, 1963.

6. G.V. Rozenberg. Dokl. AN SSSR [Proceedings of the Academy of Sciences USSR], 145, No. 4, 775, 1962.

7. G.V. Rozenberg. In collection entitled: "Spektroskopiya rasseivayushchikh sred" [Spectroscopy of Scattering Media] Minsk 1963.

Manuscript Page No.	[Transliterated Symbols]
159	sh = sinh
165	сф = sf = sfericheskiy = spherical

EQUATION FOR RELEVANCE OF INFORMATION FROM WEATHER SATELLITES AND FORMULATION OF INVERSE PROBLEMS

G.I. Marchuk

Problems of atmospheric optics and long-wave radiation transfer are considered. Functionals of the basic problems are introduced into the discussion as the readings of instruments of the weather satellite. Adjoint equations related to the corresponding functionals of the problem are constructed; these are referred to as equations for revelance of information with respect to the specified functionals. Using the basic and adjoint equations, the paper develops a theory of perturbations. The perturbation-theory formula makes it possible to formulate the corresponding inverse problems of meteorology.

* * *

The present paper will formulate an equation for relevance of information obtained from weather satellites. It is assumed that the satellite has a set of instruments that register certain characteristics of the radiation field. The instrument readings are functionals of the corresponding problems. We shall consider the process of radiation transfer at assigned frequencies in the range from the ultraviolet to long-wave radiation.

Let us introduce into the discussion a standard atmosphere that is characterized by an assigned distribution of the meteorological elements: temperature, humidity, density, aerosols, etc. Using the transfer equation for the standard atmosphere, we can formulate the problem

of radiation transfer. This problem will be referred to as the unperturbed problem.

Instruments aboard the weather satellite will register the true functionals of problems, which differ from the functionals of unperturbed problems by a certain increment, which we shall call the variation of the functional. The basic problem consists in determining the variations of the atmospheric characteristics from given variations of the functionals.

Below we shall set forth a general standpoint as to the inverse problems related to interpretation of weather-satellite data and present algorithms for solving certain inverse problems.

1. FORMULATION OF INVERSE PROBLEMS

Let φ be the intensity of the radiation and $\underline{f}$ be the radiation sources. Then the problem of radiation transfer assumes the following operational form:

$$L\varphi = f, \tag{1}$$

where L is the integrodifferential radiation-transfer operator. The functions φ and $\underline{f}$ belong to the classes of functions for which Eq. (1) has sense. Moreover, all functions from among which the solution φ is selected satisfy boundary conditions.

Let us introduce into the discussion the scalar product (g, h) as the integral, taken over the entire range of problem variables, of the product of the functions $\underline{g}$ and $\underline{h}$ and define the adjoint operator L* in the Lagrangian sense:

$$(h, Lg) = (g, L^*h). \tag{2}$$

Let us consider a certain linear functional of the radiation field, a functional that can always be presented in the form of the following product:

$$J_p(\varphi) = (p, \varphi), \tag{3}$$

and introduce into the discussion the adjoint equation with respect to this functional:

$$L^*\varphi_p^* = p, \tag{4}$$

where φ_p^* belongs to the class of functions satisfying the boundary conditions and certain differentiability properties.

We perform scalar multiplication of Eq. (1) by φ_p^* and of Eq. (4) by φ and take the difference between the expressions obtained:

$$(\varphi_p^*, L\varphi) - (\varphi, L^*\varphi_p^*) = (f, \varphi_p^*) - (p, \varphi). \tag{5}$$

Taking Relationship (2) into account, the left member of Equality (5) is zero, so that we have the formula

$$J_p(\varphi) = (f, \varphi_p^*). \tag{6}$$

Thus, the functional $J_p(\varphi)$ under consideration may be calculated either from Formula (3) or Formula (6).

This means that the functional $J_p(\varphi)$ can be calculated by either of two completely different methods: either by means of the solution to the basic problem (1), or by means of the adjoint problem (4).

This approach to determination of linear functionals has been developed particularly intensively in nuclear physics [1-6]. The general formulation of the problem was set up in [3], which gives a derivation of perturbation-theory formulas for the function $J_p(\varphi)$.

We shall regard Problems (1) and (4) as unperturbed; their solutions are found for standard characteristics of the radiation field.

Since we have at our disposal a set of functional variations, let us use them to find perturbations in the basic characteristics of the atmosphere. For this purpose, we construct the corresponding formulas of the perturbation theory for the functionals.

Let us introduce the perturbed problem

$$L'\varphi' = f', \tag{7}$$

where

$$L' = L + \delta L,$$
$$f' = f + \delta f. \qquad (8)$$

We perform scalar multiplication of Eq. (7) by the function $\varphi_p{}^*$ and of (4) by the function φ' and subtract one result from the other. Then we shall have

$$(\varphi_p{}^*, L'\varphi') - (\varphi', L^*, \varphi_p{}^*) = (f', \varphi_p{}^*) - (p, \varphi'), \qquad (9)$$

taking Relationships (5) and (8) into account, we rewrite Equality (9) in the form

$$(\varphi_p{}^*, \delta L\varphi') = (\varphi_p{}^*, \delta f) - \delta J_p, \qquad (10)$$

where

$$\delta I_p = J_p(\varphi') - J_p(\varphi).$$

Finally, we rewrite Relationship (10) in the form

$$(\varphi_p{}^*, \delta L\varphi' - \delta f) = \delta J_p. \qquad (11)$$

Formula (11) may be written for any linear functional from among the set (n = 1, 2, ..., N):

$$(\varphi_{p_n}^*, \delta L\varphi' - \delta f) = -\delta J_{p_n}. \qquad (12)$$

The functions $\varphi_{p_n}{}^*$ are statistical weights in Formulas (12) and characterize the region of influence of the perturbation $\delta L\varphi' - \delta f$ over the entire phase space. Taking this circumstance into account, we may refer to the functions $\varphi_{p_n}{}^*$ as information-value functions with respect to the functional J_{p_n}.

Let us further consider the difference between the variations of the functionals for various parameters n. Then we obtain

$$(\varphi_{p_n}^* - \varphi_{p_m}^*, \delta L\varphi' - \delta f) = \delta J_{p_m} - \delta J_{p_n}. \qquad (13)$$

Obviously, the information in the various functionals must be independent, i.e.,

$$\varphi_{p_n}^* \not\equiv \varphi_{p_m}^*.$$

Let us fix upon a certain functional J_{p_n}.

To this functional there corresponds an adjoint function $\varphi_{p_n}^*$ that is a solution of Eq. (4). To evaluate the independent information content in $\varphi_{p_m}^*$ it is convenient to examine the functions

$$\varphi^*_{p_n p_m} = \varphi^*_{p_n} - \varphi^*_{p_m}.$$

Thus, we arrive at the following set of problems:

$$\begin{aligned} L^*\varphi^*_{p_n} &= p_n, \\ L^*\varphi_{p_n p_m} &= p_n - p_m. \end{aligned} \tag{14}$$

2. INVERSE PROBLEMS OF ATMOSPHERIC OPTICS

In interpreting the results of observations from weather satellites of the radiation field in the visible region of the spectrum, it is possible to formulate various inverse problems in the determination of certain important atmospheric characteristics. For the sake of simplicity, we shall assume that the unknown atmospheric characteristic is the deviation from normal distribution of the density at a certain substation absorbing and scattering radiation. We shall regard the atmosphere as a flat layer; the external radiation source is the sun [7-9]. Then we arrive at the following equation:

$$\begin{aligned} \mu \frac{\partial \varphi}{\partial z} + \alpha_\nu \varphi - \frac{1}{2} \int_{-1}^{1} d\mu' \varphi \alpha_{s\nu} \gamma_\nu(\mu, \mu') &= f, \\ f &= -S_\nu \delta(\mu - \mu_\odot) \delta(z - h) \mu_\odot, \end{aligned} \tag{15}$$

which can be written in the operational form

$$L\varphi = f. \tag{16}$$

Here we have assumed that the problem's solution is independent of azimuth and have introduced the following symbols: φ is the intensity of the radiation at a frequency ν, $\alpha_\nu = \alpha_{s\nu} + \alpha_{c\nu}$, $\alpha_{s\nu}$ is the scattering cross section, $\alpha_{c\nu}$ is the absorption cross section, S_ν is the solar radiation spectrum, $\alpha_\nu = \alpha_{s\nu} + \alpha_{c\nu}$, $\alpha_{s\nu}$ is the altitude of the sun, $\underline{z}$ is a

vertical coordinate with its origin at the earth's surface, $\underline{h}$ is the upper limit of the atmosphere, $\mu = \cos \vartheta$, ϑ is the elevation and γ_ν (μ, μ') is the scattering indicatrix:

$$\gamma_\nu(\mu, \mu') = \sum_n \frac{2n+1}{2} \gamma_\nu P_n(\mu) P_n(\mu'). \tag{17}$$

We select the following boundary conditions for the function φ. At the upper boundary of the atmosphere, the condition is that no radiation be arriving from without. Since the sunlight is taken into account in the transfer equation itself, we shall have

$$\varphi(h, \mu) = 0 \text{ for } \mu < 0. \tag{18}$$

For the surface of the earth, we shall assume that the arriving radiation is reflected diffusely from the earth's surface with an assigned albedo a_ν. Then we arrive at the condition

$$\frac{1}{2}\varphi(0, \mu) = a_\nu \int_{-1}^{0} \varphi(0, \mu')\mu' d\mu' \text{ for } \mu > 0. \tag{19}$$

Further, we introduce into consideration the functional $J_p(\varphi)$, which is related to the reading of the instrument registering, onboard the weather satellite, the influx of radiation from the atmosphere, with its spectral characteristic $\xi(\nu)$. The following equality will obviously obtain:

$$J_p(\varphi) = \int_0^h dz \int_0^\infty d\nu \int_{-1}^{1} d\mu \, p\varphi, \tag{20}$$

where

$$p = \mu g(\mu)\xi(\nu)\delta(z-h), \qquad g(\mu) = \begin{cases} 1, & \mu > 0 \\ 0, & \mu < 0. \end{cases} \tag{21}$$

Taking the form of the function $\underline{p}$ into account, the expression for the functional $J_p(\varphi)$ will be to some extent simplified:

$$J_p(\varphi) = \int_0^\infty d\nu \int_0^1 \xi(\nu)\varphi\mu \, d\mu, \; z = h. \tag{22}$$

It is obvious that in the phase space under consideration, the scalar product will be defined as follows:

$$(\varphi, \varphi^*) = \int_0^h dz \int_0^\infty d\nu \int_{-1}^1 d\mu \varphi \varphi^*. \tag{23}$$

Let us introduce into consideration the adjoint equation

$$L^* \varphi_p^* = p, \tag{24}$$

where p is defined by Formula (21) and L* is a Lagrangian adjoint operator that satisfies Condition (2). We can satisfy ourselves by a direct check that the form of the operator L* is given by the formula

$$L^* \varphi_p^* = -\mu \frac{\partial \varphi_p^*}{\partial z} + \alpha_\nu \varphi_p^* - \frac{\alpha_{s\nu}}{2} \int_{-1}^1 d\mu' \varphi_p^* \gamma_\nu(\mu, \mu'). \tag{25}$$

Thus, the adjoint radiation-transfer equation will take the form

$$-\mu \frac{\partial \varphi_p^*}{\partial z} + \alpha_\nu \varphi_p^* - \frac{\alpha_{s\nu}}{2} \int_{-1}^1 d\mu' \varphi_p^* \gamma_\nu(\mu, \mu') = p. \tag{26}$$

We note, however, that Condition (2) will be identically satisfied only provided that, in addition to this, we bind the function φ_p^* with additional conditions, which perform the functions of boundary conditions for Eq. (26):

at the upper boundary of the atmosphere

$$\varphi_p^*(h, \mu) = 0 \quad \text{for} \quad \mu > 0, \tag{27}$$

at the earth's surface

$$\frac{1}{2} \varphi_p^*(0, \mu) = -a_\nu \int_0^1 d\mu' \mu' \varphi_p^*. \tag{28}$$

In accordance with the general theory, the problem functional may also be defined by means of the solution to the adjoint equation

$$J_p(\varphi) = \int_0^h dz \int_0^\infty d\nu \int_{-1}^1 d\mu f \varphi_p^* \tag{29}$$

or, taking into account the form of the function f,

$$J_p(\varphi) = \int_0^\infty d\nu S_\nu \varphi_p^*(h, \mu_\odot). \tag{30}$$

We note that φ and φ_p^* are functions of ν, although this fact is not pointed out specifically.

Let us now assume that the meteorological instrument fixes a devia-

tion of the functional J_p from the value corresponding to the standard atmosphere, i.e., it senses a quantity

$$\delta J_p = J\delta(\varphi') - J_p(\varphi). \tag{31}$$

This deviation is due to a change in the density of the substation being studied in the atmosphere. The problem now consists in connecting changes in the atmospheric characteristic with the variation of the functional and finding the variation of the substation density.

For this purpose, let us consider the perturbed equation (15):

$$\mu \frac{\partial \varphi'}{\partial z} + \alpha_\nu' \varphi' - \frac{1}{2} \int_{-1}^{1} d\mu' \varphi' \alpha_{s\nu}' \gamma_\nu(\mu, \mu') = f. \tag{32}$$

It is assumed that the solution φ' satisfies the boundary conditions (18) and (19).

Let us further multiply Eq. (32) by φ_p^* and Eq. (26) by φ'; we subtract one expression from the other and integrate the result over the entire region in which the solution is defined.

Then, setting

$$L' = L + \delta L,$$

where

$$L = \mu \frac{\partial}{\partial z} + \alpha_\nu - \frac{1}{2} \int_{-1}^{1} d\mu' \alpha_{s\nu} \gamma_\nu(\mu, \mu'),$$

$$\delta L = \delta\alpha_\nu - \frac{1}{2} \int_{-1}^{1} d\mu' \delta\alpha_{s\nu} \gamma_\nu(\mu, \mu'),$$

and applying Relationship (2), we arrive at the perturbation-theory formula for the functional $J_p(\varphi)$:

$$(\varphi_p^*, \delta L \varphi') = -\delta J_p. \tag{33}$$

On expansion, Formula (33) becomes

$$\int_0^h dz \int_0^\infty d\nu \int_{-1}^{1} d\mu \varphi_p^* \left[\delta\alpha_\nu \varphi' - \frac{1}{2} \int_{-1}^{1} d\mu' \varphi' \delta\alpha_{s\nu} \gamma_\nu(\mu, \mu') \right] = -\delta J_p. \tag{34}$$

The functions α_ν and $\alpha_{s\nu}$ are related to the density ρ of the absorbing and scattering substation point:

$$\alpha_\nu = \rho\sigma_\nu, \quad \alpha_{s\nu} = \rho\sigma_{s\nu},$$

where σ is the cross section referred to the unit of substation mass.

Then we shall have

$$\delta\alpha_\nu = \delta\rho(z)\,\sigma_\nu, \qquad \delta\alpha_{s\nu} = \delta\rho(z)\,\sigma_{s\nu}. \tag{35}$$

We substitute Relationships (35) in Formula (34) and obtain

$$\int_0^h \delta\rho(z)\,F_p(z)\,dz = -\,\delta J_p, \tag{36}$$

where

$$F_p(z) = \int_0^\infty d\nu \int_{-1}^{1} d\mu\varphi_p^* \left[\sigma_\nu\varphi' - \frac{1}{2}\int_{-1}^{1} d\mu'\sigma_{s\nu}\varphi'\gamma_\nu(\mu,\,\mu')\right]. \tag{37}$$

In the event that the solution perturbation is small, i.e., if we can in approximation set $\varphi' = \varphi$, the function $F_p(z)$ will be fully defined by

$$F_p(z) = \int_0^\infty d\nu \int_{-1}^{1} d\mu\varphi_p^* \left[\sigma_\nu\varphi - \frac{1}{2}\int_{-1}^{1} d\mu'\sigma_{s\nu}\varphi\gamma_\nu(\mu,\,\mu')\right] \tag{37a}$$

and can be tabulated in advance.

If there is a set of functionals J_{p_n}, then we arrive, in much the same way as above, at the equation system

$$\int_0^h \delta\rho(z)\,F_{p_n}(z)\,dz = -\,\delta J_{p_n} \quad (n = 1,\,2,\,\ldots,\,N), \tag{38}$$

where

$$F_{p_n} \int_0^\infty \nu \int_{-1}^{1} d\mu\varphi^*_{p_n}\left[\sigma_\nu\varphi' - \frac{1}{2}\int_{-1}^{1} d\mu'\varphi'\sigma_{s\nu}\gamma_\nu(\mu,\,\mu')\right]. \tag{39}$$

The system of equations (38) may be used to find functions $\delta\dot{\rho}(z)$. There are at least two approaches to solution of this problem.

The first approach consists in the following. Let us assume that the standard distribution of substation density can be described by an interpolation formula of the type

$$\rho(z) = \sum_i \varkappa_i g_i(\beta_i z), \tag{40}$$

where κ_i and β_i are parameters and $g_i(x)$ are the assigned interpolation functions.

On the assumption that the perturbed density $\rho'(z)$ can be described by Formula (40) with changed parameters κ_1', β_1', we may write in approximation that

$$\delta\rho(z) = \sum_i \left[\delta\kappa_i g_i(\beta_i z) + \delta\beta_i \kappa_i \frac{\partial g_i}{\partial \beta_i} \right]. \tag{41}$$

Strictly speaking, the representation (41) is valid only for small variations $\delta\kappa_i$ and $\delta\beta_i$. Later, however, we shall introduce into consideration a method of successive approximations that will expand the region of applicability of (41).

Formula(41) is conveniently written in the form

$$\delta\rho(z) = \sum_i \delta\varepsilon_i \psi_i(z), \tag{42}$$

where $\{\delta\varepsilon_i\}$ is the sequence of parameters $\{\delta\kappa_i\}$ and $\{\delta\beta_i\}$, and $\{\psi_i\}$ is the sequence of functions $\{g_i\}$ and $\{\kappa_i \partial g_i / \partial \beta_i\}$.

Let us substitute Expression (42) into system (38). Then we obtain

$$\sum_i \delta\varepsilon_i a_{ni} = -b_n \qquad (i, n = 1, 2, \ldots, N), \tag{43}$$

where

$$a_{ni} = \int_0^h \psi_i F_{p_n} dz, \qquad b_n = \delta J_{p_n}. \tag{44}$$

If the matrix $A = \| a_{ni} \|$ is conditioned well, the system of linear equations is solved effectively and the solution is found in the form

$$\delta\varepsilon = A^{-1} b. \tag{45}$$

If the perturbations are not small, we can formulate a method of successive approximations as follows:

$$\delta\varepsilon^{(m+1)} = A_m^{-1} b^{(m)}, \tag{46}$$

where

$$\begin{gathered} a_{ni}^{(m)} = \int_0^h \psi_i^{(m)} F_{p_n}^{(m)} dz, \\ b_n^{(m)} = -\delta J_{p_n}^{(m)} = J_{p_n}(\varphi) - J_{p_{n_i}}(\varphi^{(m)}), \\ F_{p_n}^{(m)} = \int_0^\infty d\nu \int_{-1}^1 d\mu \varphi^*_{p_n} \left[\sigma_\nu \varphi^{(m)} - \frac{1}{2} \int_{-1}^1 d\mu' \, {}^{(m)}\sigma_{s\nu} \gamma_\nu(\mu, \mu') \right]. \end{gathered} \tag{47}$$

Here $\varphi^{(m)}$ is the solution of equation (15) for

$$\rho = \rho^{(m)}(z),\ \psi_i^{(m)} = \psi_i(z;\ \beta^{(m)}).$$

The second approach involves the construction of a suitable quadrature formula for the integral in the left-hand member of Formula (38). We set

$$\int_0^h \delta\rho(z)\, F_{p_n}(z)\, dz = \sum_i c_{in}\delta\rho_i, \qquad (48)$$

where $\delta\rho_i = \delta\rho(z_i)$, and c_{in} are the coefficients of the quadrature formula taking the multiplier $F_{pn}(z)$ into account. Obviously, such a formulation of the inverse problem does not differ fundamentally from that considered previously. The successive-approximation method is defined similarly here.

One important remark: if the instrument were to sense monochromatic radiation, it would be possible to drop the integration over ν. In this case, it is not difficult to satisfy ourselves that the adjoint function would also differ from zero only for $\nu = \nu_0$. As a rule, however, the resolution of the instruments does not enable us to make this assumption, since the function σ^{ν} may vary quite substantially in the instruments's resolution interval, and this circumstance must be taken into account very carefully, since the value of information with respect to the functional J_p may vary considerably in this case from the monochromatic approximation.

The algorithm that we have formulated in setting up the inverse problems is generalized trivially for various cases. Thus, for example, it might be assumed that the atmosphere consists of a mixture of substances and that the densities of many substations are perturbed simultaneously. Further, it has been assumed in the calculations that the scattering indicatrix and albedo do not vary. If these quantities do vary, similar perturbation theory formulas may be written for them.

Other generalizations are also possible.

In conclusion, we draw attention to certain simplifications of the problem's mathematical formulation. Specifically, in the analysis given above the right-hand members of Eqs. (15) and (26) incorporated sources different from zero only at the upper boundary of the atmosphere, at z = h. It is possible to give equivalent formulations of the problems in which the sources are taken into account in the boundary conditions. In this case, the problem for the basic and adjoint functions is formulated as follows:

$$\begin{gathered}\mu\frac{\partial\varphi}{\partial z}+\alpha_\nu\varphi-\frac{1}{2}\int_{-1}^{1}d\mu'\varphi\alpha_{s\nu}\gamma_\nu(\mu,\mu')=0,\\ \varphi(h,\mu)=S_\nu\delta(\mu-\mu_\odot)\quad\text{for}\quad\mu<0,\\ \frac{1}{2}\varphi(0,\mu)=a_\nu\int_{-1}^{0}\varphi(0,\mu')\mu'd\mu'\quad\text{for}\quad\mu>0\end{gathered}\tag{49}$$

for the radiation intensity and

$$\begin{gathered}-\mu\frac{\partial\varphi_p^*}{\partial z}+\alpha_\nu\varphi_p^*\frac{\alpha_{s\nu}}{2}\int_{-1}^{1}d\mu'\varphi_p^*\gamma_\nu(\mu,\mu')=0,\\ \varphi_p^*(h,\mu)=g(\mu)\xi(\mu)\quad\text{for}\quad\mu>0\\ \frac{1}{2}\varphi_p^*(0,\mu)=-a_\nu\int_{0}^{1}\varphi_p^*(0,\mu')\mu'd\mu'\quad\text{for}\quad\mu<0\end{gathered}\tag{50}$$

for the adjoint functions.

Under the next heading, we show the equivalence of these two approaches to formulation of the system of basic and adjoint radition-transfer equations on the example provided by long-wave radiation.

3. INVERSE PROBLEMS OF LONG-WAVE RADIATION

Under the present heading, we shall formulate the problem of temperature recovery in the atmosphere over the field of receding long-wave radiation being registered by the instruments aboard the weather satelite.

As before, we shall take the reading of the instrument registering

the total long-wave radiant flux in the range of frequencies with the instrument characteristic $\xi(\nu)$ as the radiation-field functional. Then we shall have

$$J_p = \int_0^\infty d\nu \int_0^1 \xi(\nu)\,\varphi\mu\,d\mu \qquad (z = h). \tag{51}$$

The transfer equation for the long-wave radiation in the atmosphere will be written as follows:

$$\mu \frac{\partial \varphi}{\partial z} + \alpha_\nu \varphi - \frac{1}{2} \int_{-1}^{1} d\mu' \varphi \alpha_{s\nu} \gamma(\mu, \mu') = f, \tag{52}$$

where f is the atmosphere's intrinsic radiation, definable in the form

$$f = \frac{1}{2} \alpha_{c\nu} \eta_\nu(T), \tag{53}$$

where $\eta_\nu(T)$ is determined by Planck's formula:

$$\eta_\nu(T) = 2\pi \frac{2h\nu^3}{c^2} \frac{1}{e^{h\nu/kT} - 1}$$

with the following normalization:

$$\int_0^\infty \eta_\nu(T)\,d\nu = 2\pi\sigma T^4,$$

where σ is Boltzmann's constant, h is Planck's constant, c is the velocity of light in a vacuum and kT is the internal energy of the medium.

For the conditions at the upper limit of the atmosphere we take

$$\varphi(h, \mu) = 0 \text{ for } \mu < 0 \tag{54}$$

and at the surface of the earth

$$\frac{1}{2}\varphi(0, \mu) = a_\nu \int_{-1}^{0} d\mu' \mu' \varphi(0, \mu') + \frac{1}{2}\eta_\nu(T) \quad \text{for } \mu > 0, \tag{55}$$

where T_0 is the temperature of the earth's surface layer. The essential difference between this problem and the case of short-wave transfer is the fact that the boundary condition at the earth's surface (55) has now been found nonhomogeneous due to the fact that the earth's own radiation has been taken into account. If T_0 is assigned, then the direct problem (52), (54), (55) is completely formulated and its solution may

be effected by highly developed methods.

Let us proceed further to formulation of the adjoint problem with respect to the functional J_p. For this purpose, we consider the basic adjunction

$$(\varphi^*, L\varphi) = (\varphi, L^*\varphi_p^*), \tag{56}$$

where φ and φ^* are functions from the corresponding spaces recorded.

Let $\varphi^* = \varphi_p^*$, and let φ be a solution to the problem (52), (54), (55).

Let us examine the expression

$$(\varphi_p^*, L\varphi) = \int_0^\infty d\nu \int_{-1}^{1} d\mu \int_0^h \varphi_p^* \left[\mu \frac{\partial \varphi}{\partial z} + \alpha_\nu \varphi - \frac{1}{2} \int_{-1}^{1} d\mu' \varphi \alpha_{s\nu} \gamma_\nu(\mu, \mu') \right]. \tag{57}$$

We recast the first term in the form

$$\int_0^\infty d\nu \int_{-1}^{1} d\mu \int_0^h dz \varphi_p^* \mu \frac{\partial \varphi}{\partial z} = \int_0^\infty d\nu \int_{-1}^{1} d\mu \mu \varphi_p^* \varphi \Big|_{z=0}^{z=h} - \int_0^\infty d\nu \int_{-1}^{1} d\mu \int_0^h dz \, \varphi \mu \frac{\partial \varphi_p^*}{\partial z}. \tag{58}$$

Changing the orders of integration in the remaining terms of (57), we obtain

$$(\varphi_p^*, L\varphi) = \int_0^\infty d\nu \int_{-1}^{1} d\mu \int_0^h dz \varphi \left[-\mu \frac{\partial \varphi_p^*}{dz} + \alpha_\nu \varphi_p^* - \right.$$
$$\left. - \frac{\alpha_{s\nu}}{2} \int_{-1}^{1} d\mu' \varphi_p^* \gamma_\nu(\mu, \mu') \right] + \int_0^\infty d\nu \int_{-1}^{1} d\mu \, \mu \varphi_p^* \varphi \Big|_{z=0}^{z=h}. \tag{59}$$

Then we adopt the notation

$$L^* \varphi_p^* = -\mu \frac{\partial \varphi_p^*}{\partial z} + \alpha_\nu \varphi_p^* - \frac{\alpha_{s\nu}}{2} \int_{-1}^{1} d\mu' \varphi_p^* \gamma_\nu(\mu, \mu'). \tag{60}$$

Then Relationship (59) is written in the form

$$(\varphi^*, L\varphi) = (\varphi, L^*\varphi_p^*) + \int_0^\infty d\nu \int_{-1}^{1} d\mu \, \mu \varphi_p^* \varphi \Big|_{z=0}^{z=h}, \tag{61}$$

Now we require satisfaction of the equality

$$L^* \varphi_p^* = 0. \tag{62}$$

Then, applying Equation (52), we rewrite Relationship (61) in the

form

$$(\varphi_p^*, f) = \int_0^\infty d\nu \int_{-1}^{1} d\mu\, \mu \varphi_p^* \varphi \Big|_{z=0.}^{z=h.} \tag{63}$$

We present Expression (63) in the form

$$(\varphi_p^*, f) = a - b, \tag{64}$$

where

$$a = \int_0^\infty d\nu \int_{-1}^{1} d\mu\, \mu \varphi_p^*(h, \mu)\, \varphi(h, \mu),$$

$$b = \int_0^\infty d\nu \int_{-1}^{1} d\mu\, \mu \varphi_p^*(0, \mu)\, \varphi(0, \mu).$$

Let us examine the expression for the quantity b in the following form

$$b = \int_0^\infty d\nu \int_{-1}^{0} d\mu\, \mu \varphi_p^*(0, \mu)\, \varphi(0, \mu) + \int_0^\infty d\nu \int_0^1 d\mu\, \mu \varphi_p^*(0, \mu)\, \varphi(0, \mu). \tag{65}$$

Now let us recall that the solution $\varphi(0,\mu)$ satisfies the boundary condition (55), which we present in the form

$$\varphi(0, \mu) = 2a_\nu \int_{-1}^{1} d\mu'\, \mu' \varphi(0, \mu') + \eta_\nu(T_0) \quad \text{for} \quad \mu > 0. \tag{66}$$

We substitute Expression (66) in the second integral of Formula (65). Then we obtain

$$b = \int_0^\infty d\nu \int_{-1}^{0} d\mu\, \varphi(0, \mu) \left[\varphi_p^*(0, \mu) + 2a_\nu \int_0^1 d\mu'\, \mu' \varphi_p^*(0, \mu')\right] + \\ + \int_0^\infty d\nu \int_0^1 d\mu\, \mu \varphi_p^*(0, \mu)\, \eta_\nu(T_0). \tag{67}$$

We require satisfaction of the condition

$$\frac{1}{2} \varphi_p^*(0, \mu) = -a_\nu \int_0^1 d\mu'\, \mu' \varphi_p^*(0, \mu). \tag{68}$$

Then we obtain

$$b = \int_0^\infty d\nu \int_0^1 d\mu\, \mu \varphi_p^*(0, \mu)\, \eta_\nu(T_0). \tag{69}$$

Let us examine the expression for the quantity

$$a = \int_0^\infty d\nu \int_{-1}^{0} d\mu\, \mu \varphi_p^*(h, \mu)\, \varphi(h, \mu) + \int_0^\infty d\nu \int_0^1 d\mu\, \mu \varphi_p^*(h, \mu)\, \varphi(h, \mu). \tag{70}$$

From Condition (54), we may conclude that the first integral is zero, inasmuch as $\varphi(h, \mu) = 0$. We require that the second integral in Formula (70) be equal to the functional J_p, i.e.,

$$J_p = \int_0^\infty d\nu \int_0^1 d\mu\, \mu \varphi_p^*(h, \mu)\, \varphi(h, \mu). \tag{71}$$

To make Expression (71) agree with (51), it is necessary to set

$$\varphi_p^*(h, \mu) = g(\mu)\xi(\nu).$$

Taking the above into account, we may give Expression (64) the form

$$(\varphi_p^*, f) = J_p - \int_0^\infty d\nu \int_0^1 d\mu\, \mu \varphi_p^*(0, \mu)\, \eta_\nu(T_0),$$

from which it follows directly that

$$J_p = (\varphi_p^*, f) + \int_0^\infty d\nu \int_0^1 d\mu\, \mu \varphi_p^*(0, \mu)\, \eta_\nu(T_0)$$

or, in expanded form,

$$J_p = \frac{1}{2}\int_0^h dz \int_0^\infty d\nu \int_{-1}^1 d\mu\, \varphi_p^* \alpha_{c\nu} \eta_\nu(T) + \int_0^\infty d\nu \int_0^1 d\mu\, \mu \varphi_p^*(0, \mu)\, \eta_\nu(T_0). \tag{72}$$

Thus, the adjoint problem with respect to the functional will take the form

$$\begin{gathered} -\mu \frac{\partial \varphi_p^*}{\partial z} + \alpha_\nu \varphi_p^* - \frac{\alpha_{s\nu}}{2} \int_{-1}^1 d\mu' \varphi_p^* \gamma_\nu(\mu, \mu') = 0, \\ \varphi_p^*(h, \mu) = g(\mu)\xi(\nu) \text{ for } \mu > 0, \\ \frac{1}{2}\varphi_p^*(0, \mu) = -\alpha_\nu \int_0^1 d\mu' \mu' \varphi_p^*(0, \mu') \text{ for } \mu < 0. \end{gathered} \tag{73}$$

Here the functional J_p is calculated by one of the two following formulas:

$$J_p = \int_0^\infty d\nu \int_0^1 \xi(\nu)\, \varphi(h, \mu)\, \mu\, d\mu,$$

$$J_p = \frac{1}{2}\int_0^h dz \int_0^\infty d\nu \int_{-1}^1 d\mu\, \varphi_p^* \alpha_{c\nu} \eta_\nu(T) + \int_0^\infty d\nu \int_0^1 d\mu\, \mu \varphi_p^*(0, \mu)\, \eta_\nu(T_0). \tag{74}$$

Let us now assume that the functionals (74) correspond to the standard characteristics of the atmospheric temperature field. Let us consider the disturbed state of the atmosphere, which is characterized by a deviation of the temperature from the standard state. In the formulas for the functionals, this is reflected in the fact that they undergo some change in magnitude:

$$J_p + \delta J_p = \int_0^\infty d\nu \int_0^1 \xi(\nu)\varphi'(h, \mu)\mu\, d\mu,$$

$$J_p + \delta J_p = \frac{1}{2}\int_0^h dz \int_0^\infty d\nu \int_{-1}^1 d\mu \varphi_p^* \alpha_{c\nu}\eta_\nu(T + \delta T) + \tag{75}$$

$$+ \int_0^\infty d\nu \int_0^1 d\mu\, \mu\varphi_p^*(0, \mu)\,\eta_\nu(T_0 + \delta T_0).$$

Let us use the second formula of (75). Using the second formula (74) to exclude J_p, we obtain

$$\frac{1}{2}\int_0^h dz \int_0^\infty d\nu \int_{-1}^1 d\mu \varphi_p^* \alpha_{c\nu}\delta\eta_\nu(T) + \int_0^\infty d\nu \int_0^1 d\mu\, \mu\varphi_p^*(0, \mu)\,\delta\eta_\nu(T_0) = \delta J_p, \tag{76}$$

where

$$\delta\eta_\nu(T) = \eta_\nu(T + \delta T) - \eta_\nu(T). \tag{77}$$

Since the deviations of the temperature from the standard distribution do not, as a rule, exceed 10–20% of the absolute temperature, we may use the Taylor-series expansion of the function $\eta_\nu(T + \delta T)$ and drop all but the first two terms. Then we shall have in approximation

$$\eta_\nu(T + \delta T) = \eta_\nu(T) + (\partial\eta_\nu / \partial T)\delta T.$$

From this,

$$\delta\eta_\nu(T) = (\partial\eta_\nu / \partial T)\delta T. \tag{78}$$

Substituting Expression (78) into Formula (76), we get

$$\frac{1}{2}\int_0^h dz \int_0^\infty d\nu \int_{-1}^1 d\mu \varphi_p^* \alpha_{c\nu}\frac{\partial\eta_\nu}{\partial T}\delta T + \int_0^\infty d\nu \int_0^1 d\mu\, \varphi_p^*(0, \mu)\frac{\partial\eta_\nu}{\partial T_0}\delta T_0 = \delta J_p. \tag{79}$$

Thus, Formula (79) enables us to connect the variations of the functional δJ_p with the temperature variations. Formula (79) is conven-

iently recast as follows:

$$\int_0^h \delta T(z)\psi(z)dz + \Psi\delta T_0 = \delta J_p, \tag{80}$$

where

$$\psi(z) = \frac{1}{2}\int_0^\infty d\nu \int_{-1}^{1} d\mu \varphi_p^* \alpha_{c\nu} \frac{\partial \eta_\nu}{\partial T},$$
$$\Psi = \int_0^\infty d\nu \int_0^1 d\mu \varphi_p^*(0, \mu) \frac{\partial \eta_\nu}{\partial T_0}. \tag{81}$$

Let us assume that the satellite has N instruments that register various characteristics of the long-wave radiation. Then we have N functionals

$$J_{p_n} = \int_0^\infty d\nu \int_{-1}^{0} \xi_n(\nu)\varphi(h, \mu)\mu\, d\mu. \tag{82}$$

Then we obtain N equations of the form (80):

$$\int_0^h \delta T(z)\psi_n(z)dz + \Psi_n\delta T_0 = \delta J_{p_n}. \tag{83}$$

Here ψ_n and Ψ_n are determined by means of Formulas (81), where the function φ_p^* should be replaced by φ_{pn}^*.

Thus, we arrive at a system of equations for determining the deviations δT. Since the equation systems (83) and (38) are formally equivalent to one another, the methods already elaborated for application to System (38) are also usable for solution of System (83). As a result, we arrive at a solution for the inverse temperature-field problem.

Attention should be drawn to certain details of the calculation. To wit: to the extent that the function $\psi_n(z)$ and the quantities Ψ are expressed only in terms of the solutions to the unperturbed adjoint equations, the problem for $\varphi_{p_n}^*$ is solved once for assigned functions $\xi_n(\nu)$. Here it is not necessary to resort to successive approximations, which were necessary in solving the inverse problems of atmospheric optics. Even the quantity $\partial\eta_\nu/\partial T$ may be tabulated for fixed values of

BLANK PAGE

the standard temperatures. In cases where

$$\xi_n(\nu) = \xi_n \delta(\nu - \nu_n),$$

the problem becomes monochromatic and all integrations over ν are excluded.

In conclusion, we note that, simultaneously with the temperature variations, it may become necessary to account for the variations of other atmospheric characteristics, such as water-vapor density, etc.

In this case, we can first solve the inverse problem analogous to that considered above for atmospheric optics and find the substation density variations and, consequently, the form of the unperturbed equation for the standard temperature distribution. The problem of finding the $\varphi_{p_n}^*$ is solved for the operators thus found, and then Formulas (83) are used to set up and solve the inverse problem.

4. EQUATION FOR RELEVANCE OF INFORMATION FOR WEATHER SATELLITES

Under earlier headings, we derived adjoint functions, which we have used extensively in setting up inverse problems. In view of the special importance of these functions, let us dwell in greater detail on their qualitative analysis. The importance of the adjoint functions comes particularly clearly to the fore in studies of perturbation-theory formulas. For this purpose, let us consider Formula (36) with certain simplifying assumptions. Specifically, we shall assume that the problem is monochromatic, that there is no scattering of the radiation and that the function $\varphi' \cong \varphi$ does not depend on μ. Then Formulas (36), (37) are presented in the form

$$\int_0^h \delta\alpha(z)\varphi(z)\varphi_p^*(z) = -\delta J_p, \tag{84}$$

where

$$\varphi(z) = \int_{-1}^{1} \varphi(z, \mu)\, dz, \tag{85}$$

$$\varphi_p^*(z) = \frac{1}{2}\int_{-1}^{1} \varphi_p^*(z, \mu)\, dz.$$

We note that it is no longer the radiation intensity, but the radiant flux that appears in Formula (84).

Let us analyze Formula (84).

Obviously, the quantity $\delta\alpha\varphi$ describes the number of radiation absorption events per unit of atmospheric height.

We normalize the quantity $\varphi_p^*(z)$ as follows:

$$\int_0^h \varphi_p^*(z)\,dz = 1. \tag{86}$$

This can always be done by suitable normalization of J_p, i.e., we can consider cJ_p instead of J_p, where c is a constant that can be selected arbitarily. Obviously, such a substitution will effect only the scale of the functional.

Formula (84) indicates the following fact: the greater the number of radiation absorption events taking place, the smaller will be the functional J_p, since a smaller quantity of radiation will be registered by the instrument. Using the normalization (86), we may regard the function $\varphi_p^*(z)$ as the probability density. Indeed, let

$$\delta\alpha\varphi = \delta(z - z_0),$$

i.e., suppose that total absorption of the radiation has taken place at $z = z_0$, and that no additional absorptions take place outside. Then Formula (84) leads to the expression

$$\varphi_p^*(z_0) = -\delta J_p. \tag{87}$$

Formula (87) indicates the fact that

$$|\delta J_p| = \varphi_p^*(z_0), \tag{88}$$

i.e., the absolute value of the functional's variation is equal to the adjoint function. Applying the normalization (86), Formula (88) is interpreted as follows: the function $\varphi_p^*(z_0)$ is the probability that the functional will change by an amount $\varphi_p^*(z_0)$ in effecting absorption of radiation at the point $z = z_0$. This means that the variation of the

functional will depend on the magnitude of φ_p^* at this point.

If φ_p^* is vanishingly small at point z_0, then no matter how many absorption events occur in the neighborhood of this point, they will not produce essential variations δJ_p and, conversely, even not particularly intense radition-absorption events will produce significant deviations δJ_p at the points where the function φ_p has maxima. This means that the function φ_p^* can be interpreted as the relevance of the information in the region $0 \leq z \leq h$ with respect to the indication of the instrument or, what is the same thing, with respect to the functional J_p. In those regions where the function φ_p^* is small, the relevance of the information with respect to the instrument indication is also small and vice versa.

Needless to say, all of the considerations formulated above remain in force in the general case as well, when no simplifying assumptions are made.

It must be remembered, however, that although the relevance of information is of exceptional importance in the design of experiments and interpretation of data, it is also necessary to take the absolute numbers of interaction events between the radiation and the medium into account, i.e., the quantities $\delta\alpha\varphi$, which may be large precisely in the region of small values of the information relevance function. In this case, it is necessary to consider the nature and magnitude of the coefficients of the matrix A^{-1} in the solution (45), observing the requirement that the coefficient matrix A must be well conditioned.

A similar analysis can also be carried through using Eq. (80), the only difference being that this case is simpler, since the solution to the basic equations does not appear in the formula and the functions $\psi(z)$ and the quantities Ψ are related to the temperature variations and are information relevances with respect to their own functionals. In

the problem under consideration, the information relevance function is the only essential characteristic of the problem.

The information-relevance functions with respect to the corresponding functionals acquire special importance in designing research programs to be carried out with the aid of weather satellites.

In this case, it is necessary to solve a series of the equations for information relevance and give an analysis of the independent information received from the various instruments.

If the functions $\varphi_{p_n}^*$ differ little from one another in a given pair of problems, this means that the information relevance in the two problems is the same and, consequently, there is no point in studying two instruments; we may limit ourselves to only one. If, on the other hand, the difference between the functions $\varphi_{p_n}^*$ is significant, even if only on part of the interval $0 \leq z \leq h$, then the second instrument will give us information that is new with respect to the first instrument.

Such information will be useful independent information. The information relevances should be written for the normalized functions $\varphi_{p_n}^*$, i.e.,

$$\int_0^h dz \int_0^\infty dv \int_{-1}^1 d\mu \varphi_{p_n}^* = 1,$$

and, instead of the functions $\varphi_{p_n}^*$ themselves, the differences $\varphi^*_{p_n p_m} = \varphi_{p_m}^* - \varphi_{p_n}^*$, should be examined, selecting from among them only those that are linearly independent. If the functions $\varphi^*_{p_n p_m}$ have particular regions of maximum information relevance that cover the entire region $0 \leqslant z \leqslant h$ more or less uniformly, then the set of functionals $J_{p_n p_m}$ corresponding to these functions will be effective for solving inverse problems. If, on the other hand, certain regions are not presented for analysis in the appropriate manner because the information

relevance in them is low, then the inverse problem for such regions cannot be solved with sufficient effectiveness using fixed instruments. Hence it is necessary to seek other functionals that make it possible to "illuminate" such particular regions as well.

The methods examined in the present paper may be used in formulating various direct and inverse problems in meteorology.

Received 28 February 1964

REFERENCES

1. L.N. Usachev, in collection entitled "Reaktorostroyeniye i teoriya reaktorov" [Reactor Design and Reactor Theory], Izd-vo AN SSSR [Academy of Sciences USSR Press], 1955, page 376.
2. B.B. Kadomtsev, Dokl. AN SSSR [Proceedings of the Academy of Sciences USSR], 113, 3, 1957.
3. G.I. Marchuk, V.V. Orlov, in collection entitled "Neytronnaya fizika" [Neutron Physics], Gosatomizdat [State Publishing House for Literature on Atomic Energy], 1961, page 116.
4. G.I. Marchuk, Metody rascheta yadernykh reaktorov [Design Methods for Nuclear Reactors], Gosatomizdat, 1961.
5. G.I. Marchuk, Zh.N. Bel'skaya, in collection entitled "Voprosy fiziki zashchity reaktorov" [Problems of the Physics of Reactor Protection], Gosatomizdat, 1963, page 99.
6. A.A. Abagyan, V.V. Orlov, G.I. Rodionov, in collection entitled "Voprosy fiziki zashchity reaktorov" [Problems of the Physics of Reactor Protection], Gosatomizdat, 1963, page 7.
7. K.Ya. Kondratyev, Luchistaya energiya Solntsa [The Radiant Energy of the Sun], Gidrometeoizdat [State Publishing House for Literature on Hydrometeorology], 1954.
8. K.Ya. Kondrat'yev and O.P. Filippovich, Teplovoy rezhim verkhnikh

sloyev atmosfery [Thermal Regime of the Upper Layers of the Atmosphere], Gidrometeoizdat, 1960.

9. K.Ya. Kondrat'yev, Meteorologicheskiye sputniki [Weather Satellites] Gidrometeoizdat, 1963.

ANALYTICAL REPRESENTATION OF THE EARTH'S MAGNETIC FIELD IN THE ORBITAL COORDINATE SYSTEM

A.D. Shevnin

Working formulas are derived for the magnetizing-force components of the earth's constant magnetic field as functions of time and the elements of an elliptical orbit in the orbital system of coordinates.

* * *

For research conducted with artificial earth satellites (ISZ), it is important to know the magnetic field at that point on the orbit at which the satellite is situated at the given point in time. For this purpose, it is found useful to select a coordinate system fixed to the satellite and derive analytical expressions for the magnetizing-force components of the earth's magnetic field as functions of the orbit elements.

If we take the positive direction of the X-axis to be geographical North, that of the Y-axis to be East and that of the Z-axis to be vertically downward, then the rectangular field components for a fixed point in space P(r, θ, λ) will be [1, 2]:

$$X = \sum_{n=1}^{\infty}\sum_{m=0}^{n}\left[\left(I_n^m \cos m\lambda + i_n^m \sin m\lambda\right)\left(\frac{R}{r}\right)^{n+2} + \left(E_n^m \cos m\lambda + e_n^m \sin m\lambda\right)\left(\frac{r}{R}\right)^{n-1}\right]\frac{\partial P_n^m(\cos\theta)}{\partial\theta},$$

$$Y = \sum_{n=1}^{\infty}\sum_{m=0}^{n}\left[\left(I_n^m \sin m\lambda - i_n^m \cos m\lambda\right)\left(\frac{R}{r}\right)^{n+2} + \left(E_n^m \sin m\lambda - e_n^m \cos m\lambda\right)\left(\frac{r}{R}\right)^{n-1}\right]\frac{mP_n^m(\cos\theta)}{\sin\theta}, \qquad (1)$$

$$Z = -\sum_{n=1}^{\infty}\sum_{m=0}^{n}\left[\left(I_n^m \cos m\lambda + i_n^m \sin m\lambda\right)\left(\frac{R}{r}\right)^{n+2}(n+1) - \right.$$
$$\left. -\left(E_n^m \cos m\lambda + e_n^m \sin m\lambda\right)\left(\frac{r}{R}\right)^{n-1} n\right] P_n^m(\cos\theta), \qquad (1)$$

where R is the radius of the earth, $\underline{r}$ is the radius vector of the point P, θ is the complement of the geographic latitude, $P_n^m(\cos\theta)$ is an associated Legendre function of the first kind, I_n^m, i_n^m are constant coefficients corresponding to the internal part of the field and E_n^m, e_n^m correspond to the outer field; λ = geographical longitude.

Several definitions [1, 3] for the associated Legendre function of the first kind are encountered in geomagnetism. Thus, Laplace and Gauss used the functions that Schmidt denoted by $P^{n,m}(\cos\theta)$:

$$P^{n,m}(\cos\theta) = \sin^m\theta\left[\cos^{n-m}\theta - \frac{(n-m)(n-m-1)}{2(2n-1)}\cos^{n-m-2}\theta + \right.$$
$$\left. + \frac{(n-m)(n-m-1)(n-m-2)(n-m-3)}{2\cdot 4(2n-1)(2n-3)}\cos^{n-m-4}\theta + \ldots\right]. \qquad (2)$$

But according to Schmidt's second definition,

$$P_n^m(\cos\theta) = \sqrt{\frac{\varepsilon_m(n-m)!}{(n+m)!}}\,\frac{(2n)!}{2^n n!(n-m)!}P^{n,m}(\cos\theta), \qquad (3)$$

where $\varepsilon_m = 2$ for $m \geq 1$ and $\varepsilon_0 = 1$.

We shall henceforth use the first Schmidt notation (2) and the corresponding expression for the derivative with respect to θ:

$$\frac{\partial P^{n,m}(\cos\theta)}{\partial\theta} = m\,\mathrm{ctg}\,\theta\,P^{n,m}(\cos\theta) - (n-m)\,P^{n,m+1}(\cos\theta). \qquad (4)$$

This necessitates making the appropriate conversion of the coefficients. This is easily done by applying, for example, the obvious relationship

$$I^{n,m}P^{n,m}(\cos\theta) = I_n^m P_n^m(\cos\theta), \qquad (5)$$

which is written similarly also for the coefficients $\underline{i}$, E and $\underline{e}$. Substituting Expression (3) here, we write Relationship (5) in the more explicit form

$$I^{n,m} = \sqrt{\frac{\varepsilon_m (n-m)!}{(n+m)!}} \frac{(2n)!}{2^n n! (n-m)!} I_n^m. \qquad (5')$$

We shall assume that the satellite is moving along an elliptical orbit. The projection of this orbit onto the celestial sphere is shown on the figure, where Υ is the Vernal Equinox, Ω is the ascending node of the ISZ's orbit, N is the North Celestial Pole, p is the projection of point P onto the sphere, NA is the geographic meridian passing through point p, π is the projection of the perigee onto the sphere, $\Upsilon\Omega A$ is the plane of the geographical equator, $\Omega\pi p$ is the plane of the ISZ's orbit, OB is the normal to the plane of the ISZ's orbit passed from the center O of the unit sphere, and λ_u is the longitude of point p from the ascending node.

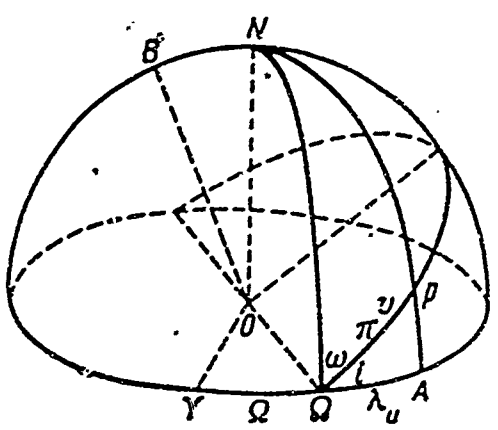

The position of the plane of the ISZ's orbit is determined by the following angles:

the longitude Ω of the ascending node and the inclination of the orbit i to the plane of the geographical equator.

The shape of the orbit is characterized by the semimajor axis a_e of the ellipse and the eccentricity e.

The position of point p on the elliptical orbit is determined by the true anomaly v (arc πp); here, $v = u - \omega$, where u is the latitude argument (arc Ωp) and ω is the angular distance of perigee from the node (arc $\Omega\pi$).

Thus, it is necessary to express the coordinates of point P(r, θ, λ) in terms of the true anomaly v, the five constants Ω, i, ω, a_e, e and the time.

For the ISZ orbit, we leave the component Z_s in the direction of the radius vector; we take the component X_s in the direction of the arc of a great circle passing through point p and the normal OB; we take Y_s perpendicular to the components X_s and Z_s.

It is easily seen that the conversion from X, Y, Z coordinates to the new coordinates X_s, Y_s, and Z_s is effected by the formulas rotating the coordinate system through the angle α formed by the meridian of point p with the great circle pB:

$$\begin{aligned} X_c &= X\cos\alpha - Y\sin\alpha, \\ Y_c &= X\sin\alpha + Y\cos\alpha, \\ Z_c &= Z. \end{aligned} \tag{6}$$

Formulas (6) can be used for all quadrants of u if we arbitrarily regard α as positive for counterclockwise rotation.

The expressions for sin θ, cos θ, sin α and cos α are found by the formulas of spherical trigonometry from the triangle ΩNp :

$$\begin{aligned} &\sin\theta = \sin u\cos i/\sin\lambda_u = \cos u/\cos\lambda_u,\ \cos\theta = \sin u\sin i, \\ &\sin\alpha = \pm\sin i\cos\lambda_u,\ \cos\alpha = \sin\lambda_u/\sin u, \\ &\operatorname{tg}\lambda_u = \cos i\operatorname{tg} u,\quad \operatorname{ctg}\theta = \sin\lambda_u\operatorname{tg} i = \sin u\sin i/\sin\theta. \end{aligned} \tag{7}$$

Following [4], let us introduce the absolute longitude λ^*, which is reckoned from the point of the Vernal Equinox:

$$\lambda^* = t_{\text{зв}}^{(\text{сек})}\frac{360^\circ}{86400} + T^{(\text{сек})}\frac{360^\circ}{86164{,}09} + \lambda. \tag{8}$$

Here $t_{zv}^{(sek)}$ is the longitude of the meridian of Greenwich, reckoned from the Vernal Equinox at Greenwich midnight in seconds of time (can be taken from the astronomical ephemeris for each day of the year), $T^{(sek)}$ is the Greenwich time (in seconds) at the point under consideration, and 86,164.09 is the length (in seconds) of the sidereal day.

On the other hand,

$$\lambda^* = \Omega + \lambda_u. \tag{9}$$

Thus we have from (8) and (9)

$$\lambda = \left[\Omega - t_{зв}^{(сек)} \frac{360^\circ}{86400} - T^{(сек)} \frac{360^\circ}{86164{,}09}\right] + \lambda_u = \lambda_\Omega + \lambda_u, \qquad (10)$$

where λ_Ω is the geographical longitude of the ascending node.

Using Formulas (6) for rotation of the coordinate system, Expression (1) for the components of the magnetic field strength, Expression (4) for the derivative of the Legendre function with respect to θ, the spherical-trigonometry formulas (7) and Relationship (10), we obtain, after a series of manipulations, working formulas for the magnetizing-force components of the earth's magnetic field in the orbital coordinate system as functions of the elements of the ISZ's orbit:

$$\begin{aligned}
X_0 = \sum_{n=1}^{\infty}\sum_{m=0}^{n} \Big\{ & [(n-m)A^{n,m+1}\cos i - mB^{n,m}\sin i]\left[\bar{I}^{n,m}\left(\frac{R}{r}\right)^{n+2} + \right. \\
& \left. + \bar{E}^{n,m}\left(\frac{r}{R}\right)^{n-1}\right] - [(n-m)B^{n,m+1}\cos i + mA^{n,m}\sin i] \times \\
& \times \left[\bar{i}^{n,m}\left(\frac{R}{r}\right)^{n+2} + \bar{e}^{n,m}\left(\frac{r}{R}\right)^{n-1}\right]\Big\}, \\
Y_0 = \sum_{n=1}^{\infty}\sum_{m=0}^{n} \Big\{ & [mB^{n,m}\sin u + (mA^{n,m}\cos i - (n-m)B^{n,m+1}\sin i)\cos u] \times \\
& \times \left[\bar{i}^{n,m}\left(\frac{R}{r}\right)^{n+2} + \bar{e}^{n,m}\left(\frac{r}{R}\right)^{n-1}\right] - [mA^{n,m}\sin u - (mB^{n,m}\cos i + \\
& + (n-m)A^{n,m+1}\sin i)\cos u]\left[\bar{I}^{n,m}\left(\frac{R}{r}\right)^{n+2} + \bar{E}^{n,m}\left(\frac{r}{R}\right)^{n-1}\right]\Big\}, \\
Z_0 = \sum_{n=1}^{\infty}\sum_{m=0}^{n} \Big\{ & [A^{n,m}\sin u\cos i - B^{n,m}\cos u]\left[\bar{i}^{n,m}\left(\frac{R}{r}\right)^{n+2}(n+1) - \right. \\
& \left. - n\bar{e}^{n,m}\left(\frac{r}{R}\right)^{n-1}\right] + [B^{n,m}\sin u\cos i + A^{n,m}\cos u] \times \\
& \times \left[\bar{I}^{n,m}\left(\frac{R}{r}\right)^{n+2}(n+1) - n\bar{E}^{n,m}\left(\frac{r}{R}\right)^{n-1}\right]\Big\},
\end{aligned} \qquad (11)$$

where we have adopted the following notation:

$$A^{n,m} = \frac{P^{n,m}(\cos\theta)}{\sin\theta}\sin(m-1)\lambda_u, \qquad (12)$$

$$B^{n,m} = \frac{P^{n,m}(\cos\theta)}{\sin\theta}\cos(m-1)\lambda_u,$$

$$I^{n,m} = I^{n,m}\sin m\lambda_\Omega - i^{n,m}\cos m\lambda_\Omega, \qquad (13)$$

$$\bar{i}^{n,m} = i^{n,m}\sin m\lambda_\Omega + I^{n,m}\cos m\lambda_\Omega.$$

Expressions similar to (13) are obtained for the coefficients corresponding to the exterior part of the field.

Now it remains to express the quantities $A^{n,m}$ and $B^{n,m}$ in terms of the orbital elements.

Using the Moivre formulas, Formula (7) from spherical trigonometry and Schmidt's first definition (2) for the associated Legendre function, we obtain

$$A^{n,0} = -\frac{b}{1-c^2} P^{n,0}(c),$$

$$B^{n,0} = \frac{a}{1-c^2} P^{n,0}(c),$$

$$A^{n,m} = (C^1_{m-1} a^{m-2} b - C^3_{m-1} a^{m-4} b^3 + C^5_{m-1} a^{m-6} b^5 - \ldots) P^{n,m}(c), \quad m \geqslant 1, \qquad (14)$$

$$B^{n,m} = (a^{m-1} - C^2_{m-1} a^{m-3} b^2 + C^4_{m-1} a^{m-5} b^4 - \ldots) P^{n,m}(c), \quad m \geqslant 1,$$

where

$$P^{n,m}(c) = \left[c^{n-m} - \frac{(n-m)(n-m-1)}{2(2n-1)} c^{n-m-2} + \right.$$
$$\left. + \frac{(n-m)(n-m-1)(n-m-2)(n-m-3)}{2 \cdot 4 (2n-1)(2n-3)} c^{n-m-4} - \ldots \right],$$

and C^n_{m-1} are binomial coefficients:

$$a = \cos u, \; b = \sin u \cos i, \; c = \sin u \sin i. \qquad (15)$$

Values of $A^{n,m}$ and $B^{n,m}$ are given in the table up to n = 6. Values of $A^{n,m+1}$ are determined by the same formulas (14) or taken from the table; it should be noted that in Formulas (11) they always appear with a multiplier (n – m), so that they vanish for m = n.

Formulas (11) for the magnetizing-force components of the earth's magnetic field were derived for a point P fixed on the ISZ's orbit. As the satellite moves on an elliptical orbit, the true anomaly v and the radius vector r of point P vary with time t. Without solving the Kepler equation, we can determine r and v by the formulas [5, 6]:

$$v = M + 2e\left(1 - \frac{e^2}{8}\right) \sin M + \frac{5}{4} e^2 \sin 2M + \frac{13}{2} e^3 \sin 3M + \ldots, \qquad (16)$$

n	m	$A^{n,m}$	$B^{n,m}$
1	0	$-\frac{bc}{1-c^2}$	$\frac{ac}{1-c^2}$
	1	0	1
2	0	$-\frac{b}{1-c^2}\left(c^2-\frac{1}{3}\right)$	$\frac{a}{1-c^2}\left(c^2-\frac{1}{3}\right)$
	1	0	c
	2	b	a
3	0	$-\frac{bc}{1-c^2}\left(c^2-\frac{3}{5}\right)$	$\frac{ac}{1-c^2}\left(c^2-\frac{3}{5}\right)$
	1	0	$c^2-\frac{1}{5}$
	2	bc	ac
	3	$2ab$	a^2-b^2
4	0	$-\frac{b}{1-c^2}\left(c^4-\frac{6}{7}c^2+\frac{3}{35}\right)$	$\frac{a}{1-c^2}\left(c^4-\frac{6}{7}c^2+\frac{3}{35}\right)$
	1	0	$c\left(c^2-\frac{3}{7}\right)$
	2	$b\left(c^2-\frac{1}{7}\right)$	$a\left(c^2-\frac{1}{7}\right)$
	3	$2abc$	$c(a^2-b^2)$
	4	$b(3a^2-b^2)$	$a(a^2-3b^2)$
5	0	$-\frac{bc}{1-c^2}\left(c^4-\frac{10}{9}c^2+\frac{5}{21}\right)$	$\frac{ac}{1-c^2}\left(c^4-\frac{10}{9}c^2+\frac{5}{21}\right)$
	1	0	$c^4-\frac{2}{3}c^2+\frac{1}{21}$
	2	$bc\left(c^2-\frac{1}{3}\right)$	$ac\left(c^2-\frac{1}{3}\right)$
	3	$2ab\left(c^2-\frac{1}{9}\right)$	$(a^2-b^2)\left(c^2-\frac{1}{9}\right)$
	4	$bc(3a^2-b^2)$	$ac(a^2-3b^2)$
	5	$4ab(a^2-b^2)$	$a^4-6a^2b^2+b^4$
6	0	$-\frac{b}{1-c^2}\left(c^6-\frac{15}{11}c^4+\frac{5}{11}c^2-\frac{5}{231}\right)$	$\frac{a}{1-c^2}\left(c^6-\frac{15}{11}c^4+\frac{5}{11}c^2-\frac{5}{231}\right)$
	1	0	$c\left(c^4-\frac{10}{11}c^2+\frac{5}{33}\right)$
	2	$b\left(c^4-\frac{6}{11}c^2+\frac{1}{33}\right)$	$a\left(c^4-\frac{6}{11}c^2+\frac{1}{33}\right)$
	3	$2abc\left(c^2-\frac{3}{11}\right)$	$c(a^2-b^2)\left(c^2-\frac{3}{11}\right)$
	4	$b(3a^2-b^2)\left(c^2-\frac{1}{11}\right)$	$a(a^2-3b^2)\left(c^2-\frac{1}{11}\right)$
	5	$4abc(a^2-b^2)$	$c(a^4-6a^2b^2+b^4)$
	6	$b(5a^4-10a^2b^2+b^4)$	$a(a^4-10a^2b^2+5b^4)$

$$\frac{r}{a_e} = 1 + \frac{e^2}{2} - e\left(1 - \frac{3}{8}e^2\right)\cos M - \frac{e^2}{2}\cos 2M - \frac{3}{8}e^2\cos 3M - \ldots \quad (17)$$

For a given point in time t the value of the mean anomaly M is found from the formula

$$M = \frac{360^\circ}{T_0}(t - t_n), \quad (18)$$

where T_0 is the period of revolution of the ISZ on the orbit and t_p is one of the times at which the satellite passes perigee.

For an elliptical orbit, Ω and i have been regarded as constant quantities. In actuality, however, due to the deviation of the earth's gravitational field from the central field, the satellite's orbit will experience perturbations, which may be represented as the following two effects [7]:

1) small periodic oscillations of the node i with an amplitude ~0°01'. We may disregard this perturbation and assume that i = const;

2) precession of the orbit – an almost uniform change in the longitude of the ascending node Ω, that can be defined by the formula

$$\Omega = \Omega_0 - 2\pi k_0 \frac{t}{T_0}, \quad k_0 = \beta\left(\frac{R}{a_e}\right)^2 \frac{\cos i}{(1-e^2)^2}, \quad (19)$$

where $\beta = 0.00163$ and Ω_0 is the initial longitude of the ascending node.

It is therefore necessary to account for the time variation of Ω by formula (19) in calculating the geographic longitude λ_Ω of the ascending node.

In conclusion, a few words on the procedure for calculating the magnetizing-force components of the earth's magnetic field in the orbital coordinate system.

We shall regard the following quantities as assigned: Ω_0, i, ω, a_e, e, T_0 and t_p. Using Formula (19), we determine Ω. For a certain fixed moment in time t, we use the expression in square brackets in Formula (10) to calculate λ_Ω, and then use Formulas (13) to calculate

the coefficients $\bar{I}^{n,m}$, $\bar{J}^{n,m}$, $\bar{E}^{n,m}$ and $\bar{e}^{n,m}$. Then we find the mean anomaly M by Formula (18) for the same moment in time. On the one hand, knowledge of M enables us to employ Formula (17) to calculate the distance to point P and, consequently, the quantities R/r and r/R as well. On the other hand, Formula (16) is used to calculate the true anomaly v and then the latitude argument u, which is equal to $v + \omega$. Using the known latitude argument, it is easy to find the quantities a, b and c and, consequently, by Formulas (14) or from the table, the quantities $A^{n,m}$ and $B^{n,m}$. At this point, Formulas (11) can be used to calculate the components X_s, Y_s, and Z_s.

Received 27 December 1963

REFERENCES

1. N.P. Ben'kova, Spokoynyye solnechno-sutochnyye variatsii zemnogo magnetizma [Quiet Solar-Diurnal Variations in Terrestrial Magnetism], Gidrometeoizdat [State Publishing House for Literature on Hydrometeorology], 1941.

2. N.V. Adam, N.P. Ben'kova, V.P. Orlov, N.K Osipov, and L.O. Tyurmina, Geomagnetizm i aeronomiya [Geomagnetism and Aeronomy], 2, No. 5, 949, 1962.

3. S. Chapman and J. Bartels, Geomagnetism, Vol. II, Oxford, 1951.

4. V.V. Beletskiy and Yu.V. Zonov, In collection entitled: "Iskusstvennyye sputniki Zemli" [Artificial Earth Satellites], No. 7. Izd-vo AN SSSR [Publishing House of the Academy of Sciences USSR], 1961, page 32.

5. G.Krauaye, Collection entitled "Ob iskusstvennom sputnike Zemli" [On the Artificial Earth Satellite], Oborongiz [State Publishing House for Literature of the Defense Industry], 1959, page 68.

6. R.Roberson, Collection entitled "Nauchnyye problemy iskusstvennykh

sputnikov" [Scientific Problems of Artificial Satellites], IL [Foreign Literature Press], Moscow, 1959, page 63.

7. D.Ye. Okhotsimskiy and V.V. Beletskiy, Collection entitled "Iskusstvennyye sputniki Zemli" [Artificial Earth Satellites], No. 16. Izd-vo AN SSSR [Publishing House of the Academy of Sciences USSR], 1963, page 94.

Manuscript Page No.	[Transliterated Symbols]
193	ИСЗ = ISZ = iskusstvennyy sputnik zemli = artificial earth satellite
194	ctg = cot
195	э = e = ellips = ellipse
196	с = s = sputnik = satellite
196	tg = tan
196	зв = zv = zvezdnyy = sidereal
196	сек = sek = sekundy = seconds
200	п = p = perigey = perigee

GEOGRAPHICAL DISTRIBUTION OF RADIATION INTENSITY IN THE REGION OF THE BRAZILIAN MAGNETIC ANOMALY AT AN ALTITUDE OF ABOUT 300 km

S.N. Vernov, V.Ye. Nesterov, I.A. Savenko,

P.I. Shavrin and K.N. Sharvina

The subject is the geographic distribution of radiation intensit in the region of the Brazilian magnetic anomaly according to the data from the Kosmos-7 and Kosmos-15 satellites. The distribution obtained is compared with the results of measurements made on the satellites Kosmos-3 and Kosmos-5 [4], as well as on the satellite Discoverer 31 [3, 5].

* * *

The anomalously small magnitudes of the terrestrial magnetic fiel along the Brazilian coastline make it possilbe to observe the radiatic of the earth's radiation belts at low altitudes in this region. Beginning in 1960, the distribution of radiation in the region of the Brazilian magnetic anomaly has been studied by many authors [1-4]. In the present paper, we present the results of an investigation of the geographic radiation-intensity distribution in this region by the satellites Kosmos-7 and Kosmos-15. The launching dates and orbital characteristics of the satellites are indicated in Table 1. The results of counting-rate measurements on screened STS-5 Geiger counters were used to construct the distribution of the radiation intensity in the region of the Brazilian anomaly.

TABLE 1

Спутник 1	Дата запуска 2	Перигей и апогей, км 3	Высота в районе Бразильской аномалии, км 4
5 «Космос-4»	6 26.IV.1962	298—330	312—325
«Космос-7»	28.VII.1962	210—369	235—340
«Космос-15»	22.IV.1963	173—371	235—305

1) Satellite; 2) launching date; 3) perigee and apogee, km; 4) altitude in region of Brazilian anomaly, km; 5) Kosmos-4; 6) 26 April 1962.

The minimum screening of the Geiger counters was 3 $g \cdot cm^{-2}$, i.e., the counters were capable of registering electrons with energies $E > 6$ Mev and protons with energies $E > 50$ Mev. Electrons with lower energies were registered at an efficiency < 1% from the bremsstrahlung that they generated in the casing of the satellite. The readings of the STS-5 counters were stored in the telemetry-system memory every 40 sec.

Fig. 1 presents the results of Geiger-counter counting-rate measurements obtained during the flights of the satellites Kosmos-7 and Kosmos-15 across the Brazilian magnetic anomaly; lines of equal counting rate for this counter are also plotted. The STS-5 Geiger counter registered radiation in both the internal and the artificial radiation belts of the earth, with the latter's contribution dominating, particularly during the time of measurements made with Kosmos-7. Indeed, according to Table 2, in which typical values of the counting rate for the Geiger and scintilation counters and their ratios in the region of maximum counting rate are given for comparison of the results of radiation measurements before and after the artificial belt was formed, not only had counting rate increased during the measurements with the Kosmos-7 and Kosmos-15 satellites, but the ratio of these rates had also diminished. This indicates that the basic contribution to the registered counting

BLANK PAGE

TABLE 1

Спутник 1	Дата запуска 2	Перигей и апогей, км 3	Высота в районе Бразильской аномалии, км 4
5 «Космос-4»	6 26.IV.1962	298—330	312—325
«Космос-7»	28.VII.1962	210—369	235—340
«Космос-15»	22.IV.1963	173—371	235—305

1) Satellite; 2) launching date; 3) pe and apogee, km; 4) altitude in region Brazilian anomaly, km; 5) Kosmos-4; 6) April 1962.

The minimum screening of the Geiger counters wa the counters were capable of registering electrons w > 6 Mev and protons with energies E > 50 Mev. Electr ergies were registered at an efficiency < 1% from th that they generated in the casing of the satellite. STS-5 counters were stored in the telemetry-system m

Fig. 1 presents the results of Geiger-counter c urements obtained during the flights of the satellit mos-15 across the Brazilian magnetic anomaly; lines rate for this counter are also plotted. The STS-5 Ge tered radiation in both the internal and the artific of the earth, with the latter's contribution dominati during the time of measurements made with Kosmos-7. to Table 2, in which typical values of the counting and scintilation counters and their ratios in the reg counting rate are given for comparison of the result urements before and after the artificial belt was fo counting rate increased during the measurements with Kosmos-15 satellites, but the ratio of these rates h This indicates that the basic contribution to the re rate aboard the Kosmos-7 and Kosmos-15 was made by r

artificial radiation belt. (This conclusion is obvious for Kosmos-7, since the counting rates of the Geiger counter aboard this satellite are considerably in excess of the corresponding values obtained on Kosmos-4. As for the Geiger counting rates registered on the Kosmos-15 and Kosmos-4: although they differ little from one another, this difference becomes significant when we take into account that the orbit of Kosmos-15 passes considerably lower than that of Kosmos-4).

TABLE 2

1 Спутник	2 Скорость счета, имп·см⁻²·сек⁻¹		$N_г / N_{сц}$, %
	3 гейгеровского счетчика, $N_г$	4 сцинтилляционного счетчика, $N_{сц}$	
6 «Космос-4»	$\sim 3 \cdot 10^1$	$\sim 3 \cdot 10^3$	10
«Космос-7»	$\sim 2 \cdot 10^3$	$\geqslant 10^3$	$\leqslant \frac{2}{4}$
«Космос-15»	$\sim 4 \cdot 10^1$	$\sim 10^3$	

1) Satellite; 2) counting rate, pulses $\cdot cm^{-2} \cdot sec^{-1}$; 3) Geiger counter, N_g; 4) scintillation counter, N_{sts}; 5) N_g/N_{sts}, %; 6) Kosmos-4.

It is clear from Fig. 1 that the contours of equal Geiger counter counting rate aboard the satellites Kosmos-7 and Kosmos-15 are similar, but since the measurements with Kosmos-7 were made immediately after formation of the artificial radiation belt (on 9 July 1962, the USA set off a high-altitude thermonuclear explosion over Johnston Island), the counting rate of the counter aboard this satellite was greater than the corresponding value obtained with the satellite Kosmos-15, and the region of high counting rate was therefore somewhat greater in size.

As we know, the radiation of the artificial radiation belt consists primarily of electrons with energies ~ 1-7 Mev. Therefore Fig. 1 reflects the intensity distribution of artificial radiation belt elec-

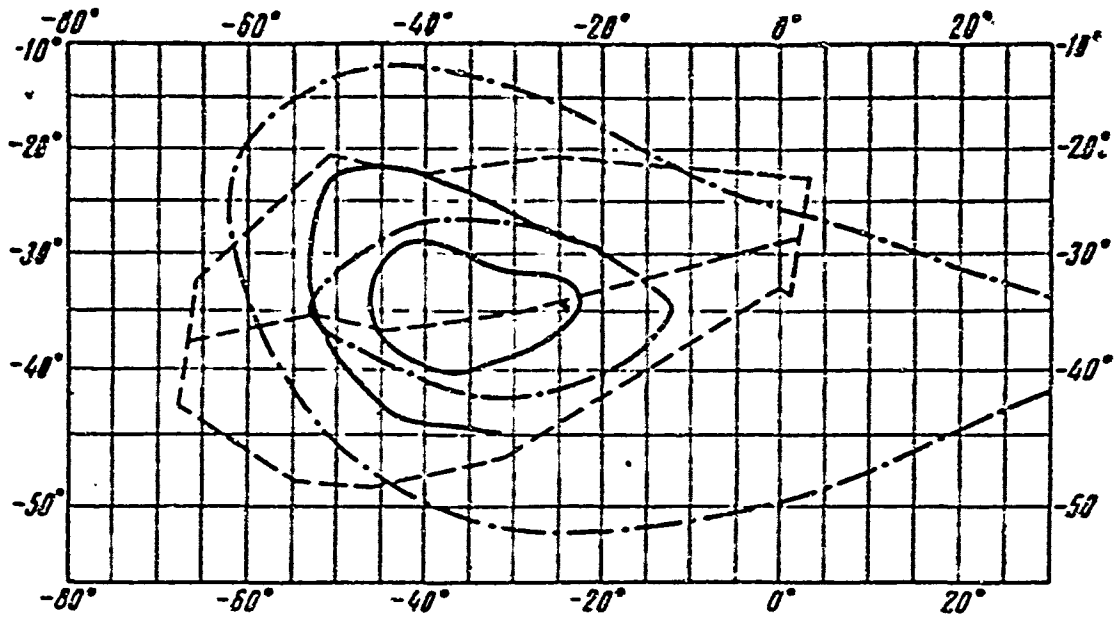

Fig. 2. Comparison of geographic distribution of radiation intensities in the internal and artificial radiation belts of the earth.

The solid lines represent lines of equal Geiger-counter rates on the satellite Kosmos-15. The dot-dash lines are lines of equal counting rate for the scintillation counter aboard the Discoverer-31 satellite [3]. The dashed contour limits the region in which the spectrum of electrons with energies from 100 to 1000 kev was measured aboard the satellite Discoverer-31; the electron intensity on the central line is 100 and more times greater than the intensity at the periphery [5].

trons with energies > 1 Mev in the region of the Brazilian anomaly.

The geographic distribution of electrons in the internal radiation belt in the region of the Brazilian anomaly (Fig. 2) was measured with the American satellite Dicoverer-31 [5] using a 10-channel permanent-magnet β-spectrometer, which registered electrons in the energy range from 100 to 1000 kev. This satellite was up in September 1961 and its altitude ranged from 240 to 410 km. It is seen from Fig. 2 that the positions of the electron-intensity maxima in the internal and artificial belts are the same in the region of the Brazilian anomaly.

The Discoverer 31 satellite was also equipped with a plastic-scintillator scintillation counter, which was screened by a layer of aluminum 1.25 mm thick and had a radio threshold of 1 Mev. This counter could register electrons with energies > 2 Mev and protons with energies > 20 Mev, as well as the bremsstrahlung that arose under the action of electrons with energies of only a few megaelectron-volts. The

contours of equal counting rate for this counter are also shown in Fig. 2.

It is evident from Fig. 2 that the position of the equal-rate contour center for the scintillation counter on the Discoverer-31 almost coincides with the center of electron-intensity distribution, while the contours themselves are similar to lines of equal electron intensity. If the scintillation counter on the Discoverer-31 satellite registered electrons preferentially, such a similarity would be natural. However, electrons with energies exceeding 2 Mev must also exist in the internal belt in this case. If we assume that the scintillation counter registered preferentially protons with energies > 20 Mev, then we must conclude from Fig. 2 that the spatial distributions of the electrons and protons in the Brazilian anomaly are the same.

An indication of the existence of differences in the spatial distributions of electrons with energies of the order of 100 kev and the radiation registered by the STS-5 Geiger counter when screened with 3.4 $g \cdot cm^{-2}$ Pb and 0.8 $g \cdot cm^{-2}$ Al in the region of the Brazilian anomaly at an altitude of ~ 650 km was obtained by V.I. Krasovskiy and his collaborators [4] as a result of studies made with the satellites Kosmos-3 and Kosmos-5 (Fig. 3). It is seen from Fig. 3 that, according to the data from detectors with fluorescent screens aboard the Kosmos-3, the center of distribution of electrons with energies of 100 kev coincides with the distribution center of the artificial-radiation-belt electrons with an average energy of ~2 Mev as obtained from measurements with the Kosmos-15 satellite, although the equal-intensity lines of these two electron groups are not fully similar.

On the other hand, the radiation distribution registered by the lead-protected Geiger counter aboard the Kosmos-3 satellite does not agree with the electron distribution in the Brazilian anomaly, either

on the basis of data from the fluorescent-screen detectors on the Kosmos-3 satellite or on the basis of the Kosmos-15 data.

TABLE 3

A № точки	Координаты B φ°	 λ°	C $N_г$, имп/см²·сек	D $N_{сц}$, имп/см²·сек	E Энерговыделение в кристалле, Мэв/см²·сек	F $N_г / N_{сц}$	G Энерговыделение на одну частицу, Мэв	H Космический фон I $N_г$, имп/см²·сек	 J $N_{сц}$, имп/см²·сек
1	—43,3	—53,5	1,5	54	43,2	2,8%	0,8	1	8,3
2	—37	—48	15	740	550	2%	0,75	1	6,2
3	—29,7	—43,5	25	655	400	3,8%	0,61		
4	—23	—40	6,0	29	71	20,6%	2,35	0,5	8,3
5	—15	—36,5	1,5	8,3	23,6	18,4%	2,85		

A) Point No.; B) coordinates; C) N_g, pulses/cm^2·sec; D) N_{sts}, pulses/cm^2·sec; E) Energy liberated in crystal, Mev/cm^2·sec; F) N_g/N_{sts}; G) energy liberated per single particle, Mev; H) cosmic background; I) N_g, pulses/cm^2·sec; J) N_{sts}, pulses/cm^2·sec.

The Geiger counters aboard the Kosmos-5 and Kosmos-15 satellites had approximately identical screening and differed only in their bremsstrahlung efficiencies. The counter aboard the Kosmos-5 was screened with lead and exhibited considerably lower registering efficiency for bremsstrahlung as compared with the counter on the Kosmos-15. For this reason, the disagreement between the particle-intensity geographic distributions registered by the Geiger counters on the Kosmos-3, Kosmos-5 and Kosmos-15 satellites can be accounted for by preferential registration of protons aboard the Kosmos-3 and the consequent differences between the proton distribution and electron distribution in the Brazilian anomaly [6].

The measurements made with the Kosmos-15 satellite confirmed this conclusion qualitatively.

Since the counting-rate ratio for the Geiger and scintillation counters and the amount of energy liberated in the crystal per single

particle registered by the scintillation counter are directly connected to the content of penetrating particles in the radiation, the geographic distribution of these quantities was studied in the Brazilian anomaly (counting rate and amount of energy liberated were averaged over a time interval of 120 sec). The dark circles in Fig. 3 denote points at which the ratio of counting rates for the Geiger and scintillation counters, N_g/N_{sts}, exceeded 5%; here, the counting rates remained high and could not be accounted for by registration of cosmic rays alone. At these points, the values of energy liberated in the crystal per single particle are two or more times as large as the analogous values in the region in which the Geiger counter rate reached its maximum.

Table 3 presents the counting rates for both counters, their ratio, and the crystal-energy values for one transit of the Brazilian magnetic anomaly by the satellite.

The change in the composition of the radiation during the passage from point 3 to point 4, which is at lower latitude, is evident from Table 3.

If we exclude the cosmic-ray background from the counter indications, we may conclude from the tabulated data that the ratio of the number of bremsstrahlung γ-quanta from electrons with energies < 6 Mev to the number of protons diminishes by approximately one order of magnitude on passage from point 3 to point 4. It is seen from Fig. 3 that these points with large proton contribution are situated to the west and north of the region in which the counting rate is highest. Further, it was found that even the points with relatively high penetrating-particle contributions, as obtained during a passage of the 2nd space vehicle over the Brazilian anomaly, are grouped in approximately the same way (open circles in Fig. 3). In the Brazilian anomaly, therefore,

the intensity of electrons drops more sharply with diminishing L than does that of protons on magnetic shells with L not too large.

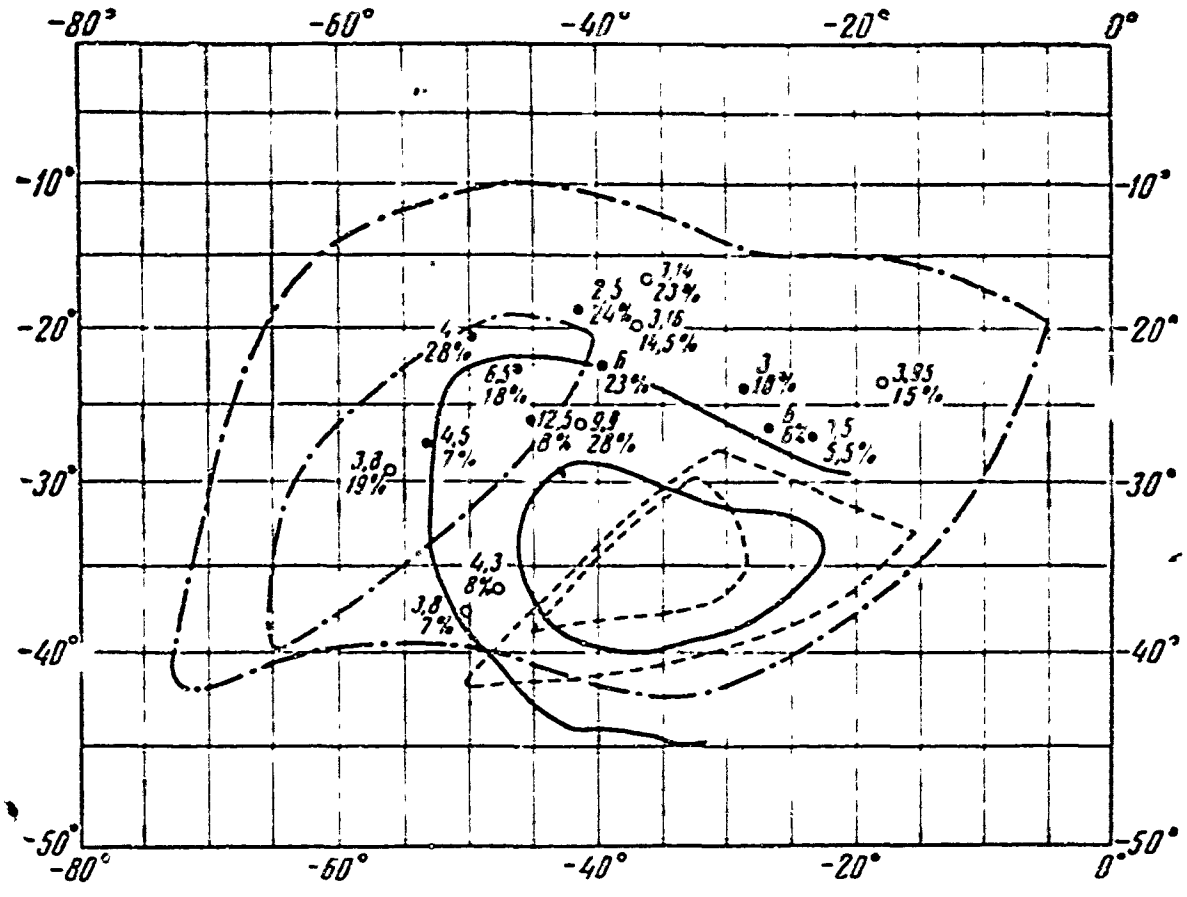

Fig.3. Radiation intensity distribution according to data obtained from the satellite Kosmos-3 [4] and Kosmos-15.

The solid lines represent lines of equal Geiger-counter rates for the satellite Kosmos-15; the dashed lines are lines of equal electron intensity, energies above 100 kev [4]; the dot-dash lines are lines of equal counting rate for a Geiger counter behind a shield of 3.4 $g \cdot cm^{-2}$ of Pb + 0.8 $g \cdot cm^{-2}$ Al [4]; the open circles are points at which, according to data obtained with the 2nd space vehicle, of the ratio $N_g / N_{sts} < 5\%$, while the dark circles are the analogous points for the Kosmos-15 satellite. The figures indicate the Geiger-counter rates averaged over 2 minutes and the value of the ratic N_g/N_{sts} over the same span of time.

It follows from comparison of the equal-electron-intensity contours obtained with the Kosmos-7 and Kosmos-15 satellites with the contours of equal scintillation-counter rates from the satellite Discoverer-31, which also appears to have registered electrons preferentially, that the electron distributions in the internal and artificial radiation belts are the same in the region of the Brazilian anomoly. It follows from this that the electron-intensity distribution in this region

is determined preferentially by the loss mechanism and not by the injection conditions.

Conclusions. 1. Using data from the satellites Kosmos-7 and Kosmos-15, the geographic distribution of the artificial belt electron intensities was determined at altitudes ~300 km in the Brazilian anomaly and found to agree approximately with the electron distribution of the internal radiation belt as obtained using the magnetic spectrometer on the satellite Discoverer-31, and with the distribution of radiation registered by a plastic-scintillator scintillation counter.

2. According to data from the 2nd space vehicle and the satellite Kosmos-15, experimental points with large Geiger-to-scintillation counting-rate ratios and large values of energy liberation per particle in the crystal are situated on magnetic shells with $L < 1.4$, which attests to a more rapid drop in electron intensity in the region of the Brazilian anomaly with diminishing L as compared with proton intensity. Thus the geographic distribution of electrons in the Brazilian anomaly is apparently somewhat different from the distribution of high-energy protons.

The authors are indebted to O.F. Gorskaya and H. Trishkina for their assistance in organizing the results.

Received 14 January 1964

REFERENCES

1. S.N. Vernov, I.A. Savenko, P.I. Shavrin and N.F. Pisarenko, in Collection entitled: "Iskusstvennyye sputniki Zemli" [Artificial Earth Satellites], No. 10. Izd-vo AN SSSR [Academy of Sciences USSR Press], 1961, page 40.

2. V.L. Ginzburg, L.V. Kurnosova, V.I. Logachev, L.A. Razorenov, I.A. Sirotkin and M.I. Fradkin, In collection entitled:"Iskusst-

vennyye sputniki Zemli," No. 10. Izd-vo AN SSSR, 1961, page 23.

3. F.D. Seward and H.N. Kornblum, Jr., Preprint, 1963.

4. V.I. Krasovskiy, Yu.I. Gal'perin, V.V. Temnyy, G.M. Mulyarchik, N.V. Dzhordzhio, M.Ya. Marov and A.D. Bolyunova, Geomagn. i aeromiya [Geomagnetics and Aeronomy], 3, No. 3, 408, 1963.

5. L.G. Mann, S.D. Bloom and H.I. West, Jr., Space Res. III, ed. W. Priester, 1963.

6. Yu.I. Gal'perin, V.I. Krasovskiy, N.V. Dzhordzhio, T.M. Mulyarchik, A.D. Bolyunova, V.V. Temnyy and M.Ya. Marov, Kosmich. issled. [Cosmic Research], 1, 126, 1963.

Manuscript Page No. [Transliterated Symbols]

206 г = geygerovskiy = Geiger

206 сц = sts = stsintillyatsionyy = scintillation

INVESTIGATION OF TERRESTRIAL RADIATION BELTS IN THE VICINITY OF THE BRAZILIAN MAGNETIC ANOMALY AT ALTITUDES OF 235-345 km

S.N. Vernov, V.Ye. Nesterov, N.F. Pisarenko, I.A. Savenko, O.I. Savun, P.I. Shavrin, K.N. Sharvina

Results are given for investigations of the terrestrial radiation belt in the vicinity of the Brazil magnetic anomaly; these investigations were carried out with the Kosmos-4, Kosmos-7, Kosmos-9, and Kosmos-15 satellites by means of Geiger and scintillation counters.

The results obtained with these satellites and from the 2nd space vehicle are presented.

During the radiation studies carried out by means of the 2nd space vehicle at altitudes of about 300 km in the low latitudes over the Atlantic Ocean, close to the coast of Brazil, a large region of high radiation intensity was detected [1, 2]. It was established that the intensity of radiation in this region rises sharply as a result of the descent of the inner radiation belt to low altitudes, this being due to a gigantic negative magnetic anomaly. The magnetizing force of the field in the Brazil anomaly is anomalously small and at an altitude 300 km attains values below 0.22 gauss, which is equivalent to an altitude of 1500 km for the same magnetic shell, but along other longitudes. For this reason the investigation of the inner radiation belt can be carried out by means of satellites launched to low heights [1-5].

On the other hand, the study of the radiation belts in the vicinity of magnetic anomalies is of independent interest, since it may yield information regarding the mechanisms of particle loss and genera-

tion in the radiation belts.

Below we present preliminary results of investigations of the terrestrial radiation belts in the vicinity of the Brazil magnetic anomaly at altitudes of 235-345 km, these investigations having been carried out with the satellites Kosmos-4, Kosmos-7, Kosmos-9, and Kosmos-15.

The launching dates and orbital characteristics of these satellites, as well as those of 2nd space vehicle, are presented in the following table.

1 Спутник	2 Дата запуска	3 Перигей и апогей, км	4 Высота в районе Бразильской аномалии, км
5 2 космический корабль	19.VIII.1960	306—339	310—335
6 «Космос-4»	26.IV.1960	298—330	312—325
«Космос-7»	28.VII.1962	210—369	235—340
«Космос-9»	27.IX.1962	301—353	314—345
«Космос-15»	22.IV.1963	173—371	235—305

1) Satellite; 2) launch date; 3) perigee and apogee, in km; 4) altitude in the vicinity of the Brazil anomaly, in km; 5) 2nd space vehicle; 6) Kosmos-4.

VARIATION IN RADIATION INTENSITY FROM THE INNER RADIATION BELT IN THE PERIOD OF TIME BETWEEN THE FLIGHTS OF THE 2nd SPACE VEHICLE AND THE KOSMOS-4 SATELLITE

In connection with the onset of the minimum in solar activity there arises interest in the study of variations in particle intensity in the inner radiation belt. The lifetime of protons in the inner radiation belt is a function of the proton energy and the density of the atmosphere, this lifetime being of the order of 10^7-10^8 sec for altitudes of 1000 km [6]. The duration of the solar cycle, equal to $4 \cdot 10^8$ sec (11 years) is greater than the lifetime of the protons at these altitudes. Consequently, at altitudes below 1000 km, the changes in atmospheric density occurring during the course of the cycle of solar activity and affecting the magnitude of the ionization proton losses may

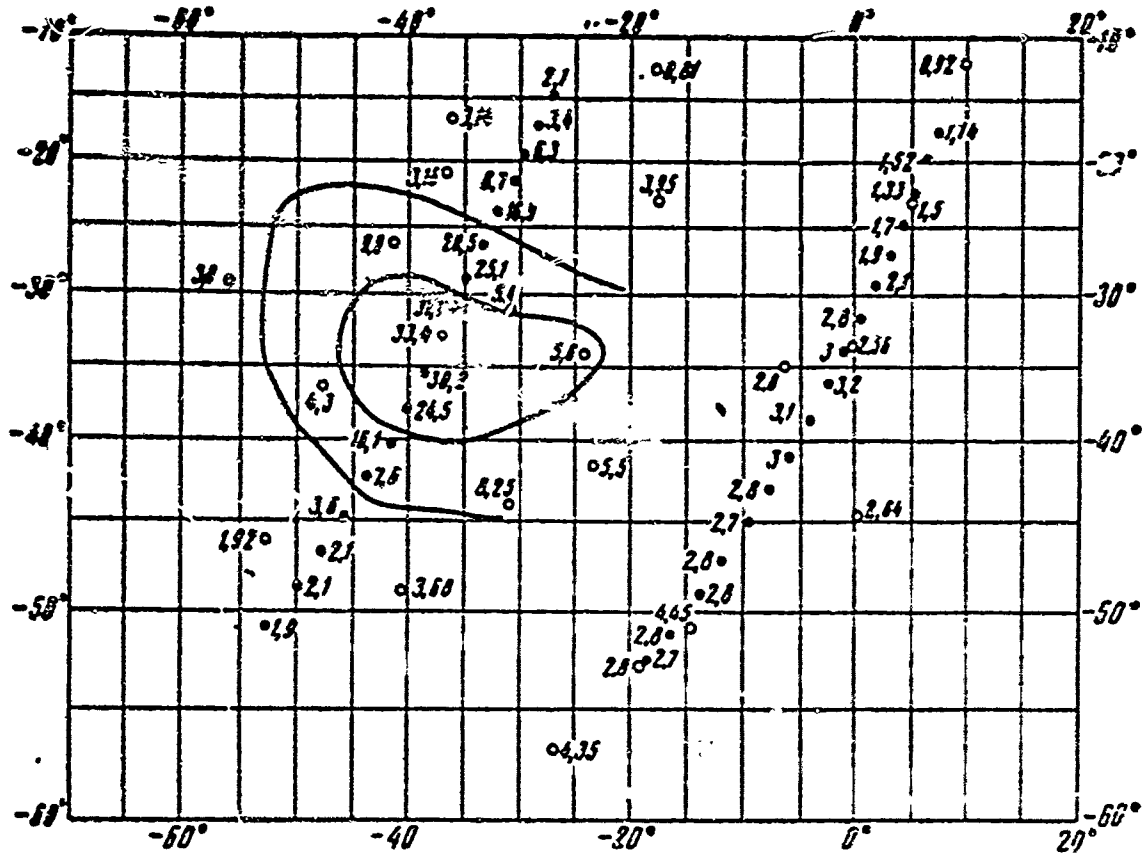

Fig. 1. Comparison of Geiger-counter data obtained from the flights of the 2nd space vehicle and the Kosmos-4 satellite through the Brazil anomaly.

Solid circles – counting rate, registered aboard the Kosmos-4 satellite, in pulses/cm^2·sec; open circles – counting rate registered aboard the 2nd space vehicle, in pulses/cm^2·sec. Solid lines – contours of counting rates equal to 25 pulses/cm^2·sec and 6 pulses/cm^2·sec as recorded aboard the Kosmos-15 satellite.

be the factors responsible for the temporary variations in proton intensity in the inner radiation belt [7] which result in an increase in particle intensity at the above-indicated altitudes during the years of minimum solar activity.

In order to reveal the nature of the variations in the vicinity of the Brazil anomaly, an attempt was made to compare the Geiger-counter data produced by the 2nd space vehicle and those of the Kosmos-4 satellite. Unfortunately, a direct comparison is impossible, since the existing information pertains to various regions of the anomaly (Fig. 1). The contours of equal Geiger-counter counting rates obtained by the Kosmos-15 satellite can be employed for an indirect comparison.

Figure 1 shows that the radiation intensity in the vicinity of

the maximum Geiger-counter count produced by the 2nd space vehicle increased in 1962 by a factor of approximately 2-3 relative to the data obtained in 1960.

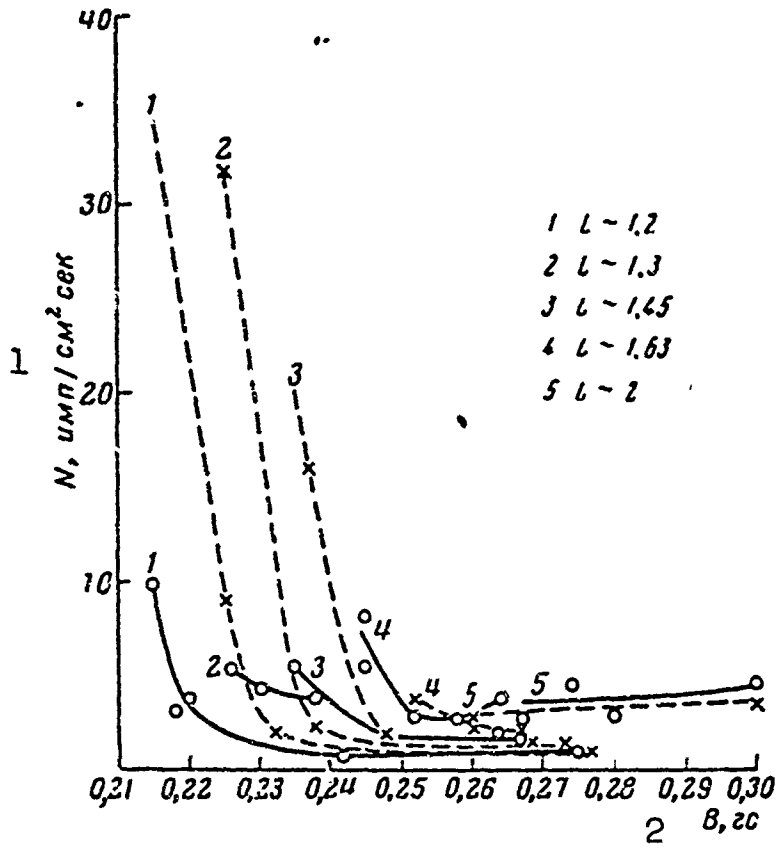

Fig. 2. Counting rates from Geiger counters as a function of B values for several values of L. Solid lines — the 2nd space vehicle; dashed lines — the Kosmos-4 satellite. 1) N, pulses/cm^2·sec; 2) B, gauss.

A more rigorous comparison can be carried out by comparing the counting rates of the Geiger counters aboard the 2nd space vehicle and Kosmos-4 satellite for identically established values of intensity for the magnetic field B for given values of L (in Fig. 2, B and L are the McIlwain coordinates). Since the readings of the counters aboard the 2nd space vehicle were taken infrequently (each 3 minutes), the average values of B and L for this interval of time were taken.

Figure 2 shows the counting rate of the Geiger counter as a function of the intensity of the magnetic field B as obtained by the 2nd space vehicle and the Kosmos-4 satellite for various values of L.

For L ~1.2, 1.3, and 1.45 the counting rate of the counter aboard

the Kosmos-4 satellite rises more steeply with a reduction in B than does the [counting rate] obtained from the 2nd space vehicle. With L ~1.3 and L ~1.45 the counting rate at the maximum obtained from the Kosmos-4 satellite exceeded the counting rate produced by the 2nd space vehicle by a factor of 4-6.

Hess calculated the curves showing the change in proton intensity in the inner radition belt during the course of the solar-activity cycle, these changes being attributable to changes in atmospheric density. Having used these curves [7] (Fig. 13), it becomes possible for us to arrive at the estimate that the intensity of protons with energies of 25 Mev must increase over the period of time between the flights of the 2nd space vehicle and the Kosmos-4 satellite by a factor of four for the magnetic shell L = 1.25 given a magnetic-field strength of B = = 0.209 gauss. For protons with energies of 100 Mev the magnitude of the increase is equal to 2.5.

There are no experimental data from the Kosmos-4 satellite for L ~1.2 and B ~0.225 gauss. Extrapolation of the experimental curve for L ~1.2 obtained for large values of magnetic-field strength B to the value B ≈ 0.215 gauss yields an increase by a factor of four. Thus the experimentally determined magnitude of the increase in radiation intensity in the inner radiation belt in the vicinity of the Brazil anomaly is in rather good agreement with the increase calculated under the assumption that the protons are injected by means of a neutron mechanism, and that the losses occur primarily as a result of ionization losses.

The increase in the counting rate of the Geiger counter recorded aboard the Kosmos-4 satellite in comparison with the measurement conducted aboard the 2nd space vehicle cannot be uniquely attributed to the increase in the proton intensity in the inner belt, since the counting rate might have changed as a result of differences in the

shielding of the counters or because of an East-West asymmetry in proton intensity in the radiation belt [8, 9]. However, the probability of such a false effect is small, since the shielding of the counters used aboard the 2nd space vehicle and Kosmos-4 satellite was virtually identical, and to explain the recording of an increase in the counting rate by means of an East-West asymmetry it would be necessary to assume that the following three conditions were simultaneously satisfied: 1) the counter aboard the Kosmos-4 satellite during the flight through the Brazil anomaly was randomly oriented to the West whereas the counter aboard the 2nd space vehicle was randomly oriented to the East (it has been calculated that for protons exhibiting energies from 60 to 120 Mev and subject to the Freden-White spectrum, $N_{vost}/N_{zap} \approx 2$ [9]); 2) the space vehicle in each flight through the Brazil anomaly, for which radiation data were available, must be oriented identically; 3) the orientation of the Kosmos-4 satellite, as well as that of the 2nd space vehicle, should not have changed during the course of the entire flight time through the anomaly.

Because of the low probability of the above-indicated false effects, it is apparently possible to draw the conclusion from the derived results that there existed a temporary variation in the intensity of particles in the inner radiation belt in the vicinity of the Brazil magnetic anomaly in 1960-1962. If it is held that the inner belt is formed as a result of a neutron mechanism, this variation must be associated primarily with the reduced density of the atmosphere in 1962 at an altitude of ~300 km and partially with the increasing intensity of cosmic radiation during this period (in Reference [10] it is estimated at 20%).

DETERMINATION OF PARTICLE LIFETIME IN AN ARTIFICIAL RADIATION BELT

An analysis of the short term relationship between the total number

of pulses recorded by the Geiger counters during the course of a day aboard the satellite Kosmos-7, Kosmos-9 and Kosmos-15 (these satellites were launched, respectively, 20 days, 2 months, and 9 months after the formation of an artificial radiation belt on 9 July 1962) make it possible to determine the lifetime of the particles in the artificial radiation belt with mirror points lying at altitudes < 370 km. This time proved to be equal to 3 months [10]. Since the artificial radiation belt descends to an altitude of 300 km primarily in the vicinity of the Brazil magnetic anomaly [11], through use of the Geiger-counter data from the Kosmos-4 and Kosmos-9 satellites for nearby positions in this area of approximately identical altitudes (~300 km), it becomes possible to evaluate the lifetime τ of the particles in the artificial radiation belt at points with various values for the terrestrial magnetic field B.

In this case we will refer to the readings of the counter aboard the Kosmos-4 satellite, resulting from cosmic radiation and the natural radiation belts, as the background. The derived results are shown in Fig. 3. These results may be regarded as estimates, since the trajectories of the Kosmos-7 and Kosmos-9 satellites in the vicinity of Brazil magnetic anomaly did not always coincide and it sometimes became necessary to compare counting rates at points differing from each other by approximately 2° of longitude. We can see from Fig. 3 that in the central part of the anomaly region, with B = 0.23 gauss and L = = 1.25-1.4, the lifetime is equal approximately to 4 months. In this part the orbit of Kosmos-4 is shifted by about 10° with respect to the orbit of the Kosmos-7, which does not yield a great error, since here the background due to cosmic radiation and the natural radiation belt is not great. As can be seen from Fig. 3, the lifetime of

the particles in the artificial radiation belt for L < 1.7 is more than a month.

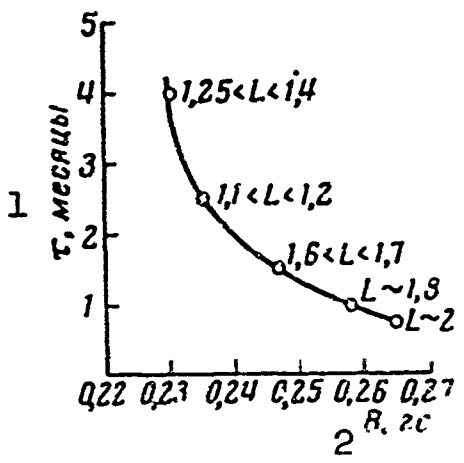

Fig. 3. Lifetime τ of particles in the artificial radiation belt as a function of B and L. The values of L are indicated around each point. 1) τ, in months; 2) B gauss.

The quantity τ for 1.25 < L < 1.4 and B = 0.23 gauss coincides with the data obtained aboard the "Injun-I" and the "Injun-III" satellites for the same B and 1.25 < L < < 1.35 [7]. With L ~2 and B = 0.265 gauss the lifetime is about 20 days. It is interesting to note that the curves showing the drop in particle intensity for the artificial radiation belt, these curves having been measured aboard the Telstar satellite during the same period as the measurements carried out aboard the Kosmos-7 and Kosmos-9 satellites, yield approximately the same lifetime for L ~2 and considerably lower values of B (0.04 gauss < B < 0.08 gauss) [7, 12]. Hence we can see that τ in this region is independent of B, i.e., [independent] of altitude. This may indicate that at L ~2 the energy losses of the particles are not governed by dissipation in the atmosphere and that there exists some mechanism of losses to which the particles in the shell with the given L are subject (for example, magnetic dissipation).

CONCLUSIONS

In the investigations of radiation in the vicinity of the Brazil magnetic anomaly by means of the Kosmos-4, Kosmos-7, Kosmos-9 and Kosmos-15 satellites, the following results were obtained.

1. During the course of the flight of the Kosmos-4 satellite in April 1962 an increase in the counting rate of Geiger counter was detected, this increase being greater by a factor of approximately 4 than the measurements carried out in August of 1960 aboard the 2nd space

vehicle. The magnitude of the increase corresponds to the anticipated change, as calculated by Hess, in the intensity of the protons in the inner belt with transition to the solar-activity minimum; this change in intensity was brought about by the reduction in atmospheric density. This fact serves as an additional argument in favor of the neutron mechanism as the source of protons in the inner radiation belt.

2. The lifetime of the electrons in the artificial radiation belt has been measured, and in the case of magnetic shells with $L < 1.8$ diminishes from values of 4 months with $B = 0.23$ gauss and $L = 1.25$–1.4 to 20 days with $B = 0.265$ gauss and $L = 2$. It follows from comparison with measurements carried out aboard the Telstar satellite that the lifetime of electrons in the magnetic shell with $L \sim 2$ is independent of B in the interval 0.04 to 0.265 gauss, which indicates the existence in this magnetic shell of a powerful loss mechanism, unlike the Coulomb scattering in the atmosphere (for example, magnetic dissipation).

The authors are indebted to T.M. Taranova and T.N. Maslova for the formulation of the results.

Received 14 January 1964

REFERENCES

1. S.N. Vernov, I.A. Savenko, P.I. Shavrin and N.F. Pisarenko, In collection entitled: "Iskusstvennyye sputniki Zemli" [Artificial Satellites of the Earth], No. 10. Izd-vo AN SSSR [Acad. Sci. USSR Press], 1961, page 40.

2. V.L. Ginzburg, L.V. Kurnosova, V.I. Logachev, L.A. Razorenov, I.A. Sirotkin and M.I. Fradkin, In collection entitled: "Iskusstvennyye sputniki Zemli," No. 10. Izd-vo AN SSSR, 1961, page 23.

3. F.D. Sieward and H.N. Kornblum, Jr., Preprint, 1963.

4. V.I. Krasovskiy, Yu.I. Gal'perin, V.V. Temnyy, G.M. Mulyarchik,

N.V. Dzhordzhio, M.Ya. Marov and A.D. Bolyunova, Geomagn. i aeronomiya [Geomagnetism and Aeronomy], 3, No. 3, 408, 1963.

5. L.G. Mann, S.D. Bloom and H.I. West, Jr., Space Res. III, ed W. Priester, 1963.
6. W.N. Hess, J. Geophys. Res., 67, No. 12, 4886, 1962.
7. W.N. Hess, Preprint, 1963.
8. A.M. Lenchek and S.F. Singer, J. Geophys. Res., 67, No. 10, 4073, 1963.
9. H.H. Heckman and G.H. Nakano, J. Geophys. Res., 68, No. 8, 2117, 1963.
10. S.N. Vernov, I.A. Savenko, P.I. Shavrin, V.Ye. Nesterov, N.F. Pisarenko, M.V. Tel'tsov, T.I. Pervaya and V.N. Yerofeyeva, Kosmich. issled. [Cosmic Research], 2, No. 1, 136, 1964.
11. W.N. Hess, J. Geophys. Res., 68, No. 3, 667, 1963.
12. W.L. Bloom and J.D. Gabbe, J. Geophys. Res., 68, No. 3, 607, 1963.

Manuscript Page No. [Transliterated Symbols]

219 ВОСТ = vost = vostok = east

219 ЗАП = zap = zapad = west

THE POSSIBILITIES OF REPLACING THE NITROGEN IN THE AIR WITH HELIUM IN SPACE-VEHICLE CABINS AND THE EFFECTIVENESS OF USING A HELIUM-OXYGEN MIXTURE FOR VENTILATION OF A SPACE-PRESSURE SUIT

A.G. Dianov

The replacement of nitrogen by helium in the atmosphere of space-vehicle cabins represents an expedient approach both from the physiological as well as from the engineering standpoints. Up to the present time there had been no prolonged experiments in which a helium-oxygen mixture was used as the medium of human environment.

Two experiments have been carried out on human beings, these tests lasting 22 and 30 days. It was established that it is possible for a human being to spend a prolonged period of time (up to 25 days) in an airtight cabin in whose atmosphere the nitrogen of the air had been replaced by helium. In view of the high thermal conductivity of the helium-oxygen mixture, the zone of thermal comfort for the test subjects during daylight hours exhibited a temperature range of 24.5-27.5°C, the temperatures ranging from 26-29°C for this zone at night. A change in the speech patterns of the test subjects was noted, this change being expressed in a shift of the speech spectrum toward frequencies higher by a magnitude of 0.7 of an octave.

It has been demonstrated in experiments lasting up to 24 hours that the utilization of a helium-oxygen mixture for ventilation of a space pressure suit at elevated ambient temperatures (27-30°C) considerably improves heat transfer on the part of the human being and makes it possible to reduce the ventilation volume of the space suit.

Among contemporary problems of space medicine, the problem of providing a microclimate within the cabins of space vehicles assumes an important place. It is quite obvious that the microclimate of the cabins must exhibit optimum physiological-hygienic characteristics and satisfy a number of engineering requirements. In this connection, the problem of replacing the nitrogen in the air of the cabins by helium takes on great significance. The concepts upon which the hypotheses of the expediency of this substitution are based follow from consideration of the primary physicochemical properties of helium and the physiological hygienic investigations involving the use of this gas which were carried out prior to this time in various areas in the field of medicine.

In view of the low solubility of helium in comparison with nitrogen in liquids and particularly in fats [1], an atmosphere consisting of oxygen and helium involves fewer dangers connected with the development of decompression disturbances which may affect a human being in the cabin of a space vehicle as a result of pressure drops. The project carried cut in connection with the utilization of helium in order to prevent caisson disease in divers [2], as well as theoretical investigations [3], have confirmed this hypothesis.

The substitution of nitrogen by helium eliminates the harmful effect on a human being of induced radioactivity which may occur under the action of cosmic radiation on nitrogen molecules [4].

Having considered the high thermal conductivity of helium (greater by a factor of 6 in comparison with nitrogen), we have a basis for the assumption that a human being in the cabin of a space vehicle with a helium-oxygen medium may more easily withstand the higher ambient temperatures than in air. Should this hypothesis be experimentally confirmed, the substitution of nitrogen by helium will play a significant

role in shielding a human being against the high temperatures (up to 35°C) which may prevail in a space vehicle.

In view of the fact that the density of helium is smaller by a factor of approximately 7 than the density of air, the utilization of a helium-oxygen mixture in space vehicles will lead to a reduction in the launching weight of the vehicles. Moreover, the presence of helium in the atmosphere of the space-vehicle cabin is expedient should it become necessary to detect the source of a breakdown in the airtightness of the vehicle, since the best method of detected this circumstance involves the utilization of a helium leakage detector. It may also be assumed that the substitution of nitroger by helium leads to a reduction in the energy required for the forced ventilation of the cabin.

Up to the present time a number of projects [2, 3, 5-13] have been devoted to the study of the influence of a helium-oxygen mixture on animal and human organisms. In the experiments with animals it has been demonstrated that it is possible to achieve a prolonged stay (up to two and a half months) in a gaseous medium in which the nitrogen of the air has been replaced by helium. In the range of temperatures from 18 to 22°C, the helium, exhibiting a greater thermal conductivity than nitrogen, raises the ability of animals to eliminate gases by increasing the losses of heat. With a rise in the temperature of the helium-oxygen mixture to 27-29°C, however, animals exhibit no significant changes.

The effect of the helium-oxygen mixture on the human organism was investigated only in brief experiments lasting no more than several hours (during dives to great depths, in the treatment of certain respiratory-organ diseases, etc.). The results of these investigations demonstrated the possibility of a human being briefly breathing a helium-oxygen mixture under both normal and elevated pressures (up to 16

atm). However, in these experiments the helium-oxygen mixture was not employed as the general gaseous medium surrounding the individual, but rather as a gaseous mixture supplied for purposes of breathing through a mask. Prolonged experiments in which a helium-oxygen mixture was used as the medium of human environment had not been carried out as of the present.

The possibility of a prolonged stay on the part of a human being in an airtight cabin at ground barometric pressure, with the nitrogen in the air of the cabin's atmosphere having been replaced by helium, is the subject of the present work. Two prolonged experiments with an over-all duration of 22 and 30 days were carried out with participation of two test subjects (the test subjects spent 10 and 25 days, respectively, in the helium-oxygen medium). The regeneration of the air in the cabin and the maintenance of the required humidity levels were achieved by means of air-conditioning systems. The temperature of the gaseous medium in the cabin was maintained by means of a heat-regulation system. The substitution of the nitrogen by helium in the air of the cabin was carried out as follows: initially the cabin was ventilated with pure medicinal oxygen in order to remove all nitrogen from the cabin and desaturate this gas from the organism of the test subject. Then, as an atmosphere consisting of 97% oxygen and 3% nitrogen was developed in the cabin, the oxygen ventilation was curtailed and ventilation with helium of high purity was undertaken to the point at which an atmosphere consisting approximately of 22.5% oxygen, 76% helium, and 1.5% nitrogen was attained. The concentration of carbon dioxide during the course of the experiment did not exceed 0.7%, the relative humidity was maintained at a level of 30-60%, and the temperature of the gaseous medium in the cabin varied within a range of 16-32°C. The variations in the temperature of the gaseous medium within such a wide range were

made necessary by the need to determine zones of thermal comfort for the test subjects both in the air and in the helium-oxygen media.

The test subjects wore cotton jersey underwear and sweatsuits. They ate four times daily, with a general average daily food intake of 3600 kcal. During the course of the entire experiment the subject was seated in an arm chair: during the hours in which he was awake he was in a sitting position, while during sleep he was lying down in a horizontal posititon (the back of the chair being folded back in this case). During the course of the experiments the functioning of the central nervous system, respiration, the cardiovascular system, gas and heat exchange, as well as speech and hearing were studied. Moreover, the behavior of the subjects was kept under observation and their moods were taken into consideration.

As a result of the experiments that were carried out it was demonstrated that a helium medium, because of its high thermal conductivity, significantly alters the transfer of heat on the part of a human being. A stay in a helium-oxygen medium at temperatures 18-24°C comfortable for air resulted in noticeable cooling of the subjects: at a cabin temperature of 21°C the average weighted surface temperature of the skin of the subject in the helium-oxygen medium was virtually two degrees lower than in air. In the helium-oxygen medium the zone of thermal comfort for the test subjects in a state of wakefulness during daylight hours ranged from 24.5-27.5°C, while at night, during sleep, it ranged from 26-29°C. Our attention is drawn to the significant reduction (by 3°) of the zone of thermal comfort in the helium-oxygen medium in comparison with an analogous zone in an air medium.

The noted changes are explained by the more pronounced cooling properties of the helium-oxygen medium in comparison with air. In a helium-oxygen medium the drop in temperature in a dry-bulb catathermo-

meter took place considerably more rapidly than in air: at an ambient temperature of 20.0°C the drop occurred approximately 39% more rapidly, while at a temperature of 24.5°C the corresponding figure was 33.5%. The body temperature of the test subjects during the course of the experiments experienced no regular variations and fluctuated between 36.2-37.0°C.

The reaction to heat on the part of the test subjects in a helium-oxygen medium was somewhat different from that in air. In the helium-oxygen medium a change in temperature was sensed more clearly than in air. Moreover, a change in the temperature of the helium-oxygen medium, whether up or down, was sensed more rapidly by the subjects than in air. The reaction to heat in a helium-oxygen medium is subject to a far greater extent to the influence of such factors as the intake of food and, particularly, physical exercise. During the course of physical exercise in a helium-oxygen medium, at a comfortable temperature for a state of rest, the subjects experienced a sensation of thermal discomfort much more rapidly and to a much greater extent. On the other hand, the return to normal sensations of heat after physical exercise in a helium-oxygen medium also occurred much more rapidly than in an air medium.

The experimental data considered below were derived primarily at comfortable temperatures for the gaseous medium in the cabin.

In investigating the functional state of the central nervous system,* determinations were made of the magnitudes of the rheobase and the chronaxy of the cutaneous, visual, vestibular, and motor analyzers, the capacity of the eye to resolve flickering light pulses of increasing frequency, the state of the taste and sensory analyzers, the bioelectric potentials of various sections of the brain in a state of relative rest, and during the course of various functional

tests, determinations were made of the conditioned-motor reflexes, the state of the higher psychic functions, and the ability to perform work.

The analysis of the bioelectric potentials and the magnitudes of the latent period of conditioned-motor reflexes showed that during the course of the experiments the test subjects exhibited gradual intensification of inhibitory processes in the cerebral cortex, which is borne out by the gradual increase in the bioelectric activity of slow rhythms in the four standard abductions, as well as a certain extension of the latent period of conditioned-motor reflexes. Both during the first and second experiments, the analysis of the electroencephalographic records was carried out by a determination of the magnitude of the total bioelectric effect over a period of 10 seconds in integral units. During the course of the first prolonged experiment, as the ability of the test subject to function was being investigated, the magnitude of the bioelectric activity of the delta-rhythm at the beginning of the experiment amounted to 14 integral units as the transmission of information by means of a coding device was being carried out, this figure gradually increasing toward the end of the experiment to 35 integral units. The magnitude of the bioelectric activity of the theta-rhythm increased, from 12 to 25 integral units, while the alpha-rhythm increased from 12 to 31 integral units. In the second experiment, the same quantitative relationship was observed for the increase in the magnitudes of the bioelectric activity of the low-frequency rhythms. The indicators of bioelectric activity for high-frequency rhythms during the course of the experiment exhibited a certain tendency to diminish both during periods of rest and during periods of work on the part of the test subjects.

The gradual increase in the magnitudes of the bioelectric activity

for low-frequency rhythms during the course of the experiments cannot be associated with any specific influence by the helium-oxygen medium on the higher nervous activity of the test subjects. This is confirmed by the fact that during the prolonged experiment involving an air medium, the test subject also exhibited a regular increase in the bioelectric activity of these rhythms [14]. Apparently, the increase in bioelectric activity of the low-frequency rhythms should be regarded as a result of the reduction in the influx of afferent information to the cerebral cortex. The recovery of bioelectric brain activity to the initial level after completion of the experiment confirms the indicated hypothesis. However, it should be pointed out that these changes are not indicative of serious disruptions of the higher nervous activity of the test subjects, since their general state and ability to function during the course of the experiment remained virtually unchanged. All remaining indicators of the functional state of the central nervous system during the stay of the test subjects in a helium-oxygen medium underwent no significant changes. In addition, no changes were detected in the general well-being and behavior of the test subjects.

The indicators for natural respiration, the cardiovascular system, gas transfer, and expenditure of energy on the part of the test subjects under the conditions of basic exchange and in a state of relative rest exhibited no significant changes. However, the application of a functional test in the form of metered physical load showed that with increasing duration of the experiments there appeared a gradual increase in the per-minute respiration volume, the frequency of cardiac contractions, the quantity of oxygen required, and the expenditure of energy upon completion of physical exercise.

Apparently, these changes are also not due to the effects of the helium-oxygen medium, but rather due to the prolonged hypodynamia and

relative isolation. The progressive deterioration of the physical condition of the test subjects was clearly brought out here as the duration of the experiments was increased. In each case the performance of physical work placed ever-increasing strain on respiration, the cardiovascular system, and exchange of gases. Thus, for example, during the course of a 30-day experiment the per-minute respiration volume, after the test subject had completed 20 squats within 30 seconds after having spent two days in the helium-oxygen medium, amounted to 18.6 liters; after eight days in this medium, the volume came to 20.4 liters, after twelve days, 22.7 liters, and after sixteen days, the respiration volume amounted to 24.5 liters [after the completion of the aforementioned exercise]. The respiration indicators subsequently stabilized and remained at this comparatively high level until the end of the experiment. During the investigations conducted during the performance of physical work on the eighth and twelth days after completion of the experiment it was noted that there appeared a reduction of the per-minute respiration volume to the initial level. The change in the frequency of the cardiac contractions and in the indicators of gas exchange followed the same trend.

The investigations showed* that a stay in a helium-oxygen medium leads to a significant change in the speech of the test subjects, this being expressed in a shift in the spectrum toward higher frequencies by an order of magnitude of 0.7 of an octave. Intelligibility of speech in this case suffered somewhat but does not drop below the level of tolerable magnitudes. The auditory function of the test subjects in the helium-oxygen medium underwent no significant change.

Up to the present time no attempt had been made to use helium for ventilation of the space suit. At the same time, considering the higher thermal conductivity of helium in comparison with air, it might be as-

sumed that the utilization of a helium-oxygen mixture for ventilation of a space pressure suit will considerably improve conditions of heat transfer on the part of the human being at high ambient temperatures and, possibly, will make it possible to reduce the level of space-suit ventilation, retaining thermal comfort for the individual. Reduction of the space-suit ventilation level represents a certain engineering advantage from the standpoint of economy in the energy required for the achievement of forced ventilation.

In order to clarify these problems, we carried out four experiments with two test subjects in an airtight cabin, in conjunction with A.D. Logunov, and the first of these test subjects was kept in the space suit for a period of 8 hours, while the second subject stayed in the suit for 24 hours. Each test subject participated in one experiment involving the use of a helium-oxygen medium and in one control experiment of the same duration in an air medium. The helium-oxygen medium in the cabin was produced in the same manner as in the prolonged experiments. The supply of the gas mixture for purposes of respiration and suit ventilation was achieved by means of an autonomous regeneration and air-conditioning system.

During the course of the experiments, the temperature and humidity of the gaseous medium of the cabin was recorded, and similar measurements were taken in the gas lines at the inlet to and outlet from the space suit, as well as in the space within the suit. The ventilation of the space suit was measured by means of a Venturi tube (in the air medium) and by means of dry-running gas flowmeters (in the helium-oxygen medium). The body and skin temperatures, as well as the rate of respiration and cardiac contractions of the test subjects were measured. The heat output of the test subjects was determined by means of indirect calorimetry in accordance with the Douglas-Holden method. The moisture

losses of the test subjects were measured in all of the experiments by means of laboratory scales. The magnitude of heat transfer on the part of the test subjects were determined on the basis of changes in body temperature and the mean-weighted skin temperatures, the quantity of evaporated moisture, and the difference between the temperatures of the ventilation air at the inlet to and the outlet from the space pressure suit. The thermal balance was determined during the comparison of these quantities with the magnitude of the heat produced by the test subjects.

During the course of the experiments in the air medium, the temperature in the airtight cabin was maintained at a level of 27-30°C and the ventilation of the space pressure suit was kept at a level of 160-180 liters/minute; the temperature of the air at the inlet to the space pressure suit fluctuated around 22°C. Under these conditions, the organisms of the test subjects experienced overheating: their reaction to heat was one of discomfiture, abundant perspiration was noted, and body temperature rose to 37.2 to 37.4°C. In the calculation of the heat balance a certain accumulation of heat in the organisms of the test subjects was noted (up to 2 kcal/hr).

During the course of the 24-hour experiment carried out in a helium-oxygen medium at the same values for the ambient temperature and the ventilation of the space pressure suit, the reactions to heat on the part of the test subjects produced no discomfort, despite the fact that the temperature of the gaseous mixture at the inlet to the space pressure suit was 3° higher than in the analogous experiment in an air medium. With a drop in the temperature of the gaseous medium at the inlet to the space pressure suit to 22°C the test subject evaluated his reaction to heat as "cool."

During the course of the 8-hour experiment in a helium-oxygen medium the reaction to heat on the part of the test subject was one of

comfort, despite the fact that the ventilation of the space pressure suit was lower by a margin of 60-80 liters/min, while the temperature of the gaseous mixture at the inlet to the space pressure suit was higher by a margin of 4-6°C than in the analogous experiment in an air medium.

In the experiments with the helium-oxygen medium the temperature of the body and the skin of the test subjects exhibted no significant change, while the loses of moisture were lower by a factor of 40%. There was no accumulation of heat in the organisms of the test subjects and a negligible heat deficit was actually noted.

Received 9 January 1964

REFERENCES

1. A.R. Behnke and O.D. Yarbrough, Amer. J. Physiol., 126, 409, 1939.
2. M.I. Yakobson, Kessonnaya bolezny. Medgiz [Caisson Disease. Medical Press], 1950.
3. D.I. Simons, J. Aviat. Med., 30, No. 5, 314, 1959.
4. N.J. Bowman and E.H. Dingman, J. Brit. Interplanet. Soc., 17, No. 10, 372, 1960.
5. V.V. Boriskin, P.V. Oblapenko, V.V. Rol'nik and B.M. Savin, Dokl. AN SSSR [Proc. Acad. Sci. USSR], 143, No. 2, 475, 1962.
6. G.L. Zal'tsman, Fiziologicheskiye osnovy prebyvaniya cheloveka v usloviyakh povyshennogo davleniya gazovoy sredy [Physiological Bases for the Stay of a Human Being under Conditions of Elevated Gas-Medium Pressures], Medgiz, 1961.
7. L.A. Orbeli, M.P. Brestkin, B.D. Kravchinskiy, K.A. Pavlovskiy and S.P. Shistovskiy, Voyenno-meditsinskiy sbornik [Military-Medical Collection], No. 1, Moscow-Leningrad, 1944.
8. A.L. Barach, Proc. Soc. Exper. Biol.and Med., 32, 462, 1934.

9. S.F. Cook, J. Cell. and Compar. Physiol., 36, No. 1, 115, 1950.

10. S.F. Cook, F.E. South and D.R. Joung, Amer. J. Physiol., 164, No. 1, 248, 1951.

11. H.A. Leon and S.F. Cook, Amer. J. Physiol., 199, No. 2, 243, 1960.

12. F.E. South and S.F. Cook, J. General Physiol., 36, No. 4, 513, 1953.

13. D.R. Joung and S.F. Cook, J. Cell and Compar. Physiol., 42, No. 2, 319, 1953.

14. F.D. Gorbov, V.I. Myasnikov and V.I. Yazdovskiy, Zh. vyssh. nervn. deyat. [Journal of Higher Nervous Activity], 13, Issue 4, 585, 1963.

Manuscript Page No.

[Footnotes]

229 The investigations were carried out by V.F. Onishchenko, V. V. Boriskin, P.A. Gul'tyayev, A.V. Sergiyenko, V.A. Pestova, and A.A. Bulat.

232 The investigations were carried out by I.Ya. Borshchevskiy, V.S. Kuznetsov, and Yu.V. Krylov.

INFORMATION FOR AUTHORS

1. Original investigations, reviews (at the request of the Editors), and brief reports are accepted for publication in this journal. Materials published earlier, as well as material accepted for publication in other journals, are not accepted by the Editors.

2. An article received for publication must be accompanied by a statement from the institution in which the given project was carried out.

3. The material must be as brief as possible and presented in completely edited form, without corrections.

4. The article must be typed with double spacing on only one side of regular-size paper, with a margin of at least 4 cm at the left. The manuscript, tabular material, and illustrations must be presented in two copies (including an original).

Drawings and graphs must be executed with india ink on white paper, tracing paper, or graph paper and of such size as to permit subsequent reduction (in the preparation of the stereotype). The author's name, the title of the article, and the number of the drawing must be indicated on the reverse side of the drawing.

5. The references must be given in a listing at the end of the article, on a separate piece of paper in the following order: the initials and name of the author, the title of the book (journal), the publisher and place of publication (for books), volume, issue number, and the first page (for journals), and the year of publication.

Literature references in the body of the article should be presen-

ted in brackets, e.g., [10]; the numbering system should be consecutive, following the order of appearance of the references in the text.

6. An article sent to the Editors must be signed by the author, and in the case of several authors, all of the co-authors must sign their surnames, given names, and patronymics, and they must indicate their complete postal address, place of work, and telephone number.

7. The Editors will submit one galley proof to the author, and this must be returned to the Editors within 24 hours after receipt.

8. In case an article is returned to the author for further processing, the date on which the article is received is regarded as the date the Editors receive the final text.

Address of the Editors: Moscow G-242, B. Gruzinskaya, 10,

Tel. D 2-10-10, ext. 686